ASSESSING THE ROLE OF TICAM1 IN HUMAN VIRAL DISEASES

IRA KARTIKA DEWI SABLI

A thesis submitted for the degree of

Doctor of Philosophy

Department of Infectious Diseases, Faculty of Medicine

Imperial College London, United Kingdom

March 2024

Abstract

Host genetic factors play a crucial role in determining an individual's vulnerability to specific infections and the outcomes of diseases caused by otherwise common pathogens. In particular, severe infectious diseases such as herpes simplex encephalitis (HSE) can be attributed to inborn errors of immunity (IEI). This thesis aimed to assess 50 different *TICAM1* variants present in individuals associated with severe viral illnesses. Firstly, we identified three variants (T4I, S60C, and Q392K) in *TICAM1* that result in a loss of function, impairing type I interferon signaling and contributing to the development of severe COVID-19 pneumonia. Secondly, our research extended beyond COVID-19 to discover a rare *TICAM1* variant linked to Mollaret's meningitis, highlighting its impact on the TLR3-TICAM1-IFN pathway. Specifically, the rare E429X *TICAM1* variant exhibited a loss of protein expression and a loss-of-function phenotype, increasing susceptibility to HSV-2 infection. Lastly, our study introduced an innovative approach, utilising cerebral organoids derived from human pluripotent stem cells (PSCs) as models for investigating viral infections. These 3D models provide insights into the intricate cellular environment of the human central nervous system (CNS) and offer a valuable platform for studying HSV-1 infection. Reprogramming induced pluripotent stem cells (iPSCs) from a patient with a potential defect in the TLR3-IFN pathway enabled the assessment of HSV-1 infection processes within iPSCs-derived CNS cells. Overall, this work aimed to understand the impact of novel genetic variants in *TICAM1* and TRL3 pathway on susceptibility to and the severity of infectious diseases.

Declaration of Originality

I hereby declare that the content presented in this thesis is the result of my own work. Parts that are not original to this work, or any work performed by anyone other than myself, have been appropriately acknowledged and referenced. This thesis is submitted to Imperial College London for the degree of Doctor of Philosophy. The data and findings presented herein have not been previously submitted by me in any form for any other qualifications at Imperial College London or any other institutions. The research was conducted in the Department of Infectious Disease, Faculty of Medicine at Imperial College London, and was co-supervised by Dr. Vanessa Sancho-Shimizu and Professor Peter O'Hare.

Copyright Declaration

The copyright of this thesis rests with the author. Unless otherwise indicated, its contents are licensed under a Creative Commons Attribution-Non Commercial 4.0 International Licence (CC BY-NC). Under this licence, you may copy and redistribute the material in any medium or format. You may also create and distribute modified versions of the work. This is on the condition that: you credit the author and do not use it, or any derivative works, for a commercial purpose. When reusing or sharing this work, ensure you make the licence terms clear to others by naming the licence and linking to the licence text. Where a work has been adapted, you should indicate that the work has been changed and describe those changes. Please seek permission from the copyright holder for uses of this work that are not included in this licence or permitted under UK Copyright Law.

Acknowledgement

I would like to express my deepest gratitude and heartfelt appreciation to Dr. Vanessa Sancho-Shimizu and Prof. Peter O'Hare for giving me the opportunity to work on this project at Imperial College London and has significantly contributed to my ongoing professional development. I am particularly grateful to Dr. Sancho-Shimizu, whose continuous encouragement, steady guidance, and belief in my abilities have absolutely crucial in this journey. Her kindness, enthusiasm, and remarkable patience have served as constant sources of motivation and inspiration throughout this endeavour.

I would also like to express a massive thank you to my family, with my deepest gratitude directed towards my parents, Sabli bin Haji Metussin and Serimah binti Awg Besar, as well as my brothers, Abang and Nabil. Their consistent and unwavering support, along with continual encouragement and belief in me, has been the most significant factor throughout my journey. I am incredibly grateful to them for being so wonderfully supportive throughout all my endeavours.

Special thanks go to all members of the Sancho-Shimizu lab, both past and present, for their amazing support and camaraderie. A special shoutout to Aneesa, Dilys, and Steph for consistently being there, making tough times more manageable with all the laughter, and for being so understanding of me! I would like to express my gratitude to everyone in the Paediatrics department, especially those who have been companions, offering support, guidance, and mentorship over the years (a special mention to Millie!). I would also like to thank all the friends I've made in Brunei Hall during these past few years (including the teachers and caretakers!) for their friendship and moral support, which have made a meaningful impact on my journey. I genuinely appreciate each one of you for making London feel like a second home.

Finally, I extend my gratitude to the Brunei Government for graciously sponsoring my education, providing me with this invaluable opportunity for learning and personal development.

Table of Contents

Abstract 2
Declaration of Originality 3
Copyright Declaration 4
Acknowledgement 5
Abbreviations 10
List of Figures 17
List of Tables 20
Foreword 21
Chapter 1 22
1. Introduction 23
1.1 Infectious diseases and genetics 23
1.2 Inborn errors of immunity 24
1.3 Herpes Simplex Virus-1 (HSV-1) 25
1.3.1 Life cycle of HSV-1 26
1.3.2 Herpes simplex encephalitis (HSE) 28
1.4 Herpes simplex virus 2 (HSV-2) 29
1.4.1 Recurrent meningitis associated with HSV-2 30
1.5 COVID-19 32
1.5.1 Severe acute respiratory syndrome coronavirus 2 (SARS-CoV-2) 32
1.5.2 Life cycle of SARS-CoV-2 33
1.6 Innate immunity 35
1.6.1 Toll-like receptors (TLRs) 36
1.6.2 Toll-like receptors 3 (TLR3) – interferon (IFN) pathway 37
1.6.3 Innate immune response to HSV-1 40
1.6.4 Inborn errors of immunity in HSE 42
1.6.5 Innate immune response to HSV-2 44
1.6.6 Innate immune response to SARS-CoV-2 45
1.7 TICAM1 46
1.7.1 TICAM1 in viral infections 49
1.8 Aims of this study 51
Chapter 2 52
2. Methods 53
2.1 Cell maintenance and culture 53
2.1.1 Dermal fibroblasts 53
2.1.2 Stem cells culture 53

2.1.2.1 Differentiation into cortical neurons 54
2.1.2.2 Differentiation into cerebral organoids 55
2.2 Isolating primary human peripheral blood mononuclear cells (PBMCs) 56
2.3 Genetic DNA editing 57
2.3.1 Plasmids 57
2.3.2 Oligonucleotides used in this thesis 61
2.4 Site-directed mutagenesis (SDM) 67
2.5 Transient transfection 68
2.6 Dual luciferase reporter assay 69
2.7 Cell viability assay 69
2.8 Western blotting 70
2.8.1 Protein isolation and quantification 70
2.8.2 Sodium dodecyl sulphate polyacrylamide gel electrophoresis (SDS-PAGE) 71
2.8.3 Membrane transfer 71
2.8.4 Protein revelation 72
2.9 Immunoprecipitation 75
2.10 Ligand stimulation 76
2.11 Cytokines measurement using Meso-scale discovery (MSD) and enzyme-linked immunosorbent assay (ELISA) 76
2.12 Viral strains and propagation 77
2.13 Infection and treatment 78
2.14 Plaque assay 78
2.15 50% Tissue culture Infective Dose ($TCID_{50}$) 79
2.16 Quantitative RT-PCR (RT-qPCR) 79
2.17 Reprogramming PBMCs into iPSCs 80
2.18 Immunofluorescence and image acquisition 82
2.18.1 Fibroblasts 82
2.18.2 Cortical neurons 82
2.18.3 Cerebral organoids 83
2.19 Statistical analysis and software 84
Chapter 3 85
3. *TICAM1* variants in SARS-COV2 infections 86
3.1 Background 86
3.2 Establishment of *TICAM1* variants in life-threatening COVID-19 pneumonia 87
3.3 Generation of *TICAM1* variants constructs 91
3.4 Optimisation of transient transfection in $TICAM^{-/-}$ cells 92
3.5 Identification of loss-of-expression *TICAM1* variants 94
3.6 Functional characterization of *TICAM1* variants 98
3.7 Complementation of Loss-of-Function *TICAM1* variants 101
3.8 Discussion 103

Chapter 4 111

4. *TICAM1* variant in HSV-2 meningitis 112

4.1 Background 112

4.2 Discovery of novel heterozygous *TICAM1* variant in a patient with recurrent HSV-2 meningitis 113

4.2.1 Clinical features 113

4.2.2 Genetic findings 115

4.3 Generation of *TICAM1* variant construct 118

4.4 Identification of loss-of-expression *TICAM1* E429X variant 118

4.5 qPCR analysis of *TICAM1* overexpression 120

4.6 Functional characterisation of E429X *TICAM1* variant using luciferase reporter assays 122

4.7 Complementation of Loss-of-Function E429X *TICAM1* variant 123

4.8 E429X TICAM1 expression using patient's cells 125

4.9 qPCR analysis of endogenous *TICAM1* from patient's cells 126

4.10 Characterisation of E429X *TICAM1* variant upon ligand stimulations 127

4.11 Characterisation of E429X *TICAM1* variant upon viral infection 130

4.12 Infection upon complementation of E429X fibroblast cells 134

4.13 Discussion 136

Chapter 5 143

5. Modelling HSV-1 infection in cerebral organoids 144

5.1 Background 144

5.2 Generation and validation of cortical neurons and cerebral organoids using ESCs 146

5.2.1 ESCs-derived cortical neurons 147

5.2.2 ESCs-derived cerebral organoids 149

5.3 Optimisation of HSV-1 infection in cortical neurons and cerebral organoids 152

5.3.1 HSV-1 infection in ESCs-derived cortical neurons 152

5.3.2 HSV-1 infection in ESCs-derived cerebral organoids 154

5.4 Effects of HSV-1 infection on patients' cells derived cortical neurons and cerebral organoids .158

5.4.1 Generation of patients' iPSCs and differentiation into cortical neurons and cerebral organoids 158

5.4.2 Effects of patients' iPSCs-derived cortical neurons upon HSV-1 infection 160

5.4.3 Effects of patients' iPSCs-derived cerebral organoids upon HSV-1 infection 163

5.4.4 Effects of patients' fibroblasts upon HSV-1 infection and ligand stimulations 165

5.5 Effects of drug treatments on H9 ESCs-derived cortical neurons 168

5.6 Discussion 172

Chapter 6 180

6. Discussion and future directions 181

6.1 General discussion 181

6.2 Main findings 183

6.3 Future directions 187
6.4 Concluding remarks 190
References 191
Appendix 228
7. Appendix 229

Abbreviations

ACE2	Angiotensin-converting enzyme 2
AD	Autosomal dominant
AP-1	Activating protein-1
AR	Autosomal recessive
ARDS	Acute respiratory distress syndrome
AZI2	5-azacytidine induced 2
BIPAP	Bilevel positive airway pressure
BSA	Bovine Serum Albumin
cDC	Conventional dendritic cells
cDNA	Complementary DNA
cGAMP	Cyclic GMP-AMP
cGAS	Cyclic guanosine monophosphate-adenosine monophosphate synthase
CLR	C-type lectin receptor
CMC	Carboxymethyl cellulose
CMV	Cytomegalovirus
CNS	Central nervous system
COVID-19	Coronavirus disease-19
COVIDHGE	COVID Human Genetic Effort
CoVs	Coronaviruses
CPAP	Continuous Positive Airway Pressure
CSF	Cerebrospinal fluid
CTIP2	COUP TF1-interacting protein 2
CVB3	Coxsackievirus B3
CVID	Common variable immunodeficiency disorder
CXCL10	C-X-C Motif Chemokine Ligand 10
DAI	DNA-dependent activator of IFN-regulatory factors

DAMP	Damage-associated molecular patterns
DBR1	Debranching enzyme 1
DCs	Dendritic cells
DMEM	Dulbecco's Modified Eagle Medium
DNA	Deoxyribonucleic acid
dsDNA	Double-stranded DNA
E	Early
E8	Essential 8
EBs	Embryoid bodies
EDTA	Ethylenediaminetetraacetic acid
EMCV	Encephalomyocarditis virus
ER	Endoplasmic reticulum
ESCs	Embryonic stem cells
FBS	Foetal bovine serum
FDA	United States Food and Drug Administration
GAGs	Glycosaminoglycans
GAPDH	Glyceraldehyde 3-phosphate dehydrogenase
GFP	Green fluorescent protein
GUSB	β-glucuronidase
H&E	Hematoxylin and Eosin
HA	Human influenza hemagglutinin
HEK293	Human embryonic kidney cells
HLA	Human leukocyte antigen
HRP	Horseradish peroxidase
HSE	Herpes simplex encephalitis
HSM	Herpes simplex meningitis
HSV-1	Herpes simplex virus-1

HSV-2	Herpes simplex virus 2
IE	Immediate Early
IEI	Inborn errors of immunity
IF	Immunofluorescence
IFI16	IFN-γ inducible protein 16
IFN	Interferon
IFNAR1	Interferon Alpha And Beta Receptor Subunit 1
IFNAR2	Interferon Alpha And Beta Receptor Subunit 2
Ig	Immunoglobulin
IHC	Immunohistochemistry
IHME	Institute of Health Metrics and Evaluation
IKK	IκB kinase
IKKε	IκB kinase-ε
IL	Interleukin
INGENIOS	Investigating the GENetics of InfectiOn Study
IP	Immunoprecipitation
iPSCs	Induced pluripotent stem cells
IRAK1	IL-1 receptor-associated kinase 1
IRAK4	IL-1 receptor-associated kinase 4
IRF3	Interferon regulatory factor 3
ISGF3	Interferon stimulated gene factor 3
ISGs	Interferon-stimulated genes
IUIS	International Union of Immunological Societies
IκBα	I kappa B alpha
JAK1	Janus kinase 1
L	Late
LAT	Latency-associated transcript

LB	Luria-Brentani
LoE	Loss-of-expression
LoF	Loss-of-function
LPS	Lipopolysaccharides
MAF	Minor allele frequency
MAP2	Microtubule-associated protein 2
MAPK	Mitogen-activated protein kinases
MAVS	Mitochondrial anti-viral signaling protein
MDA5	Melanoma differentiation-associated gene 5
MERS-CoV	Middle East respiratory syndrome coronavirus
MKK	Mitogen-activated protein kinases kinase
MMR	Measles, mumps and rubella
MOI	Multiplicity of infection
mRNAs	Messenger RNAs
MSD	Meso Scale Discovery
MyD88	Myeloid differentiation primary response protein 88
NAP1	NF-κB-activating kinase-associated protein 1
NEAA	Nonessential amino acids
NF-κB	Nuclear factor kappa-light-chain-enhancer of activated B cells
NGS	Next-generation sequencing
NK	Natural killer
NLR	Nucleotide oligomerization domain like receptor
NOD	Nucleotide oligomerization domain
NPCs	Neural progenitor cells
NSC	Neural stem cell
nsps	non-structural proteins
NTD	N-terminal domain

PAMP	Pathogen-associated molecular patterns
PBMC	Peripheral blood mononuclear cells
PBS	Phosphate buffered saline
PCA	Principal component analysis
PCR	Polymerase chain reaction
pDCs	Plasmacytoid dendritic cells
PDL	Poly-D-Lysine
PFA	Paraformaldehyde
PFU	Plaque-forming units
PKR	Protein kinase RNA-activated
PNS	Peripheral nervous system
poly I:C	Polyinosine-deoxycytidylic acid
PRR	Pattern recognition receptors
PSCs	Pluripotent stem cells
PVDF	Polyvinylidene difluoride
RBD	Receptor Binding Domain
RBLM	Recurrent benign lymphocytic meningitis
RFP	Red fluorescent protein
RHIM	RIP homotypic interaction motif
RIG	Retinoic acid-inducible gene
RIP	Receptor-interacting protein
RIP1	Receptor-interacting protein 1
RLR	Retinoic acid-inducible gene like receptor
RNA	Ribonucleic acid
RNApol III	RNA polymerase III
RPMI	Roswell Park Memorial Institute
RRV	Ross River virus

RSV	Respiratory syncytial virus
RTC	Replication and Transcription Complex
RT-qPCR	Reverse transcription-quantitative polymerase chain reaction
SARS-CoV	Severe acute respiratory syndrome coronavirus
SARS-CoV-2	Severe acute respiratory syndrome coronavirus 2
SDM	Site-directed mutagenesis
SDS-PAGE	Sodium dodecyl sulphate polyacrylamide gel electrophoresis
SnoRNA31	Small nucelolar RNA31
SNP	Single nucleotide polymorphism
ssRNA	Single-strand RNA
STAT1	Signal transducer and activator of transcription 1
STAT2	Signal transducer and activator of transcription 2
STING	Stimulator of interferon gene
T2BM	TRAF2 binding motif
T6BM	TRAF6 binding motif
TBK1	TANK-binding kinase 1
TBST	Tris-Buffered Saline-Tween20
TCID50	50% tissue culture infective dose
TICAM1	TIR domain-containing adaptor-inducing IFN-β
TICAM2	TIR domain containing adaptor molecule 2
TIR	Toll/interleukin-1 receptor
TLR	Toll-like receptor
TLR2	Toll-like receptor 2
TLR3	Toll-like receptor 3
TLR4	Toll-like receptor 4
TLR7	Toll-like receptor 7
TLR8	Toll-like receptor 8

TLR9	Toll-like receptor 9
TMPRSS2	Transmembrane serine protease
TNF	Tumour necrosis factor
TPR	Tetratricopeptide repeat
TRAF3	Tumour necrosis factor receptor-associated factor 3
TRAF6	Tumour necrosis factor receptor-associated factor 6
TRAM	TIR domain containing adaptor molecule 2
TRIF	TIR domain-containing adaptor-inducing IFN-β
TRIM	Tripartite motif
Tuj1	Beta III Tubulin
TYK2	Tyrosine kinase 2
ULA	Ultra-Low Attachment
UV	Ultraviolet
VZV	Varicella zoster virus
WES	Whole Exome Sequencing
WHO	World Health Organization
WT	Wild-type
YFV	Yellow fever virus

List of Figures

Figure 1.1 TLR3-IFN downstream signalling. 39

Figure 1.2 Schematic illustration of the TICAM1 protein. 47

Figure 1.3 TICAM1 in TLR3 and TLR4 signalling. 49

Figure 2.1 Plasmid map. 57

Figure 3.1 Lolliplot of *TICAM1* variants and their minor allele frequency. 89

Figure 3.2 Optimisation of transient transfection of WT TICAM1 plasmid in TICAM1-deficient cells. 93

Figure 3.3 Comparison of IFN-β Induction in transient transfection with and without z-VAD-fmk. 94

Figure 3.4 Impact of 49 *TICAM1* variants on protein expression 96

Figure 3.5 Impact of 20 *TICAM1* variant on protein expression by immunofluorescence 98

Figure 3.6 Impact of 49 *TICAM1* variants on IFN-β signalling. 100

Figure 3.7 Impact of 20 *TICAM1* variants on NF-κB signalling. 101

Figure 3.8 Impact of three LoF *TICAM1* variants upon complementation on IFN-β signalling. 102

Figure 4.1 Discovery of a *TICAM1* variant present in a heterozygous state among four family members. 114

Figure 4.2 Lolliplot graph of *TICAM1* variants. 117

Figure 4.3 Impact of *TICAM1* E429X variant on protein expression. 119

Figure 4.4 Impact of *TICAM1* E429X variant on protein expression by immunofluorescence. 120

Figure 4.5 *TICAM1* mRNA level in transient transfection of overexpression. 121

Figure 4.6 Impact of *TICAM1* E429X variant on IFN-β and NF-κB signalling. 122

Figure 4.7 Impact of *TICAM1* E429X variant on IFN-β and NF-κB signalling. 124

Figure 4.8 TICAM1 endogenous protein expression of P1. 126

Figure 4.9 Endogenous *TICAM1* mRNA level in SV40-fibroblasts 127

Figure 4.10 Cytokines levels in SV40-fibroblasts upon stimulation with P(I:C) and LPS. 129

Figure 4.11 Cytokines levels in SV40-fibroblasts upon stimulation with IL-1β or TNF-α. 130

Figure 4.12 Impact of HSV-1 and HSV-2 infections on SV-40 fibroblasts. 132

Figure 4.13 Cytokines levels in SV40-fibroblasts upon infection with HSV-1 and HSV-2. 133

Figure 4.14 Cytokines levels in PBMCs upon infection with HSV-1. 134

Figure 4.15 Impact of complementation on P1 SV40 fibroblasts. 135

Figure 5.1 Neuronal differentiation from H9 ESCs. 149

Figure 5.2 Characterisation of cerebral organoids derived from H9 ESCs. 151

Figure 5.3 Establishment of HSV-1 infection on H9 ESCs-derived cortical neurons. 153

Figure 5.4 Establishment of HSV-1 infection on H9 ESCs-derived cerebral organoids. 156

Figure 5.5 Viral mRNA quantification on H9 ESCs-derived cerebral organoids. 157

Figure 5.6 Pedigree of INGENIOS patient 1024. 159

Figure 5.7 Impact of HSV-1 infection on 1024M iPSCs-derived cortical neurons.....161

Figure 5.8 Immunoblot analysis of protein lysates from HSV-1 infected 1024M iPSCs-derived cortical neurons.....162

Figure 5.9 Impact of HSV-1 infection on 1024M iPSCs-derived cerebral organoids.....164

Figure 5.10 Impact of HSV-1 infection on 1024M SV40-fibroblasts. 166

Figure 5.11 Cytokines levels in 1024M SV40-fibroblasts upon stimulation with P(I:C) and LPS.....167

Figure 5.12 Impact of different treatments on H9 ESCs-derived cortical neurons upon HSV-1 infection. 170

Figure 7.1 P1 PBMCs responses to poly(I:C), LPS and IFN-α. 229

Figure 7.2 Production of cytokines by H9 ESCs-derived cortical neurons. 230

Figure 7.3 Production of cytokines by H9 ESCs-derived cerebral organoids. 231

Figure 7.4 Production of cytokines by H9 ESCs-derived cortical neurons with treatments. 232

List of Tables

Table 2.1 Plasmids used in this thesis.....58

Table 2.2 Primers used in this thesis.....61

Table 2.3 Oligonucleotides designed for site-directed mutagenesis (SDM) 62

Table 2.4 Antibodies used in this thesis.....73

Table 2.5 Primers used to detect Sendai virus vectors.....81

Table 3.1 49 *TICAM1* variants identified in COVID-19 patients.....89

Foreword

Prior to the emergence of COVID-19, our focus was set on exploring the TBK1 protein and its relationship with autophagy in the context of HSV-1 infection. Our initial intentions were clear, yet the unforeseen challenges and evolving circumstances redirected our path to the current aims listed in this thesis. In our pursuit of these original aims, significant milestones were achieved. We endeavoured to deepen our understanding of autophagy's role in infectious diseases, leading to the publication of a comprehensive review titled "**Inborn errors of autophagy and infectious diseases**" in **Current Opinion in Immunology**. Our collaborative efforts extended further as we worked with Dusan Bogunovic's team and the first author, Justin Taft, contributing to their publication titled "**Human TBK1 deficiency leads to autoinflammation driven by TNF-induced cell death**" in **Cell**. This collaboration involved the assessment of autophagy in TBK1 deficient cells obtained from their patients, marking a significant chapter in our research journey.

With the emergence of the COVID-19 pandemic, our research direction underwent a shift. We were invited to join the COVID Human Genetic Effort (COVIDHGE) consortium, tasked with the assessment of numerous *TICAM1* variants. Recognising the potential significance of this opportunity, we made the decision to delve deeper into the exploration of these TICAM1 variants. It became evident that we could not simply allow this wealth of data to remain untapped, prompting us to embark on a more comprehensive investigation of these variants. The journey of our project took an unexpected turn. The following pages unfold the journey of our exploration into the complexities of TICAM1 variants, a venture that unfolded in response to the unprecedented challenges posed by the global pandemic.

Chapter 1

1. Introduction

1.1 Infectious diseases and genetics

Infectious diseases caused by pathogens such as bacteria, fungi, parasites, and viruses, persist as a significant threat to human health, maintaining their status as one of the primary contributors to global mortality and morbidity. Recent estimates from the Institute of Health Metrics and Evaluation (IHME) Global Burden of Disease Study indicate that, a staggering 7.7 million individuals succumbed to infectious diseases in 2019, before the onset of the COVID-19 pandemic (https://www.healthdata.org/research-analysis/gbd). The significant variation in clinical outcomes observed among individuals and populations exposed to identical pathogens can be attributed to the intricate interplay between genetic diversity within both the host and the infecting microorganism, along with non-genetic environmental influences. The selective pressure for survival has profoundly influenced the dynamic genetic diversity within human immune system which enables it to effectively combat infectious diseases (Lederberg, 1999). This natural selection plays a significant role in shaping the vast diversity of immune system genes observed across diverse human populations (Murphy, 1993; Ramos et al., 2015). A publication of a thorough catalogue of alleles linked to autoimmune diseases across the genome has provided valuable insights into the potential impact of natural selection (Ramos et al., 2015). This contribution offers informative perspectives on the complex interplay among genetic diversity, immunity, and natural selection. An outstanding example of genetic diversity within the human genome is evident in the human leukocyte antigen (HLA) locus. This diversity is sustained through balancing selection which is a selective mechanism that maintains various variants at intermediate frequencies within a population to ensure prolonged persistence of each allele and surpassing the longevity of neutral counterparts (Key et al., 2014). Notably, this locus has consistently been linked to various immunological disorders including both infectious and autoimmune conditions (Dendrou et al., 2018). It is increasingly evident that host genetic factors significantly influence an individual's susceptibility to a particular infection or its outcome. It is widely acknowledged that infections stemming from the same infectious agent can yield diverse effects in different individuals. Malaria which is

caused by the parasite *Plasmodium falciparum* and its impact on red blood cells diseases (haemoglobinopathies) provide a clear example where individuals homozygous for the HbS variant of haemoglobin, commonly referred to as sickle haemoglobin, experience the manifestations of sickle-cell disease. In contrast, heterozygosity at this genetic locus confers robust protection against the development of severe malaria (Allison, 1954). Therefore, it is crucial to explore the genetic factors that could play a role in the susceptibility or emergence of severe infectious diseases in individuals who were initially healthy but fell seriously ill due to a common pathogen. This investigation is essential for gaining a deeper understanding of how certain genes might increase the likelihood of developing severe infectious diseases.

1.2 Inborn errors of immunity

Inborn errors of immunity (IEI) arise from deleterious germline variants in single genes, manifesting clinically as increased vulnerability to infections, autoinflammatory diseases, autoimmune disorders, allergies, and bone marrow failure (Tangye et al., 2022). This field has progressed from the first reported IEI in 1946, epidermodysplasia verruciformis, to the current notion that severe infectious diseases in humans can be attributed to single-gene IEIs with incomplete penetrance (Orth, 2008; Casanova & Abel, 2021). In accordance with rigorous criteria set forth by the expert committee of the International Union of Immunological Societies (IUIS), a comprehensive list of 55 monogenic defects have been incorporated into the classification system. This brings the total count to 485 genetic disorders, all of which disrupting the host's defense mechanisms against a diverse array of infectious agents and are linked to evident immunological abnormalities, often demonstrating significant or complete immunological and clinical penetrance (Casanova et al., 2014; Bousfiha et al., 2022a; Tangye et al., 2022).

The discovery of inborn errors in the Toll-like receptor 3 (TLR3) interferon (IFN) pathway of the innate immune system, which will be expanded upon later in this chapter, with mono- or biallelic mutations in six TLR3 pathway genes including *TLR3* (Zhang et al., 2007; Guo et al.,

2011; Lim et al., 2014), *UNC93B1* (Casrouge et al., 2006), *TICAM1* (Sancho-Shimizu et al., 2011), *TRAF3* (Perez de Diego et al., 2010), *TBK1* (Herman et al., 2012), and *IRF3* (Andersen et al., 2015), has been demonstrated to predispose individuals to viral herpes simplex encephalitis (HSE). Additionally, it is worth noting that two molecules not directly involved in the TLR3-IFN pathway namely debranching enzyme 1 (DBR1) encoded by *DBR1* and small nucleolar RNA31 (SnoRNA31) encoded by *SNORA31* have recently been identified predisposing individuals to HSE (Zhang et al., 2018; Lafaille et al., 2019). Variants in *IRF7* and *IRF9* have been implicated in individuals with critical influenza pneumonia or acute respiratory distress syndrome (ARDS) where IRF7 complete deficiency impairs the production of type I IFNs by its potent producer, plasmacytoid dendritic cells (pDCs), and complete IRF9 deficiency renders IFN stimulated gene factor 3 (ISGF3) inactive (Ciancanelli et al., 2015; Hernandez et al., 2018). Moreover, *TLR3* variants have also been found in individuals with ARDS including the P554S variant that causes TLR3 deficiency and has also been linked to underlie HSE (Zhang et al., 2007; Lim et al., 2019). These instances have highlighted the principle that severe infectious diseases can stem and be attributed to IEI. While several genes are mentioned in this thesis, the main focus of this study will be on *TICAM1*.

1.3 Herpes Simplex Virus-1 (HSV-1)

Herpes simplex virus-1 (HSV-1) is a member of the *Herpesviridae* family, which constitutes a large family of viruses infecting both humans and animals. The genome of the herpesvirus, consisting of linear double-stranded DNA (dsDNA) with a size ranging from 120-250 kilobases, is encased in a protein icosahedral capsid with a diameter of 100-110 nanometres (Falke et al., 1959; Furlong et al., 1972; Booy et al., 1996). Surrounding the capsid is an amorphous viral protein matrix composed of tegument proteins (Morgan et al., 1959). These structures are further enveloped by a lipid envelope containing viral glycoproteins and some host cellular proteins (Wildy & Watson, 1962; Asher et al., 1969). The Herpesviridae family encompasses eight human herpesviruses, categorised into three subfamilies: *Alphaherpesvirinae* (α), *Betaherpesvirinae* (β), and *Gammaherpesvirinae* (γ), with each subfamily classified according to its biological traits and tissue tropism during both primary lytic and latent infections (Davison et al., 2005).

HSV-1 belongs to the α subfamily and is neurotropic, exhibiting lytic infections characterised by a short reproductive cycle, leading to rapid destruction of infected host cells and they primarily infect mucosal epithelial cells during initial infection and remain in the dorsal root or trigeminal ganglia during latent infection (Baringer & Swoveland, 1973; Whitley & Roizman, 2001). HSV-1 infections are prevalent worldwide predominantly transmitted through oral contact leading to infections in or around the mouth commonly known as cold sores or oral herpes. Additionally, HSV-1 has the potential to cause genital herpes. According to World Health Organization (WHO), the latest estimate from 2016 reveals that 3.7 billion individuals below the age of 50, accounting for 67% of the global population, had experienced HSV-1 infections. Due to the fact that a substantial number of HSV-1 infections are contracted during childhood, the majority of adults worldwide have encountered this viral infection.

1.3.1 Life cycle of HSV-1

HSV-1, similar to other herpesviruses, display both lytic or productive and latent infection life cycles. In the initial lytic phase of herpesvirus infection, viral replication occurs within host cells and often leading to cell death and the generation of new viral progeny (Smiley, 2004). Symptomatic and asymptomatic shedding of the virus occurs during this phase. Subsequently, in response to the host immune system, human herpesviruses enter a latent state where they hide in secondary host cells to evade immune detection (Cohen, 2020).

HSV-1 initiates its infection process by attaching to receptors located on the surface of the host cell facilitated by the interaction between viral glycoproteins gB and gC with glycosaminoglycans (GAGs) (Herold et al., 1991). Subsequently, gD interacts with an entry receptor which initiates receptor recognition and signalling, thereby prompting fusion (Ligas & Johnson, 1988; Cocchi et al., 2004). This fusion process involves the recruitment of three additional glycoproteins – gB, gH, and gL – which collectively induce the fusion of the host cell membrane with the virus (Huff et al., 1988; Forrester et al., 1992; Roop et al., 1993; Spear et al., 2000). This fusion event leads to the introduction of the viral nucleocapsid into the

peripheral cytoplasm of the host cell. Following attachment to the host cell surface, HSV-1 proceeds to migrate towards the cell nucleus facilitated by tegument proteins UL36 and UL37, where it securely docks at a nuclear pore (Richards et al., 2017). Subsequently, the virus injects its DNA into the nucleoplasm with only the viral DNA gaining entry into the nucleus while the parental capsid remains situated outside. Upon entering the host cell nucleus, the viral DNA undergoes transcription and synthesis primarily through the action of the virus-encoded DNA polymerase. The expression of viral genes during the HSV-1 replication cycle follows a temporal sequence, with Immediate Early (IE) genes being expressed first, followed by Early (E) genes, and finally Late (L) genes. The messenger RNAs (mRNAs) produced from each gene set are transported to the cytoplasm, where they are translated into proteins. After translation, the proteins return to the nucleus to participate in the regulation of subsequent sets of viral genes, marking the orchestrated progression of the viral replication cycle. In essence, the onset of early viral gene expression triggers the initiation of viral DNA replication, while late viral structural proteins assemble into viral capsids, encapsulating the replicated viral DNA. The assembled virion or viral progeny undergo budding through the inner nuclear membrane of the infected cell and entering the intermembrane space ready to infect adjacent uninfected cells. Subsequently, the virions are transported to the endoplasmic reticulum and further conveyed to the cellular plasma membrane. The release of virions occurs through mechanisms such as cell fusion, exocytosis, or cellular lysis, marking the pinnacle of the intricate viral assembly and release process (Campadelli-Fiume et al., 2007).

HSV-1 virions undergo retrograde transport along neuronal axons to access neuronal cell bodies within the trigeminal ganglia (Antinone & Smith, 2010). The viral progeny that reaches neuronal nuclei enters a phase of latency. During the latent phase, the viral DNA has the potential to integrate into the host genome or persist as a circular episome linked to host DNA and exhibiting minimal expression of viral genes (King et al., 1980; Arthur et al., 2001; Juillard et al., 2019). The only viral gene product that demonstrates high expression during latency is the latency-associated transcript (LAT), an RNA molecule lacking protein-coding capacity, which has been significantly implicated in the epigenetic control of HSV-1 gene expression (Wang et al., 2005; Giordani et al., 2008; Cliffe et al., 2009; Nicoll et al., 2016). The recurrence of viral reactivation from latency is a phenomenon that may occur intermittently and is subject to modulation by various host-related factors such as stimuli including fever, emotional stress,

hormone imbalance, UV exposure, and immunosuppression (Knipe et al., 2013; Stoeger & Adler, 2018). Upon reactivation, the virus usually reverts to the initial site of infection and undergoes lytic replication until the host immune response compels it back into latency (Roizman & Whitley, 2013).

1.3.2 Herpes simplex encephalitis (HSE)

While HSV-1 is a prevalent pathogen affecting a substantial portion of the global population and frequently induces asymptomatic conditions, it can also give rise to more severe diseases, such as recurrent corneal infections (keratitis) and, in rare instances, invasion and replication within the central nervous system (CNS) resulting in encephalitis (Taylor et al., 2002). Herpes simplex encephalitis (HSE) is a rare but severe neurological disorder characterised by acute inflammation of the brain, primarily affecting the temporal lobe, and is caused by HSV-1 infection within the CNS (Whitley & Kimberlin, 2005). HSE represents the predominant form of sporadic encephalitis, constituting an estimated 20–30% of all encephalitis cases, with a rare annual incidence ranging from 1 in 250,000 to 1 in 500,000 (Whitley & Gnann, 2002; Davison et al., 2003; Whitley, 2006). The incidence pattern of HSE exhibits a bimodal distribution with the initial peak affecting children aged 3 months to 6 years and a subsequent peak observed in the individuals over the age of 50 years old (Babaei et al., 2021). While HSE in the later ages is frequently linked to viral reactivation, childhood HSE corresponds to primary HSV-1 infection, and interestingly, the clinical manifestations of HSE stemming from either primary infection or reactivation are indiscernible (Whitley & Gnann, 2002; Whitley & Kimberlin, 2005; Abel et al., 2010). HSE is a necrotising encephalitis where individuals typically experience symptoms such as fever, alterations in mental status, seizures, epilepsy, psychomotor disability, and focal neurological deficits (Whitley & Kimberlin, 2005; Whitley, 2006). While these assessments can provide supportive evidence, the confirmative diagnostic approach also involves detecting HSV-1 DNA in the cerebrospinal fluid (CSF) using polymerase chain reaction (PCR) (Tyler, 2004; Gnann & Whitley, 2017). The emergence of next-generation sequencing (NGS) has significantly eased the challenges faced by researchers in identifying HSV-1 viral DNA in CSF (Guan et al., 2016). Nonetheless, the accessibility of this cutting-edge technology is limited to well-equipped and developed laboratories. In less

developed regions, PCR remains the preferred method for researchers to detect HSV-1 DNA (Al-Shekhlee et al., 2006).

The repercussions of HSE can result in elevated morbidity and mortality rates, with untreated cases experiencing mortality rates as high as 70% (Whitley & Kimberlin, 2005). Aciclovir/Acyclovir is an FDA-approved antiviral treatment for genital herpes and HSE and functions as a specific inhibitor of herpesvirus DNA polymerase, thereby arresting the replication of HSV-1 (Gnann et al., 1983). Despite antiviral treatment, the combined mortality and incidence of neurological sequelae can be as high as 30% (McGrath et al., 1997; Marcocci et al., 2020; Rocha et al., 2023). Even with the recommended therapy initiated after disease onset, approximately two-thirds of patients may succumb to the condition or develop significant and lasting neurological deficits (Abel et al., 2010; Khandaker et al., 2016; Marcocci et al., 2020). A systematic review conducted back in 2016 highlighted that a substantial proportion of children affected by HSE, with a prevalence of 64%, experienced diverse neurological sequelae (Khandaker et al., 2016). Neuroinflammation stands as a potential explanation for the observed brain injuries (Piret & Boivin, 2020).

1.4 Herpes simplex virus 2 (HSV-2)

HSV-2, similar to HSV-1, is a double-stranded DNA virus belonging to the α subfamily and exhibiting neurotropic characteristics with the distinction between HSV-1 and HSV-2 established in 1962 (Schneweis, 1962). The genomic sequences of HSV-1 and HSV-2 share a 70% similarity, and the seroprevalence of HSV2 is approximately 30% among young adults (Widener & Whitley, 2014). Typically, HSV2 is associated with genital infections (Chentoufi & Benmohamed, 2012). The most recent estimate provided by the WHO in 2016 indicates that genital herpes, attributed to HSV-2, impacts approximately 491 million individuals aged 15–49 years globally, representing around 13% of this population demographic (WHO, 2023).

The clinical manifestations induced by HSV-1 and HSV-2 exhibit remarkable similarity, except for notable differences in site-specific reactivation patterns, yet both types remain confined within non-replicating neurons. HSV-1 establishes latency in the trigeminal ganglia, and upon reactivation, it causes recurrent diseases affecting the face, eyes, and oropharynx. On the other hand, HSV-2 establishes latency in the lumbar-sacral ganglia, and upon activation, it leads to recurrent diseases below the waist, primarily manifesting as genital infections (Lafferty et al., 1987; Croen et al., 1991).

HSV-1 is responsible for approximately 90% of HSE cases in immunocompetent adults, whereas HSE associated with HSV-2 tends to be more prevalent in neonates and individuals with compromised immune systems (Whitley & Gnann, 2002; Kennedy & Steiner, 2013). Substantial evidence indicates an epidemiological synergy between HSV-2 and HIV infections, as HSV-2 infection amplifies the likelihood of acquiring HIV infection by around threefold, and individuals co-infected with both HIV and HSV-2 are more prone to transmitting HIV to others (Abu-Raddad et al., 2008; Wald et al., 2011; Looker et al., 2017). In exceptional cases, both HSV-1 and HSV-2 can be transmitted from mother to child during childbirth, leading to the development of neonatal herpes (Jones, 2009). Infections during the neonatal period with either HSV-1 or HSV-2 pose substantial risks that frequently leading to severe and life-threatening conditions including disorders affecting the skin, eyes, or mouth, herpes encephalitis, or disseminated multi-organ infections (Kesson, 2001).

1.4.1 Recurrent meningitis associated with HSV-2

HSV-2 possesses the capability to induces meningitis in neonates characterised by inflammation of the meninges. This condition tends to present with greater severity and life-threatening implications when compared with recurrent benign lymphocytic meningitis (RBLM) or Mollaret meningitis—a rare form of recurrent meningitis attributed to HSV-2 in adults with prevalence rates approximated at 10 cases per 500,000 individuals (Kallio-Laine et al., 2009). Notably, Mollaret meningitis tends to manifest as aseptic, presenting milder

symptoms and typically resolving spontaneously, emphasising the characteristic benign and self-recovering nature of Mollaret meningitis even in the absence of antiviral therapy (Mollaret, 1945; Shalabi & Whitley, 2006). The confirmatory diagnostic procedure entails identifying the presence of HSV-2 DNA within CSF.

Mollaret's meningitis is believed to manifest in roughly 20% of individuals experiencing primary HSV-2 infections accompanied by symptoms of meningism such as headache, neck stiffness, photophobia, often accompanied by nausea and vomiting (Sawyer & Rotbart, 2004; Shalabi & Whitley, 2006). The demographic profile of Mollaret's meningitis patients skews heavily towards women comprising approximately 70% of cases with a reported mean age of 40 years (Davis et al., 2010). The physician Pierre Mollaret initially identified manifestation in 1944 which is characterised by widespread symptoms such as persistent headaches, fever, and meningism (Mollaret, 1945). Moreover, the current diagnostic standards have been expanded to encompass recurring episodes marked by intervals lasting weeks or months in which symptoms are absent, in addition to the occurrence of spontaneous alleviation of both symptoms and signs, coupled with cerebrospinal fluid analyses indicating a preponderance of large "endothelial" cells and lymphocytes (Bruyn et al., 1962). Similarly, the episodes occur sporadically and are typically spaced out either by several weeks, months, or years. According to one report, it has been observed that, in the period leading up to the onset of meningism in individuals with primary HSV-2 meningitis, active herpetic lesions are seen in approximately 85% of cases (Kirkland et al., 2020). However, another report presents a conflicting finding, indicating that in a substantial majority, surpassing 80% of cases, the absence of a genital lesion is documented, suggesting that HSV-2 meningitis may manifest even in the absence of the characteristic genital rash (Davies et al., 2004). Consequently, the key takeaway from these divergent observations is that the diagnosis of Mollaret meningitis, or aseptic meningitis in general, does not necessitate on the presence of herpetic lesions (Tedder et al., 1994).

Due to the rarity and its inherently self-limiting characteristics, there are currently no established therapeutic protocols outlined for the management of Mollaret meningitis. There is a notable disparity in perspectives and approaches among physicians regarding the management of HSV-2 meningitis, as revealed in a survey (Bodilsen et al., 2022). Findings

indicate that approximately 48% of Infectious Disease physicians are expressed a likelihood to administer aciclovir in clinically stable patients with presumed viral meningitis. In contrast, a substantial 10% of physicians stated their inclination to refrain from treating HSV-2 meningitis with antiviral medications altogether. In cases where individuals actually meet the diagnostic criteria administration of antiviral aciclovir is commonly initiated as part of the treatment approach (Kirkland et al., 2020; Bodilsen et al., 2022).

1.5 COVID-19

1.5.1 Severe acute respiratory syndrome coronavirus 2 (SARS-CoV-2)

Infectious diseases wield a profound influence across various aspects of human civilisation, a reality highlighted with greater intensity by the recent catastrophic emergence of severe acute respiratory syndrome coronavirus 2 (SARS-CoV-2) and its ensuing pandemic. The novel coronavirus SARS-CoV-2, responsible for the disease COVID-19, was initially identified in the city of Wuhan, China, towards the end of 2019 among a group of individuals presenting with pneumonia symptoms (Zhu et al., 2020). Coronaviruses (CoVs) belong to the *Coronaviridae* family, encompassing enveloped positive-sense single-stranded RNA viruses, and are categorized into four genera: *alphacoronavirus*, *betacoronavirus*, *gammacoronavirus*, and *deltacoronavirus* (Liu et al., 2021). Alphacoronaviruses and betacoronaviruses primarily infecting mammalian species (Cui et al., 2019), while gammacoronaviruses and deltacoronaviruses predominantly target avian species (Milek & Blicharz-Domanska, 2018; Wille & Holmes, 2020). Human coronaviruses like HCoV-229E, HCoV-OC43, HCoV-NL63, and HCoV-HKU1 are endemic pathogens transmitted through airborne droplets, leading to seasonal and typically mild respiratory tract infections characterised by symptoms of the common cold, contributing to 15–30% of cases associated with this condition (Forni et al., 2021; Liu et al., 2021).

The SARS-CoV-2 pandemic stands out as an unparalleled event, representing the third instance of a zoonotic introduction of a highly pathogenic coronavirus transitioning from animals to humans, following the earlier occurrences of severe acute respiratory syndrome coronavirus (SARS-CoV) and Middle East respiratory syndrome coronavirus (MERS-CoV), resulting in unprecedented disruptions on a global scale, affecting both societal and economic dimensions. These SARS-CoV, MERS-CoV, and SARS-CoV-2 infections can progress into severe and life-threatening respiratory pathologies and lung injuries when they infect bronchial epithelium, alveolar cells (pneumocytes), and upper respiratory tract cells in humans (Hocke et al., 2013; Choudhry et al., 2019; Carsana et al., 2020). These viruses have the ability to invade the lower respiratory tract, posing the risk of inducing a potentially lethal ARDS (Lamers & Haagmans, 2022). The FDA granted emergency use authorisation to remdesivir as the first antiviral agents to treat patients hospitalised with severe cases of COVID-19 (Rubin et al., 2020), and remdesivir functions by inhibiting the viral RNA chain-elongation reaction through the RNA-dependent RNA polymerase (Gordon et al., 2020).

SARS-CoV-2, belonging to the *betacoronavirus* genus, possesses a non-segmented positive-sense single-stranded RNA (+ssRNA) genome spanning between 27 to 32 kilobases in length which has been sequenced (Pal et al., 2020; Wu et al., 2020). Analysis of its genomic sequence indicates that SARS-CoV-2 shares a sequence identity of 79.6% with SARS-CoV and an even more notable 96.2% identity with bat coronaviruses (Zhou et al., 2020; Zandi et al., 2021). The genomic RNA, featuring a 5′-cap structure and a 3′-polyadenylate tail, which can function directly as a mRNA encoding the viral replicase while concurrently serving as a template for RNA replication and being encapsulated into progeny virions (Liu et al., 2021).

1.5.2 Life cycle of SARS-CoV-2

The virion of SARS-CoV-2 comprises structural viral proteins, namely the spike (S), envelope (E), membrane (M), and nucleocapsid (N) proteins. The +ssRNA is enveloped by the N protein, while the M and E proteins facilitate its integration into the viral particle during assembly and

the trimeric S proteins extend from the viral envelope to confer specificity for cellular entry receptors (V'Kovski et al., 2021). The structural proteins S, E, and M are embedded within the lipid-based viral envelope, while the N protein resides inside the virion, establishing electrostatic interactions with the viral genomic RNA via positively charged amino acid residues, thereby governing RNA unwinding subsequent to cellular entry (Rahman et al., 2021). The S protein facilitates the binding to host cell receptors and induces fusion between the viral and cellular membranes (Hartenian et al., 2020). The E protein serves as an ion channel and contributes to viral assembly, while the M protein plays a crucial role in integrating essential viral components into newly formed virions during the morphogenesis process (Pizzato et al., 2022).

SARS-CoV-2 gains entry into human cells by interacting with the cell surface entry receptor protein angiotensin-converting enzyme 2 (ACE2) via the Receptor Binding Domain (RBD) located on the S protein of the coronavirus (Wang & Xiang, 2020). Upon interacting with ACE2 receptors present on the target cell, the spike protein undergoes cleavage facilitated by the host transmembrane serine protease (TMPRSS2), a process that triggers the activation of the spike protein trimers causing conformational change, enabling them to merge the viral and host lipid bilayers and consequently releasing the viral nucleocapsid complex into the cell (Belouzard et al., 2009; Kleine-Weber et al., 2018; Hoffmann et al., 2020). The proteins ACE2 and TMPRSS2 exhibit significant co-expression in human lungs, notably in nasal epithelial cells, alveolar epithelial cells, and transient secretory cells of the bronchial epithelium (Lukassen et al., 2020; Sungnak et al., 2020). Upon entering the cytoplasm, the virus releases its +ssRNA, initiating direct translation to generate the viral replicase polyproteins 1a (pp1a) and pp1ab, derived from the genes *ORF1a* and *ORF1b*, respectively (Finkel et al., 2021). These two polyproteins undergo self-catalytic processing, resulting in the generation of 16 non-structural proteins (nsps), collectively constituting the Replication and Transcription Complex (RTC) responsible for viral RNA synthesis (Sola et al., 2015; Hillen, 2021; V'Kovski et al., 2021). The process of viral genomic replication commences with the production of complete negative-sense genomic duplicates within double-membrane vesicles, serving as templates for the creation of new positive-sense genomic RNA (Snijder et al., 2020). Subsequently, the virions utilise ribosomes bound to the host endoplasmic reticulum to produce a variety of S, E, and M proteins, while the translation of N protein occurs via free cytosolic ribosomes within

the host cell (Sola et al., 2015; Yadav et al., 2021). The finalisation of virion assembly occurs at the endoplasmic reticulum–Golgi intermediate compartment, wherein the M protein serves as a scaffold, intricately coordinating the construction of virions through interactions with other structural proteins and viral (Yadav et al., 2021). Following the molecular assembly, progeny virions are transported in vesicles and are conveyed to the cell membrane where they are released through exocytosis, enabling their widespread dissemination (Astuti & Ysrafil, 2020; Naqvi et al., 2020). As SARS-CoV-2 undergoes evolutionary changes via recombination and mutation, resulting in the emergence of multiple strains aimed at enhancing the virus's fitness, host pattern recognition receptors (PRRs) would be the first line of defence to detect viral pathogen-associated molecular patterns (PAMPs) to activate the innate immune responses (Amoutzias et al., 2022).

1.6 Innate immunity

Vertebrates exert two types of immunity to defend the host against infections: innate immunity and adaptive immunity. Innate immune responses act as an initial defence, occurring before the development of adaptive immune responses. The innate immune system is genetically encoded by germline genes to identify molecular structures produced by microbial pathogens known as pathogen-associated molecular patterns (PAMPs) (Janeway, 1989; Medzhitov & Janeway, 1998). It also recognises microbial products crucial for the survival of these microbes. Additionally, the innate immune system detects molecules produced by damaged or dying cells termed damage-associated molecular patterns (DAMPs). Phagocytes, such as macrophages and neutrophils, along with dendritic cells and epithelial cells forming the body's barrier express cell-associated recognition molecules, collectively known as pattern recognition receptors (PRRs), which play a crucial role in identifying pathogens and damage-associated molecules (Medzhitov, 2013). Unlike the innate immune system, the adaptive immune system involves the somatic recombination of gene segments within precursor cells of mature lymphocytes during their development resulting in the de novo generation of highly specific receptors (Chaplin, 2010). Nevertheless, the central emphasis of this study will predominantly be directed towards the intricate mechanisms and dynamics of the innate immune system.

1.6.1 Toll-like receptors (TLRs)

Mammals possess various classes of PRRs with diverse primary functions, ligand specificities, locations, and evolutionary relationships, including Toll-like receptors (TLRs), nucleotide oligomerization domain (NOD)-like receptors (NLRs), AIM2-like receptors (ALRs), retinoic acid-inducible gene- (RIG-) I-like receptors (RLRs), C-type lectin receptors (CLRs), and intracellular DNA sensors like cyclic guanosine monophosphate-adenosine monophosphate synthase (cGAS) (Akira et al., 2006; Cai et al., 2014). TLRs represent the most extensively studied class of PRRs with 222 identified in invertebrates and 28 in vertebrates (Behzadi et al., 2021). In mammals, a total of 13 Toll-like receptors (TLRs), designated as TLR1-13, have been recognized (Kawai & Akira, 2010). Interestingly, humans possess only 10 of them (TLR1-10), while mice possess all 13, although TLR10 is non-functional in mice because of a retrovirus insertion (Kawai & Akira, 2010; Nie et al., 2018). Expressed on various cell types including innate immune cells such as dendritic cells (DCs), monocytes, macrophages, neutrophils and natural killer (NK) cells as well as non-immune cells such as fibroblast cells and epithelial cells, these evolutionarily conserved receptors play a crucial role in recognizing a diverse range of microbial products as well as molecules produced or released by stressed and dying cells contributing to the regulation of inflammatory reactions and activation of the innate immune system (Akira et al., 2001). TLRs are primarily categorised into two subgroups based on their location, distinguishing between TLRs present on the cell surface and those found within the cell. Although there is considerable knowledge exists regarding the ligands and signalling pathways of TLR1-9 and TLR11, the specific biological roles of TLR10, TLR12, and TLR13 are still not fully understood (Kawasaki & Kawai, 2014; Sameer & Nissar, 2021). TLR4, the first discovery in the human TLR family, is known for its regulation of inflammatory responses triggered by lipopolysaccharides (LPS) from gram-negative bacteria and taxol from plants (Murad, 2014) whereas *TLR3*, the oldest and most conserved member without gene duplication, is categorized among viral TLRs alongside TLR7-9 (Akira et al., 2006).

Activation of TLRs occurs upon ligand interaction, initiating specific signalling pathways that lead to the production of various cytokines and chemokines. Presently, TLR signalling pathways are commonly categorised into two distinct types: the TIR domain-containing

adaptor-inducing IFN-β (TRIF/TICAM1)-dependent pathways, which will be further explained in the following Section 1.6.2, and the myeloid differentiation primary response protein 88 (MyD88)-dependent pathways (Akira & Takeda, 2004). In brief, the MyD88-dependent response is employed by nearly all TLRs except TLR3, where MyD88 binds with the TLRs through homotypic or heterotypic interactions via the Toll/IL-1 receptor (TIR) domain upon ligand recognition and TLR dimerisation. MyD88 also possess the death domain which recruits IL-1 receptor-associated kinase 4 (IRAK4) resulting in the formation of Myddosome complex and phosphorylation of IRAK1 (Lin et al., 2010). Afterwards, the protein tumour necrosis factor (TNF) receptor-associated factor 6 (TRAF6) is activated which subsequently activating mitogen-activated protein kinases (MAPK) kinase (MKK), which lead to activating protein-1 (AP-1) transcription factor activation and the IκB kinase (IKK) complex which consist of IKKα, IKKβ, and IKKg (NEMO). The IKK complex triggers phosphorylation of IκB leading to the subsequent degradation of the I kappa B alpha (IκBα) inhibitor and ultimately resulting in the nuclear translocation of the transcription factor NF-κB, which initiates the transcription of genes responsible for inflammatory cytokines (Wang et al., 2001).

1.6.2 Toll-like receptors 3 (TLR3) – interferon (IFN) pathway

TLR3 recognised dsRNA, a common product of viral replication, triggers antiviral immune responses by promoting the production of both type I IFN and inflammatory cytokines, such as TNF-a and IL-6, that can activate target cells in both autocrine and paracrine mechanisms (Jacobs & Langland, 1996). dsRNA may arise in viral infections either as a replication intermediate for ssRNA viruses, such as respiratory syncytial virus (RSV), encephalomyocarditis virus (EMCV) and West Nile virus, and certain small interfering RNAs, or as a by-product of symmetrical transcription in DNA viruses (Wang et al., 2004; Akira et al., 2006; Kawai & Akira, 2008; Bernard et al., 2012; Takemura et al., 2014). TLR3 is primarily found in conventional dendritic cells (cDCs), which engage in the phagocytosis of dying cells; however, TLR3 also exhibit a widespread expression in various human cell types, including dermal fibroblasts (Matsumoto et al., 2002), keratinocytes (Lebre et al., 2007), and CNS-resident cells such as neurons, oligodendrocytes, astrocytes, and microglia (Bsibsi et al., 2002; Jack et al., 2005; Prehaud et al., 2005). TLR3 also recognises polyinosine-deoxycytidylic acid

(poly I:C), a synthetic analog of TLR3, as PAMPs which mimic viral infection (Wong et al., 1995; Alexopoulou et al., 2001) with the expression of TLR3 undergoing rapid and substantial upregulation following poly I:C treatment (Akira et al., 2006). Poly I:C can also be detected by RLRs including both RIG-1 and melanoma differentiation-associated gene 5 (MDA5). The ability of transfected poly(I:C) to induce an IFN response is influenced by its length; specifically, long poly I:C molecules predominantly activate MDA5, while short poly I:C activates RIG-I (Kato et al., 2008). Recent discoveries highlighting the significance of TLR3 in human diseases involve the identification of single-gene disorders affecting the TLR3 pathway, thereby elevating the susceptibility to various conditions such as HSE and ARDS, topics that have been elucidated in previous sections.

UNC93B1 is a crucial transmembrane protein that facilitates the transportation of TLR3 from the endoplasmic reticulum (ER) to the endosome (Kim et al., 2008). Following ligand stimulation, TLR3 undergoes translocation to endosomes where it colocalizes and is phosphorylated by the tyrosine kinase c-Src (Johnsen et al., 2006), priming TLR3 for the initiation of subsequent signalling cascades. TLR3 exclusively recruits the TICAM1 protein as its downstream adaptor via binding interactions between their TIR domains, initiating activation of the TLR3 signaling pathway (Oshiumi et al., 2003; Yamamoto et al., 2003a). Numerous signalling pathways are initiated by the TLR3-TICAM1 interaction resulting in the phosphorylation and nuclear translocation of transcription factors like interferon regulatory factor 3 (IRF3) and nuclear factor kappa B (NF-κB). This cascade results in the expression of type-I IFNs, including IFN-a, IFN-b and IFN-l, and proinflammatory cytokines, respectively (Akira & Takeda, 2004), thereby characterising the TLR3 signalling pathway as a TICAM1-dependent pathway. Activation of IRF3 involves two non-canonical IκB-related kinases, TANK-binding kinase 1 (TBK1) and IκB kinase-ε (IKKε) ((Fitzgerald et al., 2003a), with TRAF3 serving as a crucial molecule directing these kinases towards TICAM1 (Hacker et al., 2006). It is important to highlight that TLR4 also utilises the adaptor molecule TICAM1; however, it necessitates recruiting TICAM2 or TRAM, an exclusive adaptor for TLR4, to initiate signalling through TICAM1, unlike TLR3, which does not require TRAM (Fitzgerald et al., 2003b; Yamamoto et al., 2003b).

Upon binding to their respective IFN-α/β receptors (IFNAR1/IFNAR2) on cell surfaces, IFN molecules initiate a signalling cascade orchestrated by Janus kinase 1 (JAK1), Tyrosine kinase 2 (TYK2), and signal transducer and activator of transcription (STAT1 and STAT2) resulting in phosphorylation, dimerisation, and nuclear translocation of these mediators, culminating in the activation of numerous IFN-stimulated genes (ISGs) and thus bolstering the antiviral state (Martinez-Salas et al., 2017; Stanifer et al., 2019).

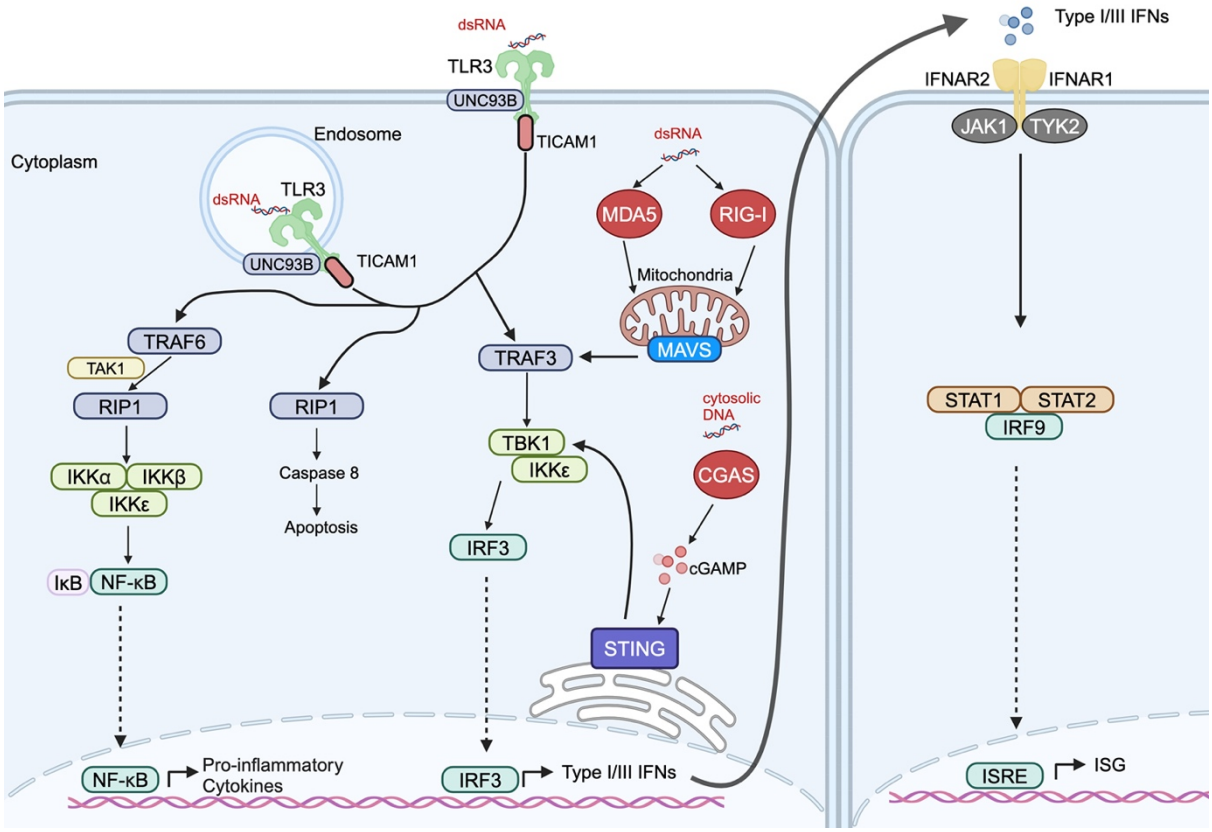


Figure 1.1 TLR3-IFN downstream signalling.

TLR3 exhibits expression both on the cell surface and within endosomal compartments, allowing it to detect extracellular viral double-stranded RNA (dsRNA) and its synthetic analog poly(I:C). This recognition initiates downstream activation of key signalling pathways involving IRF3 and NF-kB. Two non-canonical IκB-related kinases, TBK1 and IKKε, form associations with TICAM1 through the crucial mediator TRAF3. Subsequently, these two kinases play a pivotal role in phosphorylating IRF3. The activation of IRF3 results in its translocation into the cell nucleus, triggering the induction of interferons and various other cytokines. The cytoplasmic RLRs, such as RIG-I and MDA5, are also capable of sensing foreign DNA within the cytoplasm which triggers the activation of IRF-3, and subsequently initiating the production of type I interferons through a mechanism that operates independently of TLRs. The secreted interferons engage with their respective receptors (IFNAR) which triggers a cascade of events resulting in the activation of Janus kinase 1 (JAK-1) and tyrosine kinase 2

(TYK-2). This activation prompts the phosphorylation of signal transducer and activator of transcription 1 (STAT1) and STAT2 proteins. The phosphorylated STAT1 and STAT2 molecules then undergo complex formation with IRF9, ultimately facilitating the induction of interferon-stimulated genes (ISGs) within the cell nucleus.

1.6.3 Innate immune response to HSV-1

As previously discussed, HSV-1 possesses the ability to retrogradely traverse nerve pathways, circumvent the blood-brain barrier, and infiltrate the central nervous system, thereby triggering innate immune cells and initiating an innate immune response. Cells use diverse mechanisms to detect viral particles. The viral DNA and its RNA intermediates function as PAMPs that are identified by PRRs. PRRs responsible for detecting HSV-1 viral dsRNA predominantly consist of TLR3 located within endosomes, while significant cytoplasmic sensors for viral dsRNA include MDA5, RIG-I, and protein kinase RNA-activated (PKR) (Balachandran et al., 2000; Schenten & Medzhitov, 2011). Another PRR involved is the plasma membrane receptor TLR2 which senses HSV-1 protein (Leoni et al., 2012). Prominent viral DNA sensors of HSV-1 include TLR9 situated in endosomes, cGAS and DNA-dependent activator of IFN-regulatory factors (DAI) within the cytoplasm, and IFN-γ inducible protein 16 (IFI16) primarily within the nucleus (Krug et al., 2004; Takaoka et al., 2007; Li et al., 2012; Sun et al., 2013).

The detection of nucleic acids becomes crucial upon the virus's entry into the brain, where microglia, key immune cells in the brain, express cGAS, a nucleotidyl transferase and significant cytoplasmic sensor responsible for recognising DNA ligands across various cell types, and the induction of type I IFNs occurs in a cGAS–stimulator of interferon gene (STING)-dependent manner (Sun et al., 2013; Reinert et al., 2016). Following sensing and binding to viral dsDNA, cGAS undergoes activation and employs ATP and GTP to generate cyclic GMP-AMP (cGAMP), a sensor of cytoplasmic DNA (Sun et al., 2013; Wu et al., 2013). Subsequently, cGAMP acts as a second messenger and activates the STING which is translocated to the Golgi (Burdette et al., 2011; Zhang et al., 2013). STING then recruits and activates TBK1 initiating the phosphorylation of STING and the transcription factor IRF3, leading to the induction of type-I interferons and other cytokines (Cai et al., 2014; Liu et al.,

2015). This signalling pathway is of significance, as evidenced by the increased vulnerability to acute HSE observed in mice with deficiency in cGAS or STING (Reinert et al., 2016).

MDA5 and RIG-I serve as sensors for viral dsRNA. Upon activation, these sensors bind to the mitochondrial antiviral signalling protein (MAVS), triggering a cascade that involves the activation of TBK1 and IKKε (Schenten & Medzhitov, 2011). Subsequently, this activation leads to the initiation of the IRF3/7 and NF-κB pathways, ultimately resulting in the production of type I and type III interferons, along with other cytokines (Schenten & Medzhitov, 2011). Knocking down of *MDA5* in macrophages has been observed to result in reduced production of IFN-β and IFN-λ following infection with HSV-1 and HSV-2 (Rasmussen et al., 2009; Melchjorsen et al., 2010). Following HSV-1 infections, there is an observed upregulation of MDA5 expression in astrocytes, suggesting its potential involvement in exerting a protective function within this cell type (Bansode et al., 2019). Studies have shown that RIG-I works synergistically with MDA5 in the identifying viral RNA within the cytoplasm, thereby actively contributing to the induction of type I interferons (Choi et al., 2009; Rasmussen et al., 2009). In addition, RIG-I also has the capacity to recognise cytosolic DNA by engaging with RNA polymerase III (RNApol III), an intermediary enzyme that identifies the foreign DNA in the cytoplasm and transforms it into RNA with a 5'-triphosphate group (Chiu et al., 2009). This RNA is subsequently detected by RIG-I which triggers a type I interferon response.

Upon binding viral glycoproteins during viral attachment, TLR2 initiates signalling through MyD88 and TRAF6, thereby activating the NF-κB pathway, leading to the degradation of NF-κB inhibitor (Leoni et al., 2012). This allows NF-κB to translocate to the nucleus, inducing the expression of several proinflammatory cytokines (Kurt-Jones et al., 2017). Similarly, TLR9, a transmembrane protein receptor associated with endosomes and activated upon detection of viral DNA containing unmethylated CpG motifs, relies on MyD88 and TRAF6 in activating the NF-κB pathway, thereby initiating the downstream cytokine secretion upon HSV-1 recognition (Krug et al., 2004). In the earlier Section 1.6.2, we elucidated the importance of the TLR3-IFN pathway as a crucial element of the antiviral immune response, a significance that remains applicable in the context of HSE, which will be further explored in the subsequent section focusing on TLR3-IFN pathway in the context of HSE.

1.6.4 Inborn errors of immunity in HSE

Since the first discovery of inborn errors of immunity in HSE back in 2006, the condition has been studied as a paradigm of such errors that render otherwise healthy children susceptible to severe viral infections. As discussed earlier, investigations into isolated HSE affecting the forebrain have revealed single-gene inborn errors within the TLR3-IFN pathway, arising from monoallelic or biallelic mutations in six genes associated with the TLR3 pathway namely *TLR3*, *UNC93B*, *TICAM1*, *TRAF3*, *TBK1*, and *IRF3* (Casrouge et al., 2006; Zhang et al., 2007; Perez de Diego et al., 2010; Guo et al., 2011; Sancho-Shimizu et al., 2011; Herman et al., 2012; Lim et al., 2014; Andersen et al., 2015). These discoveries, along with earlier instances of HSE in combination with mycobacterial disease in patients with X-linked NEMO (*IKBKG* gene encodes for NEMO) deficiency affecting type I IFNs production during viral infection, as well as AR complete STAT1 deficiency impacting type I IFN responses, indicate the crucial role of TLR3-dependent IFNs immunity in the defence against HSV1 within the CNS (Dupuis et al., 2003; Audry et al., 2011).

In a series of experiments, it has been demonstrated that dermal fibroblasts deficient in the TLR3 pathway, including TLR3, UNC93B, TICAM1, TRAF3, TBK1, and IRF3, exhibit heightened susceptibility to HSV-1 infection compared to control cells (Casrouge et al., 2006; Zhang et al., 2007; Perez de Diego et al., 2010; Guo et al., 2011; Sancho-Shimizu et al., 2011; Herman et al., 2012; Lim et al., 2014; Andersen et al., 2015). This increased susceptibility is likely attributed to the impaired production of TLR3-dependent IFN-β and IFN-λ/IL-29. Moreover, induced pluripotent stem cells (iPSCs) differentiated into neurons and oligodendrocytes from dermal fibroblasts with deficiencies in UNC93B and TLR3 also showed increased susceptibility to HSV-1 infection, emphasising the critical role of TLR3-dependent interferon production in the antiviral defence mechanism (Lafaille et al., 2012). Conversely, TLR3-mediated antiviral defence is dispensable in numerous cell types expressing TLR3 such as leukocytes, iPSC-derived peripheral nervous system (PNS) trigeminal neurons, CNS neural stem cells (NSCs), and astrocytes (Lafaille et al., 2012; Zimmer et al., 2018). These findings indicate that TLR3-dependent IFN autonomous immunity in cortical neurons and oligodendrocytes plays a pivotal role in protecting the human forebrain against HSV-1

infection. Astrocytes or NSCs that were differentiated *in vitro* from UNC93B-deficient iPSC cells did not exhibit increased susceptibility to HSV-1 infection compared to control cells (Lafaille et al., 2012). Interestingly, this differs from the heightened susceptibility of astrocytes to HSV-2 infection observed in TLR3-deficient mice (Reinert et al., 2012). Nevertheless, there is a potential role for human astrocytes and NSCs through mechanisms mentioned in the previous Section 1.6.3, contributing to the protective immune response against HSV-1 within the CNS *in vivo*.

Other molecular mechanisms specific to forebrain HSE may be involved, as indicated by the recent identification of AD deficiency in snoRNA31 (Lafaille et al., 2019). The deficiency in snoRNA31 resulted in an increased susceptibility to HSV1 infection in fibroblasts and iPSC-derived cortical neurons, mirroring the susceptibility observed in TLR3- and STAT1-deficient fibroblasts and cortical neurons, despite these cells exhibiting normal responses through TLR3 and IFNAR1/IFNAR2 (Lafaille et al., 2019). This has set the stage for exploring inborn errors of immunity that may predispose individuals to other forms of isolated viral encephalitis. A newly identified factor contributing to brainstem viral encephalitis in five otherwise healthy children is AR partial DBR1 deficiency, resulting from biallelic hypomorphic mutations of *DBR1* (Zhang et al., 2018). This deficiency has been observed in cases induced by various viruses, including HSV-1, affecting two of the patients (Zhang et al., 2018). DBR1-deficient fibroblasts showed a high susceptibility to HSV-1 and vesicular stomatitis virus (VSV), comparable to TLR3-deficient and STAT1-deficient fibroblasts, despite maintaining intact TLR3 and IFN-α/β responsive pathways (Zhang et al., 2018). The inherited deficiency of DBR1 likely contributes to viral infection within the brainstem by disrupting brainstem-specific and cell-intrinsic immunity against HSV-1.

In essence, genetic studies on HSE conducted since 2006 have unveiled the roles of TLR3 and snoRNA31 in orchestrating cell-intrinsic immunity against HSV-1 in the forebrain whereas in the brainstem, DBR1 is pivotal for the same immunity against HSV-1. This insight opens avenues for further exploration of CNS tissue-specific cell-intrinsic immunity to HSV-1 in humans, emphasising the concept of cell specificity and distinct from the immunity mediated by hematopoietic cells.

1.6.5 Innate immune response to HSV-2

The defence against HSV-2 infection encompasses both innate and adaptive immunity, where the epithelia, covering all external and internal body surfaces, serve as the initial line of defence—a physical and chemical barrier within the innate immune system—to counteract invading pathogens (Iwasaki, 2010). Much like HSV-1, it is believed that the innate antiviral response plays a crucial role in influencing the outcome of an HSV-2 infection, with the production of type I IFN, predominantly IFN-α and IFN-β, being associated with shielding against disease progression, as evidenced in both murine models and human investigations (Pedersen et al., 1983; Ellermann-Eriksen et al., 1986a; Ellermann-Eriksen et al., 1986b; Vollstedt et al., 2004). Experiments involving mice with a knockout of the IFNAR have demonstrated heightened viral replication, exacerbated pathogenesis, and reduced survival in these animals following genital infection with HSV-2 (Svensson et al., 2007).

Several studies have demonstrated the significance of IFNs by administering ligands for TLR3 and TLR9 through mucosal delivery confers protection against genital infection with HSV-2, while with TLR2 or TLR4 ligands showing no such protective effects (Sajic et al., 2003; Ashkar et al., 2004; Gill et al., 2006; Herbst-Kralovetz & Pyles, 2006). Moreover, it has been demonstrated previously that the generation of IFN-β within the TLR3-IFN pathway is closely associated with innate protection against HSV-2 (Gill et al., 2006). As elaborated in Section 1.6.3, dsRNA is detected not only by TLR3 but also by the cytoplasmic RLRs RIG-I and MDA5, leading to the activation of IRF-3 and the subsequent production of type I IFNs in a TLR-independent manner.

In addition to the mechanisms elucidated in Section 1.6.3, as briefly alluded to earlier in the same section, PKR serves as a viral DNA sensor which functions as a cytoplasmic protein capable of recognising viral dsRNA and engaging with various PRRs. A central aspect of PKR's function involves triggering the phosphorylation of eukaryotic translation initiation factor eIF-2α, a crucial enzyme in protein synthesis to impede the translation of viral mRNA

and consequently stopping viral gene expression (Meurs et al., 1990; Balachandran et al., 2000). Upon binding to dsRNA, PKR initiates a signaling cascade that activates NF-κB and production of type I IFNs (Kumar et al., 1994). Notably, several TLRs including TLR3 and TLR4, could activate PKR thereby augmenting its effects (Horng et al., 2001; Jiang et al., 2003). Furthermore, PKR plays a pivotal role in MDA5-mediated activation of MAVS for the production of type I interferons (Pham et al., 2016). PKR-deficient mice exhibit heightened susceptibility to HSV-2, emphasising the significance of the PKR pathway in enabling IFN-α1 to orchestrate defence against HSV-2 (Al-Khatib et al., 2004; Carr et al., 2005).

1.6.6 Innate immune response to SARS-CoV-2

Upon encountering SARS-CoV-2, viral PAMPs are identified by a multitude of host PRRs in innate immune cells, primarily TLRs, RIG-I, and MDA-5. Notably, cell surface-located TLR1/2/4/6 contribute to the recognition of viral proteins, while TLR7 and TLR8, situated in the endosomal compartment, detect the viral ssRNA genome. The recognition by these TLRs initiates signalling cascade mediated by the MyD88 adaptor protein. Additionally, TLR3, RIG-I, and MDA5 have the capacity to recognise the replication intermediate double-stranded RNA (dsRNA). These pathways collectively leading to the production of type I IFNs and activation of NF-κB, orchestrating an intricate host antiviral response which has been outlined in the earlier sections.

A study has indicated the involvement of TLR2 in the recognition of the SARS-CoV-2 E protein and the initiation of inflammatory responses during infection, as demonstrated by reduced activation of pro-inflammatory signalling pathways and cytokine production in both human macrophages treated with a TLR2 inhibitor and TLR2-deficient murine macrophages upon exposure to the SARS-CoV-2 E protein (Zheng et al., 2021; Potapov et al., 2022). Additionally, in the same study, TLR2-deficient mice exhibited reduced serum IL-6 levels upon administration of the SARS-CoV-2 E protein, implying that the E protein elicits inflammation through a TLR2-dependent mechanism (Zheng et al., 2021). Research findings

also indicate that the depletion or knocking out of gene responsible for MDA5 in primary human lung airway epithelial cells or Calu-3 cells (human lung cancer) leads to a diminished expression of type I IFN during SARS-CoV-2 infection, suggesting a pivotal role for MDA5 as the primary sensor for SARS-CoV-2 (Rebendenne et al., 2021; Yin et al., 2021). Further investigations are essential to validate these findings considering the novelty of the disease and the multitude of researchers are exploring various aspects of it.

In the case of SARS-CoV, the TLR3 signalling pathway exhibits a protective function in mice, as evidenced by the increased viral load and compromised pulmonary function observed in TLR3-deficient mice compared to their control counterparts upon infection with mouse-adapted SARS-CoV (Barnard et al., 2006; Totura et al., 2015). Furthermore, the administration of a TLR3 agonist diminishes the SARS-CoV viral load in human alveolar epithelial cells and this intervention also demonstrates an absence of clinical disease in mice infected with mouse-adapted SARS-CoV (Zhao et al., 2012). As of now, there is no direct evidence establishing a connection between TLR3 and the specific recognition of SARS-CoV-2. However, a genomic analysis conducted on individuals with severe COVID-19 revealed a correlation between inborn errors in TLR3 and the severity of the disease, a connection that will be explored further in subsequent chapters of this study.

1.7 TICAM1

As discussed in Section 1.6.2, TICAM1 or TRIF, interchangeably used, is directly recruited to TLR3, whereas its association with TLR4 necessitates the involvement of TRAM or TICAM2. TICAM1 coordinates a signalling cascade marked by the inducible synthesis of type I IFN and IFN-dependent genes through the activation of the transcription factors IRF-3, NF-κB, and AP-1 (Yamamoto et al., 2002; Fitzgerald et al., 2003b; Oshiumi et al., 2003; Yamamoto et al., 2003a; Akira & Takeda, 2004). Human TICAM1 comprises 712 amino acids starting with an N-terminal protease-resistant domain predicted to have a helical structure, followed by a proline-rich unstructured region containing binding motifs for TBK1 and TRAF6, a central

TIR domain, and a C-terminal region with a receptor-interacting protein (RIP) homotypic interaction motif (RHIM) (Sato et al., 2003; Meylan et al., 2004; Sasai et al., 2010; Tatematsu et al., 2010). TICAM1 homo-oligomerization necessitates the presence of both the TIR and RHIM domains (Funami et al., 2008). The TIR domain of TICAM1 is crucial for binding to both the TIR domain of TLR3 and the TLR4 adaptor TICAM2 forming TIR-TIR domain interactions. NF-κB-activating kinase-associated protein 1 (NAP1) or also known as 5-azacytidine induced 2 (AZI2) plays a role in recruiting TBK1 and IKKε to the N-terminal region of TICAM1 leading to IRF3 activation and type I IFN production (Fujita et al., 2003; Sasai et al., 2005; Funami et al., 2008; Han et al., 2010; Tatematsu et al., 2010). While the N-terminal region is indispensable for TICAM1-mediated IRF-3 activation, the C-terminal segment is implicated in NF-κB activation and apoptosis (Yamamoto et al., 2002; Han et al., 2004; Kaiser & Offermann, 2005). The recruitment of TRAF6 leads to activation of NF-κB (Sasai et al., 2010). The RHIM domain situated in the C-terminal region of TICAM1 forms an association with receptor-interacting protein 1 (RIP1), a kinase featuring a death domain (Meylan et al., 2004). In TICAM1-mediated signalling, RIP1 serves as an inducer of NF-κB and a mediator of apoptosis (Han et al., 2004; Kaiser & Offermann, 2005).

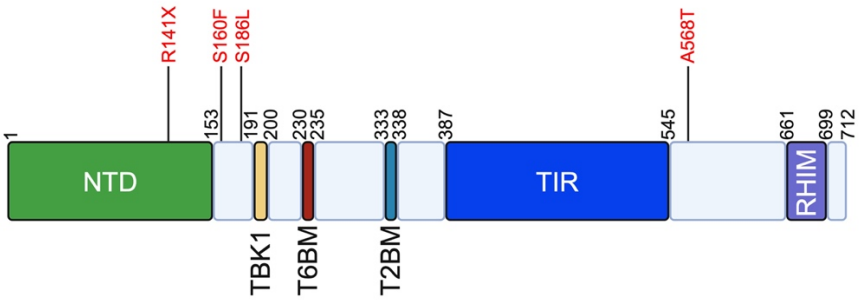


Figure 1.2 Schematic illustration of the TICAM1 protein.

TICAM1 is a 712 amino acid long protein. Functional domains are labelled. Variants in red have been reported in HSE patients. HSE: herpes simplex encephalitis, NTD: N-terminal domain, TBK1 motif: TBK1 binding motif, T6BM: TRAF6 binding motif, T2BM: TRAF2 binding motif, TIR: TIR domain, RHIM: RIP (receptor-interacting protein) homotypic interaction motif.

At the basal cellular level, TICAM1 is expressed in a low and diffuse manner in the cytoplasm (Oshiumi et al., 2003). Nevertheless, when triggered by poly(I:C) stimulation, TICAM1

experiences an initial brief interaction with TLR3, followed by the formation of speckle-like structures incorporating downstream signalling molecules (Funami et al., 2007). These structures encompass RIP1 and NAP1, marking the initiation of TICAM-1-mediated signalling (Funami et al., 2007). Various regulatory molecules, such as those from the tripartite motif (TRIM) family of proteins, play a role in modulating the signalling pathway, either positively or negatively, to sustain a balanced response (Yang et al., 2020). Both excessive activation and inadequate activation of TRIF-mediated signalling have detrimental effects, with heightened TICAM-1 expression inducing apoptosis in a caspase-dependent manner (Han et al., 2004; Ruckdeschel et al., 2004; Kaiser & Offermann, 2005; Rebsamen et al., 2008), and diminished expression resulting in the reduced production of cytokines crucial for defence (Shen et al., 2012; Xue et al., 2012; Yang et al., 2017; Ye et al., 2017). A TICAM1 mutant with deletion of the N-terminal domain (residues Δ180aa) exhibited an increased capability to activate the IFN-β promoter in comparison to the WT TICAM1 (Tatematsu et al., 2010). Inactive TICAM1 may adopt a closed conformation, concealing the essential amino acids necessary for binding with TRAF2, TRAF6, and TBK1 between the N-terminal domain and TIR domain through the folding of N-terminal domain into the TIR domain. This action serves to impede TICAM1 activation via oligomerization and acts as a barrier to prevent downstream signalling molecules from reaching TICAM1 (Tatematsu et al., 2010).

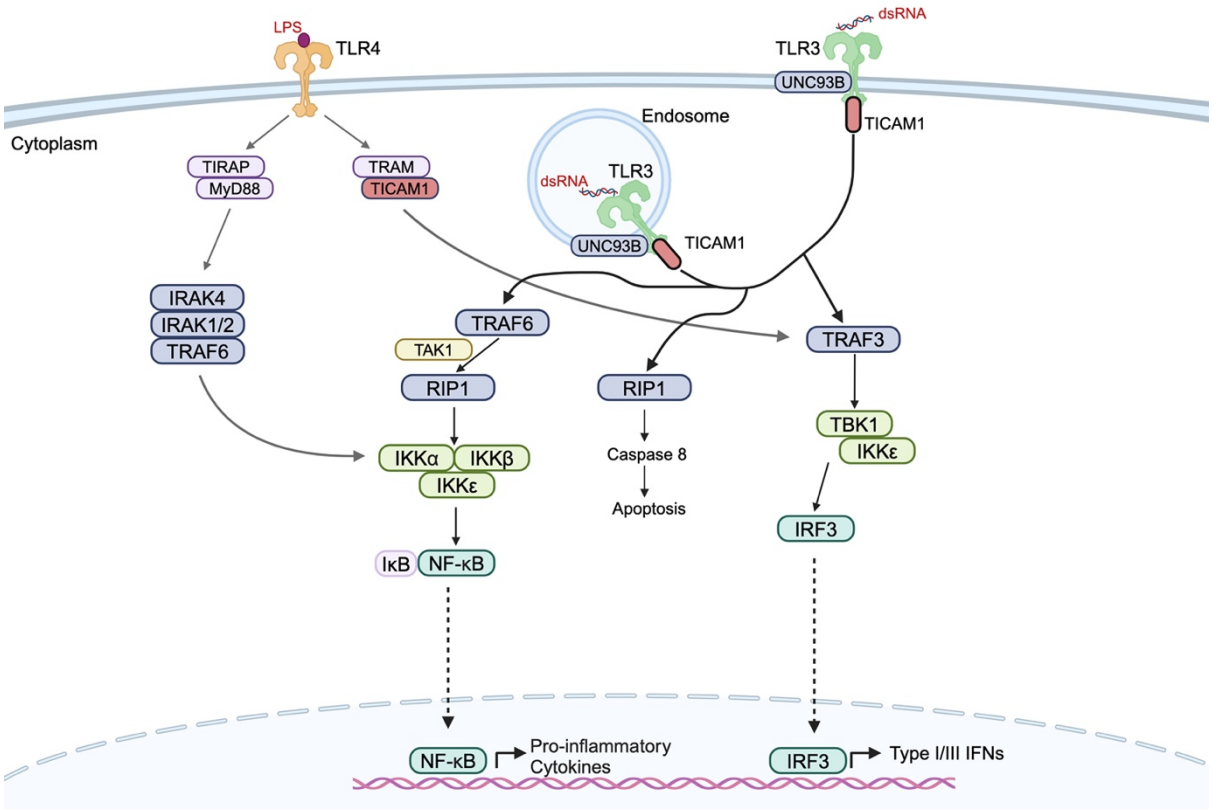


Figure 1.3 TICAM1 in TLR3 and TLR4 signalling.

TICAM1 is an adaptor protein for TLR3 and TLR4 for the induction of IFNs and pro-inflammatory cytokines. Upon stimulation, TICAM1 is directly recruited to TLR3 and indirectly, through TRAM to TLR4. TICAM1 recruits TRAF3 which, in turn, directs TICAM1 to TBK1. Once activated, TBK1 initiates the phosphorylation of the transcription factor IRF3. This activated IRF3 translocates into the nucleus and induce the production of IFNs. TICAM1 also form an association with RIP1 serves as an inducer of NF-κB and a mediator of apoptosis in a caspase-dependent manner. Furthermore, TICAM1 engages with TRAF6, facilitating the activation of TAK1-associated proteins. Upon activation, TAK1 initiates the activation of the IκB kinase-NFκB pathway. The activated NFκB subsequently undergoes translocation into the nucleus, inducing the transcriptional activation of genes responsible for encoding proinflammatory cytokines.

1.7.1 TICAM1 in viral infections

TICAM1 serves as a key mediator after the recognition of viral nucleic acids, triggering downstream signalling events that culminate in the production of cytokines including IFNs and other immune effectors. Numerous studies provide evidence indicating that the TLR3/TICAM-

1 pathway regulates the induction of IFN and contributes to host protection against diverse viral infections. In a study, TICAM1-deficient mice were intranasally infected with HSV-1, exhibiting a reduced survival rate and elevated viral load from day 5 post-infection onward in contrast to WT mice (Menasria et al., 2013). The deficiency in the TICAM1 signalling pathway also resulted in a delayed production of IFN-β, indicating an altered early response that could be crucial for controlling HSV-1 infection. Additionally, the level of phosphorylated IRF3, a crucial transcription factor responsible for activating type I IFN genes upon the stimulation of TICAM1, was significantly diminished compared to the WT. TICAM1-deficient mice were also subjected to different viruses, including Ross River virus (RRV), EMCV, Coxsackievirus B3 (CVB3), and poliovirus, revealing infectious traits resembling those observed in TLR3-deficient mice such as high viral loads, decreased survival rates and diminished IFN levels when compared to WT (Negishi et al., 2008; Oshiumi et al., 2011; Abe et al., 2012; Liu et al., 2022).

The initial identification of inborn errors of immunity associated with autosomal dominant (AD) and autosomal recessive (AR) TICAM1 deficiencies in children suffering from HSE conclusively confirms the critical role of human TLR3 immunity in the antiviral defence against HSV-1 (Sancho-Shimizu et al., 2011). In individuals with both AR (p.R141X) and AD (p.S186L) TICAM1 deficiencies, the TLR3 signalling pathway was found to be compromised while the TICAM1-dependent TLR4 pathway was specifically affected in patients with AR (p.R141X) TICAM1 deficiency. Dermal fibroblasts derived from individuals with TICAM1 deficiency exhibited reduced production of IFN-β, IFN-λ/IL-29, and IL-6 in response to either poly(I:C) stimulation, a TLR3 agonist, or infected with HSV-1 or VSV. This deficiency can be attributed to the absence of IRF-3 activation and NF-κB. Additionally, when these fibroblasts were infected with either HSV-1 or VSV, they exhibited high viral loads and low cell survival rates. Peripheral blood mononuclear cells (PBMC) extracted from the AR TICAM1 patient with the p.R141X mutation failed to initiate *IFNB1* mRNA production and exhibited a lower IL-6 induction compared to the WT. Thus, it was inferred that the observed production was attributed to the unaffected TLR4-MyD88-dependent pathway. In a separate investigation, two distinct *TICAM1* variants, AD p.S160F and AD p.A568T, were detected in unrelated males aged over 60 who manifested adult-onset HSE (Mork et al., 2015). When PBMCs from both patients were challenged with HSV-1, a significant impairment in the induction of IFN-β,

CXCL10, and TNF-α was observed. Loss-of-function (LoF) mutations in *TICAM1* have been identified in individuals experiencing severe COVID-19 pneumonia (Zhang et al., 2020). Our contribution to the functional evaluation of these *TICAM1* variants revealed impaired production of IFN-β and NF-κB, and this will be further elaborated in later chapter of this thesis.

1.8 Aims of this study

This chapter aims to elucidate the present understanding of host genetic diversity in human infectious diseases, placing particular emphasis on HSV-1, HSV-2, and SARS-CoV-2 infections, while also examining the presently identified genetic variants linked to susceptibility and the progression of severe diseases. I hypothesize that variants in the human *TICAM1* gene may play a contributory role in the manifestation of diverse viral diseases

The aims of this study:

1. To validate the functional significance of the *TICAM1* variants concerning their relevance in the context of COVID-19.
2. To examine the functional importance of the *TICAM1* variant in Mollaret Meningitis induced by HSV-2
3. To develop a cerebral organoid model of HSV-1 infection capable of replicating the pathological progression of HSE observed in humans.

Chapter 2

2. Methods

2.1 Cell maintenance and culture

2.1.1 Dermal fibroblasts

Controls and TICAM1-deficient (TICAM1$^{-/-}$) dermal fibroblasts derived from skin biopsies of healthy individuals or HSE patients have been described previously (Sancho-Shimizu et al., 2011). The team led by Dr Taco Kuijpers provided a skin biopsy from their patient (P1) with heterozygous TICAM1 E429X variant which was sent to our lab. As part of the Investigating the GENetics of InfectiOn Study (INGENIOS), our team acquired a skin biopsy from patient 1024M. These primary fibroblasts were subsequently immortalised using SV40 large T antigen, as previously described (Chapgier et al., 2006). All primary and SV40-immortalised fibroblast used here were cultured in Dulbecco's Modified Eagle Medium (DMEM) GlutaMAX (Invitrogen) supplemented with 10% of heat-inactivated foetal bovine serum (FBS) (Gibco) and grown in a humidified incubator at 37°C with 5% CO_2. Similarly, HEK293 cells derived from human embryonic kidney cells and Vero cells from African green monkey kidney were maintained in DMEM GlutaMAX supplemented with 10% of heat-inactivated FBS.

2.1.2 Stem cells culture

Pluripotent stem cells (PSCs), including H9 embryonic stem cells (ESCs) and induced pluripotent stem cells (iPSCs), were cultured in complete Essential 8 (E8) media (Gibco) or complete Essential 8 Flex (Gibco) on feeder-free culture plates pre-coated with geltrex coating matrix (Gibco). The plates were pre-coated with geltrex at a ratio of 1:100 with cold DMEM/F12 (Gibco). For cell passage, they were detached by incubating with either 0.5 μM

EDTA pH 8.0 (Gibco) or StemPro™ Accutase Cell Dissociation Reagent (Gibco) for 5 minutes at 37°C with 5% CO_2 and the resulting cell suspension was carefully added drop by drop to a new geltrex-coated plate. Ms. Aneesa Ali played a crucial role in the meticulous maintenance of PSC culture and guided the differentiation process into cortical neurons and cerebral organoids. Her invaluable contributions greatly enhanced the success of these procedures.

2.1.2.1 Differentiation into cortical neurons

To initiate the differentiation process into cortical neurons, a protocol adapted from Shi et al. (Shi et al., 2012) was performed using the dual SMAD inhibition method. PSCs were seeded on a 6-well plate to achieve full confluency and neural induction medium was introduced on day 1. The neural induction medium consisted of 500 ml N2B27 medium, 1 μM Dorsomorphin (SMAD inhibitor, Cambridge Biosciences) and 10 μM SB431542 (SMAD inhibitor, Cambridge Biosciences). The N2B27 medium is composed of a 1:1 mixture of N2 medium [242 ml of DMEM/F12 GlutaMAX (Gibco), 2.5 ml 100X N2 supplement (Gibco), 5 μg/ml insulin (Sigma), 1 mM L-glutamine (Gibco), 100 μM MEM nonessential amino acids (NEAA) (Gibco), 100 μM β-mercapto-ethanol (Gibco), 50 U/ml pen, 50 mg/ml strep (Gibco)] and B27 medium [Neurobasal™ Medium (Gibco), 5 ml B27 with vitamin A (Gibco), 200 mM L-glutamine, 50 U/ml pen, 50 mg/ml strep]. Medium was replaced everyday with fresh neural induction medium for the next 10 days. First split of the culture using EDTA was performed on day 12 to eliminate non-neuroepithelial cells and the cells were scratched to generate large cluster which were collected with N2B27 media. These cells were then added to plates that had been pre-coated with laminin (Bio-Techne Ltd.) and half the medium was replaced with a fresh media every 2 days. The second split was performed 20 days post neural induction to encourage the growth of neural rosettes and eliminate non-neural stem cells. Cells were scratched to generate smaller cell clusters than the first passage and placed onto plates that had been pre-coated with laminin with a half media change every other day. Following this passage, colonies were expected to form more neural rosettes and projections. Third split occurred on day 35 using accutase to plate cells into desired assay format such as onto coverslips for later immunofluorescence.

2.1.2.2 Differentiation into cerebral organoids

To initiate the differentiation process into cerebral organoids, a protocol adapted from Salick et al. (Salick et al., 2017) and Lancaster et al. (Lancaster & Knoblich, 2014) was performed. PSCs were dissociated using accutase and seeded in an Ultra-Low Attachment (ULA) U-bottom 96-well plates (Corning) at approximately 10,000 cells/well with E8 media supplemented with ROCK inhibitor (Sigma) to generate embryoid bodies (EBs), marking day 0. On day 2, 'dispersion' technique was used involving the drawing up and expulsion of media back into the well, performed with each media change onwards. The upward movement effectively raises cellular debris along with the organoid into suspension. Subsequently, the organoid promptly fell to the bottom of the well, while the smaller debris remained suspended, facilitating its removal through a media change. This approach helps to avert the organoid from settling amidst cellular debris during the culture process. Then, the spent medium was replaced with fresh E8 media supplemented with ROCK inhibitor. On day 3, media was replaced with E8 without ROCK inhibitor and this regimen was done every few days until experimental day. On day 4, EBs was subjected to neural induction by addition of neural induction media. This neural induction media is consisted of 500 ml of DMEM/F12 GlutaMAX, 0.5 mg heparin (Sigma), 5 ml 100X N-2 Supplement, and 5 ml 100X MEM-NEAA. On the 7th day, undiluted geltrex was dispensed onto a parafilm sheet with manually crafted rounded indentations to secure EBs in the geltrex. EBs were lifted using a 200 µl pipette tip with a bigger opening created by cutting with sterile scissors. The parafilm embedding sheet with the EBs was then incubated at 37°C with 5% CO2 for 45 minutes until the geltrex had polymerised. The EBs were washed off using neural induction media into a 24 well ULA plate (Corning) and incubated until day 38. Half media changes were performed every other day until day of experiment.

2.2 Isolating primary human peripheral blood mononuclear cells (PBMCs)

Dr Taco Kuijpers's team generously provided us with a precious sample of P1's PBMCs and Ms Dilys Santillo has kindly thawed and cultured the PBMCs in Roswell Park Memorial Institute (RPMI) 1640 Medium (Gibco) supplemented with 10 % FBS and cultured in a humidified incubator at 37°C with 5% CO_2. For the isolation of PBMC from 1024M's blood, our clinic team collected whole blood in BD Vacutainer® heparin tubes (BD biosciences). The blood then was processed through sterile density gradient centrifugation using Ficoll-Paque™ (Cytiva) by our lab team. The entire collected whole blood underwent centrifugation at 400g for 10 minutes resulting in the separation of plasma. The plasma was removed and to be replaced with phosphate buffered saline (PBS) (Gibco). Following this plasma removal, the blood was mixed in a 1:1 ratio with PBS and this PBS was carefully layered onto the one volume of Ficoll-Paque™ medium. Subsequently, the sample underwent centrifugation at 600g for 30 minutes with the centrifuge brakes disengaged (zero brakes) to prevent any mixing of gradients. After the centrifugation, there were a distinct four-layer gradient formation with a cloudy layer in the middle emerged which was abundant in PBMCs. This particular layer was carefully pipetted out into PBS and subjected to two washes involving centrifuging for 10 minutes at 600g and resuspending the cell pellet in PBS each time. The now isolated and washed PBMCs were counted with a haemocytometer manually using trypan blue (Invitrogen). PBMCs were cultured in RPMI 1640 Medium (Gibco) supplemented with 10 % FBS and maintained in a humidified incubator at 37°C with 5% CO_2.

2.3 Genetic DNA editing

2.3.1 Plasmids

Table 2.1 provided a comprehensive inventory of all plasmids used and constructed in this thesis. Meanwhile, Figure 2.1 showed detailed plasmid maps of the pEF-BOS. All pEF-BOS-TICAM1 variants presented in this study were produced by introducing point mutations into the pEF-BOS-TICAM1 wildtype through site-directed mutagenesis (see Section 2.4).

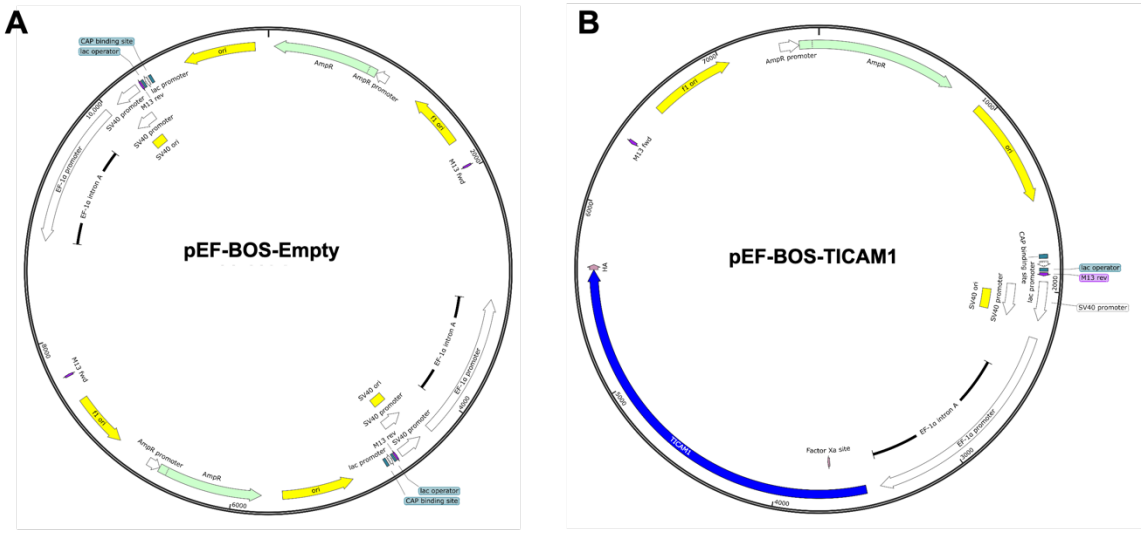


Figure 2.1 Plasmid map.

Plasmid map showing A) pEF-BOS-Empty and B) pEF-BOS-TICAM1 WT.

Table 2.1 Plasmids used in this thesis

Plasmids	Descriptions	Source
pEF-BOS-Empty	Cloning vector, HA-tagged (C-terminus), used to control uniformity in transfection efficiency, ampicillin resistant cassette	(Sancho-Shimizu et al., 2011)
pEF-BOS-TICAM1	Expression vector, HA-tagged (C-terminus) human wild-type TICAM1, ampicillin resistant cassette	(Sancho-Shimizu et al., 2011)
pEF-Bos-TICAM1-T4I	Cloned from pEF-BOS-TICAM1, T4I variant incorporated using site-directed mutagenesis	This study
pEF-Bos-TICAM1-S10N	Cloned from pEF-BOS-TICAM1, S10 variant incorporated using site-directed mutagenesis	This study
pEF-Bos-TICAM1-T32I	Cloned from pEF-BOS-TICAM1, T32I variant incorporated using site-directed mutagenesis	This study
pEF-Bos-TICAM1-G52S	Cloned from pEF-BOS-TICAM1, G52S variant incorporated using site-directed mutagenesis	This study
pEF-Bos-TICAM1-S60C	Cloned from pEF-BOS-TICAM1, S60C variant incorporated using site-directed mutagenesis	This study
pEF-Bos-TICAM1-R71Q	Cloned from pEF-BOS-TICAM1, R71Q variant incorporated using site-directed mutagenesis	This study
pEF-Bos-TICAM1-V80M	Cloned from pEF-BOS-TICAM1, V80M variant incorporated using site-directed mutagenesis	This study
pEF-Bos-TICAM1-A111T	Cloned from pEF-BOS-TICAM1, A111T variant incorporated using site-directed mutagenesis	This study
pEF-Bos-TICAM1-V122I	Cloned from pEF-BOS-TICAM1, V122I variant incorporated using site-directed mutagenesis	This study
pEF-Bos-TICAM1-R128K	Cloned from pEF-BOS-TICAM1, R128K variant incorporated using site-directed mutagenesis	This study
pEF-Bos-TICAM1-R141X	Cloned from pEF-BOS-TICAM1, R141X variant incorporated using site-directed mutagenesis	(Sancho-Shimizu et al., 2011)
pEF-Bos-TICAM1-T157M	Cloned from pEF-BOS-TICAM1, R157M variant incorporated using site-directed mutagenesis	This study
pEF-Bos-TICAM1-S160F	Cloned from pEF-BOS-TICAM1, S160F variant incorporated using site-directed mutagenesis	This study
pEF-Bos-TICAM1-L162V	Cloned from pEF-BOS-TICAM1, L162V variant incorporated using site-directed mutagenesis	This study
pEF-Bos-TICAM1-R176S	Cloned from pEF-BOS-TICAM1, R176S variant incorporated using site-directed mutagenesis	This study

pEF-Bos-TICAM1-R180C	Cloned from pEF-BOS-TICAM1, R180C variant incorporated using site-directed mutagenesis	This study
pEF-Bos-TICAM1-S186L	Cloned from pEF-BOS-TICAM1, S186L variant incorporated using site-directed mutagenesis	(Sancho-Shimizu et al., 2011)
pEF-Bos-TICAM1-S189T	Cloned from pEF-BOS-TICAM1, S189T variant incorporated using site-directed mutagenesis	This study
pEF-Bos-TICAM1-R195Q	Cloned from pEF-BOS-TICAM1, R195Q variant incorporated using site-directed mutagenesis	This study
pEF-Bos-TICAM1-L207W	Cloned from pEF-BOS-TICAM1, L207W variant incorporated using site-directed mutagenesis	This study
pEF-Bos-TICAM1-S219R	Cloned from pEF-BOS-TICAM1, S219R variant incorporated using site-directed mutagenesis	This study
pEF-Bos-TICAM1-P234S	Cloned from pEF-BOS-TICAM1, P234S variant incorporated using site-directed mutagenesis	This study
pEF-Bos-TICAM1-P244L	Cloned from pEF-BOS-TICAM1, P244L variant incorporated using site-directed mutagenesis	This study
pEF-Bos-TICAM1-G245S	Cloned from pEF-BOS-TICAM1, G245S variant incorporated using site-directed mutagenesis	This study
pEF-Bos-TICAM1-S258L	Cloned from pEF-BOS-TICAM1, S258L variant incorporated using site-directed mutagenesis	This study
pEF-Bos-TICAM1-P271S	Cloned from pEF-BOS-TICAM1, P271S variant incorporated using site-directed mutagenesis	This study
pEF-Bos-TICAM1-D281H	Cloned from pEF-BOS-TICAM1, D281H variant incorporated using site-directed mutagenesis	This study
pEF-Bos-TICAM1-A282G	Cloned from pEF-BOS-TICAM1, A282G variant incorporated using site-directed mutagenesis	This study
pEF-Bos-TICAM1-T283N	Cloned from pEF-BOS-TICAM1, T283N variant incorporated using site-directed mutagenesis	This study
pEF-Bos-TICAM1-D289N	Cloned from pEF-BOS-TICAM1, D289N variant incorporated using site-directed mutagenesis	This study
pEF-Bos-TICAM1-V302L	Cloned from pEF-BOS-TICAM1, V302L variant incorporated using site-directed mutagenesis	This study
pEF-Bos-TICAM1-T346A	Cloned from pEF-BOS-TICAM1, T346A variant incorporated using site-directed mutagenesis	This study
pEF-Bos-TICAM1-T377I	Cloned from pEF-BOS-TICAM1, T377I variant incorporated using site-directed mutagenesis	This study
pEF-Bos-TICAM1-T377N	Cloned from pEF-BOS-TICAM1, T377N variant incorporated using site-directed mutagenesis	This study
pEF-Bos-TICAM1-L386P	Cloned from pEF-BOS-TICAM1, L386P variant incorporated using site-directed mutagenesis	This study
pEF-Bos-TICAM1-Q392K	Cloned from pEF-BOS-TICAM1, Q392K variant incorporated using site-directed mutagenesis	This study
pEF-Bos-TICAM1-E429X	Cloned from pEF-BOS-TICAM1, E429X variant incorporated using site-directed mutagenesis	This study

pEF-Bos-TICAM1-I452T	Cloned from pEF-BOS-TICAM1, I452T variant incorporated using site-directed mutagenesis	This study
pEF-Bos-TICAM1-S465N	Cloned from pEF-BOS-TICAM1, S465N variant incorporated using site-directed mutagenesis	This study
pEF-Bos-TICAM1-G481A	Cloned from pEF-BOS-TICAM1, G481A variant incorporated using site-directed mutagenesis	This study
pEF-Bos-TICAM1-L533F	Cloned from pEF-BOS-TICAM1, L533F variant incorporated using site-directed mutagenesis	This study
pEF-Bos-TICAM1-D557N	Cloned from pEF-BOS-TICAM1, D557N variant incorporated using site-directed mutagenesis	This study
pEF-Bos-TICAM1-A565S	Cloned from pEF-BOS-TICAM1, A565S variant incorporated using site-directed mutagenesis	This study
pEF-Bos-TICAM1-L574V	Cloned from pEF-BOS-TICAM1, L574V variant incorporated using site-directed mutagenesis	This study
pEF-Bos-TICAM1-M595L	Cloned from pEF-BOS-TICAM1, M595L variant incorporated using site-directed mutagenesis	This study
pEF-Bos-TICAM1-G598W	Cloned from pEF-BOS-TICAM1, G598W variant incorporated using site-directed mutagenesis	This study
pEF-Bos-TICAM1-G611S	Cloned from pEF-BOS-TICAM1, G611S variant incorporated using site-directed mutagenesis	This study
pEF-Bos-TICAM1-P620S	Cloned from pEF-BOS-TICAM1, P620S variant incorporated using site-directed mutagenesis	This study
pEF-Bos-TICAM1-P628S	Cloned from pEF-BOS-TICAM1, P628S variant incorporated using site-directed mutagenesis	This study
pEF-Bos-TICAM1-P658L	Cloned from pEF-BOS-TICAM1, P658L variant incorporated using site-directed mutagenesis	This study
pEF-Bos-TICAM1-A666T	Cloned from pEF-BOS-TICAM1, A666T variant incorporated using site-directed mutagenesis	This study
pEF-Bos-TICAM1-Q702R	Cloned from pEF-BOS-TICAM1, Q702R variant incorporated using site-directed mutagenesis	This study
IFN-β promoter-luciferase	Firefly reporter vector, used in the dual luciferase reporter assay	(Sancho-Shimizu et al., 2011)
NF-κB promoter luciferase	Firefly reporter vector, used in the dual luciferase reporter assay	(Sancho-Shimizu et al., 2011)
pRL-TK Renilla luciferase	Renilla reporter vector, used in the dual luciferase reporter assay	(Sancho-Shimizu et al., 2011)
pEGFP	Expression vector, used for visualising transfection efficiency	Abcam

2.3.2 Oligonucleotides used in this thesis

The primers used for confirming the plasmid sequence of *TICAM1* were previously designed by Dr. Vanessa Sancho-Shimizu (Sancho-Shimizu et al., 2011) and their details are outlined in Table 2.2. For site-directed mutagenesis, Dr Stephanie Hodeib manually designed overlapping primer pairs to introduce the single nucleotide substitution at the targeted area of interest. The specific details of these primers are catalogue in Table 2.3.

Table 2.2 Primers used in this thesis

Primer	Sequence 5'-3'
TICAM1-31F	GCGCCTTCGACATTCTAGG
TICAM1-351F	TACCAGGAAGCCGTCCGCA
TICAM1-537F	CTGGCTGAGGAGAAGCTGTG
TICAM1-681F	AGCAAGCTCTGTGACGACC
TICAM1-1021F	ACCACCTCTCCAAATACCAAGC
TICAM1-1945F	CAGCCAGCAGCCTTTCCA
TICAM1-407R	GACCACCGGCTGGGGGAACT
TICAM1-1134R	CTGGGTAGTTGGTGCTGGTT
TICAM1-1298R	ACCTGGAAATCCTCGCAGAA
TICAM11945R	TGGAAAGGCTGCTGGCTG
TICAM1-2201R	GAAGGGCAGTGACTGTGGA

Table 2.3 Oligonucleotides designed for site-directed mutagenesis (SDM)

Primer	Sequence 5' to 3'	Descriptions
TICAM1_T4I_F	tggtaccatggcctgcaTaggcccatcacttcct	Generation of T4I variant in pEF-BOS-TICAM1
TICAM1_T4I_R	aggaagtgatgggccAttgcaggccatggtacca	Generation of T4I variant in pEF-BOS-TICAM1
TICAM1_S10N_F	ggcccatcacttcctaAcgccttcgacattc	Generation of S10N variant in pEF-BOS-TICAM1
TICAM1_S10N_R	gaatgtcgaaggcgTtaggaagtgatgggcc	Generation of S10N variant in pEF-BOS-TICAM1
TICAM1_T32I_F	agcacaaactgaagaTcccacgcccaggct	Generation of T32I variant in pEF-BOS-TICAM1
TICAM1_T32I_R	agcctgggcgtgggAtcttcagtttgtgct	Generation of T32I variant in pEF-BOS-TICAM1
TICAM1_G52S_F	ctgaagctgAgccaggaaactgaggccagg	Generation of G52S variant in pEF-BOS-TICAM1
TICAM1_G52S_R	cctggcctcagtttcctggcTcagcttcag	Generation of G52S variant in pEF-BOS-TICAM1
TICAM1_S60C_F	gaggccaggatctGtctagaggcattg	Generation of S60C variant in pEF-BOS-TICAM1
TICAM1_S60C_R	caatgcctctagaCagatcctggcctc	Generation of S60C variant in pEF-BOS-TICAM1
TICAM1_R71Q_F	ccgatgcggtggcccAgctggtggcccgccagt	Generation of R71Q variant in pEF-BOS-TICAM1
TICAM1_R71Q_R	actggcgggccaccagcTgggccaccgcatcg	Generation of R71Q variant in pEF-BOS-TICAM1
TICAM1_V80M_F	gccagtgggctggcAtggacagcaccgagga	Generation of V80M variant in pEF-BOS-TICAM1
TICAM1_V80M_R	tcctcggtgctgtccaTgccagcccactggc	Generation of V80M variant in pEF-BOS-TICAM1
TICAM1_A111T_F	gagaagctgtgccccAcctcgctgcgggacgtg	Generation of A111T variant in pEF-BOS-TICAM1
TICAM1_A111T_R	cacgtcccgcagcgaggTggggcacagcttctc	Generation of A111T variant in pEF-BOS-TICAM1
TICAM1_V122I_F	ccaggaagccAtccgcaccctcagctcc	Generation of V122I variant in pEF-BOS-TICAM1
TICAM1_V122I_R	ggagctgagggtgcggaTggcttcctgg	Generation of V122I variant in pEF-BOS-TICAM1
TICAM1_R128K_F	cctcagctccaAggacgaccaccggc	Generation of R128K variant in pEF-BOS-TICAM1
TICAM1_R128K_R	gccggtggtcgtccTtggagctgagg	Generation of R128K variant in pEF-BOS-TICAM1

TICAM1_T157M_F	atccagggagcatccggaTgctccagtccaatctgggct	Generation of R157M variant in pEF-BOS-TICAM1
TICAM1_T157M_R	agcccagattggactggagcAtccggatgctccctggat	Generation of R157M variant in pEF-BOS-TICAM1
TICAM1_S160F_F	atccggacgctccagtTcaatctgggctgcct	Generation of S160F variant in pEF-BOS-TICAM1
TICAM1_S160F_R	aggcagcccagattgAactggagcgtccggat	Generation of S160F variant in pEF-BOS-TICAM1
TICAM1_L162V_F	gacgctccagtccaatGtgggctgcc	Generation of L162V variant in pEF-BOS-TICAM1
TICAM1_L162V_R	ggcagcccaCattggactggagcgtc	Generation of L162V variant in pEF-BOS-TICAM1
TICAM1_R176S_F	ctttgccctctgggaccagCagcctcccac	Generation of R176S variant in pEF-BOS-TICAM1
TICAM1_R176S_R	gtgggaggctGctggtcccagagggcaaag	Generation of R176S variant in pEF-BOS-TICAM1
TICAM1_R180C_F	gagcctcccaTgccccattgacggtg	Generation of R180C variant in pEF-BOS-TICAM1
TICAM1_R180C_R	caccgtcaatggggcAtgggaggctc	Generation of R180C variant in pEF-BOS-TICAM1
TICAM1_S189T_F	cggtgtttcggactggaCccaagggtgctccc	Generation of S189T variant in pEF-BOS-TICAM1
TICAM1_S189T_R	gggagcacccttggGtccagtccgaaacaccg	Generation of S189T variant in pEF-BOS-TICAM1
TICAM1_R195E_F	tgctccctgcAatccactggc	Generation of R195E variant in pEF-BOS-TICAM1
TICAM1_R195E_R	gccagtggatGgcagggagca	Generation of R195E variant in pEF-BOS-TICAM1
TICAM1_L207W_F	ctccctggccagcaactGggaaatcagcc	Generation of L207W variant in pEF-BOS-TICAM1
TICAM1_L207W_R	ggctgatttccCagttgctggccagggag	Generation of L207W variant in pEF-BOS-TICAM1
TICAM1_S219R_F	catgcccttcctcCgcctgcaccgcagcccac	Generation of S219R variant in pEF-BOS-TICAM1
TICAM1_S219R_R	gtgggctgcggtgcaggcGgaggaagggcatg	Generation of S219R variant in pEF-BOS-TICAM1
TICAM1_P234S_F	gctctgtgacgacTcccaggccagcttggtgcccg	Generation of P234S variant in pEF-BOS-TICAM1
TICAM1_P234S_R	cgggcaccaagctggcctgggAgtcgtcacagagc	Generation of P234S variant in pEF-BOS-TICAM1
TICAM1_P244L_F	ccagcttggtgcccgagcctgtccTcggtggc	Generation of P244L variant in pEF-BOS-TICAM1
TICAM1_P244L_R	gccaccgAggacaggctcgggcaccaagctgg	Generation of P244L variant in pEF-BOS-TICAM1
TICAM1_G245S_F	tgcccgagcctgtccccAgtggctgccaggagcc	Generation of G245S variant in pEF-BOS-TICAM1

TICAM1_G245S_R	ggctcctggcagccacTggggacaggctcgggca	Generation of G245S variant in pEF-BOS-TICAM1
TICAM1_S258L_F	ccgccatTgggggagattgccag	Generation of S258L variant in pEF-BOS-TICAM1
TICAM1_S258L_R	ctggcaatctcccccAatggcgg	Generation of S258L variant in pEF-BOS-TICAM1
TICAM1_P271S_F	cagagctgccaagcagcTcacctcctgggcttccc	Generation of P271S variant in pEF-BOS-TICAM1
TICAM1_P271S_R	gggaagcccaggaggtgAgctgcttggcagctctg	Generation of P271S variant in pEF-BOS-TICAM1
TICAM1_D281H_F	gaagtggccccaCatgcaacctcc	Generation of D281H variant in pEF-BOS-TICAM1
TICAM1_D281H_R	ggaggttgcatGtggggccacttc	Generation of D281H variant in pEF-BOS-TICAM1
TICAM1_A282G_F	gccccagatgGaacctccactggcctccc	Generation of A282G variant in pEF-BOS-TICAM1
TICAM1_A282G_R	gggaggccagtggaggTtccatctggggc	Generation of A282G variant in pEF-BOS-TICAM1
TICAM1_T283N_F	cagatgcaaActccactggcctccctgatacc	Generation of T283N variant in pEF-BOS-TICAM1
TICAM1_T283N_R	ggtatcagggaggccagtggagTttgcatctg	Generation of T283N variant in pEF-BOS-TICAM1
TICAM1_D289N_F	ccactggcctccctAatacccccgcagc	Generation of D289N variant in pEF-BOS-TICAM1
TICAM1_D289N_R	gctgcgggggtatTagggaggccagtgg	Generation of D289N variant in pEF-BOS-TICAM1
TICAM1_V302L_F	agcaccaactacccaCtggagtgcaccgaggggt	Generation of V302L variant in pEF-BOS-TICAM1
TICAM1_V302L_R	acccctcggtgcactccaGtgggtagttggtgct	Generation of V302L variant in pEF-BOS-TICAM1
TICAM1_T346A_F	cacctctccaaatGccaagccgtgccc	Generation of T346A variant in pEF-BOS-TICAM1
TICAM1_T346A_R	gggcacggcttggCatttggagaggtg	Generation of T346A variant in pEF-BOS-TICAM1
TICAM1_T377I_F	ttcagctcacctgaTcccctcctccctgtt	Generation of T377I variant in pEF-BOS-TICAM1
TICAM1_T377I_R	aacagggaggaggggAtcaggtgagctgaa	Generation of T377I variant in pEF-BOS-TICAM1
TICAM1_T377N_F	gctcacctgaAcccctcctccctg	Generation of T377N variant in pEF-BOS-TICAM1
TICAM1_T377N_R	cagggaggaggggTtcaggtgagc	Generation of T377N variant in pEF-BOS-TICAM1
TICAM1_L386P_F	ccctgttcccttcctcccCggaatcatcatcggaac	Generation of L386P variant in pEF-BOS-TICAM1
TICAM1_L386P_R	gttccgatgatgattccGgggaggaagggaacaggg	Generation of L386P variant in pEF-BOS-TICAM1

TICAM1_Q392K_F	catcatcggaaAagaaattctataactttgtg	Generation of Q392K variant in pEF-BOS-TICAM1
TICAM1_Q392K_R	cacaaagttatagaatttctTttccgatgatg	Generation of Q392K variant in pEF-BOS-TICAM1
TICAM1_E429X_F	ggccaccttctgcTaggatttccagg	Generation of E429X variant in pEF-BOS-TICAM1
TICAM1_E429X_R	cctggaaatcctAgcagaaggtggcc	Generation of E429X variant in pEF-BOS-TICAM1
TICAM1_I452T_F	gaccactcagctttcaCcatcctacttctcacc	Generation of I452T variant in pEF-BOS-TICAM1
TICAM1_I452T_R	ggtgagaagtaggatgGtgaaagctgagtggtc	Generation of I452T variant in pEF-BOS-TICAM1
TICAM1_S465N_F	cttcgactgtcgcctgaAcctgcaccaggtg	Generation of S465N variant in pEF-BOS-TICAM1
TICAM1_S465N_R	cacctggtgcaggTtcaggcgacagtcgaag	Generation of S465N variant in pEF-BOS-TICAM1
TICAM1_G481A_F	acctcacgcgacaggCgtcgccagac	Generation of G481A variant in pEF-BOS-TICAM1
TICAM1_G481A_R	gtctggcgacGcctgtcgcgtgaggt	Generation of G481A variant in pEF-BOS-TICAM1
TICAM1_L533F_F	ccccacaggTttcaggcccgaaagg	Generation of L533F variant in pEF-BOS-TICAM1
TICAM1_L533F_R	cctttcgggcctgaaAcctgtgggg	Generation of L533F variant in pEF-BOS-TICAM1
TICAM1_D557N_F	agagccaacacctgAacggtgagcggatgc	Generation of D557N variant in pEF-BOS-TICAM1
TICAM1_D557N_R	gcatccgctcaccgtTcaggtgttggctct	Generation of D557N variant in pEF-BOS-TICAM1
TICAM1_A565S_F	gatgcaggcggcgTcactgaacgcag	Generation of A565S variant in pEF-BOS-TICAM1
TICAM1_A565S_R	ctgcgttcagtgAcgccgcctgcatc	Generation of A565S variant in pEF-BOS-TICAM1
TICAM1_L574V_F	cgcagcctactcagcctacGtccagagctacttgtcc	Generation of L574V variant in pEF-BOS-TICAM1
TICAM1_L574V_R	ggacaagtagctctggaCgtaggctgagtaggctgcg	Generation of L574V variant in pEF-BOS-TICAM1
TICAM1_M595L_F	gtggcttttgggagccacTtgtcatttgggactg	Generation of M595L variant in pEF-BOS-TICAM1
TICAM1_M595L_R	cagtcccaaatgacaAgtggctcccaaaagccac	Generation of M595L variant in pEF-BOS-TICAM1
TICAM1_G598W_F	ccacatgtcatttTggactggggcgccctat	Generation of G598W variant in pEF-BOS-TICAM1
TICAM1_G598W_R	atagggcgccccagtccAaaatgacatgtgg	Generation of G598W variant in pEF-BOS-TICAM1
TICAM1_G611S_F	gaatgccctttgggAgccaggtgccc	Generation of G611S variant in pEF-BOS-TICAM1

TICAM1_G611S_R	gggcacctggcTcccaaagggcattc	Generation of G611S variant in pEF-BOS-TICAM1
TICAM1_P620S_F	ggagccccgccaTcctttcccacttgg	Generation of P620S variant in pEF-BOS-TICAM1
TICAM1_P620S_R	ccaagtgggaaaggAtggcggggctcc	Generation of P620S variant in pEF-BOS-TICAM1
TICAM1_P628S_F	ttggccggggtgcTcgcagccgcc	Generation of P628S variant in pEF-BOS-TICAM1
TICAM1_P628S_R	ggcggctgcgAgcaccccggccaa	Generation of P628S variant in pEF-BOS-TICAM1
TICAM1_P658L_F	gcccttccTgcagtccccagccttc	Generation of P658L variant in pEF-BOS-TICAM1
TICAM1_P658L_R	gaaggctggggactgcAggaagggc	Generation of P658L variant in pEF-BOS-TICAM1
TICAM1_A666T_F	gccttccctacgAcctcacccgcaccccc	Generation of A666T variant in pEF-BOS-TICAM1
TICAM1_A666T_R	gggggtgcgggtgaggTcgtagggaaggc	Generation of A666T variant in pEF-BOS-TICAM1
TICAM1_Q702R_F	accagagagggtcccGggcgcccgaggacaa	Generation of Q702R variant in pEF-BOS-TICAM1
TICAM1_Q702R_R	ttgtcctcgggcgccCgggaccctctctggt	Generation of Q702R variant in pEF-BOS-TICAM1

2.4 Site-directed mutagenesis (SDM)

Dr Stephanie Hodeib conducted site-directed mutagenesis (SDM) using the QuikChange Lightning Site-Directed Mutagenesis Kit (Agilent Technologies) following the guidelines provided by the manufacturer for the introduction of the point mutation into the wildtype expression vector, pEF-BOS-TICAM1. The generation of mutant alleles was achieved through PCR under the following conditions: an initial denaturation at 95°C for 10 minutes, followed by 18 cycles of amplification with each consisting of denaturation 95°C for 20 seconds, annealing at X°C for 10 seconds, 68°C for 4.5 minutes and one final extension at 68°C for 5 minutes after the completion of 18 cycles. The annealing temperatures were adjusted based on the custom designed primer pairs (Table 2.3), typically aiming for a temperature approximately 5°C lower than the melting temperature. The PCR product's parental plasmids were subjected to digestion with the restriction enzyme DpnI at 37°C for 5 minutes and the followed by transformation. Dpn1-treated PCR products from SDM were transformed into E. coli XL10-Gold ultracompetent cells (Agilent). In the transformation stage, 2 µl of Dpn1-treated PCR mutagenesis products were combined with 25 µl of competent cells and chilled on ice for 30 minutes. Subsequently, a 30-second heat shock at precisely 42°C in a water bath was followed by immediate return to ice for an additional 2 minutes. Next, 200 µl of SOC media (Invitrogen) was added to the mixture and placed in a shaking incubator (225 rpm) at 37°C and 5% CO_2 for 30-60 minutes. Following the incubation period, the cells were then plated onto Luria-Brentani (LB) agar plates [mix of LB powder (Sigma) and agar (Sigma)] and supplemented with ampicillin (100 µg/ml), and left to incubate overnight at 37°C and 5% CO_2. The next day, individual colonies from the overnight culture were selected and cultured in LB liquid broth with ampicillin and left to grow overnight in a shaking incubator (225 rpm) at 37°C and 5% CO_2.

The plasmids obtained from the overnight LB broth culture were extracted and isolated using the QIAprep® Spin Miniprep Kit (QIAGEN), following the manufacturer's instructions. Quantification of the eluted plasmids was accomplished using a Nanodrop™ 2000/2000c spectrophotometer (Thermo Fisher Scientific). To validate the successful introduction of the single nucleotide substitution within the specified target regions, the isolated plasmids were

sent off for sanger sequencing. Genewiz, Azenta Life Sciences (https://www.genewiz.com/en-GB) performed this sequencing procedure using the designed primers in Table 2.2. Furthermore, comprehensive sequencing of the full-length plasmids was carried out by another company, Plasmidsaurus (https://www.plasmidsaurus.com).

2.5 Transient transfection

TICAM1-deficient (TICAM1$^{-/-}$) SV40 fibroblasts or HEK293 cells were seeded in 24-well plate at a density of 0.16 x 10^6 cells/well overnight to achieve approximately 90% confluent monolayer the next day. The culture media was removed and replaced with 500 µl of fresh supplemented culture media before transfection. Transient transfections were conducted using the Lipofectamine™ 3000 Transfection Reagent (Invitrogen) in accordance with the manufacturer's instructions. Plasmid DNA was diluted to appropriate concentration in 25 µl of Opti-MEM medium (Gibco) in a tube and the total amount of DNA (500 ng/well) was maintained constant by the addition of pEF-BOS empty vector. Typically, the mixture consisted of 100 ng of pEF-BOS-TICAM1 variant, 100 ng of IFN-β or NF-κB promoter luciferase, 10 ng of pRL-TK renilla luciferase, and the necessary pEF-BOS empty vector to reach the specified total amount of DNA quantity (500 ng/well). In a separate tube, 1.5 µl of Lipofectamine™ 3000 Reagent was mixed with 23.5 µl of Opti-MEM medium. The contents of both tubes were subsequently combined and allowed to incubate at room temperature for at least 15 minutes. The combined mixture was then carefully added drop by drop to the cells. Following this, the plates were incubated at 37°C with 5% CO_2 for a minimum of 24 hours. Transfection efficiency was assessed in the beginning using fluorescent microscopy with an EVOS™ FL Auto 2 (Invitrogen) looking for GFP expression, where applicable. For western blot and immunofluorescence assay involving the transfection of TICAM1, apoptosis was inhibited by adding 20 µM z-VAD-fmk (Sigma-Aldrich) to each well before transfection.

2.6 Dual luciferase reporter assay

TICAM1-deficient fibroblasts cells were seeded in 24-well plates and subjected to transfection with the designated expression vectors following the previously outlined procedure (see Section 2.5). After 24 hours of transfection, spent media were removed and cells were washed once with PBS. Passive lysis buffer from the Dual-Luciferase Reporter Assay System (Promega Corporation) kit was added to the cells and placed onto a plate shaker for 15 minutes. The resulting cell lysates were mechanically harvested and transferred to a 96-well flat-bottom white cell culture treated plate (Corning Costar). Subsequent analysis was carried out using the Dual-Luciferase Reporter Assay System according to the manufacturer's guidelines and measurements were acquired using FLUOstar® Omega (BMG Labtech). The values of Firefly luciferase were normalized against Renilla luciferase activity and presented as a fold change relative to cells transfected wildtype vector.

2.7 Cell viability assay

Cell viability was evaluated using the CellTiter 96® AQueous One Solution Cell Proliferation Assay (MTS assay) from Promega Corporation, following the manufacturer's instructions. In the same setting consistent with the procedure outlined in Section 2.5, TICAM1-deficient fibroblasts cells were seeded in 24-well plates and subsequently, the cells were transiently transfected with either TICAM1 WT or TICAM1 variants. The MTS reagent was introduced to all wells 24 hours post-transfection, while the control wells containing only TICAM1-deficient cells received lysis buffer (Promega Corporation) 15 minutes before the addition of the MTS reagent. Photometric measurement of the endpoint colour was performed one hour after the addition of MTS into the wells at 490 nm using a Versamax microplate reader (Molecular Devices). To obtain accurate values, background absorbance calculated for lysed cells was subtracted from the other samples, and 100% viability was correlated with the absorbance of non-transfected cells. The calculation was based on this formula:

$$\% \text{ Viability} = \frac{(x\text{-Min})}{(\text{Max-Min})} \times 100\%$$

Min – wells containing lysis buffer that served as the negative control

Max – positive control wells

2.8 Western blotting

2.8.1 Protein isolation and quantification

The adherent cells were washed with PBS and then followed by mechanically detachment, harvesting, and immediate placement on ice to prevent degradation of lysates. Subsequently, the cells underwent centrifugation at 500g for 5 minutes at 4°C, and the supernatant was discarded. As for cerebral organoids, they were gently washed with PBS and centrifuged at 6000g for 5 minutes at 4°C, with the supernatant then being discarded. To proceed with cell lysis, the cell pellets or cerebral organoids were resuspended in RIPA buffer (Sigma), complemented with 1x Halt™ Protease and Phosphatase Inhibitor Cocktail (Thermo Scientific) and then allowed to incubate on ice for at least 30 minutes. Following this, samples were centrifuged at 13,000g for 20 minutes at 4°C, and the resulting cell lysates were returned to ice. These cells lysates were transferred to a fresh Protein LoBind® Tubes (Eppendorf) and were ready for immediate use in the downstream applications or for storage at -80 °C. Protein was quantified using the Pierce™ Coomassie (Bradford) Protein Assay Kit (Thermo Fisher Scientific) following the manufacturer's Standard Microplate Protocol. Absorbance was measured at 595 nm using a Versamax microplate reader (Molecular Devices).

2.8.2 Sodium dodecyl sulphate polyacrylamide gel electrophoresis (SDS-PAGE)

After protein quantification, protein lysates concentrations were made equal across samples to a total volume of 6.5 µl, supplemented with additional 1 µl of 10x NuPAGE Sample Reducing Agent (Thermo Fisher Scientific) and 2.5 µl of 4x NuPAGE LDS Sample Buffer (Thermo Fisher Scientific), resulting in a final volume of 10 µl for one well. The prepared protein lysated mixture were subsequently denatured for 10 minutes at 70 °C and promptly cooled on ice. A precast 4-12% gradient polyacrylamide NuPAGE™ Bis-Tris, 1.0 mm, Midi Protein Gels (Thermo Fisher Scientific) were set up using adaptors for the reservoir and positioned in a Criterion™ Cell tank (Bio-Rad). The tank and gel reservoirs were filled with 1x XT MES Running Buffer (Bio Rad). Individual wells were loaded with 10 µl of each sample. Precision Plus Protein Dual Colour Standards ladder (Bio Rad) was run on each end of the gel and served as the protein ladder. Gel electrophoresis was then conducted at 100 Volts for a minimum of 3 hours to ensure optimal protein separation.

2.8.3 Membrane transfer

After gel electrophoresis, the separated proteins were transferred from the polyacrylamide gel to a polyvinylidene difluoride (PVDF) membrane using the semi-dry transfer system iBlot™ Transfer Stacks (Invitrogen) and iBlot™ 2 Gel Transfer Device system (Invitrogen) in accordance with the manufacturer's instructions. The semi-dry blotting transfer method involved applying 20 V for 1 minute, followed by 23 V for 4 minutes, and finally, 25 V for 2 minutes. Subsequently, the membranes containing the transferred proteins were trimmed to the desired size and placed in a blocking buffer consisting of 5% Bovine Serum Albumin (BSA) in 1X Tris-Buffered Saline, 0.1% Tween (Sigma) (TBS-T) for a minimum of 1 hour with gentle rocking.

2.8.4 Protein revelation

Membranes were incubated with primary antibodies (Table 2.4) diluted in either 5% BSA or 5% 1X Pierce™ Clear Milk Blocking Buffer (Thermo Fisher Scientific) in 1X TBS-T buffer overnight at 4°C with gentle rocking. The antibody specification and dilution can be found in the accompanying Table. Following day, the membranes were retrieved and washed at least three times with 1X TBS-T for 5 minutes each round with gentle rocking to remove excess antibody. Subsequently, the membranes were incubated in either 1% BSA or 1% milk in 1x TBS-T buffer, with secondary IgG antibodies conjugated to horseradish peroxidase (HRP) (Table 2.4) at room temperature for 1 hour with gentle rocking. The antibodies bound to proteins were detected using the ECL Western Blotting kit from Cytiva, visualised through Azure BioSystems c600, and analyzed with Fiji/ImageJ software.

Table 2.4 Antibodies used in this thesis

Antibodies	Dilutions	Diluent buffer	Application		Source and catalogue number
TICAM1	1 in 1000	5% BSA in 1x TBS-T (0.1%)	Western blot	Primary	Cell Signaling Technology, 4596S
	1 in 100	1% BSA in PBS	Immunofluorescence	Primary	
HA	1 in 1000	5% BSA in 1x TBS-T (0.1%)	Western blot	Primary	Sigma, H6908
	1 in 100	1% BSA in PBS	Immunofluorescence	Primary	
GAPDH	1 in 1000	5% milk in 1x TBS-T (0.1%)	Western blot	Primary	Cell Signaling Technology, 3683S
TLR3	1 in 1000	5% BSA in 1x TBS-T (0.1%)	Western blot	Primary	R&D Systems, AF1487
LC3B	1 in 1000	5% BSA in 1x TBS-T (0.1%)	Western blot	Primary	Abcam, ab48394
	1 in 100	1% BSA in PBS	Immunofluorescence	Primary	
p62	1 in 1000	5% BSA in 1x TBS-T (0.1%)	Western blot	Primary	MBL Intl, PM045
TBK1	1 in 1000	5% BSA in 1x TBS-T (0.1%)	Western blot	Primary	Cell Signaling Technology, 3013S
pTBK1 (Ser172)	1 in 1000	5% BSA in 1x TBS-T (0.1%)	Western blot	Primary	Cell Signaling Technology, 5483S
IRF3	1 in 1000	5% BSA in 1x TBS-T (0.1%)	Western blot	Primary	Cell Signaling Technology, 4302S
pIRF3 (Ser396)	1 in 1000	5% BSA in 1x TBS-T (0.1%)	Western blot	Primary	Cell Signaling Technology, 4947S

Donkey anti-rabbit IgG HRP	1 in 10,000	1% BSA in 1x TBS-T (0.1%)	Western blot	Secondary	GE Healthcare, NA934
Rabbit anti-Goat IgG HRP	1 in 10,000	1% BSA in 1x TBS-T (0.1%)	Western blot	Secondary	Invitrogen, 31402
Beta-III Tubulin/Tuj1	1 in 100	1% BSA in PBS	Immunofluorescence	Primary	Bio-Techne Ltd., NL1195V
CTIP2	1 in 750	1% BSA in PBS	Immunofluorescence	Primary	Abcam, ab18456
MAP2	1 in 2000	1% BSA in PBS	Immunofluorescence	Primary	Abcam, ab5392
Nestin	1 in 1000	1% BSA in PBS	Immunofluorescence	Primary	Sigma-Aldrich, ABD69
SOX2	1 in 750	1% BSA in PBS	Immunofluorescence	Primary	Bio-Techne Ltd., mab2018
TBR2	1 in 750	1% BSA in PBS	Immunofluorescence	Primary	Abcam, ab23345
DyLight™ 488 Goat anti-Rabbit IgG	1 in 1000	1% BSA in PBS	Immunofluorescence	Secondary	Invitrogen, A-11001
Alexa Fluor™ 488 Goat anti-Chicken IgG	1 in 1000	1% BSA in PBS	Immunofluorescence	Secondary	Invitrogen, A-11039
Alexa Fluor™ 488 Goat anti-Mouse IgG	1 in 1000	1% BSA in PBS	Immunofluorescence	Secondary	Invitrogen, A28175
Alexa Fluor™ 488 Goat anti-Rat IgG	1 in 1000	1% BSA in PBS	Immunofluorescence	Secondary	Invitrogen, A-11006
Alexa Fluor™ Plus 594 Goat anti-Chicken IgY	1 in 1000	1% BSA in PBS	Immunofluorescence	Secondary	Invitrogen, A32759
Alexa Fluor™ 594 Goat anti-Mouse IgG	1 in 1000	1% BSA in PBS	Immunofluorescence	Secondary	Invitrogen, A-11020
Alexa Fluor™ 594 Goat anti-Rabbit IgG	1 in 1000	1% BSA in PBS	Immunofluorescence	Secondary	Invitrogen, A-11012
Alexa Fluor™ 647 Goat anti-Chicken IgY	1 in 1000	1% BSA in PBS	Immunofluorescence	Secondary	Invitrogen, A-21449
Alexa Fluor™ 647 Goat anti-Mouse IgG	1 in 1000	1% BSA in PBS	Immunofluorescence	Secondary	Invitrogen, A-21235
Alexa Fluor™ 647 Goat anti-Rat IgG	1 in 1000	1% BSA in PBS	Immunofluorescence	Secondary	Invitrogen, A-21247

2.9 Immunoprecipitation

Total cell extracts were harvested the same way as outlined in Section 2.8.1 with a slight modification involving the use of a milder lysis buffer. The cell pellets were resuspended with a lysis buffer composed of 5 ml TRIS 1M (pH 7.4), 3 ml NaCl 5M, 5 ml 10% Triton, 0.2 ml EDTA 0.5M and topped up with 87 ml double distilled water. The lysis buffer was also supplemented with 1x Halt™ Protease and Phosphatase Inhibitor Cocktail (Thermo Scientific). The lysates were left to incubate on ice for at least 30 minutes before undergoing for sonification using Bioruptor® Sonication System (Diagenode). This step was implemented to further disrupt cell membranes and facilitate DNA degradation thereby preventing the lysates from becoming viscous. To maintain a low temperature during sonication, the sonicator's water bath was filled with cold water and crushed ice, ensuring it remained at 4°C throughout the process. The sonicator operated in cycles of 15 seconds on and 45 seconds off, repeated three times to prevent overheating of the samples. The lysates were returned on ice for an additional 30 minutes before undergoing centrifugation at 13,000g for 20 minutes at 4°C and subsequent transfer to Protein LoBind tubes. The protein concentrations were quantified as described previously (Section 2.8.1).

Dynabeads™ Protein G Immunoprecipitation Kit (Invitrogen) was used here for protein immunoprecipitation (IP) following the manufacturer's protocol. To initiate the process, Dynabeads™ magnetic beads were resuspended by vortexing for 30 seconds and 50 µl of the suspension were transferred into a tube. Subsequently, the tube was then placed on a DynaMag™-2 Magnet (Invitrogen) to separate the beads from the supernatant which was then discarded. Antibodies at concentration of 1 µg were added to the beads and bound to the magnetic beads through their Fc-region during a 30-minute incubation at 4°C. After the incubation, the tube was positioned on the magnet and the supernatant was removed. The magnetic bead-antibody complex was resuspended with 200 µl of Ab Binding and Washing buffer provided in the kit by gentle pipetting. Subsequently, the tube was placed on the magnet and supernatant was once again removed. Protein lysates at a concentration of 50 µg were added into the tube to resuspend the magnetic bead-antibody complex followed by incubation

at 4°C with rotation for 2 hours to enable the binding of protein lysates antigens to the magnetic bead-antibody complex Following incubation, the tube was placed on the magnet and the supernatant was transferred into a new tube, constituting the flowthrough sample. The magnetic bead-antibody-antigen complex was washed three times using the Ab Binding and Washing buffer by gentle pipetting. Subsequently, the elution of the magnetic bead-antibody-antigen complex was carried out using an elution buffer consisting of 2.5 µl 4x NuPAGE LDS Sample Buffer, 1 µl 10x NuPAGE Sample Reducing Agent, 0.5 µl β-mercapto-ethanol, and water added to top up the buffer to 10µl. These samples then followed heating, gel loading, membrane transfer and imaging procedures outline in Sections 2.8.2 - 2.8.4. In addition to these samples, normal lysates prepared for Western blot and the flowthrough samples were also run on the gel.

2.10 Ligand stimulation

Stimulations were conducted in DMEM GlutaMAX supplemented with 10% FBS unless specified otherwise. A synthetic analog of double-stranded RNA, poly(I:C) (GE Healthcare), was applied at concentrations ranging from 10 to 50 µg/ml. Additionally, lipopolysaccharide (LPS E. Coli K12, Invivogen) was used at a concentration of 100 ng/ml, interleukin-1β (IL-1β) (R&D Systems) at 20 ng/ml, and tumor necrosis factor-α (TNF-α) (R&D Systems) at 20 ng/ml. Lipofectamine™ 3000 Transfection Reagent (Invitrogen) was used to transfect 25 µg/ml of poly(I:C). Both primary and SV40-fibroblast cell lines underwent stimulation for 24 hours with supernatants being collected at the end of this period.

2.11 Cytokines measurement using Meso-scale discovery (MSD) and enzyme-linked immunosorbent assay (ELISA)

The quantification of IFN-β, IFN-λ/IL-29 and IL-6 cytokines in culture supernatants was performed using the MesoScale Discovery (MSD) platform (U-PLEX Biomarker Group 1

human Assays) following the manufacturer's instructions with the incorporation of two extra serial dilution concentrations at the lower end. The quantification of IL-2, IL-4 and IL-10 cytokines in culture supernatants was measured using the MSD platform (V-PLEX Proinflammatory Panel 1 Human Kit) following the manufacturer's instructions. All MSD plates were read using MESO QuickPlex SQ 120 (MSD).

The quantification of IL-6 cytokines in some experiments was carried out using Human IL-6 DuoSet ELISA (R&D Systems) and performed in accordance with the manufacturer's instructions. Absorbance readings were taken at 450 nm and 540 nm using a Versamax microplate reader with readings at 540 nm subtracted from those at 450 nm.

2.12 Viral strains and propagation

In the course of this research, we used the HSV1-GFP (KOS) strain that features green fluorescent protein (GFP) tag attached to its capsid protein VP26 (Desai & Person, 1998). Additionally, Professor Trine Mogensen in Aarhus University, Denmark, has graciously gifted us HSV-2-mCherry (Hait et al., 2020). Both of these strains were propagated through inoculation of Vero cell. In brief, Vero cells were cultivated to full confluency in a T75 cm^2 culture flask and subsequently infected with either HSV-1 or HSV-2. Infections were allowed to progress for several days until the monolayer of Vero cells exhibited cytopathic effects characterised by the rounding up of the Vero cells. The flask then was subjected to freezing at -80°C overnight and thawed on ice the following day. The flask was mechanically scrapped, and the culture medium was collected and centrifuged at 2000 rpm for 5 minutes at 4°C to pellet the cells. The resulting supernatants containing either HSV-1 or HSV-2 viruses were harvested and further filtered through a 0.45 μm filter to separate the infectious viral stock from the cellular debris. The multiplicity of infection (MOI) or titre of viral stocks was determined by titrating on control dermal fibroblasts using the 50% tissue culture infective dose ($TCID_{50}$).

2.13 Infection and treatment

Cells seeded in plates were grown to 80-90% confluency before being exposed to the virus. In infection experiments, the duration of infection and viral dosage (MOI) are specified in the figure legends. Viral inoculums were prepared in DMEM GlutaMAX supplemented with 2% of FBS and added to the cells for a two-hour of adsorption period. Following this, the culture media was replaced with a fresh DMEM GlutaMAX supplemented with 2% of FBS, with or without added treatments and maintained until the end of the experiment. The drug treatments used in this study were Human IFN-α2a (PBL Assay Science) at a concentration of 100 units/ml, Aciclovir (Sigma) at 100 μM, and Dexamethasone (Sigma) at 1 μg/ml.

2.14 Plaque assay

Plaque assay was used as one of the techniques used to assess viral titers obtained from experiments. Instead of collecting the supernatants solely, lysates were prepared by mechanically scraping infected cells and collecting the entire cell lysates in the supernatants into a tube. The tubes were then centrifuged at 500g at 4°C and the resulting supernatants were collected. In brief, Vero cells were plated in 12-well plates at a density of 0.25 x 10^6 cells/well and allowed to grow overnight. On the following day, the viral inoculum was prepared through serial dilution at a ratio of 1:10 in DMEM GlutaMAX supplemented with 2% of FBS, resulting in dilutions ranging from 10^{-1} to 10^{-6}. Duplicates of 0.6 ml inoculum were added per well and incubated on Vero cells for a two-hour of adsorption before replacing the medium with fresh DMEM GlutaMAX 2% of FBS mixed with 3% carboxymethyl cellulose (CMC, 1:1 ratio of high viscosity CMC and low viscosity CMC, Sigma). The addition of CMC created an overlay on the cells, confining the infection and facilitating the formation of distinct plaques. The cells were then incubated in 37°C with 5% CO_2 for 3 days. Well images were captured using an EVOS™ FL Auto 2 (Invitrogen) with 25% well coverage, and the total number of plaques was multiplied by four. The count of plaques was tallied, and the plaque-forming units (PFU) per ml were calculated using the following formula:

$$\text{PFU/ml} = \frac{\text{Average number of plaques}}{\text{Dilution factor} \times \text{Inoculum volume}}$$

2.15 50% Tissue culture Infective Dose ($TCID_{50}$)

$TCID_{50}$ was used as another technique used to evaluate viral titres obtained from experiments using Vero cells. Vero cells were seeded in a 96-well plate to full confluency. Subsequently, 10 µl of harvested supernatants was added to the first-row wells which contained 90 µl of DMEM GlutaMAX supplemented with 2% of FBS, resulting in a dilution of 10^{-1}. Serial dilutions were carried out, ranging from 10^{-1} to 10^{-8} and three biological samples were used each with three replicates. These plates were then incubated for 7 days. The data were calculated using an online calculator employing the Spearman–Kärber method (https://www.virosin.org/tcid50/TCID50) (Lei et al., 2021).

2.16 Quantitative RT-PCR (RT-qPCR)

Total RNA extraction was performed using the RNeasy Plus Mini Kit (Qiagen) following the manufacturer's guidelines. Briefly, cells and tissues were first lysed and homogenised in Buffer RLT plus. The lysates were subsequently processed through a gDNA Eliminator spin column, effectively removing genomic DNA selectively and efficiently. To establish suitable binding conditions for RNA, 70% ethanol was added. The samples were then transferred to a RNeasy spin column and centrifuged, where RNA bound to the membrane while contaminants were removed. High-quality RNA was then eluted from the column. For cerebral organoids, the initial step involves the gentle enzymatic dissociation of the organoids using Neural Tissue Dissociation Kits (Miltenyi Biotec), ensuring the efficient harvest of viable cells. Cerebral organoids were washed with HBSS (without calcium and magnesium, Gibco), followed by the addition of enzyme mix 1, and a subsequent incubation at 37°C for 15 minutes. This was

succeeded by the addition of enzyme mix 2, accompanied by a 10-minute incubation at 37°C. The resultant mixture was centrifuged for 5 minutes at 6000g, following which the supernatant was removed and the remaining material was resuspended in Buffer RLT plus. The subsequent RNA extraction process proceeded as detailed above.

RNA was reverse transcribed into cDNA using the High-capacity RNA-to-cDNA kit (Thermo Fisher Scientific). The resulting cDNA was subjected to amplification with designated probes through real-time PCR with TaqMan™ Universal Master Mix II, no UNG (Thermo Fisher Scientific) following the manufacturer's protocol. Probes used were as follows: human TICAM1 (assay ID Hs00706140_s1), with human β-glucuronidase (GUSB) (assay ID Hs00939627_m1) used as normalisation. Additionally, we designed Taqman custom human assay probes tagged with fluorescent labels targeting HSV-1 *US12* gene that encodes for ICP47 in alignment with the approach outlined by Salgado et al. (Salgado et al., 2023). ICP47 (US12) - Taqman forward primer: 5′-CGTACGCGATGAGATCAATAAAAGG-3′; reverse primer: 5′-GCTCCGGGTCGTGCA-3′; TaqMan probe: 5″-AGGCGGCCAGAACC-3. The qPCR process was performed on an ABI StepOnePlus Real-Time PCR System (Applied Biosystems). Results are expressed according to the ΔΔCt method. Data analysis was performed using StepOne Software V2.1.

2.17 Reprogramming PBMCs into iPSCs

PBMCs from 1024M's blood was extracted by our team following procedures in Section 2.2. The PBMC was sent it to Harry Leitch's lab at Hammersmith campus of Imperial College London where his research associate, Lucy Watson, kindly reprogrammed the PBMCs into iPSCs using CytoTuneTM-iPS 2.0 Sendai Reprogramming Kit (Thermo Fisher Scientific). Briefly, PBMCs were transduced with the Sendai virus vectors provided in the kit. These harbor transgenes encoding hOct3/4, hSox2, hKlf4, and hc-Myc factors. Upon transduction, these viral vectors induce the expression of these four genes within the cells leading to the reprogramming process. Media was replaced every day and on day 7, cells were transferred to

geltrex coated plates. iPSC colonies became apparent within a week, and by the end of four weeks, they were prepared for isolation and subsequent expansion onto new geltrex-coated plates. Ms Aneesa Ali has graciously continued culturing these iPSCs through more than 10 passages and regularly testing for the presence of Sendai virus vectors by RT-PCR with primers (shown in Table 2.5) at final concentration of 200 nM. Total RNA extraction was performed using the RNeasy Plus Mini Kit (Qiagen) following the manufacturer's guidelines. RNA was reverse transcribed into cDNA using the High-capacity RNA-to-cDNA kit (Thermo Fisher Scientific). RT-PCR was performed under the following conditions: an initial denaturation at 95°C for 30 seconds, followed by 30 cycles of amplification with each consisting of denaturation 95°C for 30 seconds, annealing at 52°C for 30 seconds, 68°C for 1 minute and one final extension at 68°C for 5 minutes after the completion of 30 cycles. After confirming the clearance of the Sendai virus vectors, these iPSCs were deemed ready for differentiation into cortical neurons and cerebral organoids.

Table 2.5 Primers used to detect Sendai virus vectors

Primer	Sequence (5' to 3')	Product size	Anneal temperature
SeV F	GGA TCA CTA GGT GAT ATC GAG C	181 bp	52°C
SeV R	ACC AGA CAA GAG TTT AAG AGA TAT GTA TC		
KOS F	ATG CAC CGC TAC GAC GTG AGC GC	528 bp	52°C
KOS R	ACC TTG ACA ATC CTG ATG TGG		
KLF4 F	TTC CTG CAT GCC AGA GGA GCC C	410 bp	52°C
KLF4 R	AAT GTA TCG AAG GTG CTC AA		
cMYC F	TAA CTG ACT AGC AGG CTT GTC G	532 bp	52°C
cMYC R	TCC ACA TAC AGT CCT GGA TGA TGA TG		

2.18 Immunofluorescence and image acquisition

2.18.1 Fibroblasts

Fibroblasts cells were seeded onto coverslips (VWR) that had been sterilised using ethanol in 24-well plates and transfected following the previously described procedure (Section 2.5) for 24 hours in a humidified incubator at 37°C with 5% CO_2. Subsequently, these cells were washed once with PBS and fixed using pre-chilled 100% methanol (Sigma) on ice for 15 minutes. After removing the methanol, cells were washed three times with PBS and permeabilized with 0.1% Triton-X-PBS (BDH) for 4 minutes at room temperature. Following another round of PBS wash, the coverslips were blocked with 1% BSA in PBS for at least 10 minutes at room temperature. The coverslips were then placed in a dark humidified chamber and incubated with primary antibody (Table 2.4) for 45 minutes at room temperature. Following seven washes with PBS, the coverslips were incubated with secondary antibody (Table 2.4) in a dark humidified chamber for 45 minutes at room temperature. Subsequently, the coverslips underwent for seven additional washes with PBS and mounted on SuperFrost Microscope Slides (VWR) using ProLong™ Gold Antifade Mountant with DAPI (Invitrogen). The coverslips were sealed with clear varnish on the slides and incubated at 4°C overnight. Imaging was performed on LSM 5 Pascal Confocal microscope (Zeiss). Images were captured 63X oil-immersion lens and image processing was carried out using Fiji/ImageJ Software.

2.18.2 Cortical neurons

On day 35, cortical neurons were passaged onto Poly-D-Lysine (PDL)-coated coverslips (Corning) within 24-well plates with a density of 200,000 cells per well. These cells were subjected to infection following procedure in Section 2.13. Subsequently, these cells were washed once with PBS and fixed using 4% Paraformaldehyde (PFA) solution in PBS (Thermo Fisher Scientific) for 15 minutes. After removing the 4% PFA, cells were washed carefully

three times with PBS and permeabilized with 0.1% Triton-X-PBS for 4 minutes at room temperature. Following another round of PBS wash, the coverslips were blocked with 1% BSA in PBS for at least an hour at room temperature. The coverslips were then incubated with primary antibody (Table 2.4) and placed in a dark humidified chamber overnight at 4°C. The following day, the coverslips were washed three times with PBS and incubated with secondary antibody (Table 2.4) in a dark humidified chamber for an hour at room temperature. Subsequently, the coverslips underwent for three additional washes with PBS and mounted on SuperFrost Microscope Slides using ProLong™ Gold Antifade Mountant with DAPI. Imaging was performed on either Widefield Axio Observer (Zeiss) and Axiovert 135 TV inverted fluorescence microscope (Zeiss). Images were captured with either 40X or 63X oil-immersion lens and image processing was carried out using Fiji/ImageJ Software.

2.18.3 Cerebral organoids

Cerebral organoids embedded in Tissue-Tek® O.C.T. Compound (Sakura) were frozen at -80°C and sent to Experimental Histopathology department at The Francis Crick Institute for cryosectioning. The sections were sliced into 10 μm thickness using a cryostat and mounted onto slides. The sections on the slides were washed with PBS, and then permeabilized with 0.1% Triton-X-PBS for one hour at room temperature. After three washes, the sections were blocked with 5% goat serum in PBS for at least an hour at room temperature. Subsequently, the slides were incubated with the primary antibody (Table 2.4) and placed in a dark humidified chamber overnight at 4°C. The next day, the sections were washed three times with PBS and incubated with the secondary antibody (Table 2.4) in a dark humidified chamber for an hour at room temperature. After three additional washes with PBS, coverslips were mounted on the sections with ProLong™ Gold Antifade Mountant with DAPI sandwiched between the section and coverslip. Imaging was conducted using either Widefield Axio Observer (Zeiss) and Axiovert 135 TV inverted fluorescence microscope (Zeiss). Images were captured with either 20X or 40X and image processing was carried out using Fiji/ImageJ Software.

2.19 Statistical analysis and software

The nucleotide sequences, plasmid mapping, and analyses of sequence chromatograms were performed using SnapGene software (www.snapgene.com). Densitometry analyses of immunoblots was conducted using Fiji/ImageJ software with Band/Peak Quantification Tool macro (Kenji Ohgane, 2019). Immunofluorescence images were processed and analysed using Fiji/ImageJ software. MSD reading data were taken using MESO QuickPlex SQ 120 (MSD) and analysed using Discovery Workbench (MSD). ELISA absorbance data were evaluated using SoftMax Pro 7 software (Molecular Devices). Statistical analyses were carried out using Prism 10 software (GraphPad 10).

Chapter 3

3. *TICAM1* variants in SARS-COV2 infections

The research detailed in this chapter was conducted amidst the peak of the SARS-CoV2 pandemic lockdowns. We were given the opportunity to be a part of COVID Human Genetic Effort (COVIDHGE, https://www.covidhge.com). The urgency of the situation was heightened which demanded a swift response. Given the abrupt initiation of the project and the stringent deadline it entailed, the necessity for prompt and efficient work became paramount. Most of the work conducted in this chapter involved a close collaboration with a fellow laboratory colleague, Dr. Stephanie Hodeib.

3.1 Background

Single-gene inborn errors of immunity affecting the TLR3-IFN pathway were originally associated with HSE but more recently have been implicated in respiratory viral infections (Casrouge et al., 2006; Zhang et al., 2007; Perez de Diego et al., 2010; Guo et al., 2011; Sancho-Shimizu et al., 2011; Herman et al., 2012; Lim et al., 2014; Andersen et al., 2015). Acute respiratory distress syndrome (ARDS) is a rare manifestation of human influenza infection which may lead to life-threatening pneumonitis caused by human influenza virus. A study (Lim et al., 2019) has reported unrelated children with influenza A virus infection manifesting ARDS and harbouring heterozygous *TLR3* variants, P554S and P680S, causing AD TLR3 deficiency. Both missense mutations are located in the N-terminal extracellular domain of TLR3. The P554S variant has been shown to be both LoF and dominant negative and to underlie HSE (Zhang et al., 2007). The P680 residue is crucial in both TLR3 dimerization and dsRNA binding (Wang et al., 2010). The P680L TLR3 protein could not induce IFN-β mRNA when stimulated with poly(I:C) despite having similar TLR3 mRNA levels to controls (Lim et al., 2019). This finding is consistent with another study where the P680L TLR3 mutant in HEK293 cells was found to be LoF for NF-κB activation (Wang et al., 2010). Altogether, (Lim et al., 2019) identifies AD TLR3 deficiency as a novel human genetic etiology of ARDS and highlight that functional TLR3-IFN pathway is important in host defence against influenza

ARDS. Given these findings, COVIDHGE was established to test the hypothesis that previously healthy and young individuals may develop life-threatening COVID-19 due to monogenic inborn errors of immunity to SARS-Cov2 exhibiting either incomplete or complete penetrance (Zhang et al., 2020). In addition to TLR3 described above, inborn errors of immunity in the TLR3, IRF7, and IRF9 pathways have been demonstrated to render individuals susceptible to severe, life-threatening pneumonia caused by influenza through impaired production of type I IFNs (Zhang et al., 2020). Given the established role of these type I IFN pathways in ARDS, this particular pathway was investigated in patients presenting with severe COVID-19.

This research has the potential to enhance our understanding of the extensive interindividual clinical variations within infected populations in collaboration with the international COVIDHGE network which has more than 40 laboratories joined as members and situated all over the world (COVIDGHE, https://www.covidhge.com). Part of the work detailed in this chapter has been published in Zhang et al. (2020) "Inborn errors of type I IFN immunity in patients with life-threatening COVID-19" where I am a second co-author. The primary objective of the project was to investigate the roles of TLR3, IRF7, IRF9 and associated loci within these pathways, including *UNC93B1, TICAM1, TBK1, IRF3, IFNAR1, IFNAR2, STAT1, and STAT2*, in the context of COVID-19 pneumonia. Building on our laboratory's prior expertise in investigating TICAM1 in HSE, our special assignment was to uncover the potential impact of *TICAM1* variants on SARS-COV2 infection and the development of COVID-19 disease.

3.2 Establishment of *TICAM1* variants in life-threatening COVID-19 pneumonia

The COVIDHGE consortia had gathered comprehensive sets of whole-genome (N=364) and whole-exome (N=295) sequences from 659 patients admitted to intensive care due to critical COVID-19 pneumonia (Zhang et al., 2020). Life-threatening COVID-19 pneumonia here was

characterised as patients with pneumonia who progressed to critical disease conditions, including pulmonary cases necessitating mechanical ventilation (BIPAP, CPAP, intubation, hi-flow oxygen), septic shock, or any other organ damage that mandated admission to the intensive care unit. In this cohort of 659 patients, 74.5% were male and 25.5% were female, and a mortality rate of 13.9%. The participants were from diverse ancestral backgrounds and ranged in age from 1 month to 99 years with mean age of 51.8 years (SD 15.9 years). As controls, they included 534 individuals who tested positive for SARS-CoV2 using PCR and/or serological test. Additionally, individuals with typical symptoms like anosmia or ageusia, following exposure to a confirmed COVID-19 case, were enrolled. This group remained either asymptomatic or experienced mild, self-resolving, ambulatory illness.

Genetic analysis was undertaken, specifically searching for nonsynonymous variants, both monoallelic and biallelic, with a minor allele frequency (MAF) < 0.001 across all 13 loci which are *TLR3, IRF7, IRF9, TICAM1, UNC93B1, TRAF3, TBK1, IRF3, NEMO/IKBKG, IFNAR1, IFNAR2, STAT1*, and *STAT2*. They found 118 variants either monoallelic or biallelic at these loci. In addition, a principal component analysis (PCA) adjusted burden test on the 12 autosomal loci (excluding *NEMO* which is X-linked) demonstrated significant enrichment in pathogenic loss-of-function (pLOF) variants in patients relative to controls [P = 0.01; odds ratio (OR) = 8.28; 95% confidence interval (CI) = 1.04 to 65.64] under an AD mode of inheritance. None of the patients enrolled in the study had a history of hospitalisation for severe viral infections prior to contracting COVID-19. From this study of severe COVID-19 patients (hereafter referred to as Zhang's cohort), 20 heterozygous *TICAM1* variants were identified which were functionally tested in our laboratory. After further analysis which takes into account the variant's MAF and patient's illness severity, only 15 *TICAM1* variants were carried forward in the published version (Zhang et al., 2020). However, after the publication we were given 29 additional variants to be tested and here all 49 *TICAM1* variants results will be covered. Figure 3.1 illustrates the identified *TICAM1* variants in a lolliplot which depicts the relationship of the MAF of these variants and their location within the TICAM1 protein domains. Controls used in this chapter involved previously documented *TICAM1* variants which includes R141X, a loss-of-function (LoF) variant, and S186L, a hypomorphic variant (Sancho-Shimizu et al., 2011). Table 3.1 shows list of variants together with their MAF and phenotype of illness severity.

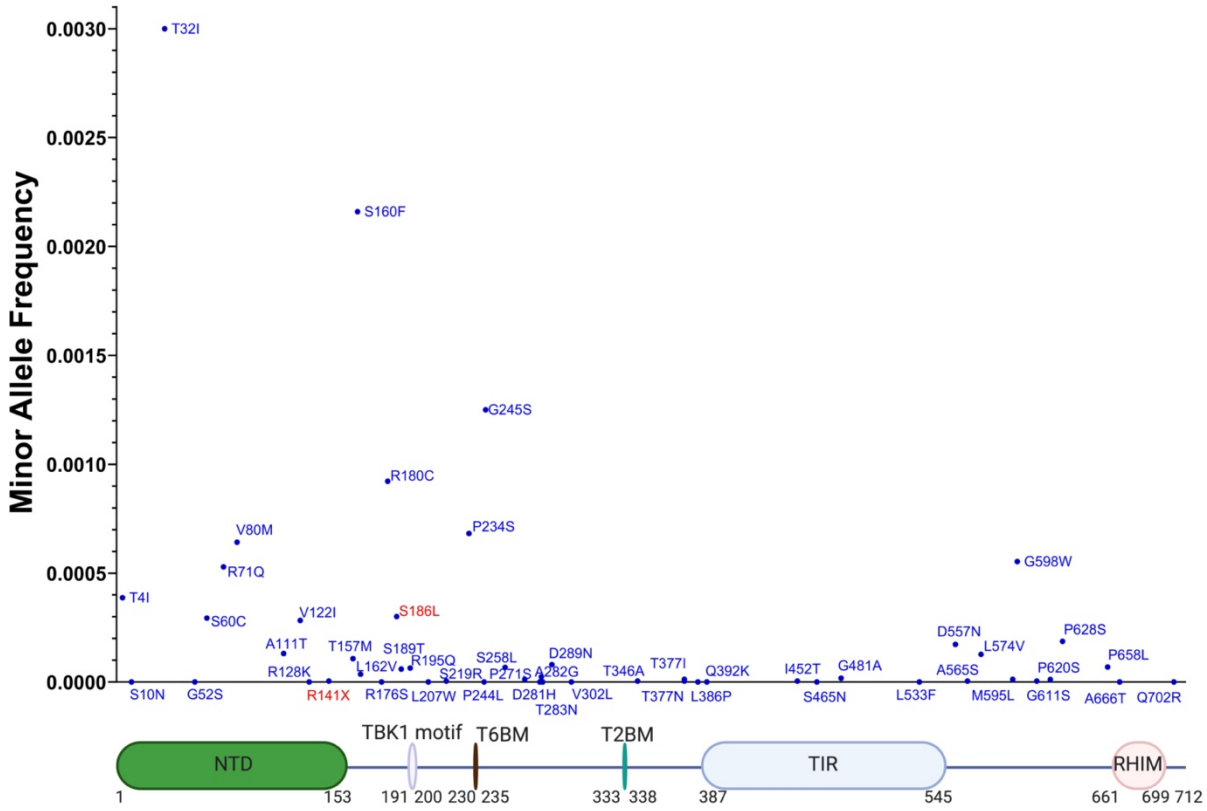


Figure 3.1 Lolliplot of *TICAM1* variants and their minor allele frequency.

This lolliplot illustrating the allele frequency of *TICAM1* variants along a schematic representation of the TICAM1 protein to show their respective locations. Variants in blue are reported in SARS-CoV-2 pneumonia patients, and in red is reported here in HSE. NTD: N-terminal domain, TBK1 motif: TBK1 binding motif, T6BM: TRAF6 binding motif, T2BM: TRAF2 binding motif, TIR: TIR domain, RHIM: RIP (receptor-interacting protein) homotypic interaction motif, HSE: herpes simplex encephalitis.

Table 3.1 49 *TICAM1* variants identified in COVID-19 patients.

Protein Variant	Minor Allele Frequency (MAF, Global gnomAD)	Number of cases, phenotype
T4I *	0.0003874	1 Severe
S10N	0	1 Severe
T32I	0.003	1 Severe
G52S	0	1 Mild
S60C *	0.000294	1 Severe
R71Q *	0.000529	3 Severe
V80M *	0.000642	1 Severe; 1 Asymptomatic

A111T *	0.000131	1 Critical
V122I	0.0002831	1 Severe
R128K	0	1 Unsure
T157M *	0.000107	1 Critical
S160F	0.00216	1 Severe
L162V	0.00003616	1 Severe
R176S	0	1 Severe
R180C	0.0009221	1 Severe; 1 Mild; 1 Unsure
S189T	0.0000596	1 Severe; 1 Mild
R195Q	0.0000641	1 Severe
L207W	0	1 Mild
S219R	0.000004227	2 Mild
P234S	0.0006822	2 Mild; 1 Unsure
P244L	0	1 Severe
G245S	0.00125	1 Severe
S258L	0.00006693	1 Severe
P271S	0.00001207	1 Unsure
D281H	0	1 Mild
A282G	0.00002399	1 Unsure
T283N	0	1 MISC
D289N	0.00007984	1 Unsure
V302L *	0	1 Severe
T346A	0.000004007	1 Mild
T377I *	0.0000119	1 Severe
T377N	0.000003982	1 Mild
L386P *	0	1 Severe
Q392K *	0	1 Severe
I452T	0.000003981	1 Unsure
S465N *	0	1 Severe
G481A	0.00001773	1 Unsure
L533F	0	1 Severe
D557N *	0.000173	1 Severe
A565S	0.000003981	1 Unsure

L574V	0.0001273	1 Severe
M595L *	0.000012	1 Severe
G598W *	0.000553	1 Severe
G611S	0.000004099	1 Severe
P620S	0.0000114	1 Severe; 1 Asymptomatic
P628S	0.0001868	1 Unsure
P658L	0.00006854	1 Severe
A666T	0	1 Unsure
Q702R *	0	1 Severe

The asterisk (*) indicates variants that were documented and published in the Zhang et al. (2020) study.

3.3 Generation of *TICAM1* variants constructs

My fellow laboratory colleague, Dr. Stephanie Hodeib, constructed all the *TICAM1* variants identified in the COVID-19 pneumonia cohort and subsequently, I carried out all the functional tests. Previously described pEF-BOS mammalian expression vector containing the wild-type (WT) TICAM1 with its C-terminal tagged with HA, served as the foundation for incorporating missense variants. This was achieved through site-directed mutagenesis employing overlapping primer pairs featuring the specific single nucleotide substitution. Plasmids resulting from site-directed mutagenesis underwent Sanger sequencing to validate the successful incorporation of target variants. This confirmation was achieved by aligning the constructed plasmid sequences with the WT *TICAM1* sequence.

3.4 Optimisation of transient transfection in TICAM$^{-/-}$ cells

Transient transfection was carried out using Lipofectamine 3000 in TICAM$^{-/-}$ or TICAM1-deficient SV40-fibroblast cells, which has been shown previously (Sancho-Shimizu et al., 2011) to have homozygous *TICAM1* R141X null allele causing complete TICAM1 deficiency. It has been described before that the transient transfection of WT *TICAM1* and *TICAM1* variants through the use of high expression plasmids (pEF-BOS) resulted in overexpression of TICAM1 leads to pronounced cell death due to accelerated apoptosis, as shown in various other systems (Yamamoto et al., 2002; Han et al., 2004; Kaiser & Offermann, 2005; Sancho-Shimizu et al., 2011). We compared WT TICAM1 plasmid concentration of 10ng and 100ng for the experiment. We opted to proceed with 100ng for subsequent experiments as the IFN-β promoter induction, which was the main outcome measured here. Specifically, the 100 ng dosage exhibited an 80-fold induction compared to the 23-fold induction observed with the 10 ng dosage, with minimal difference in terms of cellular mortality, with rates of 32% and 37%, respectively, between these two conditions. (Figure 3.2).

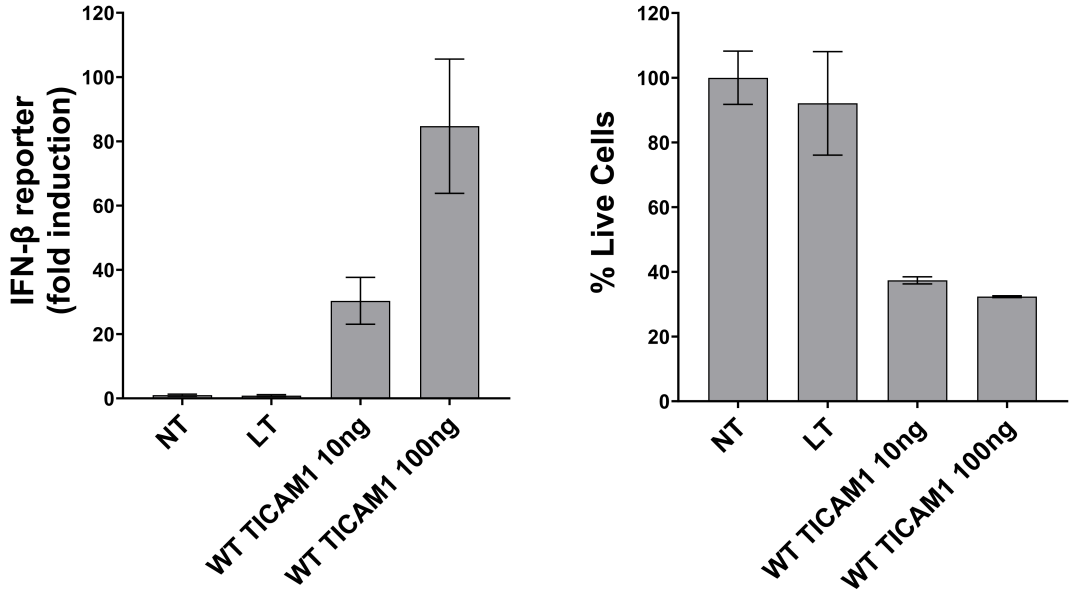


Figure 3.2 Optimisation of transient transfection of WT TICAM1 plasmid in TICAM1-deficient cells.

TICAM1-deficient SV40-fibroblast cells were transiently transfected with WT TICAM1 together with an IFN-β Firefly luciferase reporter to assess promoter induction upon TICAM1 overexpression. The Firefly luciferase values were normalised against Renilla luciferase activity and expressed as fold change with respect to non-transfected cells. The data shown are means and SEM of three biological replicates from three independent experiment (n=3). NT; non-transfected, LT; lipofectamine transfected, WT; wild type.

Given our intention to incorporate z-VAD-fmk, a pan-caspase inhibitor, during the transfection process for the protein works to prevent cell apoptosis, it is imperative to ensure that the inclusion of this compound does not exert any confounding effects on the obtained results. Thus, we conducted a comparative analysis of the fold changes observed in the reporter assay between transient transfections performed with and without the pan-caspase inhibitor (Figure 3.3). The outcomes revealed a consistent pattern, with the fold changes remaining comparable in both scenarios, attributed to the normalisation process utilising their respective controls within the experimental sets. Hence, the results indicate that it is acceptable to use z-VAD-FMK, as previously demonstrated (Sancho-Shimizu et al., 2011).

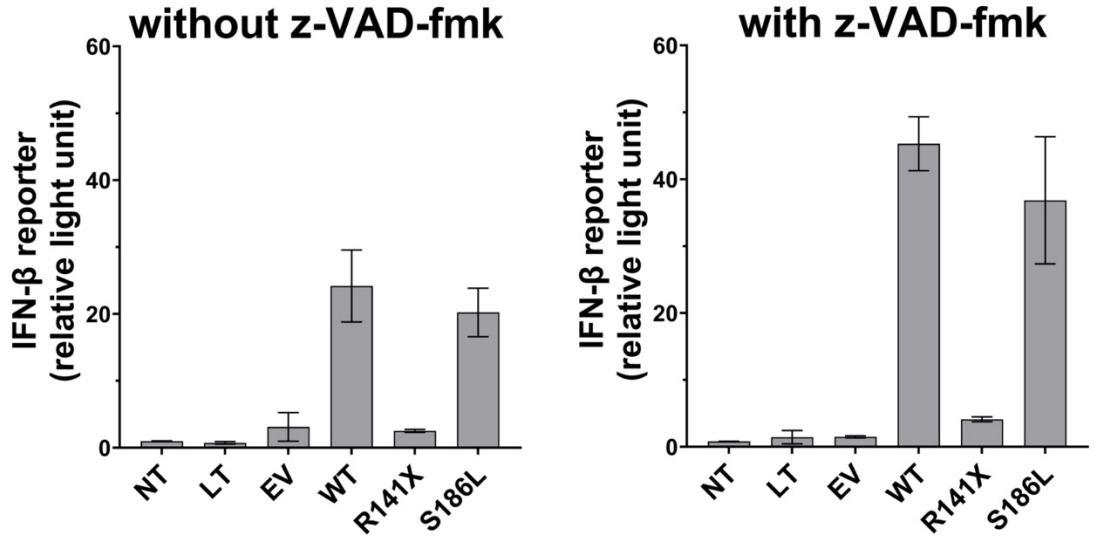


Figure 3.3 Comparison of IFN-β Induction in transient transfection with and without z-VAD-fmk.

TICAM1-deficient SV40-fibroblast cells were transiently transfected with WT, R141X, or S186L TICAM1 together with an IFN-β Firefly luciferase reporter to assess promoter induction upon TICAM1 overexpression with or without the presence of z-VAD-fmk, a pan-caspase inhibitor. The Firefly luciferase values were normalised against Renilla luciferase activity and expressed in relative light unit (RLU). The data shown are means and SEM of three biological replicates from three independent experiment (n=3). NT; non-transfected, LT; lipofectamine transfected, EV; empty vector, WT; wild type.

3.5 Identification of loss-of-expression *TICAM1* variants

With regards to protein experiments, the transient transfection was done in the presence of z-VAD-fmk, to inhibit cell apoptosis and hence ensuring a sufficient protein yield for subsequent testing. The RHIM domain located in the C-terminal region of TICAM1, associates with RIP1, a kinase containing a death domain, which acts as a mediator of apoptosis (Han et al., 2004; Meylan et al., 2004; Kaiser & Offermann, 2005). Notably, the overexpression of TICAM-1 triggers apoptosis in a caspase-dependent manner (Han et al., 2004; Ruckdeschel et al., 2004; Kaiser & Offermann, 2005; Rebsamen et al., 2008). Protein extraction from cell lysates and quantification were carried out in accordance with the procedures outlined in Section 2.8. TICAM1 protein expression was assessed by immunoblot where we used an antibody that

recognised the HA antigen positioned at the C-terminal of TICAM1. Enhanced chemiluminescence was used because of its high sensitivity to detect the antibody and the images were captured by digital OCD camera. The pEF-BOS-*TICAM1* construct of R141X was used as loss-of-expression (LoE) and the pEF-BOS-*TICAM1* construct of S186L was used as hypomorphic control (Sancho-Shimizu et al., 2011). All 49 TICAM1 variants were tested and the three variants (T41, S60C, and Q392K) were seen to be LoE with no detectable proteins showed by immunoblotting (Figure 3.4). Protein expression levels were quantified by densitometry results normalised to WT levels and expressed as relative intensity of TICAM1-HA (Figure 3.4). To mitigate the risk of error when comparing multiple population groups, rather than employing a t-test, we utilise ANOVA (Analysis of Variance).

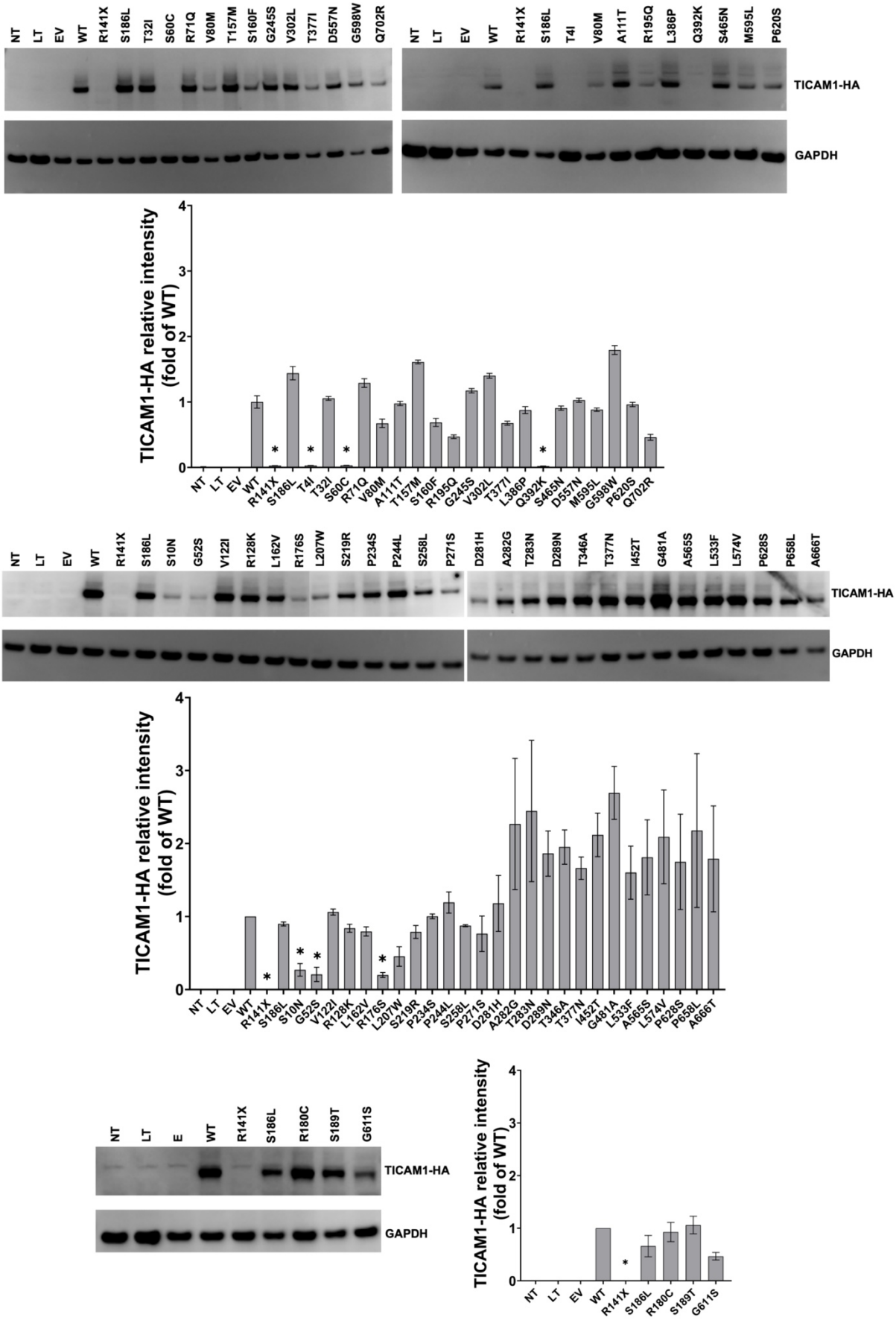


Figure 3.4 Impact of 49 *TICAM1* variants on protein expression.

TICAM1-deficient SV40-fibroblast cells were transiently transfected with TICAM1 variants or WT in the presence of z-VAD-fmk. Immunoblots representative of n=3 and shows resolved TICAM1 proteins using antibody against HA protein tagged on TICAM1, with GAPDH used as a loading control. Respective densitometries were analysed with Fiji/ImageJ and shown alongside. Data shown as mean ± SEM and the differences between variants and wild type were tested in one-way ANOVA, significance shown with *p<0.05. NT; non-transfected, LT; lipofectamine transfected, EV; empty vector, WT; wild type.

Furthermore, to corroborate the finding of the three LoE variants observed in the immunoblots, immunofluorescent assay was utilised to detect the protein expressions where TICAM1-deficient cells were transiently transfected with *TICAM1* variants constructs in the presence of pan caspase inhibitor. These cells were then fixed and probed with HA antibody to detect HA antigen at the C-terminal of TICAM1. Immunofluorescence (IF) was able to show protein at single cell level using confocal microscopy. Only a subset of 20 TICAM1 variants sourced from Zhang's cohort underwent testing. The three LoE variants (T41, S60C, and Q392K) showed absence of fluorescence of TICAM1-HA (Figure 3.5) and hence, confirming the LoE phenotype corroborating the findings from the immunoblot data.

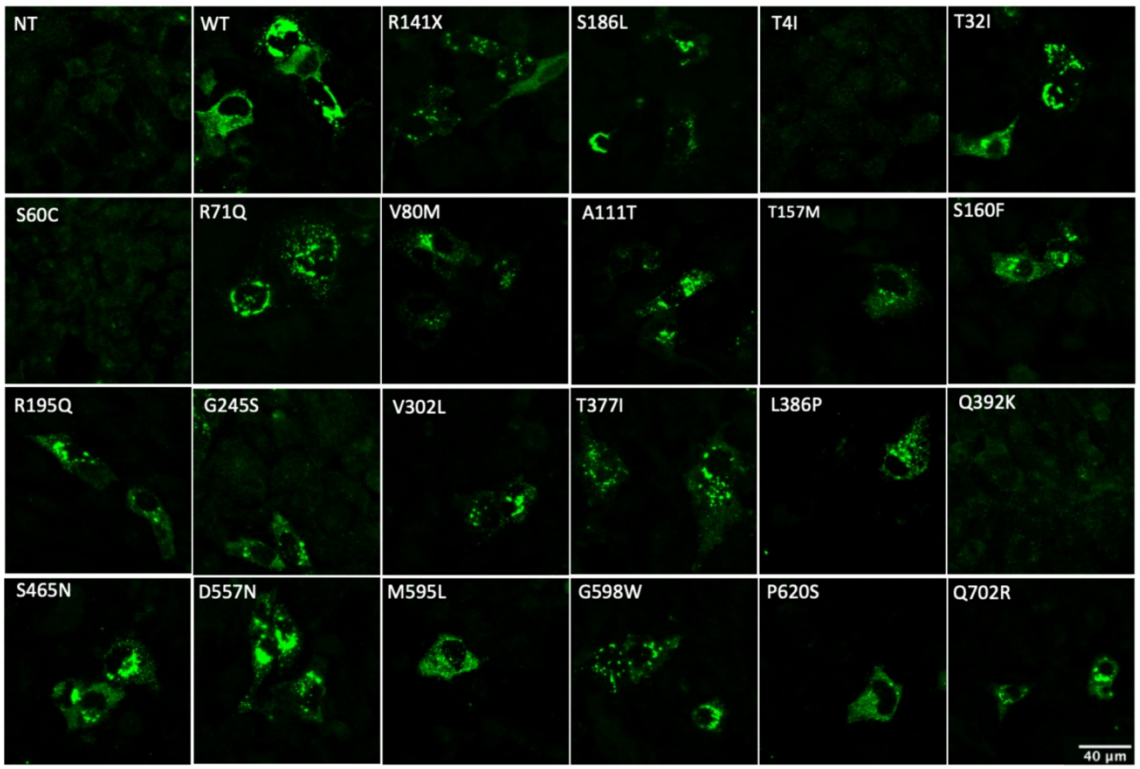


Figure 3.5 Impact of 20 *TICAM1* variant on protein expression by immunofluorescence.

TICAM1-deficient SV40-fibroblast cells were transiently transfected with TICAM1 variants or WT in the presence of z-VAD-fmk. A primary antibody against HA protein tagged on TICAM (1:100) followed by a secondary antibody DyLight™ 488 Goat anti-Rabbit IgG (1:1000) was employed to stain the cells. R141X and S186L were used as a loss-of-expression and hypomorphic controls, respectively. Visualisation of immunofluorescence was achieved with LSM 5 Pascal Confocal microscope (Zeiss) using 63X oil-immersion lens. Scale bar represents 40 µm. Figure shows a representative replicate of n=3. NT; non-transfected, WT; wild type.

3.6 Functional characterization of *TICAM1* variants

Luciferase reporter assays were employed to assess the impact of all 49 *TICAM1* variants on signalling function by overexpression system in TICAM1-deficient fibroblast cells. pEF-BOS-*TICAM1* construct of R141X was used as loss-of-function (LoF) and pEF-BOS-*TICAM1* construct of S186L was used as hypomorphic control (Sancho-Shimizu et al., 2011). R141X variant was previously reported (Sancho-Shimizu et al., 2011) to result in total TICAM1 deficiency, as evidenced by the lack of both IFN-β and NF-κB promoter induction. The level

of induction was similar to that of cells transfected with pEF-BOS empty plasmid. Additionally, this R141X variant, which has a premature termination codon, was also shown to have complete loss-of-expression (LoE) due to absence of detectable protein expression in immunoblotting. S186L variant was previously characterised as hypomorphic, particularly in a doxycycline-inducible retroviral transduction system where TICAM1 protein levels closely resemble endogenous expression whereas when the S186L variant was transfected transiently, no hypomorphic characteristics were observed (Sancho-Shimizu et al., 2011). Three out of the 49 variants assessed, namely T4I, S60C, and Q392K, exhibited loss-of-function characteristics concerning IFN-β promoter inductions when compared to WT (Figure 3.6). The remaining 46 variants exhibited either neutral or possibly overactive profiles. Moreover, when considering NF-κB promoter inductions, these same three variants, among a total of 20 variants from Zhang's cohort tested, also demonstrated a loss of function when compared to WT (Figure 3.7). The remaining 17 variants were either biochemically neutral or possibly overactive. Notably, the induction levels of these three LoF variants were similar to the previously described LoF variant, R141X, concerning both IFN-β and NF-κB promoter inductions (Sancho-Shimizu et al., 2011). The three patients harbouring these LoF *TICAM1* variants did not carry candidate variants at other loci known to be involved in underlying inborn errors of immunity (Zhang et al., 2020).

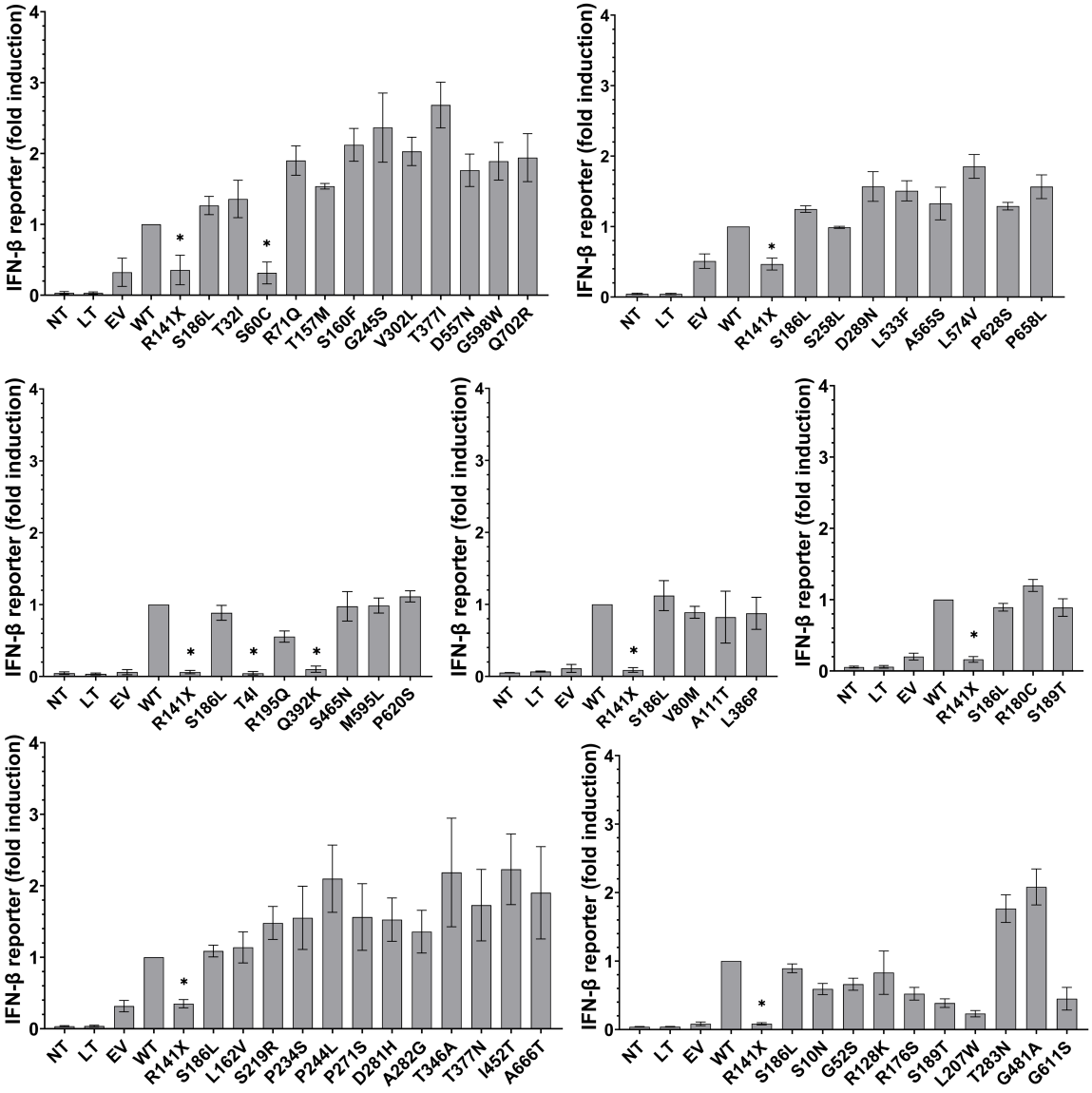


Figure 3.6 Impact of 49 *TICAM1* variants on IFN-β signalling.

TICAM1-deficient SV40-fibroblast cells were transiently transfected with with TICAM1 variants or WT together with an IFN-β Firefly luciferase reporter to assess promoter induction upon TICAM1 overexpression. The Firefly luciferase values were normalised against Renilla luciferase activity and expressed as fold change with respect to cells transfected with WT TICAM1 vector. The data shown are means and SEM of three biological replicates from three independent experiment (n=3), and one-way ANOVA used to assess statistical significance when compared to WT indicated by an asterisks (*$p<0.05$). R141X variant is a known null variant and served as negative control whereas S186L variant was used as hypomorphic control. NT; non-transfected, LT; lipofectamine transfected, EV; empty vector, WT; wild type.

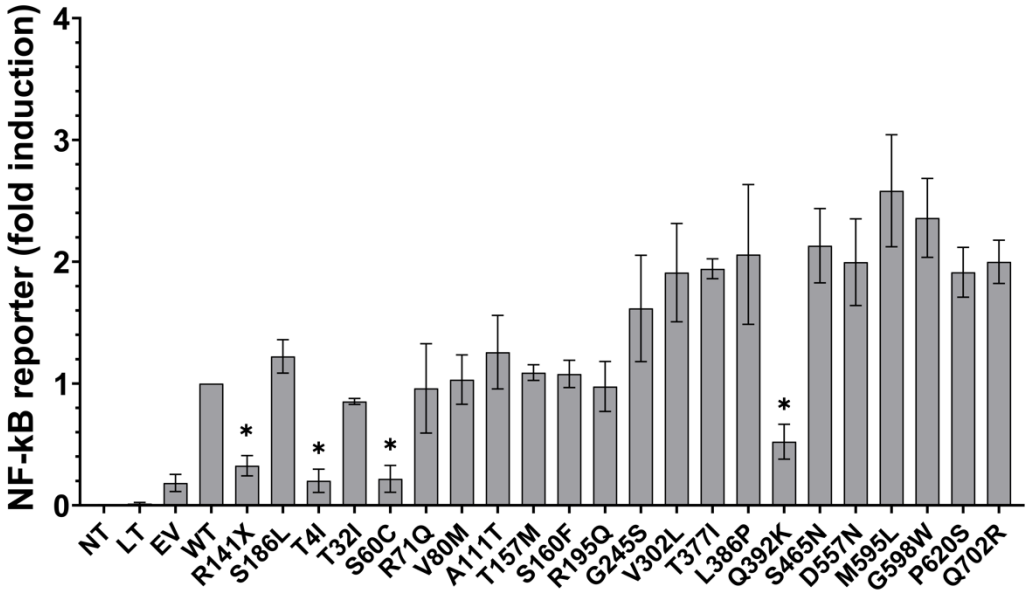


Figure 3.7 Impact of 20 *TICAM1* variants on NF-κB signalling.

TICAM1-deficient SV40-fibroblast cells were transiently transfected with TICAM1 variants or WT together with an NF-κB Firefly luciferase reporter to assess promoter induction upon TICAM1 overexpression. The Firefly luciferase values were normalised against Renilla luciferase activity and expressed as fold change with respect to cells transfected with WT TICAM1 vector. The data shown are means and SEM of three biological replicates from three independent experiment (n=3), and one-way ANOVA used to assess statistical significance when compared to WT indicated by an asterisks (*$p<0.05$). R141X variant is a known null variant and served as negative control whereas S186L variant was used as hypomorphic control. NT; non-transfected, LT; lipofectamine transfected, EV; empty vector, WT; wild type.

3.7 Complementation of Loss-of-Function *TICAM1* variants

We further investigate the impact of the three LoF variants (T4I, S60C, and Q392K). We wanted to identify if these mutations were dominant negative mutations using luciferase reporter assays. ΔNΔC TICAM1 construct encodes a truncated dominant-negative TICAM1, consisting of only 162 amino acids of the TIR domain (Yamamoto et al., 2002), which served as a control for dominant negativity. When TICAM1-deficient cells were transfected with equal amounts of WT and ΔNΔC TICAM1 plasmids, minimal levels of IFN-β activity were observed (Figure 3.8). This aligned with the original findings, where proteins encoded by ΔNΔC

TICAM1 would bind to the available TIR domain of WT TICAM1 proteins, thereby preventing the activation of IFN-β promoter (Yamamoto et al., 2002). When TICAM1-deficient cells were transfected with equal amounts of WT and R141X plasmids, the levels of IFN-β activity were similar to WT 200ng suggesting that R141X allele does not exert a dominant-negative effect which was consistent with the original findings (Sancho-Shimizu et al., 2011) and we utilised this as control in the assay. TICAM1-deficient cells were transfected with equal amounts of WT and T41 or S60C or Q392K plasmids, the levels of IFN-β activity were similar or greater to WT 200ng and WT with ΔNΔC TICAM1 (Figure 3.8). This suggested all three alleles does not exert a dominant-negative effect.

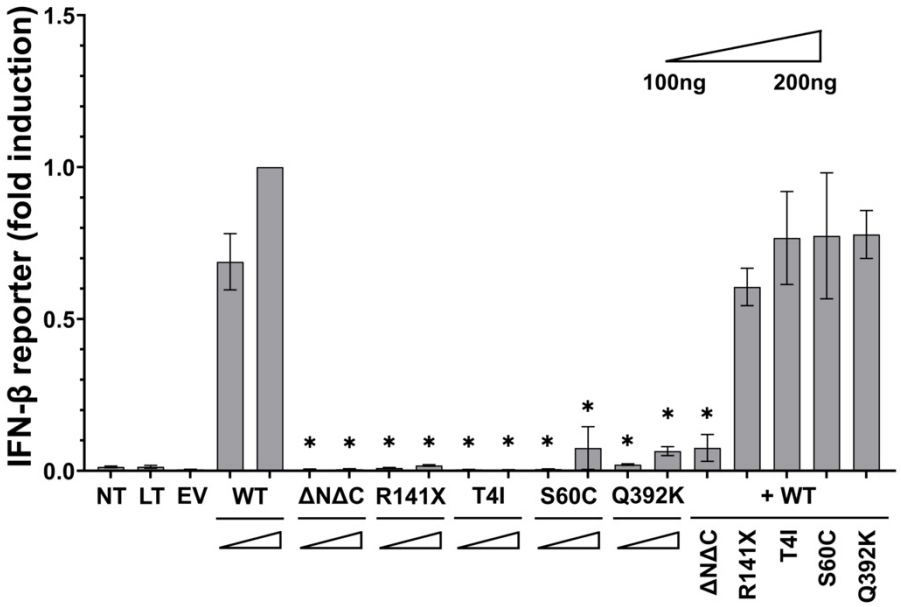


Figure 3.8 Impact of three LoF *TICAM1* variants upon complementation on IFN-β signalling.

TICAM1-deficient SV40-fibroblast cells were transiently transfected with TICAM1 variants or WT together with an IFN-β (top) Firefly luciferase reporter to assess dominant negative impact of TICAM1 variant. The Firefly luciferase values were normalised against Renilla luciferase activity and expressed as fold induction with respect to cells transfected with 200 ng WT TICAM1 vector. The data shown are means and SEM of three biological replicates from three independent experiments (n=3), and one-way ANOVA used to assess statistical significance when comparing WT co-transfections (100 ng +100 ng) to 200 ng WT TICAM1 indicated by an asterisks (*$p<0.05$). NT; non-transfected, LT; lipofectamine transfected, EV; empty vector, WT; wild type, ΔNΔC; dominant negative construct of TICAM1 harbouring solely TIR domain with absence of both N and C terminal domains (Yamamoto et al., 2002).

3.8 Discussion

Numerous investigations have identified specific monogenic deficiencies within the TLR3 pathway that led to impaired TLR3-IFN signalling, which have been previously linked to various viral infections (Miot et al., 2017; Lim et al., 2019; Liang et al., 2020; Kuo et al., 2022), particularly herpes simplex virus 1 (HSV-1) infection in the brain (Casrouge et al., 2006; Zhang et al., 2007; Perez de Diego et al., 2010; Guo et al., 2011; Sancho-Shimizu et al., 2011; Herman et al., 2012; Lim et al., 2014; Andersen et al., 2015). These single-gene inborn errors include autosomal recessive (AR) *UNC93B1*, autosomal dominant (AD) *TRAF3*, AD and AR *TLR3*, AD and AR *TICAM1*, AD *TBK1*, AD *IRF3*, X-linked *NEMO*, AR *DBR1*, and AD *SNORA31* (Casrouge et al., 2006; Zhang et al., 2007; Perez de Diego et al., 2010; Audry et al., 2011; Guo et al., 2011; Sancho-Shimizu et al., 2011; Herman et al., 2012; Lim et al., 2014; Andersen et al., 2015; Zhang et al., 2018; Lafaille et al., 2019). A study (Lafaille et al., 2012) cultivated induced pluripotent stem cells (iPSCs) derived neurons and oligodendrocytes from control, UNC93B- and TLR3-deficient dermal fibroblasts which revealed that cells lacking UNC93B and TLR3 exhibited increased susceptibility to HSV-1 infection compared to control cells, attributable to deficiencies in TLR3-dependent IFN production. This investigation highlighted the crucial antiviral role played by TLR3 in the CNS. Both AR R141X and AD S186L *TICAM1* deficiencies were described in children with HSE and also exhibited impaired TLR3 signalling.

As outlined earlier in this chapter, these two previously published *TICAM1* variants were utilised as controls, with R141X serving as LoF control and S186L as the hypomorphic control. R141X variant was determined as LoF variant due to absence of both IFN-β and NF-κB promoter inductions in the previous study, and those findings were reproduced in the current chapter (Figure 3.6, Figure 3.7). While the S186L variant was previously characterised as hypomorphic in a doxycycline-inducible retroviral transduction system, no hypomorphic characteristics were observed in transient transfections, and the promoter inductions either resembled or exceeded those the WT TICAM1 as seen by the reporter assay (Figure 3.6, Figure 3.7). Given the association of inborn errors of immunity with the onset of life-threatening pneumonia and ARDS in influenza infections due to deficiencies in TLR-3, IRF-7, and IRF-9 (Lim et al., 2019), the COVIDHGE consortium was established with one of its aims to

investigate these three loci, together with 10 other loci intricately linked to these three core genes contributing to influenza susceptibility. This encompassed genes in the TLR3-dependent type I IFN induction pathway (*UNC93B1, TICAM1, TBK1, TRAF3, IRF3,* and *NEMO/IKBKG*) and those located in the IRF7- and IRF9-dependent type I IFN amplification pathway (*IFNAR1, IFNAR2, STAT1*, and *STAT2*) (Zhang et al., 2020). The deficiencies in these genes were found to be the genetic aetiology of various viral diseases including HSE, influenza, yellow fever virus (YFV), varicella zoster virus (VZV), and measles, mumps and rubella (MMR) (Casanova & Anderson, 2023). Due to the abrupt initiation of this project amid the COVID19 pandemic, the COVIDHGE consortium invited us to be part of this extensive work, assigning us the task of investigating the impact of rare *TICAM1* variants with the hypothesis that life-threatening COVID-19 may be caused by monogenic inborn errors of immunity to SARS-CoV-2 with incomplete or complete penetrance.

In this chapter, 49 *TICAM1* variants were identified in patients hospitalised for life-threatening pneumonia caused by SARS-CoV-2 (or critical COVID-19). As mentioned earlier, none of the COVID-19 patients with severe pneumonia with mutations in the *TICAM1* gene investigated here carried variants at other candidate loci known to be involved in underlying inborn errors of immunity (Zhang et al., 2020). These *TICAM1* variants were successfully integrated into a mammalian expression vector pEF-Bos-TICAM1 by a colleague Dr Stephanie Hodeib, as described previously. The confirmation of the incorporation of the target single nucleotide polymorphism (SNP) into the backbone plasmid was confirmed through Sanger sequencing. Subsequent validation was done to ensure the absence of any unintended additional errors introduced during the mutagenesis process (data not shown). This precaution aimed to eliminate any potential impact on the observed variant-specific outcomes.

Two luciferase reporter assays were conducted to investigate the functional impact of the TICAM1 variants. These assays aimed to explore the induction of IFN-β and NF-κB promoters, which are critical key molecule downstream of TICAM1 signalling pathway. These investigations revealed three LoF variants, T4I, S60C, and Q392K, in terms of IFN-β and NF-κB promoter induction, with the induction levels were significantly decreased when compared to WT and consistent with the induction level of previously published LoF variant's, R141X

(Figure 3.6, Figure 3.7). To further investigate the impact of the *TICAM1* variants, we assessed TICAM1 protein expression through immunoblotting and immunofluorescence techniques to visualise the TICAM1-HA expressing proteins. Both immunoblotting and immunofluorescence showed the three LoF variants to also exhibit LoE, with no detectable protein observed (Figure 3.4, Figure 3.5). Immunofluorescence exhibited higher sensitivity, capable of detecting the protein at single-cell level. The protein levels of all other TICAM1 variants in the immunoblot were either similar or lower than the WT; however, the densitometry analysis indicated that they did not mount any significance differences. Due to the time constraint at the time, we were unable to procure an appropriate TICAM1 antibody to probe this immunoblot. However, the HA antibody we used to detect the TICAM1-HA is considered sufficient, as it accurately reflected the expected results in the controls.

TICAM1-deficient fibroblast cells (Sancho-Shimizu et al., 2011) were employed in this chapter because of their absence of endogenous TICAM1 protein. This characteristic allowed for the evaluation of both the expression and functionality of the *TICAM1* variants. The transient transfection of *TICAM1* variants utilising high-expression plasmids resulted in elevated cell mortality, as previously documented (Sancho-Shimizu et al., 2011). This phenomenon can be attributed to the overexpression of TICAM1, leading to rapid apoptosis, as shown in other experimental systems (Yamamoto et al., 2002; Han et al., 2004; Kaiser & Offermann, 2005). Furthermore, overexpression and accumulation of TICAM1 could induce its own degradation through NDP52-mediated selective autophagy (Inomata et al., 2012). Additionally, another study (Tao et al., 2012) presented findings supporting a negative regulation mechanism in the context of TLR3, leading to down-regulation of TICAM1 through lysosomal degradation. These processes occur because the cellular levels of TICAM1 are tightly regulated as TICAM1 served as a key adaptor molecule in the TLR3/4 pathway, and increased TICAM1 expression could initiate the signalling cascade. Nonetheless, the levels of TICAM1 produced under conditions of overexpression in this chapter do not reflect physiologically relevant functions of TICAM1, as they lead to constitutive activation and apoptosis. However, it is also important to note that the transient transfection system has been effectively utilised by numerous research groups before to investigate the function of TICAM1 in conditions of overexpression (Yamamoto et al., 2002; Oshiumi et al., 2003; Jiang et al., 2004; Kaiser & Offermann, 2005; Funami et al., 2008; Tatematsu et al., 2010; Sancho-Shimizu et al., 2011).

The reporter assay we employed in this chapter was sufficiently sensitive to detect significant fold changes, indicative of an intact signalling pathway, even with the increased cell death, resulting in approximately 32% cell viability (Figure 3.2). Nevertheless, during our initial protein works, the overexpression of TICAM1 in transient transfection did not yield sufficient cells or proteins for downstream applications such as western blot and immunofluorescence. Hence, to address this increased cell death caused by rapid apoptosis occurring in transient transfection, z-VAD-FMK, a pan caspase inhibitor, was used during transfection and the cell viability was enhanced considerably (data not shown). z-VAD-FMK is a cell-permeable pan-caspase inhibitor designed to prevent apoptosis by irreversibly binding to the catalytic site of caspase proteases (Slee et al., 1996). To ensure the validity of our initial reporter assay results without the addition of this compound, we compared the fold changes in the reporter assay between the transient transfections conducted with and without the pan-caspase inhibitor. The results exhibited a similar pattern, and the fold changes were comparable to each other due to the normalisation with their respective controls in the sets (Figure 3.3). Thus, we opted to utilise z-VAD-FMK exclusively for western blot and immunofluorescence assays.

In addition to the three LoF TICAM1 variants tested in our laboratory, the collaborative efforts of various research groups involved in the Zhang et al. study identified 21 other variants deemed deleterious (Zhang et al., 2020). These variants, inclusive of those analysed in our laboratory, contribute to AR deficiencies, involving *IRF7* and *IFNAR1*, and AD deficiencies encompassing *TLR3*, *UNC93B1*, *TICAM1*, *TBK1*, *IRF3*, *IRF7*, *IFNAR1*, and *IFNAR2*, affecting four and 19 patients, respectively. The study demonstrated that AR IRF7 deficiency led to a reduction in the production of type I IFN by pDCs when infected with SARS-CoV-2. Additionally, both AR and AD deficiencies of TLR3, along with AR deficiency of IFNAR1, were identified to compromise type I IFN immunity to SARS-CoV-2 infection in fibroblasts. These findings unveil the crucial significance of the dsRNA receptor TLR3 and the cell-intrinsic immunity governed by type I IFN in the regulation of SARS-CoV-2 infection within the pulmonary environment. This aligns seamlessly with their extensively recognized roles in orchestrating pulmonary immunity against the influenza virus (Ciancanelli et al., 2015; Hernandez et al., 2018; Lim et al., 2019; Zhang, 2020). The genetic characteristics implicated remained latent until the advent of infection with SARS-CoV-2.

We also briefly investigated the impact of the three LoF variants (T4I, S60C, and Q392K) to assess whether these mutations manifest dominant-negative characteristics using the luciferase reporter assays. In this chapter, we utilised ΔNΔC TICAM1 construct which encodes a truncated dominant-negative TICAM1, encompassing the TIR domain, as a true dominant-negative control (Yamamoto et al., 2002). Upon transfecting TICAM1-deficient cells with equivalent amount of WT and ΔNΔC TICAM1 plasmids, minimal activity of IFN-β was detected. This observation corroborates with earlier research (Yamamoto et al., 2002), indicating that proteins encoded by ΔNΔC TICAM1 interact with accessible TIR domain of WT TICAM1 proteins and consequently preventing the activation of IFN-β promoter. In similar fashion of testing, upon transfecting TICAM1-deficient cells with equivalent amount of WT and T4I or S60C or Q392K plasmids, the levels of IFN-β activity did not significantly differ from the WT suggesting that all three alleles do not exert a dominant-negative effect. We also utilised R141X as a control in this assay, considering in the original findings where cells transfected with equal amounts of WT and R141X plasmids showed IFN-β activity levels were similar to WT which suggested that R141X allele does not exert a dominant-negative effect. Furthermore, the levels of IFN-β activity induced by combination of WT with either T4I or S60C or Q392K variants were comparable to of combination of WT with R141X. Thus, reinforcing the observation that these three LoF variants did not demonstrate a dominant-negative effect. These findings may probably suggestive of haploinsufficiency as a potential mechanism for the observed LoF. To explore this further, immunoblotting and a similar transfection approach can be employed, wherein cells are transfected with equivalent amounts of WT and TICAM1 variants. If the allele exhibits haploinsufficiency trait, the TICAM1 band on the immunoblot would demonstrate 50% intensity or less than the full WT.

The three LoF variant alleles result in the total absence of the TICAM1 protein. Specifically, the T4I and S60C variants are located in the N-terminal domain (NTD) of the TICAM1 protein, while the Q392K variant is positioned in the TIR domain of the protein. The NTD plays an essential role in TICAM1-mediated IRF-3 activation, while the TIR domain is critical for facilitating interactions with both the TIR domain of TLR3 and the TLR4 adaptor TICAM2, thereby forming TIR-TIR domain interactions (Fujita et al., 2003; Sasai et al., 2005; Funami et al., 2008; Han et al., 2010; Tatematsu et al., 2010). It was widely acknowledged that missense mutations have the potential to influence the transcription and translation factors, thereby

impacting the expression of the corresponding protein (Zhang et al., 2012). This premise is supported by evidence indicating that specific disease-causing missense mutations in the pancreatic secretory trypsin inhibitor (*SPINK1*) gene, responsible for encoding pancreatic secretory trypsin inhibitor (PSTI), result in the complete loss of PSTI expression (Boulling et al., 2007).

Similarly, we observe a parallel phenomenon with the total absence of the protein in the case of the three LoF TICAM1 variants leading to complete loss of TLR3-mediated IFN activation. Concerning T4I, it is plausible that the missense mutation induces protein instability, particularly given its location in the early portion of the protein. Notably, existing research has demonstrated that approximately 80% of missense mutations linked to diseases involve amino acid substitutions that influence protein stability (Wang & Moult, 2001). This suggests that alterations in protein stability might be a contributing factor in the observed effects of the T4I missense mutation. In an investigative analysis using nuclear magnetic resonance spectroscopy to examine NTD structure of TICAM1, it was discovered that the NTD constitutes a singular, compact structure consisting of eight α-helices (Kumeta et al., 2014). Ser60 is situated within one of these helices, which is part of the tetratricopeptide repeat (TPR) motif-like region. TPR proteins are known to facilitate protein-protein interactions and the inter-domain assembly of proteins with multiple domains (Cerveny et al., 2013). Consequently, the S60C variant may potentially disrupt this helical structure, consequently interfering with the inter-domain assembly of proteins with multiple domains, ultimately leading to the absence of TICAM1 protein.

Regarding the Q392K variant situated within the TIR domain, it is conceivable that a mutation within this region might undermine the capacity of TICAM1 to participate in pivotal interactions, consequently disrupting the downstream signalling pathway. A relevant example illustrating this phenomenon is the discovery of the human TICAM-1 variant P434H, wherein the resultant complete loss of TLR3-mediated IFN activation has shed light on its significant influence on this specific signalling pathway (Oshiumi et al., 2003; Funami et al., 2008; Enokizono et al., 2013). In its core, variation within the amino acid sequence possesses the potential to modify the protein's structure without inevitably impacting its function; however,

mutations at specific locations, such as conserved sites, may instigate both the structural and functional changes within the protein (Prabantu et al., 2020). Nevertheless, numerous variants tested in this chapter are located within crucial domains and appeared not to influence TICAM1 expression and IFN induction. Given the extensive catalogue of characterised TICAM1 variants here, there arises an interest in complementing this wealth of functional data with a computational model of TICAM1's structure. This computational model aims to discern specific residues associated with loss of function and potentially predict additional sites that may lead to diseases in the presence of a variant. The anticipation is that the computational approach can serve as a learning tool to enhance our understanding of the intricacies of TICAM1 variants and their impact on functionality.

While there were three *TICAM1* variants identified as LoF in this chapter, it would be premature to dismiss the potential effects of the remaining variants may have. Previous research (Sancho-Shimizu et al., 2011) indicates that AD *TICAM1* variant (S186L) exhibits hypomorphic characteristics, contributing to severe clinical phenotype (HSE) with incomplete clinical penetrance. TICAM1 S186L was used as a hypomorphic control in these experiments. However, it is essential to note that hypomorphic phenotypes are often subtle and may not readily apparent in a transient overexpression system, as employed in this chapter. This is attributed to cellular levels of TICAM1 reaching a saturation, rendering subsequent analyses less sensitive to discern potential impacts. Thus, in this transient overexpression system, TICAM1 S186L consistently yielded induction levels of both IFN-β and NF-κB promoters, and protein expression similar to WT, consistent with previous reports (Oshiumi et al., 2003; Yamamoto et al., 2003a) where TICAM1 overexpression led to TLR3-independent activation of IFN-β and NF-κB. In the original study of TICAM1 S186L, it was identified as a hypomorphic variant exhibiting significantly impaired production of IFN-β, IFN-λ, and IL-6 in a doxycycline-inducible retroviral transduction system. In experimental setup, the TICAM1 levels were significantly lower compared to those achieved through transient overexpression transfection, aligning more closely with endogenous TICAM1 levels as suggested by the absence of constitutive activation together with low level of apoptosis. This approach can be applied to the identified *TICAM1* variants in this cohort to unveil potential the subtle hypomorphic effects on TICAM1 function. This doxycycline-inducible retroviral transduction system would also address the issue of rapid apoptosis observed in transient transfection

(without the addition of pan-caspase inhibitor), ensuring that TICAM1 protein levels are maintained at a physiological level tolerable for the cells. We anticipate observing the same LoF outcomes in T4I, S60C, and Q392K, but the implementation of this approach would require more additional time and we were constrained by time limitations, which restricted our ability to pursue this approach.

A limitation in our study, in contrast to other well-documented inborn errors of immunity in the TLR3 pathway (Casrouge et al., 2006; Zhang et al., 2007; Perez de Diego et al., 2010; Guo et al., 2011; Sancho-Shimizu et al., 2011; Herman et al., 2012; Lim et al., 2014; Andersen et al., 2015), lies in the unavailability of heterozygous fibroblasts from patients harbouring the three LoF variants. Consequently, the data presented here primarily revolves around the molecular characterisation. The absence of these cells hinders our ability to conduct comprehensive tests on the TLR3-IFN pathway, including evaluating endogenous TICAM1 protein expression. With access to such cells, we could conduct further investigations into the integrity of the TLR3-IFN response, assessing immune reactions in response to viral infections. These cellular assays would have provided valuable insights into the functional implications of these *TICAM1* variants in the context of immune response.

In summary, three *TICAM1* variants (T4I, S60C, and Q392K) were identified as LoF. The functional evaluation of these *TICAM1* variants, as presented in this chapter, has been published alongside other monogenic inborn errors of immunity affecting the TLR3-IFN pathway that may underlie the COVID-19 pneumonia. The study revealed that at least 3.5% of patients with life-threatening COVID-19 pneumonia had known genetic defects in genes involved in the TLR3- and IRF7-dependent induction and amplification of type I IFNs which includes *TLR3*, *UNC93B1, TICAM1, TBK1, IRF3, IRF7, IFNAR1,* and *IFNAR2*. This highlights the significance of type-1 IFN immunity in combating the life-threatening COVID-19 pneumonia. This concept is further reinforced by a companion paper, published alongside our genetic study, which describes the presence of neutralizing antibodies against type-I IFN in patients with life-threatening COVID-19 pneumonia (Bastard et al., 2020).

Chapter 4

4. *TICAM1* variant in HSV-2 meningitis

The research detailed in this chapter was conducted in collaboration with Dr Taco Kuijpers' team from Amsterdam UMC. The identified patient belongs to his cohort. We were given the opportunity to work together due to our lab's previous expertise in investigating TICAM1 in HSE. Part of the work conducted in this chapter involved a close collaboration with fellow laboratory colleagues, Ms Dilys Santillo and Dr Stephanie Hodeib.

4.1 Background

HSV-2 commonly results in HSE among neonates, presenting with disseminated infection or as a less severe infection confined to the meninges called herpes simplex meningitis (HSM) (Miller et al., 2013; Steiner & Benninger, 2013), whereas in adults, HSV-2 infection can give rise to a rare manifestation of meningitis known as recurrent benign lymphocytic meningitis (RBLM), alternatively referred to as Mollaret's meningitis (Shalabi & Whitley, 2006). This condition is characterised by recurrent episodes of aseptic lymphocytic meningitis, each episode being of short duration and followed by asymptomatic intervals (Bruyn et al., 1962). In this chapter, Dr. Taco Kuijpers along with our group has made a significant contribution by identifying a patient presenting with recurrent meningitis and found to harbour a novel heterozygous mutation within the *TICAM1* gene. This discovery adds another element to the broader understanding of genetic factors associated with recurrent meningitis, thereby contributing to the ongoing research and comprehension of the intricate molecular pathways involved in such clinical presentations.

I conducted functional testing of the variant, which involved luciferase promoter assays, protein expression using immunoblotting, infecting patient's fibroblasts with HSV-1 and HSV-2, and subsequently measuring the cytokine levels. Dr Stephanie Hodeib kindly constructed the nonsense *TICAM1* variant and integrated it into previously described pEF-BOS-*TICAM1*,

thereby enabling all of my subsequent work possible. Ms Dilys Santillo has been tremendously helpful in performing WES analysis and conducting assays to test for dominant negativity and protein expression through immunofluorescence. We decided to divide the work with the intention of publishing it as soon as possible where the manuscript has been submitted to Journal of Clinical Immunology and currently under review. In this collaboration, I would be the joint first author with Dr Dorit Verhoeven, who is the lead investigator on Dr Taco Kuijpers' team.

4.2 Discovery of novel heterozygous *TICAM1* variant in a patient with recurrent HSV-2 meningitis

4.2.1 Clinical features

The clinical information presented here was collected by our collaborators, Dr Dorit Verhoeven and Dr Taco Kuijpers. The patient is a female of Surinamese descent (P1) who suffered from meningitis and keratitis at the age of 20, during which HSV-2 DNA was detected in the patient's CSF (Figure 4.1). At the time of hospital admission, she received intravenous aciclovir treatment for 4 weeks because of the combined neurological and serious ophthalmic manifestations, which improved her symptoms and prevented neurological sequelae. However, recurrent herpes uveitis caused severe eye damage to her. Discontinuing aciclovir treatment led to recurrent herpes meningitis, now diagnosed as Mollaret meningitis based on the characteristics of recurrent benign lymphocytic meningitis (RBLM) (Bruyn et al., 1962; Mirakhur & McKenna, 2004; Farazmand et al., 2011). In addition to infections of herpes uveitis, herpes genitalis, and herpes labialis, this condition necessitated daily prophylaxis with valaciclovir. During recurrent flares, which manifest approximately one to three times annually and are characterised by symptoms such as photophobia and headaches, she was prescribed to higher dosage of valaciclovir. This adjustment in medication proved effective in preventing the exacerbation of symptoms and contributing to symptom management. The patient had not suffered from any other unusually severe infectious diseases, whether of viral origin or

otherwise. She has been infected by the varicella-zoster virus (VZV) and cytomegalovirus (CMV), as demonstrated by positive serology. Additionally, she has been immunised against live MMR vaccines with no adverse effects.

The mother of the index patient tested positive for HSV-IgG serology, encompassing combined testing for both HSV-1 and HSV-2, making it indistinguishable between the two strains. Additionally, the mother was afflicted with small fiber neuropathy diagnosed at the age of 59, with no recorded occurrences of HSE, HSM, or any other severe diseases. The index patient's brother experienced meningitis at 9 months of age, resulting in impaired hearing in the left ear despite antibiotic intervention. No viral or bacterial pathogen was identified at that time, and there is no history of other severe infections, testing negative for HSV-IgG.

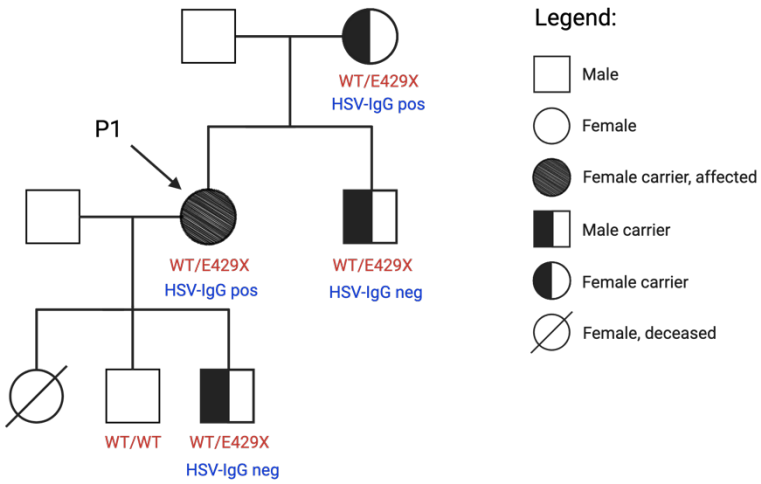


Figure 4.1 Discovery of a *TICAM1* variant present in a heterozygous state among four family members.

This family pedigree illustration showing four affected family members who exhibit the heterozygous E429X TICAM1 mutation. The designated arrow in the diagram indicates the index patient characterised by a history of recurrent HSV-2 meningitis, highlighted with black shading for clarity. The HSV-IgG status is documented for each individual within the familial cohort which determined through a combined serological assessment for both HSV-1 and HSV-2. WT: Wild-type.

4.2.2 Genetic findings

Since 2014, there has been a systematic updating process for the IEI gene panel, which is guided by the latest insights and recommendations from the International Union of Immunological Societies (IUIS). This iterative process occurs every three months and is informed by annual updates from the IUIS and insights gained from expert meetings in the field. This dynamic approach ensures that the IEI gene panel remains current and reflective of the evolving landscape of immunological research and clinical practice. Whole exome sequencing was performed using targeted IEI gene panel and was followed by genetic analysis representative of the 2014 International Union of Immunological Societies (IUIS) gene list (Elsink et al., 2021). WES followed by filtering for the 2014 IEI genes panel, identified a heterozygous mutation in the *TICAM1* gene (c.1285G>T, p.Glu429*), predicting a nonsense mutation at amino acid position 429 (E429X) located at the TIR domain of the TICAM1 protein. Furthermore, after the birth of her newborn son, the analysis of family members led to the discovery of a total of four genetically affected family members with incomplete clinical penetrance (HSV serology is shown in Figure 4.1). In an effort to eliminate the possibility of common variable immunodeficiency disorder (CVID) due to the occasional occurrence of HSV in CVID cases, the subsequent immunological screening revealed no manifestations indicative of CVID (Borish et al., 2011). The index patient's three years old son was diagnosed with the *TICAM1* E429X variant at birth and received valaciclovir treatment for the first four months of life. As of now, he displayed an extensive vesicular rash due to VZV with no clinical necessity for antiviral intervention. Notably, his older brother does not carry the mutation.

As of 2022, the panel consists of 454 genes (Bousfiha et al., 2022a; Tangye et al., 2022). Genetic analysis was rerun in 2023 by Ms Dilys Santillo using the latest 2022 IEI gene panel together with genes involved in HSV-2 meningitis or inborn errors of autophagy (*ATG4A*, *MAPILC3B2*) (Hait et al., 2020). No variants were found in the *ATG4A* and *MAPILC3B2* genes.

Gene analysis performed in 2023, included genes:

ACD; ACP5; TRAF3IP2; ACTB; ADA; ADA2; ADAM17; ADAR1; AICDA; AIRE; AK2; ALPI; AP1S3; AP3B1; AP3D1; APOL1; APOLLO; ARHGEF1; ARPC1B; ATAD3A; ATG4A; ATM; ATP6AP1; B2M; BACH2; BCL10; BCL11B; BLM; BLNK; BRCA1; BRCA2; BRIP1; BTK; C16ORF57; C1QA; C1QB; C1QC; C1R; C1S; C2; C2orf69; C3; C4A; C4B; C6; C7; C8A; C8B; C8G; C9; CARD11; CARD14; CARD9; CASP10; CASP8; CCBE1; CD19; CD20; CD27; CD28;CD3D; CD3E; CD3G; CD3Z; CD40; CD40LG; CD46; CD55; CD59; CD70; CD79A; CD79B; CD81; CDC42; CDCA7; CEBPE; CFB; CFD; CFH; CFHR1; CFHR2; CFHR3; CFHR4; CFHR5; CFI; CFTR; CHD7; CIB1; CIITA; CLBP; CLCN7; COH1; COPA; COPG1; CORO1A; CR2; CRACR2A; CSF2RA; CSF2RB; CSF3R; CTC1; CTLA4; CTNNBL1; CTPS1; CTSC; CXCR2; CXCR4; CYBA; CYBB; CYBC1; DBR1; DCAB1; DCLRE1B; DCLRE1C; DEF6; DIAPH1; DKC1; DNAJC21; DNASE1L3;DNASE2; DNMT3B; DOCK2; DOCK8; EFL1; ELANE; ELF4; EPG5; ERBB2IP; ERCC4; ERCC6L2; EXTL3; FAAP24; FADD; FANCA; FANCB; FANCC; FANCD2; FANCE; FANCF; FANCI; FANCM; FAT4; FCGR3A; FCHO1; FCN3; FERMT1; FERMT3; FNIP1; FOXN1; FOXP3; FPR1; G6PC3; G6PD; G6PT1; GATA2; GFI1; GINS1; HAVCR2; HAX1; HCK; HELLS; HMOX; HYOU1; ICOS; ICOSLG; IFIH1; IFNAR1; IFNAR2; IFNG; IFNGR1; IFNGR2; IGHM; IGKC; IGLL1; IKBB; IKBKB; IKBKG; IKFZ2; IKKa; IKZF1; IKZF2; IKZF3; IL10; IL10RA; IL10RB; IL12B; IL12RB1; IL12RB2; IL17F; IL17RA; IL17RC; IL18BP; IL1RN; IL21; IL21R; IL23R; IL2RA; IL2RB; IL2RG; IL36RN; IL6R; IL6ST; IL7R; INO80; IRAK1; IRAK4; IRF2BP2; IRF3; IRF4; IRF7; IRF8; IRF9; ISG15; ITCH; ITGB2; ITK; ITPKB; JAGN1; JAK1; JAK3; KDM6A; KMT2A; KMT2D; KRAS; LAMTOR2; LAT; LCK; LIG1; LIG4; LPIN2; LRBA; LSM11; LYST; MAD2L2; MAGT1; MALT1; MAN2B2; MAP1LC3B2; MAP3K14; MAPK8; MASP2; MCM10; MCM4; MECOM; MEFV; MKL1; MOGS; MSH6; MSN; MTHFD1; MVK; MYD88; MYSM1; NBAS; NBS1; NCF1; NCF2; NCF4; NCKAP1L; NCSTN; NFAT5; NFE2L2; NFKB1; NFKB2; NFKBIA; NHEJ1; NLRC4; NLRP1; NLRP12; NLRP3; NOD2; NOLA2; NOLA3; NOS2; NRAS; NSMCE3; OAS1; ORAI1; OSTM1; OTULIN; PALB2; PARN; PAX1; PDCD1; PEPD; PFC; PGM3; PIK3CD; PIK3CG; PIK3R1; PLCG2; PLEKHM1; PMS2; PNP; POLA1; POLD1; POLD2; POLE; POLE2; POLR3A; POLR3C; POLR3F; POU2AF1; PRF1; PRKDC; PSEN; PSENEN; PSMB8; PSMB9; PSMG2; PSTPIP1; PTEN; PTPRC; RAB27A; RAC2; RAD51; RAD51C; RAG1; RAG2; RANBP2; RASGRP1; RBCK1; REL; RELA; RELB; RFWD3; RFX5; RFXANK; RFXAP; RHOG; RHOH; RIPK1; RLTPR; RMRP; RNASEH2A; RNASEH2B; RNASEH2C; RNF168; RNF31; RNU4ATAC; RNU71; RORC;

RPSA; RTEL1; SAMD9; SAMD9L; SAMHD1; SASH3; SBDS; SEC61A1; SEMA3E; SERPING1; SH2DIA; SH3BP2; SH3KBP1; SKIV2L; SLC29A3; SLC35C1; SLC39A7; SLC46A1; SLC7A7; SLP76; SLX4; SMARCAL1; SMARCD2; SNM1; SNORA31; SNX10; SOCS1; SP110; SPI1; SPINK5; SPPL2A; SRP54; SRP72; STAT1; STAT2; STAT3; STAT5B; STIM1; STK4; STN1; STX11; STXBP2; SYK; TAP1; TAP2; TAPBP; TAZ; TBK1; TBX1; TBX21; TCF3; TCIRG1; TCN2; TERC; TERT; TET2; TFRC; TGFB1; TGFBR1; TGFBR2;THBD; TICAM1; TINF2; TIRAP; TLR3; TLR7; TLR8; TMC6; TMC8; TMEM173; TNFAIP3; TNFRS13B; TNFRS13C; TNFRSF11A; TNFRSF1A;TNFRSF4; TNFRSF6; TNFRSF9; TNFSF11; TNFSF13; TNFSF6; TOP2B; TP53; TPP1; TPP2; TRAC; TRAF3; TREX1; TRIM22; TRNT1; TTC37; TTC7A; TWEAK; TYK2; UBA1; UBE2T; UNC13D; UNC93B1; UNG; USP18; VPS45; WAS; WDR1; WIPF1; WRAP53; XIAP; XRCC2; XRCC9; ZAP70; ZBTB24; ZNF341; ZNFX1.

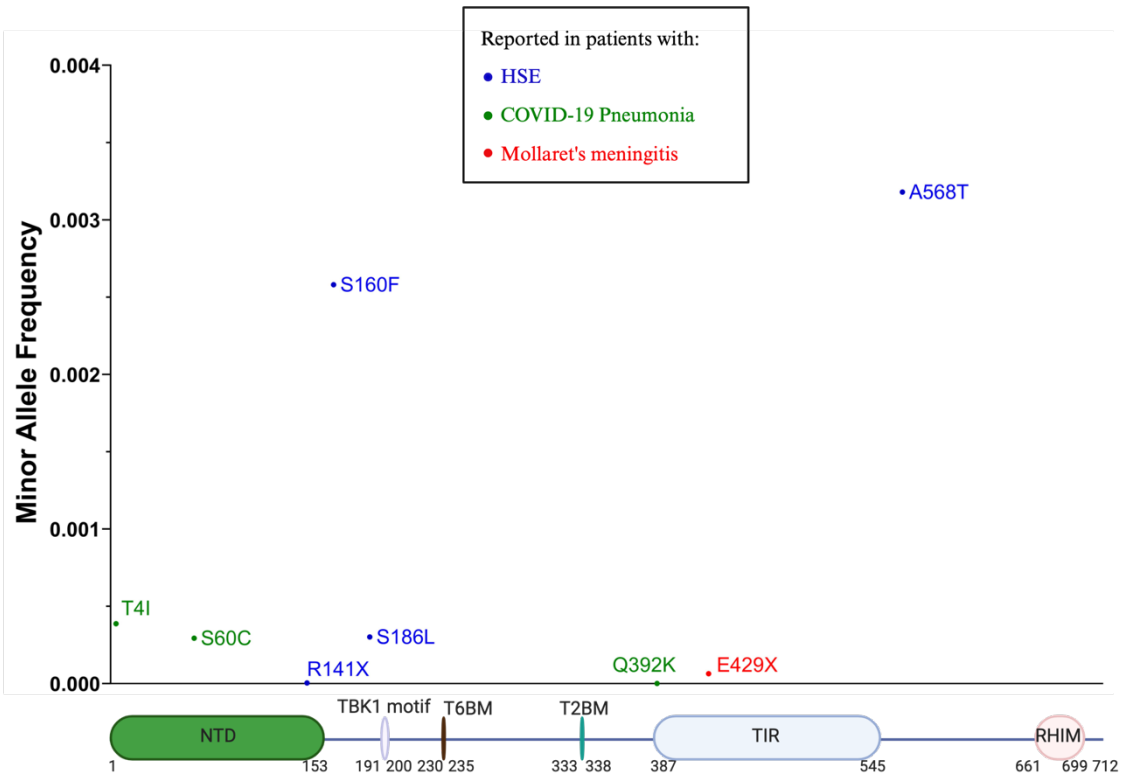


Figure 4.2 Lolliplot graph of *TICAM1* variants.

This lolliplot illustrating the allele frequency of *TICAM1* variants along a schematic representation of the TICAM1 protein to show their respective locations. Variants in blue are reported in HSE, in green

are reported in SARS-CoV-2 pneumonia patients, and in red is reported here in Mollaret's meningitis patient. HSE: herpes simplex encephalitis, NTD: N-terminal domain, TBK1 motif: TBK1 binding motif, T6BM: TRAF6 binding motif, T2BM: TRAF2 binding motif, TIR: TIR domain, RHIM: RIP (receptor-interacting protein) homotypic interaction motif.

4.3 Generation of *TICAM1* variant construct

My fellow laboratory colleague, Dr. Stephanie Hodeib, constructed the nonsense TICAM1 variant (E429X) identified here and subsequently, I carried out most of the functional tests. As mentioned in the previous chapter (Section 3.3), the previously described pEF-BOS mammalian expression vector containing the WT TICAM1 with its C-terminal tagged with HA, served as the foundation for incorporating nonsense variants. This was achieved through site-directed mutagenesis employing overlapping primer pairs featuring the specific single nucleotide substitution. Plasmids resulting from site-directed mutagenesis underwent Sanger sequencing to validate the successful incorporation of target variants. This confirmation was achieved by aligning the constructed plasmid sequences with the WT *TICAM1* sequence.

4.4 Identification of loss-of-expression *TICAM1* E429X variant

As mentioned in Section 3.5 previously, with regards to protein experiments, the transient transfection was done in the presence of z-VAD-fmk, which is a pan caspase inhibitor. This inhibitor was employed to prevent cell apoptosis, which is a feature of *TICAM1* overexpression, and hence ensuring a sufficient protein yield for subsequent testing. The transient transfection here was done in TICAM1-deficient cells (Sancho-Shimizu et al., 2011). Protein extraction from cell lysates and quantification were carried out in accordance with the procedures outlined in Section 2.8. TICAM1 protein expression was assessed by immunoblot where we used an antibody that recognised the TICAM1 peptide positioned at the N-terminal of TICAM1. Enhanced chemiluminescence was used because of its high sensitivity to detect the antibody and the images were captured by digital OCD camera. As mentioned in Section 3.5 previously,

the pEF-BOS-*TICAM1* construct of R141X was used as LoF (Sancho-Shimizu et al., 2011). The E429X variant did not produce any detectable TICAM1 protein similar to R141X. Protein expression levels of at least three independent experiments were quantified by densitometry results normalised to WT levels and expressed as relative intensity of TICAM1 (Figure 4.3).

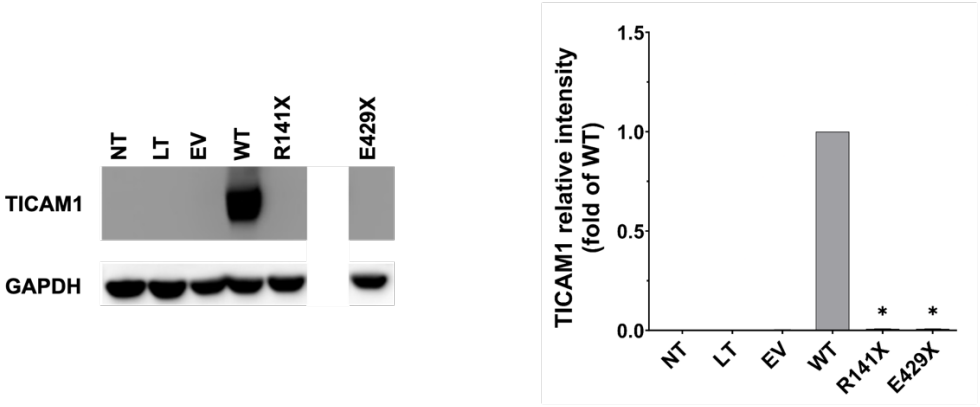


Figure 4.3 Impact of *TICAM1* E429X variant on protein expression.

TICAM1-deficient SV40-fibroblast cells were transiently transfected with WT, R141X, or E429X TICAM1**.** Immunoblots representative of n=3 and shows resolved TICAM1 proteins using antibody against an epitope on the N-terminal of TICAM1, with GAPDH used as a loading control. Densitometry analysed with Fiji/ImageJ, data shown as mean ± SEM and the differences between variants and wild type were tested in one-way ANOVA, significance shown with *$p<0.05$. NT; non-transfected, LT; lipofectamine transfected, EV; empty vector, WT; wild type.

Furthermore, to corroborate the finding of LoE variants observed in the immunoblots, immunofluorescent assay was utilised to detect the protein expressions where TICAM1-deficient cells were transiently transfected with the E429X *TICAM1* variant construct in the presence of pan caspase inhibitor. These cells were then fixed and probed with TICAM1 antibody to detect TICAM1 peptide at the N-terminal of TICAM1. Immunofluorescence was able to show protein at single cell level using confocal microscopy. The E429X variant showed absence of fluorescence of TICAM1 (Figure 4.4) and hence, confirming the LoE phenotype corroborating the findings from the immunoblot data. This immunofluorescence assay was conducted by Ms Dilys Santillo.

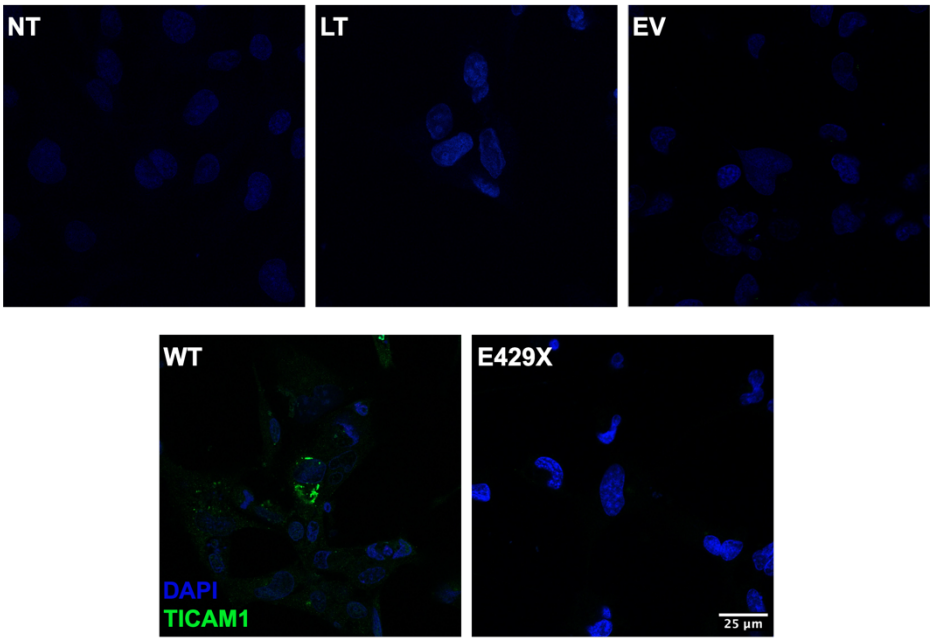


Figure 4.4 Impact of *TICAM1* E429X variant on protein expression by immunofluorescence.

TICAM1-deficient SV40-fibroblast cells were transiently transfected with WT, R141X, or E429X TICAM1. A primary antibody against an epitope on the N-terminal of TICAM (1:100) followed by a secondary antibody DyLight™ 488 Goat anti-Rabbit IgG (1:1000) was employed to stain the cells and visualisation of immunofluorescence was achieved with Widefield Axio Observer (Zeiss) using 63X oil-immersion lens. Scale bar represents 25 µm. Figure shows a representative replicate of n=3 and was performed by Ms Dilys Santillo. NT; non-transfected, LT; lipofectamine transfected, EV; empty vector, WT; wild type.

4.5 qPCR analysis of *TICAM1* overexpression

Next, we wanted to confirm that the expression at the protein level corresponds with the expression at transcriptional level in the overexpression system. Hence, the transient transfection here was conducted in TICAM1-deficient cells as outlined previously in Section 2.5. RNA samples were extracted from the transfected TICAM1-deficient cells using a protocol detailed in Section 2.16. Subsequently, the RNA samples were converted into cDNA via reverse transcription and RT-qPCR was performed using the cDNA product to determine *TICAM1* gene expression using Taqman-based qPCR. The level of E429X *TICAM1* mRNA expression (Figure 4.5) from at least three independent experiments was consistent with the

protein expression (Figure 4.3) in that there was no E429X *TICAM1* mRNA expression. This observation suggested the loss of expression is likely caused by nonsense-mediated mRNA decay. This differs from the previously reported (Sancho-Shimizu et al., 2011) R141X variant where no nonsense-mediated decay was observed, as evidenced by its mRNA level being similar to WT, and that result was reproducible in this chapter (Figure 4.5). I performed the transient transfections and subsequent collection of RNA samples, while Ms Dilys Santillo kindly performed the RT-qPCR assay.

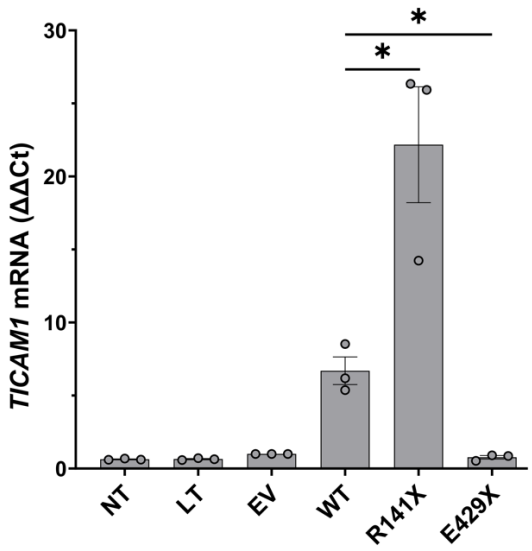


Figure 4.5 *TICAM1* mRNA level in transient transfection of overexpression.

The mRNA expression level of *TICAM1* were determined by RT-qPCR in TICAM1-deficient SV40-fibroblast transfected with WT or mutant TICAM1. Values are expressed as fold change with respect to Empty vector. Mean and SEM were calculated and t-test was used to assess statistical significance indicated by an asterisks (*$p<0.05$). The data shown are means of three biological replicates from three independent experiments (n=3). GUSB was used for normalisation. I conducted the transient transfections and subsequent RNA sample collection with the RT-qPCR assay being graciously conducted by Ms. Dilys Santillo. NT; non-transfected, LT; lipofectamine transfected, EV; empty vector, WT; wild type.

4.6 Functional characterisation of E429X *TICAM1* variant using luciferase reporter assays

As we have optimised the luciferase reporter assays in the previous chapter (Section 3.4), we promptly utilised the same luciferase reporter assays to assess the impact of E429X *TICAM1* variants on signalling function by overexpression system in TICAM1-deficient fibroblast cells. As mentioned previously in Section 3.5, pEF-BOS-*TICAM1* construct of R141X was used as loss-of-function (LoF) and pEF-BOS-*TICAM1* construct of S186L was used as hypomorphic control (Sancho-Shimizu et al., 2011). R141X variant was previously reported (Sancho-Shimizu et al., 2011) to result in complete TICAM1 deficiency with complete loss of expression, as evidenced by the lack of both IFN-β and NF-κB promoter induction. The level of induction was similar to that of cells transfected with pEF-BOS empty plasmid. Consistent with the lack of expression of the E429X variant, it was shown to be loss-of-function in terms of both IFN-β and NF-κB promoter inductions (Figure 4.6) when compared to WT.

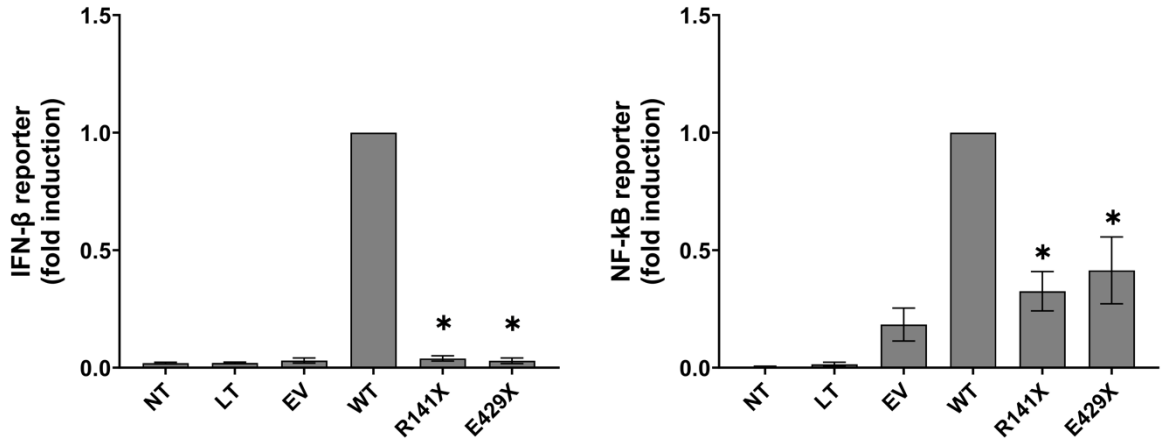


Figure 4.6 Impact of *TICAM1* E429X variant on IFN-β and NF-κB signalling.

TICAM1-deficient SV40-fibroblast cells were transiently transfected with WT, R141X, or E429X TICAM1 together with an IFN-β (left) or NF-κB (right) Firefly luciferase reporter to assess promoter induction upon TICAM1 overexpression. The Firefly luciferase values were normalised against Renilla luciferase activity and expressed as fold change with respect to cells transfected with WT TICAM1 vector. The data shown are means and SEM of three biological replicates from three independent experiment (n=3), and one-way ANOVA used to assess statistical significance when compared to WT indicated by an asterisks (*$p<0.05$). R141X variant is a known null variant and served as negative control. NT; non-transfected, LT; lipofectamine transfected, EV; empty vector, WT; wild type.

4.7 Complementation of Loss-of-Function E429X *TICAM1* variant

We further investigate the impact of this LoF variant. Ms Dilys Santillo has graciously volunteered to conduct the luciferase reporter assays in this section. We wanted to identify if these mutations were dominant negative mutations using luciferase reporter assays. As mentioned in the previous chapter (Section 3.7) ΔNΔC TICAM1 construct encodes a truncated dominant-negative TICAM1, consisting of only 162 amino acids of the TIR domain (Yamamoto et al., 2002), which served as a control for dominant negativity. In this section, 293HEK cells were used because of their ease of transfection and undetectable endogenous TICAM1 proteins similar to TICAM1-deficient cells. When 293HEK cells were transfected with equal amounts of WT and ΔNΔC TICAM1 plasmids, low levels of IFN-β and NF-κB inductions were observed. This aligned with the original findings, where proteins encoded by ΔNΔC TICAM1 would bind to the available TIR domain of WT TICAM1 proteins, thereby preventing the activation of IFN-β (Yamamoto et al., 2002). When 293HEK cells were transfected with equal amounts of WT and R141X plasmids, the levels of IFN-β and NF-κB inductions were similar to WT 200ng suggesting that R141X allele does not exert a dominant-negative effect which was consistent with the original findings (Sancho-Shimizu et al., 2011) and we utilised this as control in the assay. 293HEK cells were transfected with equal amounts of WT and E429X plasmids, the levels of IFN-β and NF-κB inductions were similar or greater to WT 200ng and WT with ΔNΔC TICAM1 (Figure 4.7). This suggested this allele does not exert a dominant-negative effect.

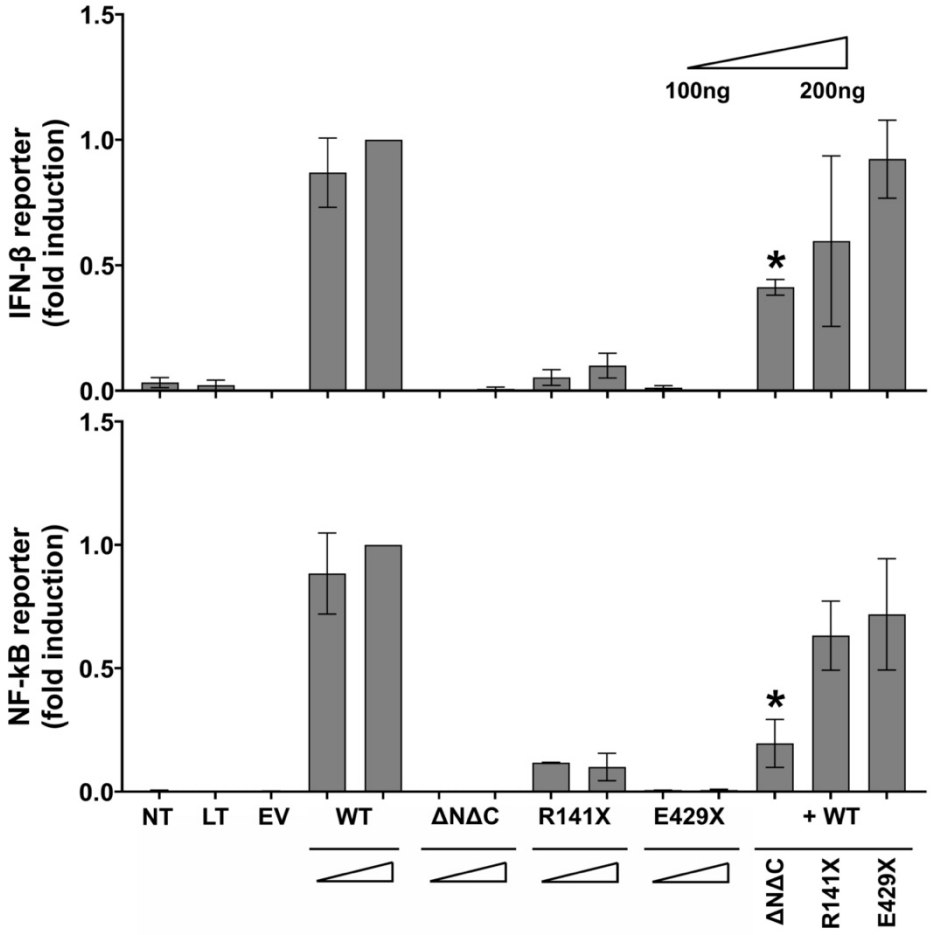


Figure 4.7 Impact of *TICAM1* E429X variant on IFN-β and NF-κB signalling.

HEK293 cells were transiently transfected with WT, R141X, or E429X TICAM1 together with an IFN-β (top) or NF-κB (bottom) Firefly luciferase reporter to assess dominant negative impact of *TICAM1* variant. The Firefly luciferase values were normalised against Renilla luciferase activity and expressed as fold induction with respect to cells transfected with 200 ng WT TICAM1 vector. The data shown are means and SEM of three biological replicates from three independent experiments (n=3), and one-way ANOVA used to assess statistical significance when comparing WT co-transfections (100 ng +100 ng) to 200 ng WT TICAM1 indicated by an asterisks (*$p<0.05$). NT; non-transfected, LT; lipofectamine transfected, EV; empty vector, WT; wild type, ΔNΔC; dominant negative construct of TICAM1 harbouring solely TIR domain with absence of both N and C terminal domains (Yamamoto et al., 2002).

4.8 E429X TICAM1 expression using patient's cells

We received patient's primary fibroblast cells from Dr Dorit Verhoven and Dr Taco Kuijpers, which were subsequently immortalised using SV40 large T antigen, as previously described (Chapgier et al., 2006). Total cellular extracts were obtained from both SV40 healthy control fibroblasts and SV40 Patient (P1) fibroblasts harbouring heterozygous nonsense E429X mutation in *TICAM1*, as previously described in Section 2.8 and Section 2.9. The detection of the endogenous TICAM1 protein was performed using immunoprecipitation (IP) due to its low basal expression in cells. As TICAM1 expression is tightly regulated, this method enabled the isolation and pooling of the available TICAM1 protein. We utilised a TICAM1 antibody recognising the N-terminal to bind with the magnetic beads, which gives sufficient surface area for a balanced high-capacity antibody binding and antigen yield. In this chapter, Protein G magnetic beads were utilised where the Protein G served as an affinity ligand that bind to the heavy chains on the Fc region of the IgG antibodies. This effectively orients the immobilised IgG antibodies, positioning their antigen-binding sites facing outward (Bjorck & Kronvall, 1984; Wikstrom et al., 1995). Immunoblot analysis of IP revealed that fibroblasts from the heterozygous P1 cells exhibited approximately 32% of TICAM1 protein levels when compared to TICAM1 in the healthy control (Figure 4.8). Protein expression levels were quantified by densitometry results normalised to healthy control level of TICAM1 in IP sample and expressed as relative intensity of TICAM1 (Figure 4.8).

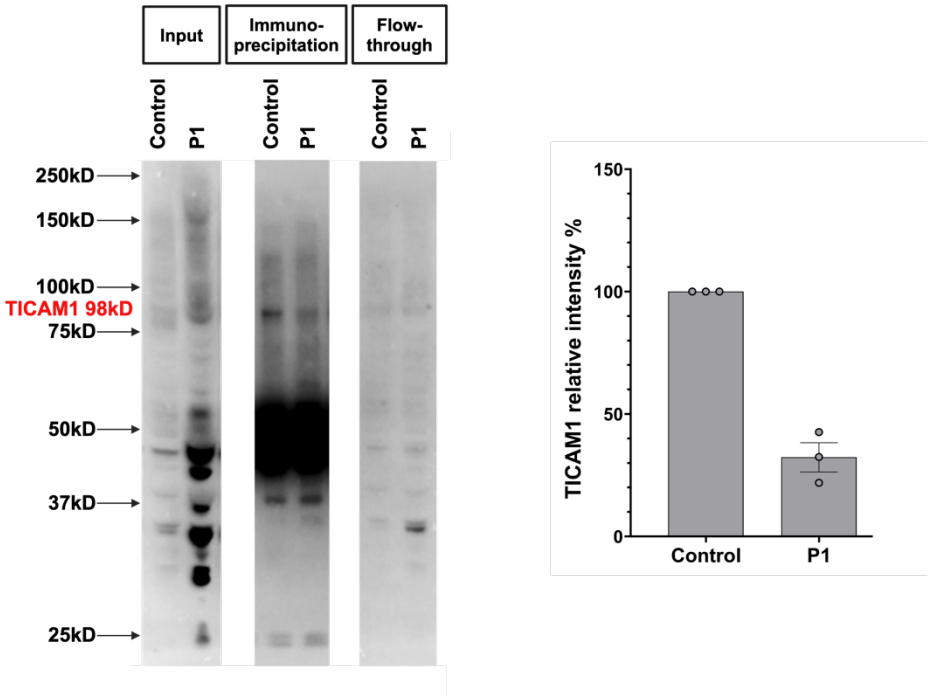


Figure 4.8 TICAM1 endogenous protein expression of P1.

Detection of endogenous TICAM1 protein in SV40-fibroblasts from both control and patient samples using immunoprecipitation and SDS-PAGE. Immunoblots shows resolved TICAM1 proteins using antibody against an epitope on the N-terminal of TICAM1. The results shown are representative of three independent experiments (n=3). Relative protein levels from the IP by comparing P1 to the control were assessed by densitometry using Fiji/ImageJ. P1 showed a TICAM1 protein expression level approximately equivalent to 32% of that observed in the TICAM1 expression of healthy control. Data shown as mean ± SEM.

4.9 qPCR analysis of endogenous *TICAM1* from patient's cells

Similarly, we wanted to confirm that the endogenous expression at the protein level corresponds with the endogenous expression at transcriptional level in the basal state of patient's cells. RNA samples were extracted from multiple SV40 healthy control fibroblasts and SV40 P1 fibroblasts using a protocol detailed in Section 2.16. *TICAM1* mRNA transcript level of P1 did not show a significant difference when compared to the *TICAM1* mRNA transcript in controls, based on at least three independent experiments (Figure 4.9). This result contrasts with the observations we observed in the overexpression system (Figure 4.5), which

could be attributed to the heterozygous state of P1. I extracted the RNA samples, while Ms Dilys Santillo kindly performed the RT-qPCR assay.

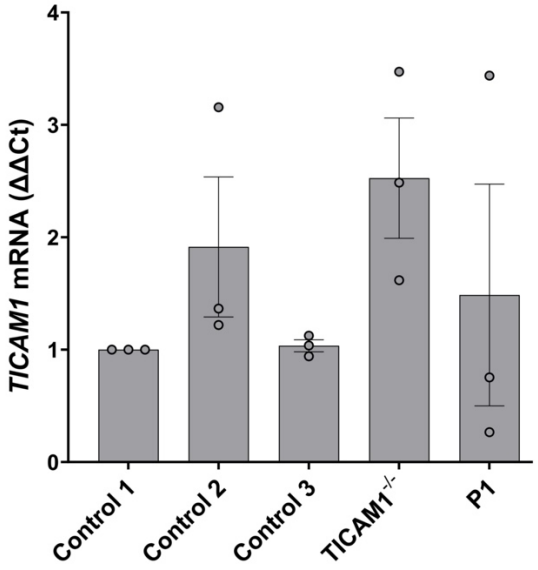


Figure 4.9 Endogenous *TICAM1* mRNA level in SV40-fibroblasts.

The mRNA expression level of TICAM1 were determined by RT-qPCR in three human healthy control SV40-fibroblasts labelled as Control 1-3, alongside TICAM1-deficient and P1 SV40-fibroblasts. The obtained values are presented as fold changes relative to Control 1, providing a normalised comparison. Mean and SEM were calculated. Data are represented as relative fold change (ΔΔCt units), where GUSB was used for normalisation. Data shown are means of three biological replicates from three independent experiments (n=3). I collected the RNA samples with the RT-qPCR assay being graciously conducted by Ms. Dilys Santillo.

4.10 Characterisation of E429X *TICAM1* variant upon ligand stimulations

Dermal fibroblasts in human express TLR3 and TLR4 on the cell membrane, exhibiting the ability to produce IFN-β and IFN-λ upon stimulation (Zhang et al., 2007; Israel et al., 2017). To evaluate the impact of the E429X *TICAM1* mutation on the antiviral response, fibroblasts from patient (P1) and healthy controls were stimulated with increasing concentration of poly(I:C), a synthetic analog of dsRNA and a TLR3 agonist. Given their previously established characterisation of having deficiency in TLR3 signalling, the TICAM1-deficient fibroblast cells were utilised here as a negative control (Sancho-Shimizu et al., 2011). We observed that

P1 fibroblasts displayed a deficiency in the production of IFN-β, IFN-λ/IL-29 and IL-6 across all concentrations (Figure 4.10). This impaired response occurred despite maintaining a normal cytokine secretion following stimulation of transfected poly(I:C), a known trigger for the TLR3-independent cytosolic dsRNA receptors MDA5/RLR signalling pathways (Kato et al., 2008).

TICAM1 is recognised for its interaction with TLR4 in both humans and mice (Fitzgerald et al., 2003b) and has been demonstrated to regulate IFN induction by LPS in mouse models (Hoebe et al., 2003; Yamamoto et al., 2003a; Yamamoto et al., 2003b). Consequently, we evaluated the induction of IFN-β, IFN-λ, and IL-6 cytokines in response to LPS stimulation in primary fibroblast cells from the patient (P1), primary fibroblasts cells from a healthy control, as well as SV40-transformed fibroblast cells from the patient (P1), SV40 TICAM1-deficient fibroblast cells and SV40 fibroblast cells from healthy controls. As anticipated, P1 SV40 fibroblasts exhibited an unresponsive reaction to LPS, a TLR4 agonist, in terms of IFN-β, IFN-λ/IL-29, and IL-6 levels production (Figure 4.10). P1 SV40 fibroblast cells were also stimulated with IL-1β and TNF-α to demonstrate the response integrity of other non-TICAM1 dependent pathways and these cells exhibited normal IL-6 production (Figure 4.11).

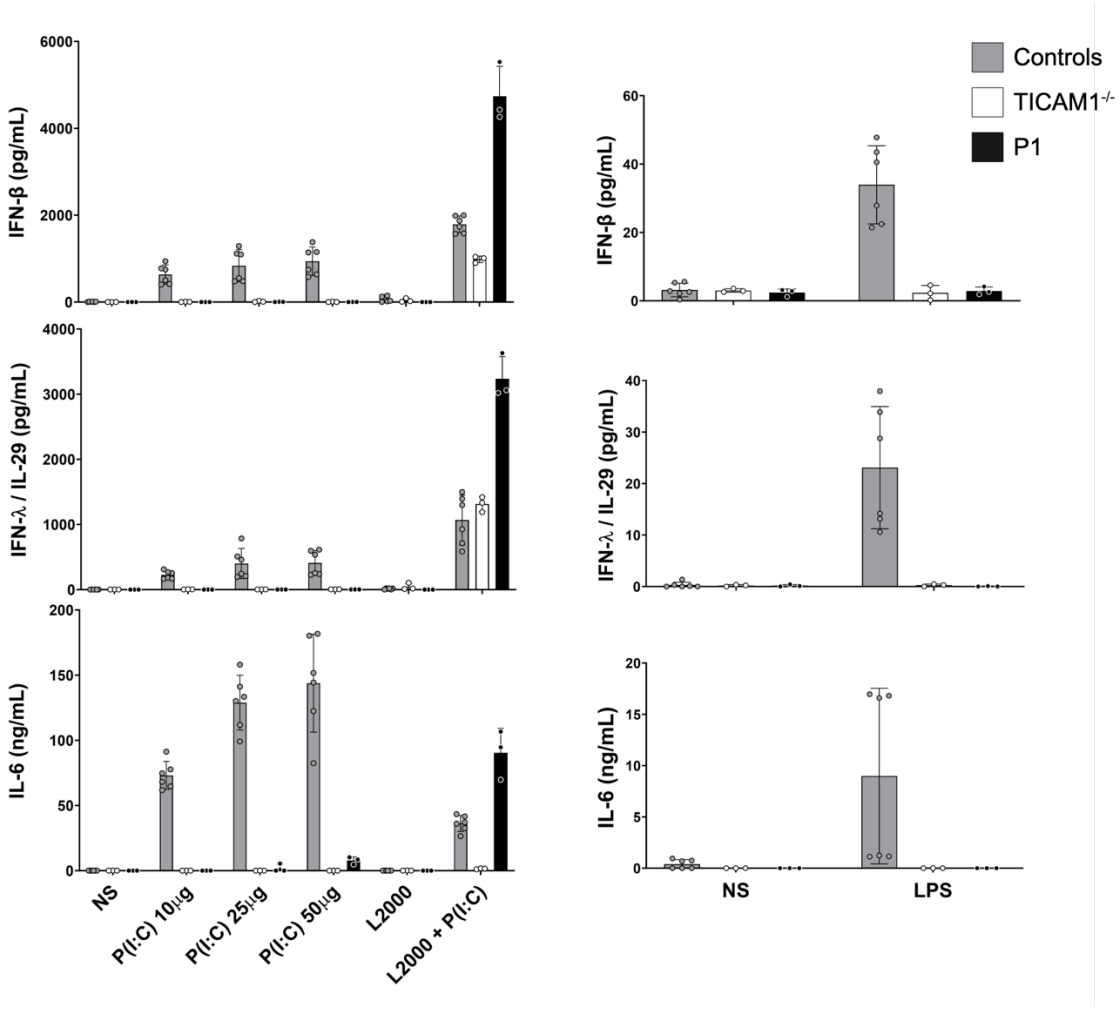


Figure 4.10 Cytokines levels in SV40-fibroblasts upon stimulation with P(I:C) and LPS.

Controls (Control 1 and Control 2), TICAM1-deficient and P1 SV40-fibroblast cells were left unstimulated (NS) or stimulated with different amounts of poly(I:C) (10-50 µg/ml) (left) or stimulated with LPS (100 ng/ml) (right) for 24 hours. In this experiment settings, two fibroblast controls were utilised and represented on the same bar to provide an average of two different fibroblasts controls. The results shown are representative of three independent experiments (n=3) and production of cytokines was assessed by Meso Scale Discovery immunoassays and ELISA. Mean and SD were calculated. NS; non-stimulated, L2000; lipofectamine transfected, P(I:C); polyinosinic:polycytidylic, LPS; lipopolysacharides.

These observations align with the recognised function of TICAM1 as the exclusive adaptor to TLR3 and a variable adaptor to TLR4. This indicates that the discernible levels of WT TICAM1 observed in the fibroblasts of P1 through IP (Figure 4.8) may not be adequate for IFN production.

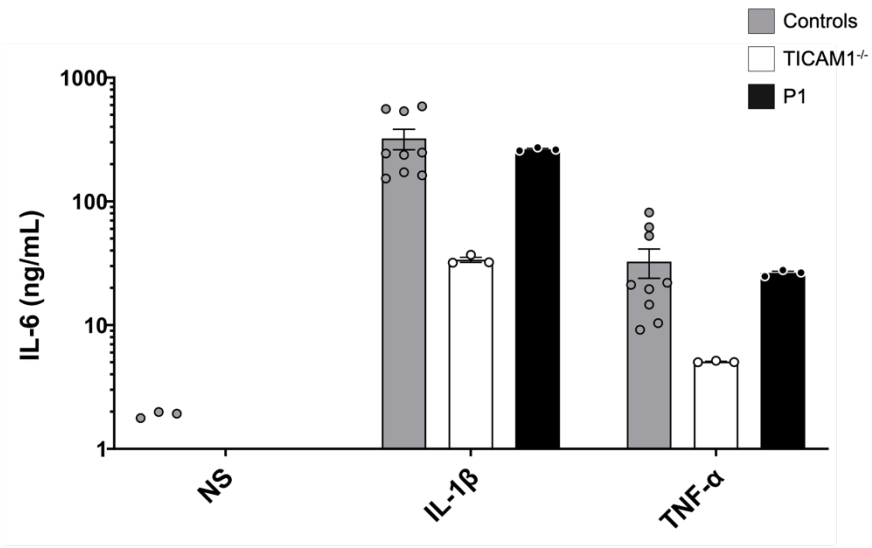


Figure 4.11 Cytokines levels in SV40-fibroblasts upon stimulation with IL-1β or TNF-α.

Controls (Control 1, Control 2 and Control 3), TICAM1-deficient and P1 SV40-fibroblast cells were left unstimulated (NS) or stimulated with IL-1β or TNF-α for 24 hours. In this experiment settings, three fibroblast controls were utilised and represented on the same bar to provide an average of two different fibroblasts controls. The results shown are representative of three independent experiments (n=3) and production of IL-6 cytokines was assessed by ELISA. Mean and SD were calculated. NS; non-stimulated. NS; non-stimulated.

4.11 Characterisation of E429X *TICAM1* variant upon viral infection

Next, we examined the *in vitro* antiviral response to HSV-1 and HSV-2. Given P1's history of HSV-2 meningitis, we subjected P1 cells not only to HSV-2 infection but also to HSV-1 infection. This was done to demonstrate P1's susceptibility to infections from other similar neurotropic viruses and given the observation of TICAM1 deficiency underlying HSE. P1 SV40 fibroblasts cells, SV40 TICAM1-deficient fibroblast cells, and SV40 fibroblast cells from healthy controls were infected with GFP-tagged HSV-1 at MOI 1, and RFP-tagged HSV-2 at MOI 1 and MOI 10, allowing viral replication to proceed for 24 hours. Viral replication of HSV-1 and HSV-2 were visualised by GFP and RFP fluorescence, respectively, using immunofluorescence imaging at 24 hours post-infection (Figure 4.12). Considering their

previously established characterisation of having deficiency in TLR3 signalling, TICAM1-deficient fibroblast cells were used as a control. We observed enhanced viral replication of HSV-1 under immunofluorescence imaging, indicated by positive GFP fluorescence in P1 fibroblasts compared to the control fibroblasts (Figure 4.12). In addition, there appears to be a more pronounced infection in P1 than in TICAM-1-deficient fibroblasts (Figure 4.12). At MOI 1 of HSV-2 infection, the viral replication was observed through the positive RFP fluorescence but the difference between P1 and TICAM1-deficient fibroblasts was not obvious (Figure 4.12). Hence, we infected the cells at a higher MOI (MOI 10) and indeed, there was more pronounced infection in P1 than in TICAM1-deficient fibroblasts (Figure 4.12). The fibroblasts from healthy control utilised in this chapter appeared to be resistant to both HSV-1 and HSV-2 indicated by minimal positive GFP and RFP fluorescence, respectively. These infection experiments were conducted in triplicate and independent of each other to ensure robustness and reliability.

To quantify the observation seen in fluorescence imaging, we employed titration by plaque assay technique on Vero cells with detailed protocol outlined in Section 2.14. The viral titre of MOI 1 infections was determined using the plaque assay, and the result were consistent with the findings from fluorescence imaging, revealing a significant difference between P1 and healthy control fibroblasts in both viruses (Figure 4.12). These observations suggested that P1 fibroblasts cells are susceptible to both viruses.

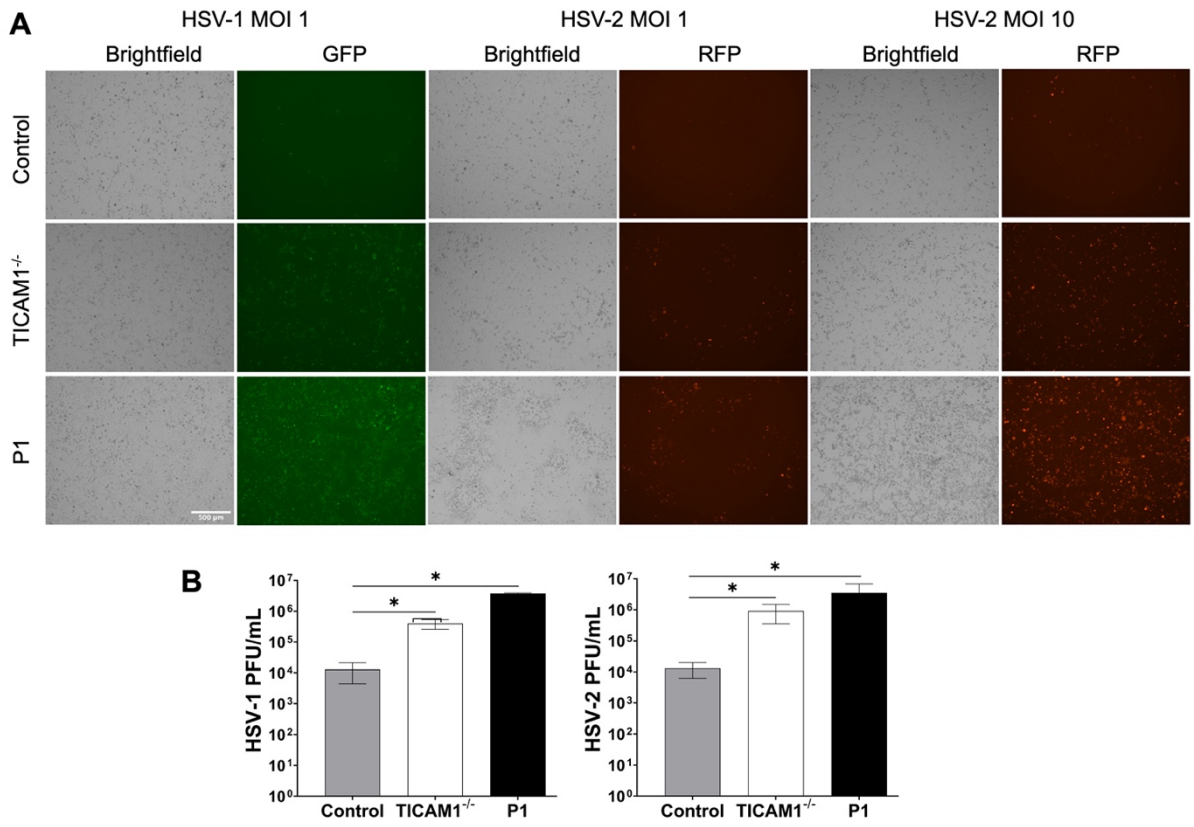


Figure 4.12 Impact of HSV-1 and HSV-2 infections on SV-40 fibroblasts.

Control, TICAM1-deficient and P1 SV40-fibroblast cells were infected with HSV-1-GFP or HSV-2-mCherry (RFP) for 24 hours and viral replication assessed by A) fluorescence imaging at 4x magnification using EVOS™ FL Auto 2 (Invitrogen). Scale bar represents 500 µm. Figure shows a representative replicate of n=3. B) HSV-1 and HSV-2 replication in cells infected with MOI 1 were titrated by plaque assay on Vero cells. The results shown are representative of three independent experiments. Mean and SD were calculated. T-test was used to assess statistical significance indicated by an asterisks (*$p<0.05$).

Subsequently, we wanted to measure the cytokines produced during the infection and thus, we collected supernatants from infected fibroblasts 24 hours post-infection. We employed both immunoassay technologies of Meso Scale Discovery (MSD) and ELISA to quantify the cytokines produced from MOI 1 infected cells. There was a lack of IFN-β and IFN-λ/IL-29 production in both HSV-1 infected and HSV-2 infected P1 fibroblasts (Figure 4.13). Taken together, the susceptibility of P1 to viruses likely arises from lack of protective IFN-β and/or IFN-λ/IL-29 during viral infection. This outcome was anticipated due to the TICAM1 deficiency, resulting in the abolished TLR3 signalling required for IFNs production.

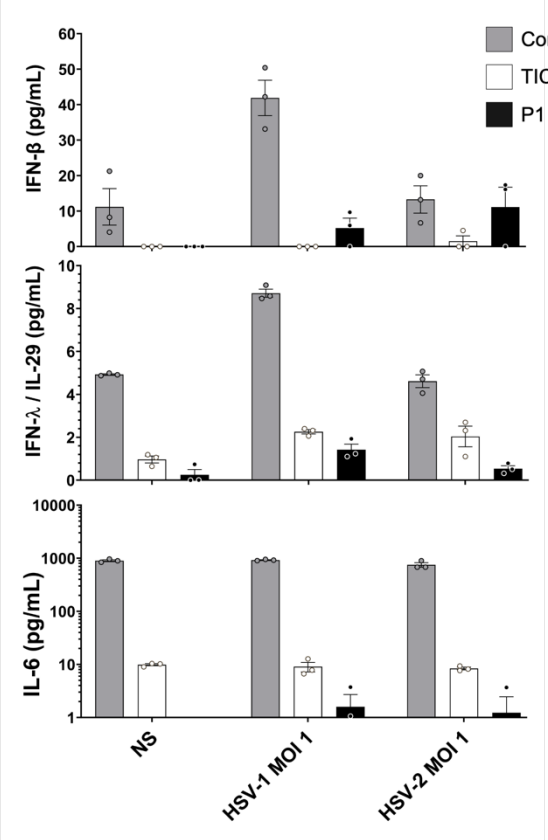


Figure 4.13 Cytokines levels in SV40-fibroblasts upon infection with HSV-1 and HSV-2.

Control, TICAM1-deficient and P1 SV40-fibroblast cells were infected with HSV-1-GFP or HSV-2-mCherry for 24 hours. Supernatants collected from the infected cells were assayed for production of cytokines IFN-β and IFN-λ/IL-29 by Meso Scale Discovery immunoassays and IL-6 by ELISA. The results shown are representative of three independent experiments (n=3). Mean and SD were calculated. NS; non-stimulated.

We received a last remaining frozen vial of P1 PBMCs from Amsterdam and Ms Dilys Santillo generously volunteered to salvage and infect the limited available PBMCs with HSV-1. Given our laboratory's extensive experience with HSV-1 virus, and limited PBMC cell numbers we opted to infect the PBMCs with HSV-1 instead of HSV-2. This PBMCs experiment was conducted only once. PBMCs from P1 and healthy controls were infected with GFP-tagged HSV-1 at MOI 1 for 24 hours. Their supernatants were harvested 24 hours post-infection and cytokines concentrations were measured using MSD immunoassay by me. The induction of cytokines in P1 PBMCs following HSV-1 infection demonstrated normal cytokine production including IFN-α2a, TNF-α, IFN-λ/IL-29, and IL-6 (Figure 4.14). This result suggested that the viral response in PBMCs was maintained.

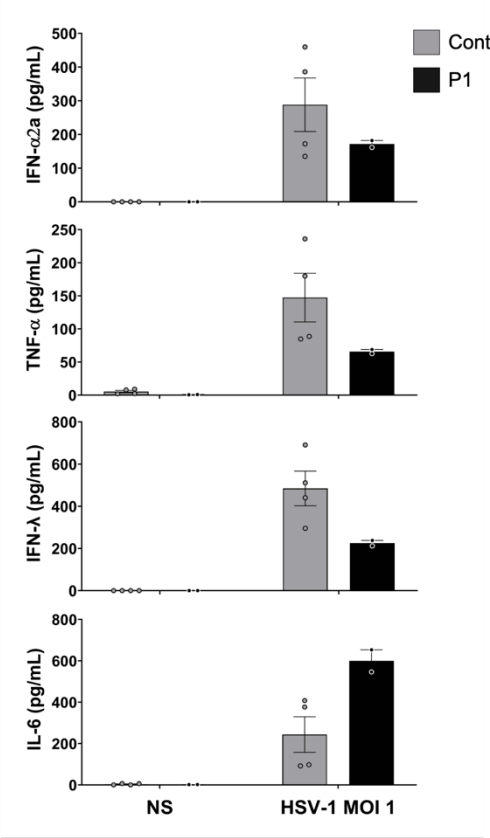


Figure 4.14 Cytokines levels in PBMCs upon infection with HSV-1.

Controls (from two healthy donor) and P1 PBMCs were left unstimulated (NS) or stimulated with HSV-1 for 24 hours. In this experiment settings, two PBMC controls were utilised and represented on the same bar to provide an average of two different PBMC controls. Supernatants collected from the infected cells were assayed for production of cytokines IFN-α2a, TNF-α and IFN-λ by Meso Scale Discovery immunoassays. This experiment has only been performed once. Mean and SD were calculated. NS; non-stimulated.

4.12 Infection upon complementation of E429X fibroblast cells

Having demonstrated the susceptibility of P1 fibroblast cells in the previous section, we posed the question of whether patient's fibroblast cells can be rescued with expression of WT *TICAM1* gene using luciferase reporter assay. We performed transient transfection of either pEF-BOS-*TICAM1* WT or E429X construct plasmid into P1 SV40 fibroblast cells in the presence of z-VAD-FMK, a pan caspase inhibitor, for 24 hours. As mentioned before, this inhibitor was employed to prevent cell apoptosis, ensuring a sufficient number of viable cells

for subsequent infection. After 24 hours of transfection, these fibroblast cells complemented either with WT *TICAM1* or with P1's mutation E429X were subjected to RFP-tagged HSV-2 infection. The complementation of WT *TICAM1* into P1 fibroblast cells restored the IFN-β promoter induction upon HSV-2 infection (Figure 4.15). Conversely, the complementation of E429X *TICAM1* into P1 fibroblast cells failed to restore the IFN-β promoter induction upon HSV-2 infection (Figure 4.15). This highlights the important role of TICAM1 in viral infections.

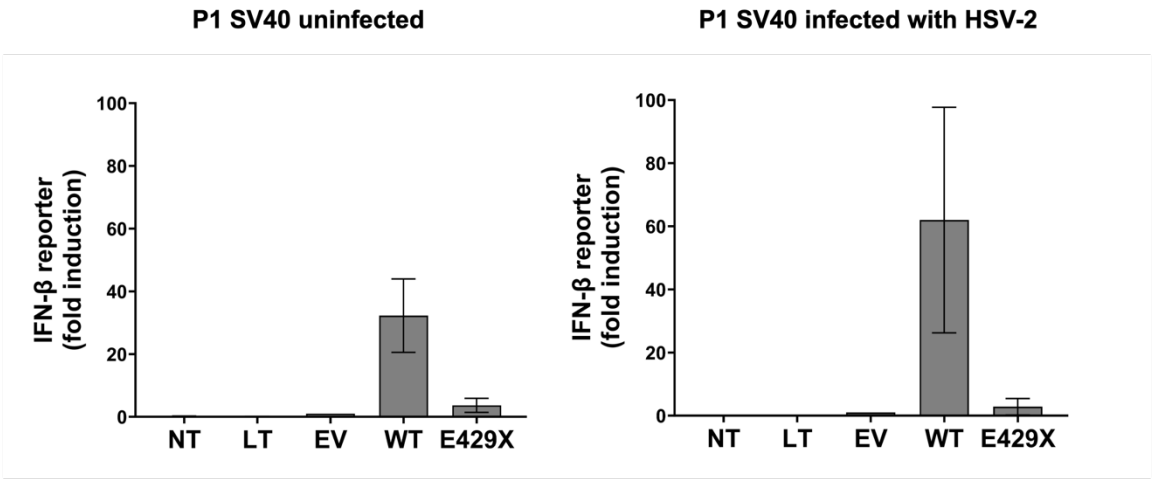


Figure 4.15 Impact of complementation on P1 SV40 fibroblasts.

P1 SV40-fibroblasts were transiently transfected with empty vector, WT or E429X TICAM1 and/or infected with HSV-2. z-VAD-fmk (a cell-permeable pan-caspase inhibitor) was used to prevent apoptosis upon transfection. IFN-β luciferase reporter assays to assess the complementation effect and the values were expressed as fold change with respect to cells transfected with empty vector. The results shown are representative of three independent experiments (n=3). Mean and SD were calculated. NT; non-transfected, LT; lipofectamine transfected, EV; empty vector, WT; wild type.

4.13 Discussion

Although HSE rarely exhibits recurrence and is characterised by its potentially lethal nature, coupled with severe neurological sequelae, Mollaret's meningitis is distinguished by recurrent episodes marked by meningeal irritation, accompanied by fever and mononuclear pleocytosis (Min & Baddley, 2014). While it has been documented that around 85% of individuals with primary HSV-2 meningitis exhibit active herpetic lesions in the days preceding the onset of meningism (Kirkland et al., 2020), it is noteworthy that existing case reports in the literature have not provided accounts of any additional extra-cerebral manifestations, such as ocular or orolabial lesions, at the time of presentation (Abu Khattab et al., 2009; Goyal & Ali, 2020; Grinney & Mohseni, 2022; Ahmad & Alsaeed, 2023). Moreover, it has been reported that over 50% of patients experiencing recurrent lymphocytic meningitis attributed to HSV-2 do not have a history of genital herpes (Rosenberg & Galen, 2017). The presence of active genital vesicular lesions during episodes of viral HSV-2 meningitis is not consistently observed, adding a layer of complexity to the clinical presentation of HSV-2 meningitis beyond the commonly associated genital manifestations (Rosenberg & Galen, 2017). This unique observation renders our study distinctive, potentially marking it as one of the few reports to document such findings.

The loss of expression (LoE) and loss of function (LoF) E429X allele leads to the complete abolishment of TLR3-mediated signaling pathways and TICAM1-dependent TLR4 production of IFNs and pro-inflammatory cytokines within the heterozygous cells of P1. There were quite a few of P1’s family members that are heterozygous for this mutation, yet they have not suffered any instances of HSE or HSM. This indicates an incomplete penetrance where the presence of the mutation does not necessarily correlate with the manifestation of severe infections in the family members. Additionally, it's noteworthy that the E429X allele did not demonstrate dominant-negative effects in transfection assays conducted with HEK293 cells. The E429X variant exhibits a LoE at both the mRNA and protein levels, leading to decreased protein levels in the heterozygous state of P1 (WT/E429X) (Figure 4.3, Figure 4.5). This suggests TICAM1 haploinsufficiency as a mechanism of LoE similar to the previous reported

R141X variant in a homozygous patient where no nonsense-mediated mRNA decay occurred and no detectable protein was observed (Sancho-Shimizu et al., 2011).

Even though there was a reduction in TICAM1 protein levels observed in P1's heterozygous cells, their leukocytes exhibited a robust normal response to HSV-1 infection through the induction of IFN-α2a, TNF-α, IFN-λ/IL-29, and IL-6 cytokines (Figure 4.14). This implies that despite the decreased levels of TICAM1 protein, its functional capacity remained intact in facilitating the cellular response to HSV-2 within the leukocytes of P1. Dr Dorit Verhoeven also conducted an investigation into the phosphorylation of signalling proteins downstream of TLR3, TLR4, and the IFN-α/β receptor in PBMCs stimulated with poly(I:C), LPS, and IFN-α (Figure 7.1 in the Appendix). Notably, the fold induction of poly(I:C)-induced phosphorylation of NF-κB-p65 and IRF3, but not LPS-induced, was significantly diminished in the monocytes of the patient compared to those in healthy controls. Interestingly, the levels of induced pSTAT1 and CD169 upregulation were comparable to control cells across all stimuli tested. These findings suggest that while poly(I:C)-induced TLR3 signalling in patient monocytes is diminished, the subsequent IFN-dependent signalling pathway remains intact. These observations align with previous investigations into monogenic defects associated with HSE, such AD and AR TLR3 mutations (Zhang et al., 2007; Guo et al., 2011), AR UNC93B mutations (Casrouge et al., 2006), AD TRAF3 mutations (Perez de Diego et al., 2010), AD and AR TICAM1 mutations (Sancho-Shimizu et al., 2011), and AD TBK1 mutations (Herman et al., 2012). In these cases, the response to TLR3 ligands in patients' leukocytes remained unaffected despite the genetic defects indicating a TLR3-independent response. This observation may suggest alternative pathways for responding to dsRNA mediated by MDA5 or RIG-I, and potentially other pathways yet to be fully elucidated (Yoneyama et al., 2004; Gitlin et al., 2006).

Interestingly, a monoallelic variant in the *IKBKE* gene, responsible for encoding the IKKε kinase crucial for initiating the expression of antiviral IFN genes, was identified in a patient who had experienced recurrent episodes of HSV-2 meningitis (Reyahi et al., 2023). The patient's PBMC exhibited compromised induction of IFN-β expression upon HSV-2 infection or exposure to dsDNA. Notably, there was a failure to induce the phosphorylation of IKKε,

crucial for its kinase activation, as well as STING within the cGAS/STING pathway, which is essential for recruiting IRF3 and initiating IFN-β expression. Intriguingly, the IKKε patient's PBMCs exhibited no impairment in response to the poly(I:C) or HSV-1 infection or various RNA viruses in terms of *IFNB1* mRNA expression suggesting a potential central role for other cytoplasmic dsRNA sensors in identifying HSV-1 in the PBMC. This aligns with our study findings, where PBMCs from our patient, despite harbouring a LoF TICAM1 variant, displayed a robust response to HSV-1, suggesting the existence of intricate compensatory mechanisms in antiviral responses.

Conversely, when they were assessing fibroblasts from the IKKε patient, a distinct pattern emerged. The patient's fibroblasts showcased impaired virus-induced expression of *IFNB1* mRNA in response to both HSV-1 and HSV-2, coupled with an augmented HSV-2 load and this substantiates the notion of defective anti–HSV-2 defence in the fibroblasts and establishes a link between defective *IFNB1* expression and heightened susceptibility to HSV-2 replication (Reyahi et al., 2023). Similarly, we observe a parallel pattern in our study, where P1 fibroblasts also exhibit defective IFN-β induction with the *TICAM1* variant, aligning with an increased susceptibility to HSV-2 replication.

Even more remarkably, the depletion of *IKBKE* in induced pluripotent stem cells (iPSCs)-derived microglia demonstrated a notable reduction in HSV-2–induced expression of *IFNB1*, while this effect was not observed in iPSC-derived neurons (Reyahi et al., 2023). Interestingly, the reduction of cGAS expression, rather than TLR3 expression, had a substantial impact on impairing HSV-2–induced IFNB expression in iPSCs-derived microglia, highlighting the dependence of HSV-2–induced expression of *IFNB1* on cGAS as the primary sensor. These findings shed light on the distinct roles played by specific cellular components in the intricate signalling pathways activated in response to HSV-2 infection, providing valuable insights into the underlying mechanisms of antiviral responses in different cell types. Additionally, it's noteworthy that several pivotal immune regulatory elements implicated in type I IFN signaling, including RIG-I, MAVS, cGAS, and STING, are subject to regulation by autophagy mechanisms (Zhang et al., 2021). This intricate interplay suggests that autophagy modulation could have far-reaching effects on the regulation of type I IFN production. Understanding these

mechanisms provides crucial knowledge about the antiviral responses in different cell types within the meninges, which include CNS fibroblasts, vascular networks, lymphatic vessels, neural stem cells, and specialized immune cells (Derk et al., 2021). Given this complexity, it is plausible that cells other than neurons play essential roles in the anti-HSV-2 response within the meninges. Exploring innovative *in vitro* models tailored to study the intricacies of CNS-resident cells could significantly enhance our ability to address relevant translational research questions which could significantly contribute to advancing our understanding of various neurological processes involved in antiviral responses.

The nonsense E429X variant allele leads to the complete absence of the TICAM1 protein. Situated within the TIR domain of TICAM1, this variant is of critical significance as the TIR domain plays a pivotal role in facilitating interactions with both the TIR domain of TLR3 and the TLR4 adaptor TICAM2, thereby forming TIR-TIR domain interactions. An early investigation has pinpointed a pivotal functional site within the TIR domain of TICAM1, unravelling the significance of this domain in orchestrating essential molecular interactions (Oshiumi et al., 2003). Specifically, the identification of the human *TICAM-1* variant P434H has illuminated its profound impact on TLR3-mediated IFN activation, resulting in the complete loss of TLR3-mediated IFN activation (Oshiumi et al., 2003; Funami et al., 2008; Enokizono et al., 2013). This observation underscores the indispensability of the 434Pro residue for both the binding and signalling functions of TICAM-1. The position of the E429X variant (at amino acid 429) is in close proximity to the identified functional site (at amino acid 434). Drawing parallels with the observed impact of the P434H variant, one could postulate that a mutation in the vicinity, as seen in the E429X variant, would yield a similar effect. Consequently, the disruption caused by the E429X variant within this domain is expected to compromise TICAM1's ability to engage in critical interactions, thereby affecting the downstream signalling cascade. This is consistent with the experimental findings demonstrating the absence of IFN-β induction. Exploring the interaction between the *TICAM1* E429X variant and TLR3 through immunoprecipitation could provide valuable insights into the molecular dynamics. Given that TIR domain is affected by the E429X variant, conducting IP experiments may elucidate the potential disruption of TIR-TIR domain interactions. Furthermore, the premature termination of the protein sequence resulting from the mutation leads to the loss of the RHIM domain which resides in the C-terminal region of TICAM1. The

RHIM domain is essential for forming associations with RIP1, a crucial mediator in the activation of the NF-κB pathway by TICAM1 (Sharma et al., 2003; Han et al., 2004; Kaiser & Offermann, 2005). Given this integral role of the RHIM domain in the interaction with RIP1, it is not surprising that the observed lack of NF-κB induction in the experimental findings aligns with expectations.

In addition to the established susceptibility to HSV-1 as documented previously (Sancho-Shimizu et al., 2011; Mork et al., 2015), this study contributes novel evidence indicating that TICAM1 deficiency serves as the underlying cause not only for HSV-2 cerebral infections but also for extra-cerebral manifestations. Our findings highlight the pivotal role of TICAM1 in regulating the replication of both HSV-1 and HSV-2 aligns with the concept implicating TLR3 in the detection of dsRNA intermediates stemming from HSV-1 and HSV-2 infections. However, beyond its involvement in dsRNA sensing, TLR3 is also recognized recently for its crucial contribution to governing the constitutive production of IFN-β in fibroblasts (Gao et al., 2021). This constitutive IFN production deemed crucial in facilitating the early clearance of viral pathogens. In that investigation, the researchers discovered that, under basal conditions, human fibroblasts predominantly expressed IFN-β among the IFN genes. Notably, control fibroblasts exhibited elevated levels of basal IFN-β secretion compared to TLR3-deficient or UNC93B-deficient fibroblasts. Furthermore, the fibroblasts with deficiencies in either TLR3 or IFN signalling showcased diminished basal expression levels of both IFN and interferon-stimulated genes (ISGs). These experiments emphasize the pivotal role of TLR3 in preserving the constitutive expression of antiviral genes, highlighting its contribution to the intrinsic antiviral immune response in human fibroblasts. Furthermore, they provided compelling evidence for the necessity of TLR3 signalling in orchestrating this constitutive antiviral response, ultimately restricting early viral replication. The findings collectively support the notion that TLR3-dependent IFN-β acts as a protective cytokine, and the maintenance of constitutive IFN-β production governs the intrinsic antiviral immunity in human fibroblasts. Importantly, these insights hold potential relevance to our understanding of *TICAM1* E429X variant cells and their increased susceptibility to HSV-1 and HSV-2 infections, along with a reduced induction of IFN-β. By elucidating the underlying mechanisms governing the innate immune response in the context of TICAM1 mutations, this research could offer invaluable insights into the pathogenesis of viral infections. Therefore, ensuring adequate sensing

mechanisms during viral replication and infection appears imperative for the immune regulation of HSV.

Although we have provided initial evidence suggesting that the introduction of WT TICAM1 into P1 fibroblast cells reinstated IFN-β promoter induction during HSV-2 infection, and conversely, the introduction of E429X TICAM1 into P1 fibroblast cells failed to restore the IFN-β promoter induction during HSV-2 infection, we have yet to present the viral titre data, which would serve as conclusive evidence of successful rescue. Our attempts to conduct a plaque assay were hindered by challenges in quantifying the plaques, attributed to the phenomenon wherein transfecting mammalian cells with bacterial, viral, or synthetic nucleic acids to induce type I IFN responses, thereby complicating the quantification of HSV-2 replication (Huerfano et al., 2013). Moving forward, our next course of action entails exploring the feasibility of utilising RT-qPCR to measure the viral mRNA of these transfected and infected cells. However, the ideal strategy would be to employ CRISPR/Cas9 gene modification in P1 cells to introduce the WT *TICAM1* and its E429X variant. Subsequently, infecting these cells and measuring outcomes, such as IFN-β cytokine induction and viral titre. This comprehensive approach will offer a more robust assessment of the functional implications of the *TICAM1* E429X variant in the context of HSV-2 infection.

Expanding the range of clinical manifestations, both our research and that of other investigators have revealed the presence of pathogenic heterozygous variants in the *TICAM1* gene among adults who had not previously experienced hospitalization for any other viral illnesses (Figure 4.2) (Sancho-Shimizu et al., 2011; Mork et al., 2015; Zhang et al., 2020). The identification of *TICAM1* genetic variants and their association with severe SARS-CoV-2 pneumonia in three adults suggests a broader implication of the TLR3-TICAM1-IFN pathway, extending beyond susceptibility to HSV-1 and HSV-2 to encompass other viral conditions with life-threatening manifestations outside the CNS. Notably, the observed incomplete penetrance in this and similar families raises the intriguing possibility that the TLR3-TICAM1-IFN pathway might be dispensable for host defence against HSV in certain individuals. Further exploration is warranted to elucidate the intricate interplay of viral and host modifying factors that could

contribute to differential susceptibility to HSV reactivation and, consequently, account for the observed incomplete penetrance in the familial cases.

In conclusion, our investigation offers evidence highlighting the significance of TICAM1 in regulating not only cerebral but also extra-cerebral manifestations of HSV-2. This implies a broader clinical spectrum of the disease beyond the confines of HSE. While these novel insights are significant, they also unveil numerous captivating avenues for future investigation, thereby offering promising opportunities for ongoing research endeavours in this field.

Chapter 5

5. Modelling HSV-1 infection in cerebral organoids

The research detailed in this chapter was conducted in collaboration with fellow laboratory colleague, Ms Aneesa Ali who developed and optimized the protocols for neuronal and organoid differentiation described here.

5.1 Background

In the case of HSE, following exposure to HSV-1, the virus is thought to infect and replicate in the mucosal-epithelial cells with the resultant manifestation of HSE stemming from the robust replication of HSV-1 within neuronal cells situated in the brain (Gnann & Whitley, 2017). Various pathways and mechanisms have been postulated regarding the route of HSV-1 to the CNS and the subsequent development of HSE, either due to primary infection or viral reactivations (Bradshaw & Venkatesan, 2016). One proposed route involves the spread of HSV-1 from the oral cavity or nasal cavity to the CNS following infection of the olfactory epithelium where this intricate path is intertwined with the olfactory bulb, consequently exerting an influence on the limbic system, ultimately culminating in focal encephalitis within the brain, as evidenced in animal studies (Twomey et al., 1979; Dinn, 1980; Jennische et al., 2015).

The modern capability to generate *in vitro* cultures of neuronal cells has significantly contributed to further understanding of the intricacies of the nervous system, significantly enhancing our knowledge in this field (Schulz et al., 2003; Schulz et al., 2004; Elkabetz et al., 2008; Compagnucci et al., 2014). The existing data on understanding the mechanisms involved in HSV-1 infection within the central nervous system are obtained through either *in vitro* differentiated neurons or animal models (Knotts et al., 1973; Steiner et al., 1990; Kastrukoff et al., 2012; D'Aiuto et al., 2019; Sehl et al., 2020). However, these models fall short in fully addressing the specificity of human host-pathogen interactions and the diversity in cellular and

functional aspects within the neural tissues (D'Aiuto et al., 2019; Sehl et al., 2020). In recent years, cerebral brain organoids derived from human iPSCs have become prominent as models that encapsulate various important elements of human brain development, tissue architecture, and physiology (Lancaster et al., 2013; Lancaster & Knoblich, 2014). Specifically, cerebral brain organoids derived from human iPSCs are gaining recognition as 3D model to study viral infections (Salick et al., 2017; D'Aiuto et al., 2019; Krenn et al., 2021; Rybak-Wolf et al., 2023). These cerebral organoids have the capability to form neuroepithelial rosettes resembling the developing cerebral cortex, encompassing intermediate progenitor cells and various subtypes of cortical neurons (Lancaster et al., 2013; Lancaster & Knoblich, 2014; Pasca et al., 2015; Qian et al., 2016). Transcriptomics investigations done by several studies reveal that the neuronal cells types produced in the cerebral organoids closely resemble their counterparts found in the human embryonic brain (Camp et al., 2015; Qian et al., 2016; Quadrato et al., 2017).

Initially the original purpose of developing these cerebral organoids was not only to establish a relevant model for HSE but also to delve into the investigation of the autophagy response triggered by HSV-1 infection. This stemmed from our lab's previous findings indicating TBK1's involvement in autophagy (Ahmad et al., 2019). The AD *TBK1* variant has been described in children with HSE, producing a mutant TBK1 protein carrying the G159A substitution. This variant is a LoF variant, exhibiting no enzymatic kinase activity and exerting a dominant-negative effect on the WT TBK1 activity (Herman et al., 2012). This G159A *TBK1* LoF variant has been demonstrated to lead to the uncontrolled spread of HSV-1 infection and impaired HSV-1-induced IFN production. Furthermore, TBK1 has been shown to play a crucial role in initiating cytoprotective autophagy during the early phases of HSV-1 infection where G159A TBK1 failed to induce autophagy and anti-viral IFN response upon HSV-1 infection when compared to WT TBK1 which affected the cell survival during infection. Following this, a compelling notion surfaced, suggesting that HSV1 infection of post-mitotic cells, such as those in the CNS, may depend more significantly on autophagy mechanisms rather than type 1 IFN responses (Nikoletopoulou et al., 2015; Ahmad et al., 2019; Verzosa et al., 2021; Gomez-Virgilio et al., 2022). This notion presents a promising avenue for investigating the relative contributions of type 1 IFN versus autophagy pathways across diverse cellular contexts. Due to the COVID-19 pandemic we had to switch our focus and we were only able to start this work

in the past year. In this chapter, I will present some of the preliminary data we obtained during the optimisation stage.

I conducted functional testing of the various cell types which includes infecting these cells with HSV-1. Subsequently, I measured the cytokine levels, protein expressions using immunoblotting, and gene expression through RT-qPCR. Ms Aneesa Ali has been tremendously helpful and accommodating in culturing and differentiating iPSCs into either cortical neurons or cerebral organoids. Both of us work hand in hand in conducting assays to test protein expression through immunofluorescence and imaging them. We decided to divide the work due to the duration of culturing these different types of cells.

5.2 Generation and validation of cortical neurons and cerebral organoids using ESCs

Embryonic stem cell (ESC) lines have the capacity for indefinite *in vitro* propagation and the potential to undergo differentiation into any cell lineages (Reubinoff et al., 2000). Human ESC (hESC) line H9 cells derived from University of Wisconsin are a commonly used NIH-approved cell line that has been widely employed in the field (Loser et al., 2010). A study revealed the genetic profiles of hESCs and human iPSCs (hiPSC) exhibited clear similarities, providing evidence for a close molecular resemblance between genetically distinct hESCs and hiPSCs in terms of both gene expression and signaling pathways (Marei et al., 2017). Hence, we decided to use H9 cell line as our control in all of our experiments.

5.2.1 ESCs-derived cortical neurons

We opted to differentiate H9 hESCs into neuronal cells to investigate the impact of HSV-1 infection on hESC-derived neurons in subsequent investigations. We adapted our approach to differentiate PSCs into neuronal cells based on protocol described by Shi et al. (Shi et al., 2012). This method employs a double SMAD signalling inhibition strategy directing the differentiation toward the neuroectodermal lineage and the details can be found in Methods Section. The stages of differentiation involve the formation of neural rosettes which consist of neural stem cells (NSCs), as well as the progression to neural progenitor cells (NPCs), and eventually the development of mature neurons (data of progression not shown). The cortical neurons reach maturity by day 35 and from that day onwards, they are deemed ready for investigations. According to the original protocol, these neurons can be cultured up to day 60 but we would begin our investigations on day 36.

The objective of staining these neurons was to verify the composition of neuronal cultures and determine the proportions of cells that are mature or immature within the culture. In our early optimisation stage, we fixed the cells and stained with primary antibodies including microtubule-associated protein 2 (MAP2), Beta III Tubulin (βIII-Tubulin/Tuj1), COUP TF1-interacting protein 2 (CTIP2), SOX2, Nestin, and TBR2. MAP2 is a neuron-specific protein in the dendrites involved in organising the microtuble cytoskeleton (Soltani et al., 2005; Bodakuntla et al., 2019) and optimisation of this marker is essential to identify mature neurons and confirm the neuronal composition of cultures. βIII-Tubulin or Tuj1 is one of the earliest cytoskeletal marker proteins associated with neurons and that appears to be expressed exclusively in the neurons when compared to its other classes (Moody et al., 1989; Lee et al., 1990; Easter et al., 1993; Katsetos et al., 1993; Katsetos et al., 2003). The expression of βIII-Tubulin occurs immediately before or during terminal mitosis in the CNS and its incorporation aligns with the development of dendrites and correlates with the expression of MAP2 (Burgoyne et al., 1988; Ferreira & Caceres, 1992). CTIP2 serves as a specific marker in the cell body of a subtype of cortical neurons where high level expression is observed particularly within motor neurons (Arlotta et al., 2005). Sox2 is typically recognised as a marker for NSCs

in various embryonic and adult brain regions (Mercurio et al., 2019b). Nevertheless, Sox2 expression has also been reported in differentiated neurons across various areas of the nervous system (Hoefflin & Carter, 2014; Mercurio et al., 2019a). Nestin is an intermediate filament protein and identified as a marker for NSCs (Lendahl et al., 1990). The expression of nestin is detected in adult NSCs both *in vitro* and *in vivo* (Reynolds & Weiss, 1992; Morshead et al., 1994), and downregulated when NSCs cells undergo differentiation into neurons (Dahlstrand et al., 1995). TBR2 is a transcription factor that is localised to the cell body and its expression indicates the transition from radial glia to intermediate progenitors (Englund et al., 2005). The subsequent downregulation of TBR2 denotes the transition from intermediate progenitors to postmitotic neurons (Englund et al., 2005).

Our cultures showed high proportions of MAP2-positive and Tuj1-positive cells which indicated mature neuronal culture (Figure 5.1). We observed a limited number of CTIP2-positive cells in our mature culture as anticipated since CTIP2 is not expected to be present in every cell type within the culture. Given that TBR2 as a marker for the early stages of neuronal development, we expect to observe relatively low number of TBR2-positive cells as seen in Figure 5.1. Ultimately, our neuronal cultures comprised a higher proportion of mature neurons.

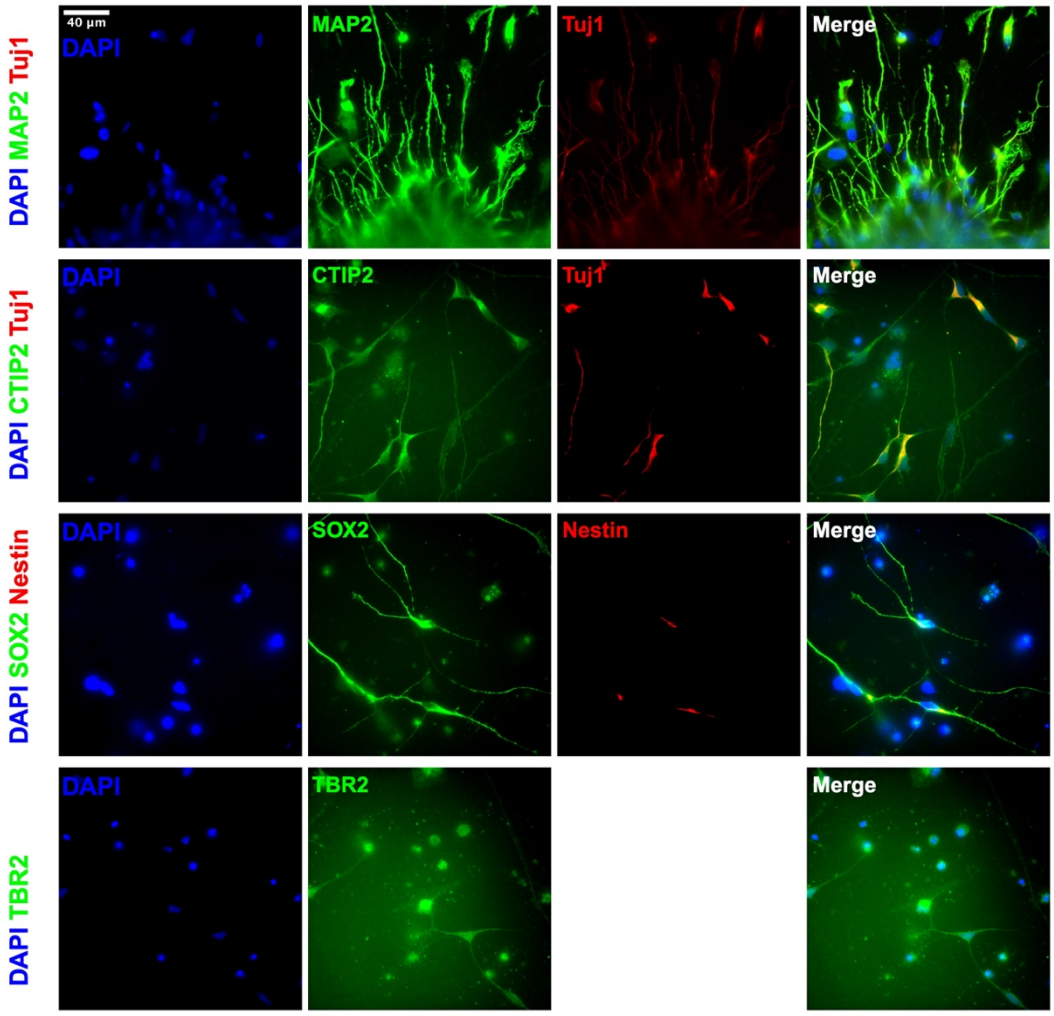


Figure 5.1 Neuronal differentiation from H9 ESCs.

H9 ESCs-derived cortical neurons were cultured, fixed on day 36, and subjected to immunostaining with various markers including MAP2, Tuj1, CTIP2, SOX2, nestin, and TBR2. The results shown are representative of three independent experiments (n=3). Visualisation of immunofluorescence was achieved with Widefield Axio Observer (Zeiss) using oil-immersion 63X lens. Scale bar represents 40 µm.

5.2.2 ESCs-derived cerebral organoids

Cerebral brain organoids are 3D cultures of neural cells originating from pluripotent stem cells (PSCs) replicating the organisational, developmental, and functional aspects of the brain within a controlled environment (Lancaster et al., 2013). There are several strategies that have been

devised to generate cerebral organoids that typically categorised as guided (patterned) or unguided (unpatterned). We developed our cerebral organoids using unguided protocols of intrinsic neuroectoderm differentiation, where hESCs are cultured together in signal-free media leading to differentiation into neural cells by default (Lancaster & Knoblich, 2014). We adapted our method from Salick et al. protocol (Salick et al., 2017) and also incorporated steps from the original Lancaster and Knoblich protocol (Lancaster & Knoblich, 2014) into the development of our cerebral organoids where the details can be found in Methods Section. The cerebral organoid will expand quickly once placed in Geltrex, a substitute for Matrigel which was used in the original protocol (Lancaster & Knoblich, 2014), and according to the Madeline et al., these cerebral organoids can be sustained up to 15 months. However, the organoids start to shrinking in size after 6 months which is attributed to depletion of progenitors and most likely indicative of a progressive neuronal cell loss (Lancaster & Knoblich, 2014). We chose to designate day 38-40 as our optimal time for investigations on the cerebral organoids aligning with Lancaster et al. findings that these organoids exhibited neuronal differentiation after a month which is also observed here (Figure 5.2).

Hematoxylin and Eosin (H&E) stains are routine staining in immunohistochemistry (IHC) to examine the underlying cellular and tissue structures by staining distinct colours to nuclei and cytoplasm upon cryosectioning (Chan, 2014). The sectioned cerebral organoids exhibited rosettes that have morphologically resemblance to ventricles as seen in H&E stains (Figure 5.2B) and brightfield microscopy (Figure 5.2A). The neuroepithelium-like structures expressed the progenitor marker, SOX2, neural differentiation marker, Vimentin, and neuronal marker, MAP2 (Figure 5.2C). Nestin, a marker that undergoes downregulation when NSCs cells undergo differentiation into neurons (Dahlstrand et al., 1995) and also for radial glia, was detected in the outer surface through IF staining in our cerebral organoids consistent with the findings of Lancaster et al. (Lancaster et al., 2017) where radial glial cells covering the brain's surface as scaffold for the migration and orientation of neurons (Torii et al., 2009) (Figure 5.2C). IF staining revealed positive for neural marker MAP2 (Figure 5.2C). To conclude, our day 38 cerebral organoids are deemed good enough as they exhibit rosette structures and neurons populate the outer regions of these formations (Figure 5.2B).

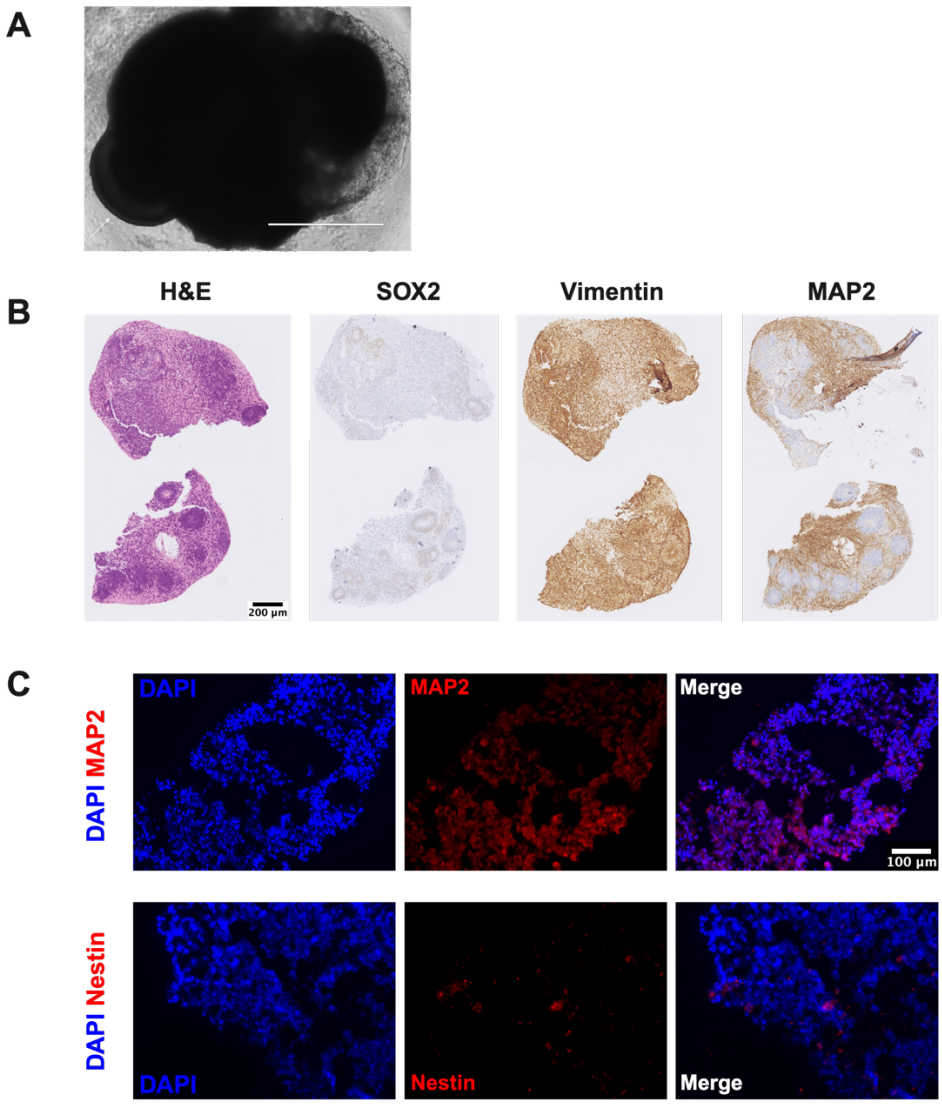


Figure 5.2 Characterisation of cerebral organoids derived from H9 ESCs.

A) H9 ESCs-derived cerebral organoid at day 38 exhibit budding neuroepithelium formations, denoted by a white arrow positioned at the lower left corner. Figure shows a representative replicate of n=3. Imaging using EVOS™ FL Auto 2 (Invitrogen). Scale bar represents 1000 µm. B) Cerebral organoids were sent to IQPath of UCL for IHC staining including H&E, as well as specific markers such as SOX2, Vimentin, and MAP2. Images were captured by IQPath of UCL. Scale bar represents 200 µm. C) Cerebral organoids derived from H9 ESCs on day 38 were fixed and sent to the Experimental Histopathology department at The Francis Crick Institute for cryosectioning. Immunostaining with MAP2 and nestin was conducted. The results shown are representative of three independent experiments (n=3). Visualisation of immunofluorescence was achieved with Axiovert 135 TV inverted fluorescence microscope (Zeiss) using 20X lens. Scale bar represents 100 µm. IF images here were being graciously captured by Ms. Aneesa Ali.

5.3 Optimisation of HSV-1 infection in cortical neurons and cerebral organoids

5.3.1 HSV-1 infection in ESCs-derived cortical neurons

We first sought to determine whether our cultured ESCs-derived cortical neurons could be infected with HSV-1. We subjected these cortical neurons to GFP-tagged HSV-1 infection at MOI 1 and allowing viral replication to proceed for 24 hours. We demonstrated that these ESCs-derived cortical neurons are susceptible to acute HSV-1 infection *in vitro* as evidenced by the presence of positive GFP fluorescence in the nuclei of the cell bodies (Figure 5.3A). We observed dendrites projections were protruding from clumps of cell bodies in uninfected cultures. The differential staining for nestin and βIII-Tubulin highlighted the presence of more mature neurons within the culture (Figure 5.3A). This observation was corroborated by the differential staining for SOX2 and MAP2 where it revealed there were high proportion of MAP2 positive cells (Figure 5.3A). Upon HSV-1 infection, a reduction in nestin-positive cells and a decrease in protruding βIII-Tubulin projections were observed compared to uninfected culture, suggesting neural degeneration (D'Aiuto et al., 2012). The latter observation aligned with the retraction of neurites observed in infected MAP2 positive cells.

To quantify the observation seen in fluorescence imaging, we employed titration by $TCID_{50}$ assay on Vero cells with detailed protocol outlined in Section 2.15. We opted for $TCID_{50}$ assay over plaque assay due to the absence of plaque formation when assessing the viral titre using plaque assay despite clear evidence of HSV-1 infection in fluorescence imaging. The viral titre of MOI 1 infections was determined using the $TCID_{50}$ assay, and the result were consistent with the findings from fluorescence imaging, indicating a significant difference between infected and non-infected cortical neurons (Figure 5.3B). These observations suggested that these cortical neurons cells are susceptible to HSV-1.

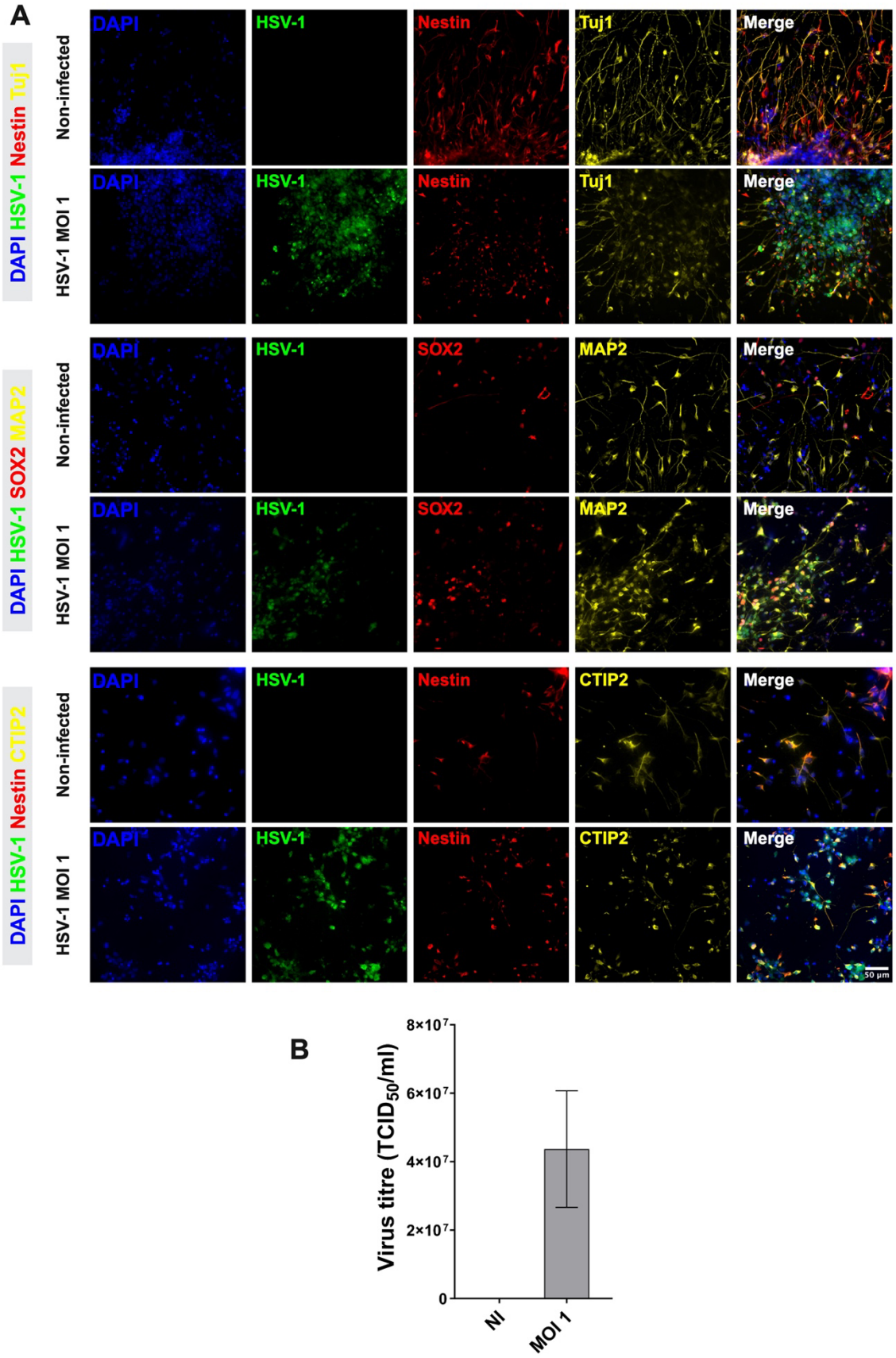


Figure 5.3 Establishment of HSV-1 infection on H9 ESCs-derived cortical neurons.

A) On day 36, H9 ESCs-derived cortical neurons were subjected to HSV-1 infection at MOI 1 for 24 hours, followed by fixation and subsequent immunostaining with various markers including nestin, Tuj1, SOX2, MAP2, and CTIP2. This experiment has only been performed once. Visualisation of immunofluorescence was achieved with Widefield Axio Observer (Zeiss) using 40X lens. Scale bar represents 50 μm. B) The viral titres were determined by TCID50 on Vero cells. Supernatants from cortical neurons were collected 24 hours post-infection. Mean and SD were calculated. NI; non-infected.

Following this, we wanted to measure the cytokines produced during the infection. Consequently, we collected supernatants from infected cortical neurons 24 hours post-infection. We employed immunoassay technologies of MSD to quantify the cytokines produced from MOI 1 infected cells. Both non-infected and HSV-1 infected samples exhibited a lack of IFN-β and IFN-λ/IL-29 production (Figure 7.2 in the Appendix) with levels of these cytokines falling below the detection range despite the high sensitivity of the MSD technology. It is likely that were insufficient cells to generate detectable levels of cytokines.

5.3.2 HSV-1 infection in ESCs-derived cerebral organoids

Next, we sought to determine the susceptibility of our cultured ESCs-derived cerebral organoid to HSV-1 infection. We subjected these cerebral organoids to GFP-tagged HSV-1 infection at MOI 1 and MOI 10, and allowing viral replication to proceed for 24 hours. Subsequently, cerebral organoids were sent for cyrosectioning followed by IHC (Figure 5.4A). We established that these ESCs-derived cerebral organoids can be infected with HSV-1 *in vitro* as indicated by the presence of positive GFP fluorescence (Figure 5.4B). IF staining revealed the HSV-1 viral protein overlapping with MAP2 positive neuron cells in the cryosectioned cerebral organoid following HSV-1 infection (Figure 5.4B). After cerebral organoids were infected with HSV-1, there appeared to be an apparent upregulation in the expression of LC3 which also colocalised with the HSV-1 viral protein.

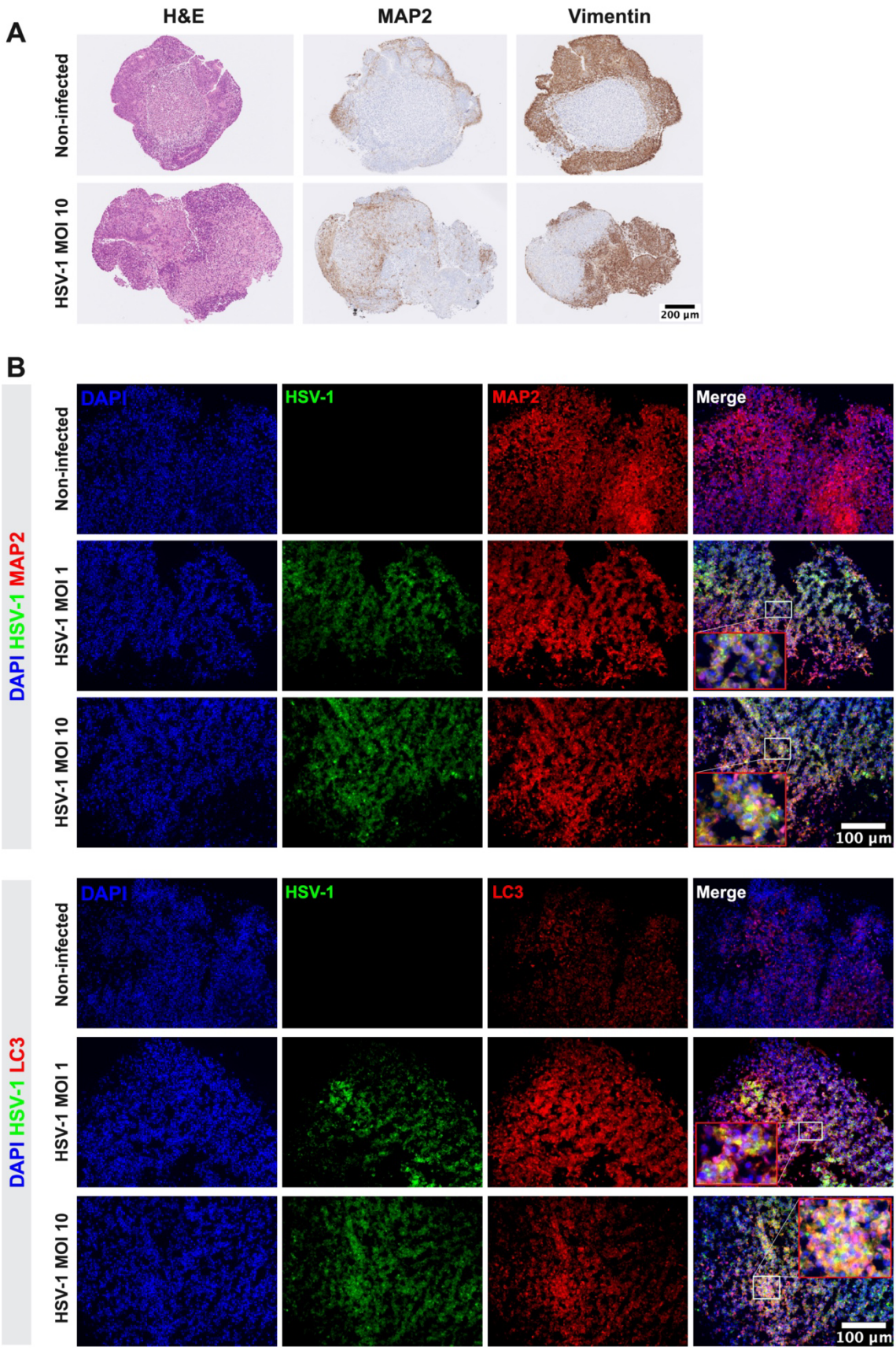

A
H&E
MAP2
Vimentin
Non-infected
HSV-1 MOI 10
200 μm
B
DAPI HSV-1 MAP2
DAPI
HSV-1
MAP2
Merge
Non-infected
HSV-1 MOI 1
HSV-1 MOI 10
100 μm
DAPI HSV-1 LC3
DAPI
HSV-1
LC3
Merge
Non-infected
HSV-1 MOI 1
HSV-1 MOI 10
100 μm

Figure 5.4 Establishment of HSV-1 infection on H9 ESCs-derived cerebral organoids.

A) H9 ESCs-derived cerebral organoids on day 38, subjected to either uninfected conditions or HSV-1 infection at MOI 10 for 48 hours, were sent to IQPath of UCL for IHC staining including H&E, along with specific markers like MAP2 and Vimentin. Images were captured by IQPath of UCL. Scale bar represents 200 μm. B) Cerebral organoids derived from H9 ESCs on day 38 underwent either no infection or were subjected to HSV-1 infection at MOI 1 or MOI 10 for a duration of 24 hours. Subsequently, they were fixed and sent to the Experimental Histopathology department at The Francis Crick Institute for cryosectioning. The subsequent step involved immunostaining with markers MAP2 and LC3. Visualisation of immunofluorescence was achieved with Axiovert 135 TV inverted fluorescence microscope (Zeiss) using 20X lens. Scale bar represents 100 μm. IF images here were being graciously captured by Ms. Aneesa Ali.

To quantify the observation seen in fluorescence imaging, we employed RT-qPCR assay using Taqman-based qPCR with detailed protocol outlined in Section 2.16. We chose the RT-qPCR assay over both $TCID_{50}$ and plaque assays due to the lack of plaque formation when evaluating the viral titre using both assays (data not shown) despite clear evidence of HSV-1 infection in fluorescence imaging. Subsequently, we quantified the viral cDNA through RT-qPCR targeting HSV-1 *US12* that encodes ICP47, an immediate early protein (York et al., 1994; Goldsmith et al., 1998), revealing an increase of approximately 1700-fold in HSV-1 MOI 1 infected cerebral organoids compared to the non-infected (Figure 5.5). Despite the observed rise in the viral RNA within the cerebral organoid tissues, no detectable viral particles were detected in the supernatants, as assessed through $TCID_{50}$ and plaque assays (data not shown), a phenomenon consistent with findings reported elsewhere (Ramani et al., 2020).

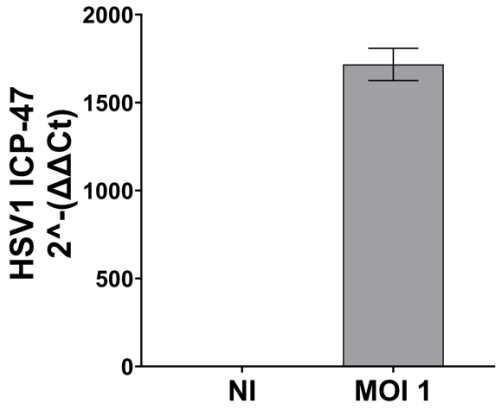


Figure 5.5 Viral mRNA quantification on H9 ESCs-derived cerebral organoids.

At the 24-hour time point, RNA extraction was performed on H9 ESCs-derived cerebral organoids, followed by the conversion of the extracted RNA into cDNA. Subsequently, the cDNA was subjected to analysis for the presence of HSV-1 *US12*, which encodes for ICP47, viral RNA through RT–qPCR. Data are represented as relative fold change (ΔΔCt units), where GUSB was used for normalisation. This experiment has only been performed once. Mean and SD were calculated. NI; non-infected.

Similar to the approach with cortical neurons, we aimed to assess the cytokines produced during the infection. Therefore, we collected supernatants from infected cerebral organoids 24 hours post-infection. We again utilised immunoassay technologies from MSD to quantify the IL-2, IL-4, IL-6, and IL-10 cytokines produced from MOI 10 infected cells. However, both non-infected and HSV-1 infected samples showed a deficiency in cytokine production (Figure 7.3 in the Appendix), with the levels of these cytokines falling below the detection range despite the high sensitivity of the MSD technology.

5.4 Effects of HSV-1 infection on patients' cells derived cortical neurons and cerebral organoids

5.4.1 Generation of patients' iPSCs and differentiation into cortical neurons and cerebral organoids

There is a specialised clinic centre based at St Mary's Hospital (London, England), recruiting eligible patients who meet the criteria for the Investigating the GENetics of InfectiOn Study (INGENIOS). The recruitment criteria encompassed children presenting with a severe or uncommon infectious disease, who were otherwise healthy and lacked known underlying risk factors for infection. The primary objective of this clinic was to recruit cases and explore the potential mechanisms underlying severe disease in children. The clinic identified a male paediatric patient (Patient 1024) with multiple variants in the *OAS1* and one variant in *IRAK4* (p.R391C) who unfortunately succumbed to HSE after coming in contact with HSV-1 (Figure 5.6). These were inherited from the mother and IRAK4 p.R391C is predicted to be deleterious or damaging (Alipoor et al., 2016). The biological mother (Patient 1024M) of this index case had HSV-1 colitis during delivery but otherwise healthy with no significant family history (Figure 5.6). Shortly after birth, the baby experienced seizures, bleeding, and liver failure. Natural killer cells were not detected even at 10 days after birth. The mother consistently tested positive for HSV-1 in the blood, despite receiving intravenous aciclovir treatment. The mother was found to have a novel missense *TLR3* variant, p.T650R, of uncertain significance and it has been established that HSE could arise from single-gene inborn errors of TLR3-mediated immunity involving variants within the TLR3 pathway (Casrouge et al., 2006; Zhang et al., 2007; Perez de Diego et al., 2010; Guo et al., 2011; Sancho-Shimizu et al., 2011; Herman et al., 2012; Lim et al., 2014; Andersen et al., 2015). Hence, this variant was further tested to assess its impact on TLR3 mediated immunity following HSV-1 infection. Following the recruitment of index case, a biological sample, usually blood or saliva, was collected from index case and the biological mother. Subsequently, DNA was extracted being sent to Novogene (Cambridge, UK) for Whole Exome Sequencing (WES). Blood sample was acquired from both the index case and biological mother to conduct immune functional testing in the

lab. The clinic was unable to procure additional samples from the index case due to his passing away, but they did obtain additional blood sample and skin biopsy from the biological mother.

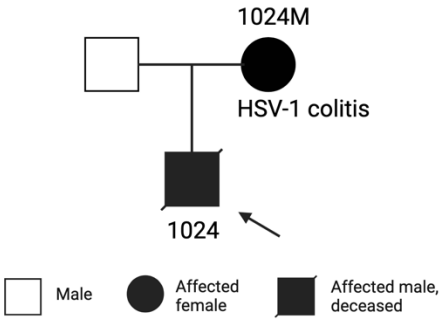


Figure 5.6 Pedigree of INGENIOS patient 1024.

The pedigree illustrates the relationship of INGENIOS patient 1024, denoted by the arrow, who is affected by herpes simplex encephalitis (HSE). The biological mother, 1024M, experienced HSV-1 colitis during the delivery of 1024 and carries the *IRAK4* variant (p.R391C) and *TLR3* variant (p.T650R). The genetic status of the father has not been investigated.

PBMCs were isolated from 1024M's blood and sent to Harry Leitch's lab at Hammersmith campus of Imperial College London through a collaborative effort where his research associate, Lucy Watson, kindly reprogrammed the PBMCs into iPSCs using Sendai virus vectors. Ms Aneesa Ali has graciously cultured these iPSCs through more than 10 passages and regularly testing for the presence of Sendai virus vectors by PCR. After confirming the clearance of the Sendai virus vectors, these iPSCs were deemed ready for differentiation into cortical neurons and cerebral organoids. Despite the index case that contracted neonatal HSE and the biological mother not having a history of HSE, we opted to generate iPSCs from the biological mother to model the HSV-1 infection in the cortical neurons and cerebral organoid. This decision was justified by the fact that 1024M shared all the potentially damaging variants, including the *IRAK4* variant (p.R391C), with 1024 when the WES data was analysed by the team. In addition, 1024M possesses a *TLR3* variant (p.T650R) which would add interesting dimension to observe its effects on the cortical neurons and cerebral organoids. This variant could serve as a valuable neurological model for testing susceptibility, given reports indicating that AD and AR TLR3

deficiencies contribute to an increased susceptibility to HSV-1 and consequently to HSE (Zhang et al., 2007; Guo et al., 2011; Lim et al., 2014).

5.4.2 Effects of patients' iPSCs-derived cortical neurons upon HSV-1 infection

Following that, we infected H9 ESCs- and 1024M iPSCs-derived cortical neurons with GFP-tagged HSV-1 infection at an MOI of 1 for either 8 hours or 24 hours. The expression of HSV-1 viral capsid proteins, VP26, was detected in the nuclei of the cell bodies of 1024M iPSCs-derived cortical neurons 24 hours post-infection and a decrease in neuron cultures was apparent when compared to the uninfected neuron culture (Figure 5.7A). In HSV-1 infected 1024M cortical neurons, a reduction in nestin-positive cells was seen and the immunoreactivity for βIII-Tubulin appeared to be severely punctated on most of the neurons with barely any protruding βIII-Tubulin projections observed indicating neural degeneration as seen in previous report (D'Aiuto et al., 2012). Surprisingly, when we assessed the viral cDNA levels using RT-qPCR targeting HSV-1 *US12* encoding for ICP47, there was no significant difference between 1024M and the control in MOI 1 8 hours post-infection (Figure 5.7B). However, it is essential to note that further repetitions of this experiment, along with assessment of the RNA at the 24-hour post-infection, are required to confirm the absence of any difference. Nonetheless, these observations suggested that 1024M iPSCs-derived cortical neurons are susceptible to HSV-1 infection.

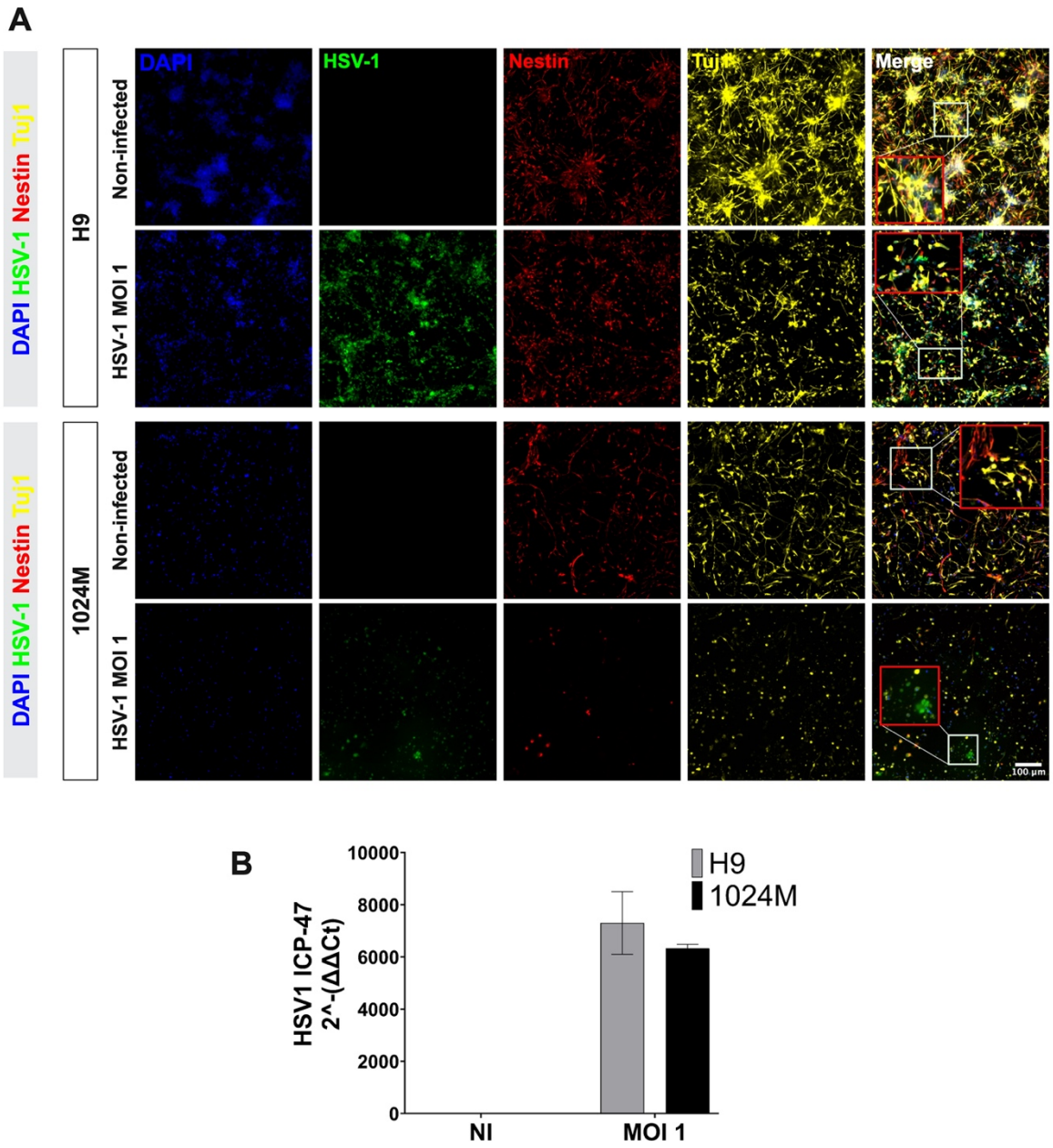


Figure 5.7 Impact of HSV-1 infection on 1024M iPSCs-derived cortical neurons.

Cortical neurons derived from both H9 ESCs and 1024M iPSCs underwent HSV-1 infection at an MOI of 1 for a duration of 24 hours on day 36. The neurons were fixed and subjected to subsequent immunostaining using Tuj1 and nestin. This experiment has only been performed once. Visualisation of immunofluorescence was achieved with Widefield Axio Observer (Zeiss) using 20X lens. Scale bar represents 100 µm. B) RNA was extracted from cortical neurons derived from both H9 ESCs and 1024M iPSCs 8 hours post-infection, with the extracted RNA then converted into cDNA. The resulting cDNA underwent analysis to detect the presence of HSV-1 *US12*, which encodes for ICP47, viral RNA using RT–qPCR. This experiment has only been performed once. Data are represented as relative fold change (ΔΔCt units), where GUSB was used for normalisation. Mean and SD were calculated. NI; non-infected.

Subsequently, we investigated the proteins expressed upon HSV-1 infection by immunoblotting. The protein lysates used in this immunoblot were extracted at the 8-hour time point, and western blots were subsequently conducted utilising antibodies specific to TBK1, IRF3, phosphorylated and activated forms of TBK1 and IRF3, as well as autophagy markers p62 and LC3B, with GAPDH serving as a loading control (Figure 5.8). The western blot of these cortical neurons is currently at optimisation stage, as it has only been conducted once, and unfortunately, we observed unequal loading in the H9 control when compared to the 1024M. However, no distinct difference between the infected and non-infected conditions observed in 1024M across all tested antibodies. This implies the need to explore earlier time points to unveil any potential significant differences.

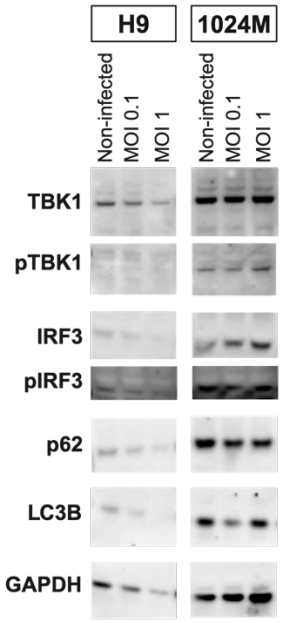


Figure 5.8 Immunoblot analysis of protein lysates from HSV-1 infected 1024M iPSCs-derived cortical neurons.

Cortical neurons derived from H9 ESCs and 1024M iPSCs were either infected with HSV-1 at varying MOIs, or remained uninfected, with subsequent collection of lysates at 8 hours post-infection. Immunoblots were then probed for TBK1, pTBK1, IRF3, pIRF3, p62, and LC3B, while GAPDH served as a loading control. This experiment has only been performed once.

5.4.3 Effects of patients' iPSCs-derived cerebral organoids upon HSV-1 infection

Next, we subjected H9 ESCs- and 1024M iPSCs-derived cerebral organoids to infection using GFP-tagged HSV-1 at MOI 1 and MOI 10, allowing the infection to progress for 24 hours and 48 hours. Cerebral organoids were fixed and subjected to cryosectioning, followed by staining for MAP2 and LC3 proteins. IF staining revealed the presence of HSV-1 viral protein, VP26, overlapping with MAP2-positive neuron cells in the cryosectioned cerebral organoids of both H9 and 1024M after HSV-1 infection (Figure 5.9A). Upregulation in LC3 expression was observed in both H9 and 1024M, which colocalized with the HSV-1 viral protein. Interestingly, no difference in infection was observed between MOI 1 and MOI 10 in the IF. Moreover, quantification of viral cDNA through RT-qPCR targeting HSV-1 *US12*, which encodes for ICP47, showed no significant difference between HSV-1 MOI 1 and HSV-1 MOI 10 infected cerebral organoids (Figure 5.9B). Additionally, no significant difference was observed between the control and infected cerebral organoids in MOI 1 and MOI 10.

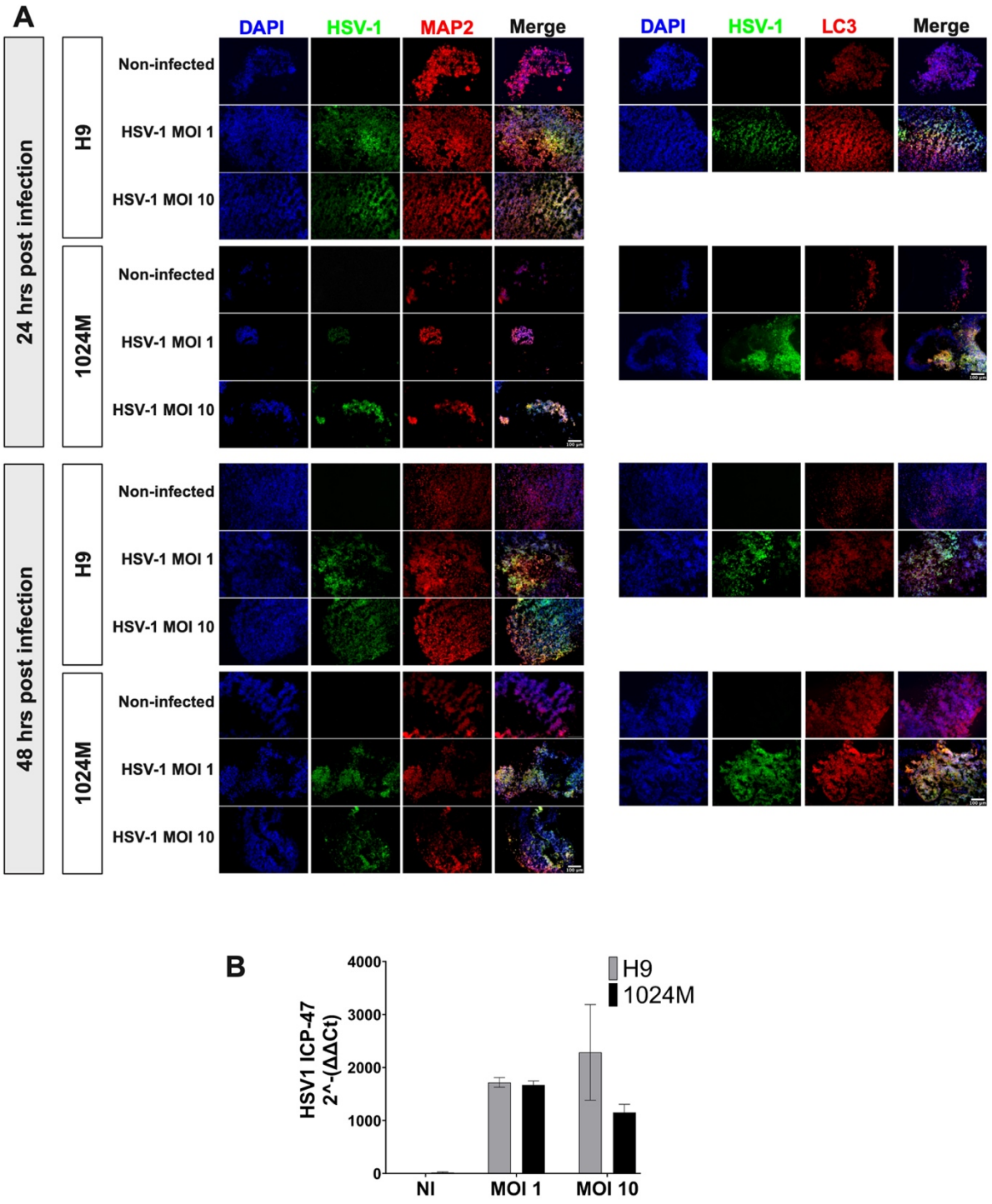


Figure 5.9 Impact of HSV-1 infection on 1024M iPSCs-derived cerebral organoids.

H9 ESCs- and 1024M iPSCs-derived cerebral organoids on day 38 were subjected to either uninfected conditions or HSV-1 infection at MOI 1 or 10 for durations of 24 hours or 48 hours. Subsequently, they were fixed and sent to the Experimental Histopathology department at The Francis Crick Institute for cryosectioning, followed by immunostaining using markers MAP2 and LC3. Visualisation of immunofluorescence was achieved with Axiovert 135 TV inverted fluorescence microscope (Zeiss) using 20X lens. Scale bar represents 100 µm. IF images here were being graciously captured by Ms. Aneesa Ali. B) RNA was extracted from cerebral organoids derived from both H9 ESCs and 1024M

iPSCs, with the extracted RNA then converted into cDNA. The resulting cDNA underwent analysis to detect the presence of HSV-1 *US12*, which encodes for ICP47, viral RNA using RT–qPCR. This experiment has only been performed once. Data are represented as relative fold change (ΔΔCt units), where GUSB was used for normalisation. Mean and SD were calculated. NI; non-infected.

5.4.4 Effects of patients' fibroblasts upon HSV-1 infection and ligand stimulations

Subsequently, we investigated the *in vitro* antiviral response of 1024M to HSV-1 since the patient's primary fibroblasts were available from skin biopsy. Human dermal fibroblasts were shown to express TLR3 and TLR4 on the cell membrane, indicating their capability to produce IFN-β and IFN-λ upon stimulation (Zhang et al., 2007; Israel et al., 2017). 1024M's primary fibroblasts were immortalised using SV40 large T antigen, as previously described (Chapgier et al., 2006). 1024M SV40 fibroblasts cells and SV40 fibroblast cells from healthy control were infected with GFP-tagged HSV-1 at MOI 0.1, 1, and 10, allowing viral replication to proceed for 24 hours. Viral replication of HSV-1 was visualised by GFP fluorescence using immunofluorescence imaging at 24 hours post-infection. There appeared to be a more pronounced infection in 1024M SV40 fibroblasts cells when compared to the control which particularly noticeable at MOI 0.1 (Figure 5.10). However, we cannot confirm the viral titre and the cytokines produced by this infection yet due to time constraints. This experiment has only been conducted once and requires additional repeats to validate the findings.

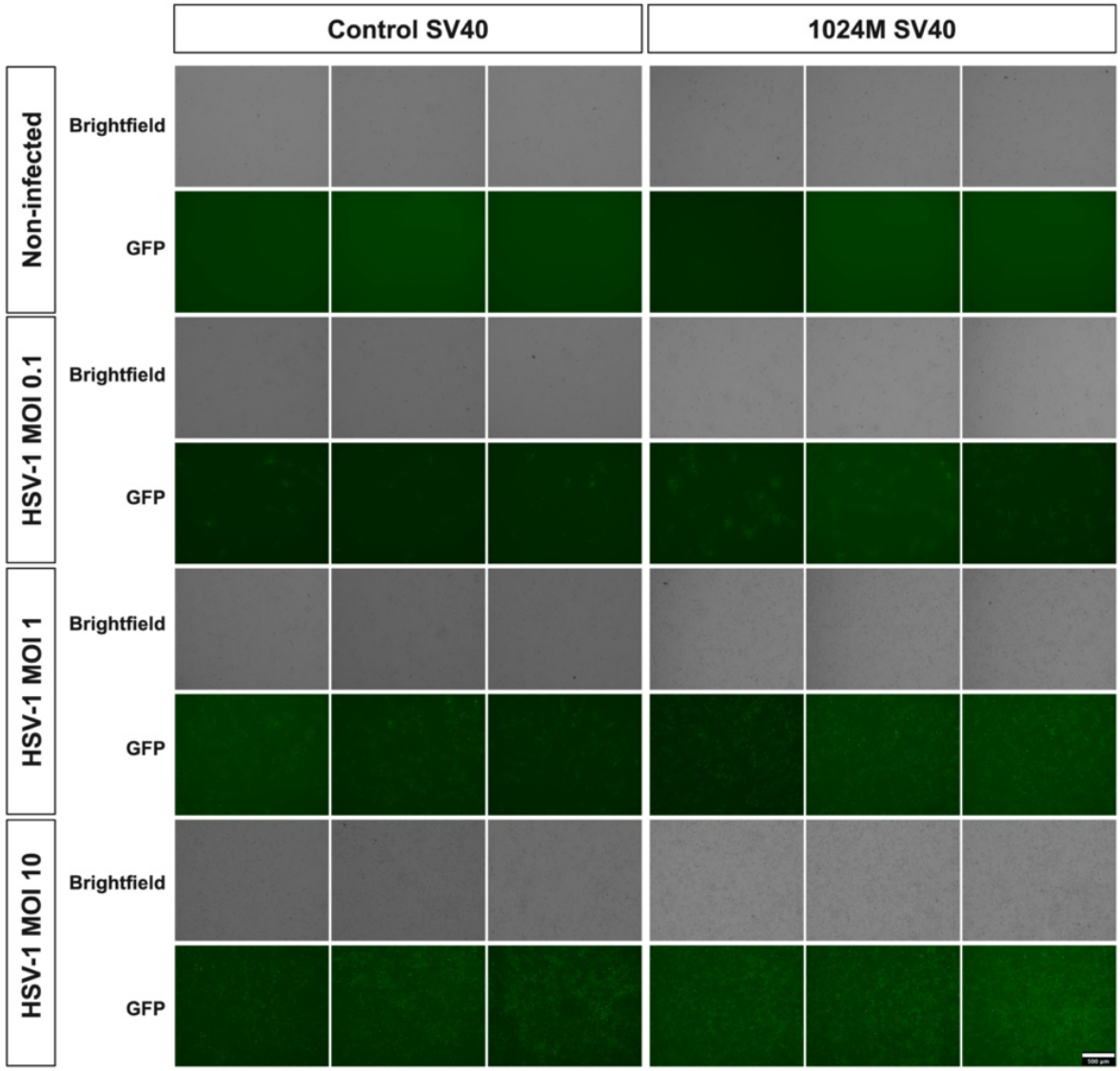


Figure 5.10 Impact of HSV-1 infection on 1024M SV40-fibroblasts.

Control and 1024M SV40-fibroblast cells were infected with HSV-1-GFP for 24 hours and visualised using fluorescence imaging at 4x magnification using EVOS™ FL Auto 2 (Invitrogen). Scale bar represents 500 μm. This experiment has only been performed once.

Nevertheless, we managed to evaluate the response of 1024M SV40 fibroblasts to poly(I:C) and LPS, known agonists for TLR3 and TLR4, respectively. We observed that 1024M SV40 fibroblasts exhibited a deficiency in the production of IFN-β, IFN-λ, and IL-6 cytokines across all concentrations of poly(I:C) when compared to the control (Figure 5.11). This deficiency persisted even though normal cytokine secretion was maintained following stimulation with transfected poly(I:C). It is interesting that 1024M SV40 fibroblasts exhibited an unresponsive

reaction to LPS, in terms of IFN-β and IL-6 production (Figure 5.11). However, it's crucial to acknowledge that this experiment has been conducted only once and requires further repetition to confirm the findings.

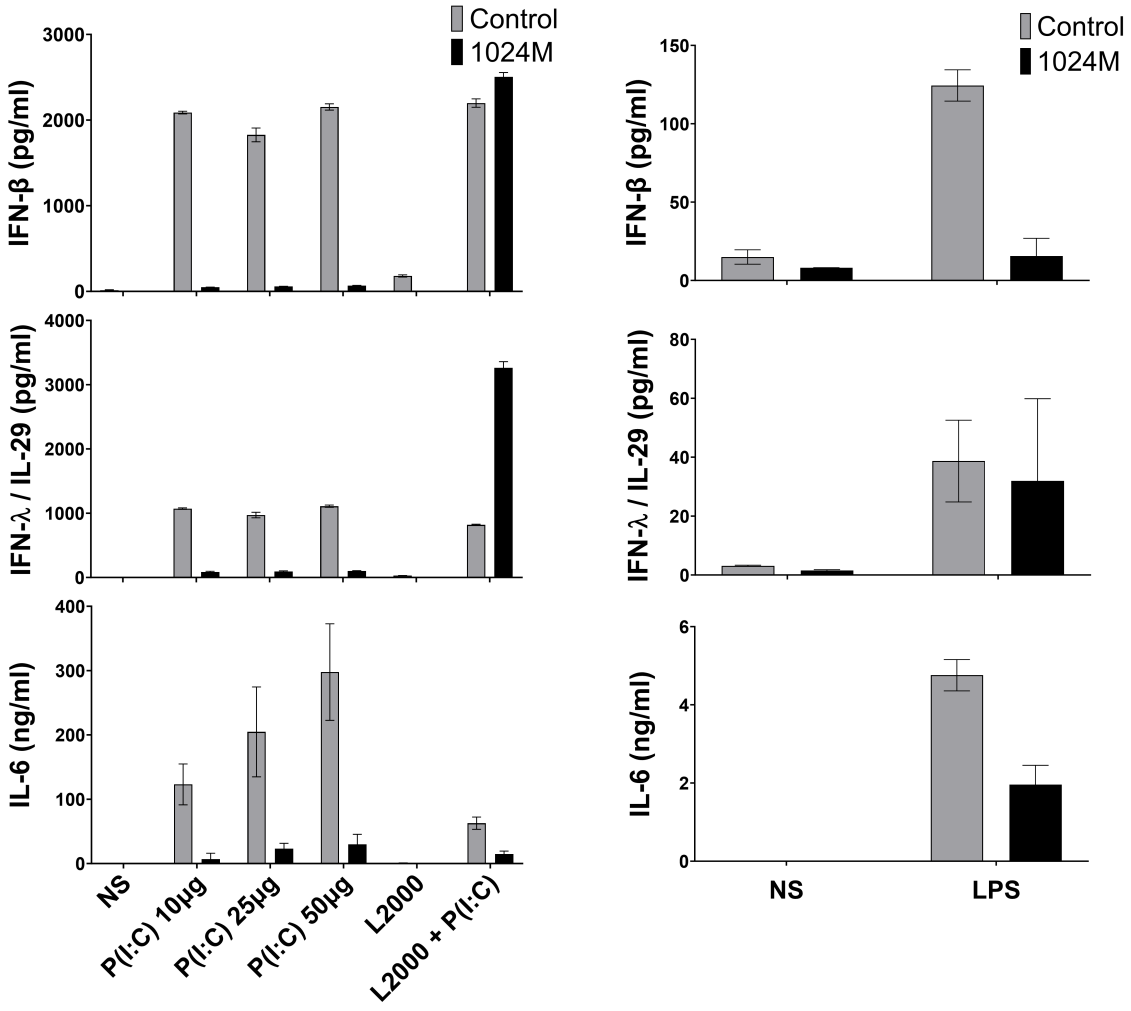


Figure 5.11 Cytokines levels in 1024M SV40-fibroblasts upon stimulation with P(I:C) and LPS.

Control, and 1024M SV40-fibroblast cells were left unstimulated (NS) or stimulated with different amounts of poly(I:C) (10-50 µg/ml) (left) or stimulated with LPS (100 ng/ml) (right) for 24 hours. Supernatants were collected and production of cytokines was assessed by Meso Scale Discovery immunoassays and ELISA. This experiment has only been performed once. Mean and SD were calculated. NS; non-stimulated, L2000; lipofectamine transfected, P(I:C); polyinosinic:polycytidylic, LPS; Lipopolysaccharides..

In summary, the imaging results suggest increased susceptibility of 1024M to HSV-1 in cortical neurons and SV40 fibroblasts. However, when quantifying the viral mRNA, no discernible

difference was observed between 1024M and the control. Notably, 1024M SV40 fibroblasts exhibited unresponsiveness to poly(I:C), a TLR3 agonist, and LPS, a TLR4 agonist. This observation suggests that the *TLR3* variant and *IRAK4* variant present in 1024M may contribute to defective production after stimulation of TLR3 and TLR4, respectively. Additionally, investigating the IFN cytokine production after HSV-1 infection would be interesting to determine if impairment exists, though this experiment was not conducted due to time constraints.

5.5 Effects of drug treatments on H9 ESCs-derived cortical neurons

Shifting the focus from infection alone to the realm of pharmacological interventions, we are intrigued by the potential efficacy of various treatments in managing HSV-1 infection. Current standard therapeutic strategy for HSE is the administration of aciclovir which is a viral replication inhibitor (Tunkel et al., 2008). Managing inflammation in HSE could improve the outcome as demonstrated in several mouse model studies (Meyding-Lamade et al., 2002; Meyding-Lamade et al., 2003; Sellner et al., 2005). Corticosteroids were occasionally used as a treatment for individuals with HSE prior to the introduction of aciclovir (Upton et al., 1971; Habel & Brown, 1972). Patients administered corticosteroids exhibited a reduction in both cerebral oedema on imaging and CSF IL-6 levels (Kamei et al., 2009). However, corticosteroids possess immunosuppressive effects and thus not recommended in HSE as they could potentially enhance viral replication. Accordingly, we aimed to test the effect of different treatments to H9 ESCs-derived cortical neurons.

The H9-derived cortical neurons were infected with GFP-tagged HSV-1 at MOI 1, allowing viral replication to occur for 2 hours. Subsequently, different treatments were added at that time point, and the cultures were left to continue for an additional 22 hours. For the pre-treatment, IFN-α2a was added a day before the experiment and left on for overnight. At 24 hours post-infection, the pre-treatment with exogenous IFN-α2a appeared to confer resistance to HSV-1 infection in these cortical neurons, evidenced by minimal GFP fluorescence and low

$TCID_{50}$ (Figure 5.12). This effect was also observed in the combined pre- and post-IFN treatment. However, for the post-IFN treatment, it showed similar GFP fluorescence as the infected cortical neurons without any treatments (Figure 5.12A). Nevertheless, the $TCID_{50}$ showed a low number and comparable to the pre-treatment with IFN (Figure 5.12B). Similarly, for the aciclovir treatment, it showed similar GFP fluorescence as the infected cortical neurons without any treatments, yet the $TCID_{50}$ also demonstrated a low number and comparable to the combined pre- and post-treatment with IFN (Figure 5.12). With dexamethasone, a corticosteroid treatment, the infection appeared to be similar as the infected cortical neurons without any treatments and once again the $TCID_{50}$ also demonstrated a low number and comparable to the post-treatment with IFN (Figure 5.12). Finally, treatment with combined aciclovir and dexamethasone appeared to have reduced GFP fluorescence than the aciclovir treatment alone but the $TCID_{50}$ was actually higher than aciclovir treatment alone and comparable to dexamethasone treatment alone (Figure 5.12). Nonetheless, it's crucial to acknowledge that this experiment has been performed only once and necessitates additional repeats to validate the results.

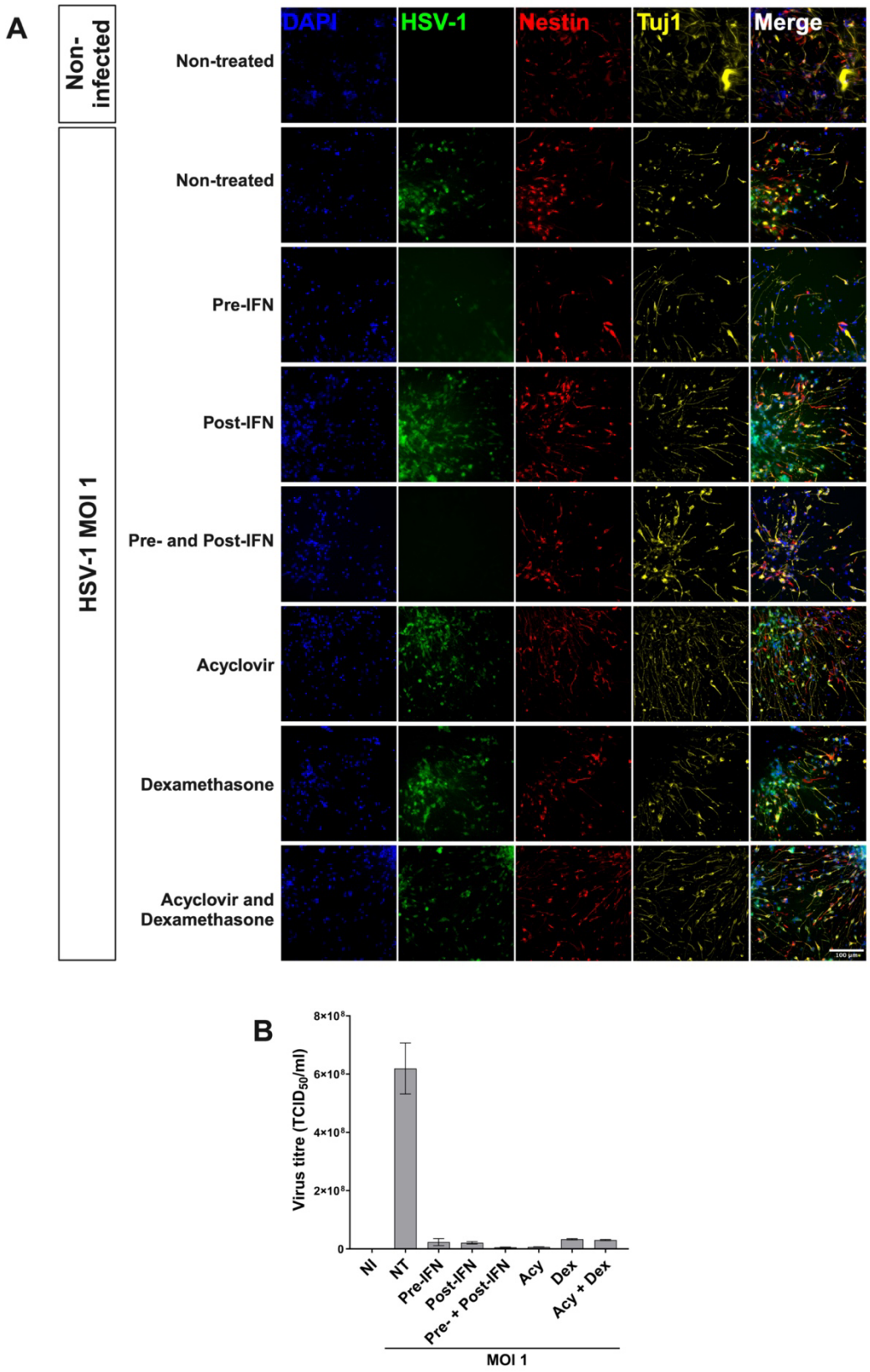


Figure 5.12 Impact of different treatments on H9 ESCs-derived cortical neurons upon HSV-1 infection.

A) Cortical neurons derived from both H9 ESCs were either uninfected or infected with HSV-1 at MOI 1. Post 2 hours of inoculation, the media were replaced to introduce various treatments, left for an additional 22 hours. Subsequently, the neurons were fixed and subjected to subsequent immunostaining using nestin and Tuj1. This experiment has only been performed once. Visualisation of immunofluorescence was achieved with Widefield Axio Observer (Zeiss) using 40X lens. Scale bar represents 100 μm. B) The viral titres were determined by TCID50 on Vero cells. Supernatants from cortical neurons were collected 24 hours post-infection. This experiment has only been performed once. Mean and SD were calculated. NI; non-infected, NT; non-transfected, Acy: Aciclovir, Dex; Dexamethasone.

Consequently, we collected supernatants from infected cortical neurons 24 hours post-infection. Employing immunoassay technologies from MSD, we sought to quantify the IL-2, IL-6, IL-10, IFN-β and IFN-λ/IL-29 cytokines produced in both MOI 0.1 and MOI 1 infected cells. However, both non-infected and HSV-1 infected samples displayed a shortfall in cytokine production (Figure 7.4 in the Appendix), with the levels of these cytokines plummeting below the detection threshold. Once again, this observation aligns with the trend observed throughout this study, highlighting the challenges in detecting cytokine levels within this experimental context.

5.6 Discussion

Investigation aimed at unravelling the intricacies of neurological and pathogenesis of CNS diseases have long been impeded by the absence of reliable human neuronal model. Recent strides in technology facilitating the reprogramming of adult human somatic cells into induced pluripotent stem cells (iPSCs) have brought about a transformative shift in our ability to conduct investigations in this realm (Takahashi et al., 2007; Yu et al., 2007). As a result, we have gained the remarkable ability to generate and manipulate iPSCs, transforming them into a diverse array of cell types, all derived from these somatic cells, providing an unprecedented avenue for exploration (Gore et al., 2011; Ji et al., 2012). Indeed, these ground-breaking advances in the applications of human iPSC technologies have significantly reshaped the experimental framework for modelling CNS diseases and infections (Bellin et al., 2012; Aboul-Soud et al., 2021; Nicholson et al., 2022). Historical challenges, stemming from the unavailability of relevant live tissues and cell types, have posed considerable obstacles to research in this domain.

The development of iPSCs-derived cells from somatic cells stands as a pivotal advancement in the realm of personalised medicine, driven by the recognition of inherent variations among individuals in their response to environmental, genetic, or infectious factors (Chun et al., 2011; Paik et al., 2020; Hao et al., 2022). Consequently, iPSC-based models emerge as a powerful tool for delving into the intricacies of the pathogenesis associated with neurotropic viruses, as well as neuropsychiatric and neurodegenerative diseases (Qian et al., 2016; D'Aiuto et al., 2019; Sison et al., 2019; Chang et al., 2020; Yi et al., 2020; Barreras et al., 2022; Zhang et al., 2022). These models replicate the unique susceptibilities of individuals and cell types to mutations, or pathogens, offering insights into the complex processes involved. Taking innovation a step further, the development of brain organoids models, achieved through the cultivation of iPSCs under conditions favouring 3D neuroectoderm differentiation, represents a significant breakthrough in understanding and replicating the intricate workings of the brain (Lancaster et al., 2013; Pavoni et al., 2018).

In this study, we opted to utilise H9 ESCs as our control due to the challenges in obtaining a suitable iPSCs control. A research investigation (Marei et al., 2017) revealed that the vast majority of both induced and repressed modulated genes in undifferentiated human iPSCs and human ESCs lines exhibited similar expression profiles, evidently associated with common biological processes and pathways. The identification of commonly induced and repressed genes across hiPSCs and hESCs lines further implies a close resemblance between the two cell types (Marei et al., 2017). This choice was thereby justified.

To recreate the scenario of HSE, wherein the replication of HSV-1 within neuronal cells in the brain is believed to be the causative factor (Gnann & Whitley, 2017), we aim to establish a neuronal model of HSV-1 infection as the initial step. Given our consistent use of fibroblasts in the laboratory for testing HSV-1 infection, we decided to explore the use of ESCs-derived neurons. This decision also stemmed from the understanding that distinct cell types exhibit varying responses to HSV-1 or TLR3 agonists, such as poly(I:C). For instance, leukocytes and fibroblasts have been observed to respond differently, with studies indicating that fibroblasts carrying specific monogenic error implicated in HSE exhibit defective responses to TLR3 ligands, while their leukocytes respond normally (Casrouge et al., 2006; Zhang et al., 2007; Perez de Diego et al., 2010; Guo et al., 2011; Sancho-Shimizu et al., 2011; Herman et al., 2012). This choice also offers distinct advantages, providing a highly scalable and efficient platform for rapid experiments aimed at observing transcriptional expression, and signalling mechanisms. Certainly, we effectively cultivated ESCs-derived cortical neurons, ensuring the expression of appropriate markers and exhibiting a higher degree of neuronal maturity (Figure 5.1). Subsequently, these neurons displayed susceptibility to HSV-1 infection (Figure 5.3) resulting in a general reduction in the number of neurons within infected neuron-enriched cultures compared to the control. It is noteworthy that the immunoreactivity for βIII-Tubulin displayed pronounced punctation on the majority of neurons, accompanied by a scarcity of protruding βIII-Tubulin projections, indicative of neural degeneration, a phenomenon also observed in neurons infected with HCMV (D'Aiuto et al., 2012). This neural degeneration might be attributed to apoptosis.

We also managed to culture patient derived (1024M) iPSCs into cortical neurons (Figure 5.7). This is of significance as 1024M has a *TLR3* variant (p.T650R) of unknown significance and it has been reported previously that TLR3 deficiencies lead to increased susceptibility to HSV-1 infection and subsequently HSE (Zhang et al., 2007; Guo et al., 2011; Lim et al., 2014). A prior study found that cortical neurons derived from TLR3-deficient iPSCs exhibited increased levels of viral replication as early as six hours post-infection (Gao et al., 2021) and we expected to see similar results in our experiment. However, the unclear significance of our specific *TLR3* variant might explain why we observed no difference in HSV-1 infection between the 1024M and control (Figure 5.7B). Moreover, since this experiment was only conducted once, additional repetitions are necessary to validate these findings. Although our efforts led to the HSV-1 infection of 1024M iPSCs-derived cortical neurons and the quantification of viral mRNA on a single occasion, we have yet to ascertain the levels of IFN-α/β and/or IFN-λ cytokines. Exploring these cytokine levels would be intriguing as they could shed light on the potential susceptibility to HSV-1 stemming from the absence of protective endogenous IFN production during viral infection. This investigations aligns with the premise that TLR3 plays a pivotal role in orchestrating the continuous production of IFN-β in fibroblasts and iPSCs-derived cortical neurons (Gao et al., 2021) where the cumulative findings substantiate the concept that TLR3-dependent IFN-β functions as a safeguarding cytokine to pre-empt viral infection, highlighting the importance of maintaining constitutive IFN-β production in governing the intrinsic antiviral immunity within the cortical neurons. Despite our RT-qPCR data (Figure 5.9B) revealing no significant difference in viral mRNA copies between the patient and control in cerebral organoid models, it's crucial to note that this measurement pertains to viral mRNA within the cells and does not extend to assessing the active infectious viral particles present outside the cells. Another potential factor contributing to this discrepancy could be the variation in the size of the organoids between the 1024M and the control. Consequently, the number of available cells for infection may exhibit variability as a result of these differences in organoid size.

The preliminary IF imaging analysis indicates that 1024M SV40 fibroblasts seemed to exhibit an increased susceptibility to HSV-1 infection in comparison to the control SV40 fibroblasts, although it is imperative to validate this observation through the quantification of viral titres (Figure 5.10). Intriguingly, these 1024M SV40 fibroblasts demonstrated an impaired response

to poly(I:C), a TLR3 agonist, as well as LPS, a TLR4 agonist (Figure 5.11). This observation implies that the presence of the *TLR3* variant and *IRAK4* variant in 1024M may contribute to deficiencies in cytokine production following stimulation of TLR3 and TLR4, respectively. Further exploration could involve the measurement of cytokine levels in 1024M SV40 fibroblasts following HSV-1 infection, providing a comprehensive understanding of the intricate cellular responses.

Over the past few years, brain organoids derived from human stem cells have garnered significant attention, emerging as models that encompass various crucial facets of human brain development, structural tissue composition, and physiology (Lancaster et al., 2013; Quadrato et al., 2017; Qian et al., 2018; D'Aiuto et al., 2019). Furthermore, in contrast to conventional 2D differentiation cultures, cerebral organoids showcase a sophisticated cellular architecture essential for corticogenesis, a process marked by differentiative divisions giving rise to neurons (Agirman et al., 2017; Qian et al., 2019). Recent research has highlighted that this intricate architecture could be compromised following Zika viral infection (Gabriel et al., 2017). Given that these cerebral organoids derived from PSC cultures and autonomously form three-dimensional tissues, this methodology provides a platform to address the pathogenesis of viral infection in the developing brain, particularly our keen interest in HSV-1 infection (D'Aiuto et al., 2019; Sun et al., 2021; Rybak-Wolf et al., 2023). Deciphering the intricate complexities surrounding the initiation of HSV-1 infection within the brain, navigating through the progression of HSE, and deciphering its intricate association with brain tissue damage remains a challenge. Our research has illustrated that our human cerebral organoids display remarkable neuronal differentiation (Figure 5.2) and susceptibility to HSV-1 infection (Figure 5.4). This can serve as a model for advancing our comprehension of HSV-1 infection within the brain. While acknowledging that organoids do not perfectly replicate the intricate architecture of the adult temporal and frontal lobes, which are frequently afflicted in cases of HSE, they represent the most sophisticated human brain-like tissue system available to date for *in vitro* investigations into HSV-1 infections in the brain (Su et al., 2021).

Cerebral organoids exhibit a remarkable level of heterogeneity, encompassing different cell types into a cohesive system and this cellular heterogeneity within cerebral organoids

encapsulates a diverse array of neuronal subtypes capable of establishing intricate connections (Arlotta & Pasca, 2019; Sabate-Soler et al., 2024). One research utilised single-cell RNA sequencing to dissect the cellular diversity within 3D whole-brain organoid cultures (Camp et al., 2015). Examining organoids undergoing two months of differentiation in culture, the study identified the coexistence of dorsal and ventral forebrain fates. Notably, a compelling revelation emerged as a direct comparison with primary tissue showcased noteworthy resemblances to the human foetal cerebral cortex. This resonates with our own cerebral organoids which emulate the characteristics of a developing fetal brain. Hence, it's essential to acknowledge our limitation, as the HSV-1 infection observed in this model may not necessarily mirror the dynamics of HSV-1 infection in the neonatal brain leading to HSE. Prolonging the culture duration is both time and labor-intensive, with associated costs often serving as a constraining factor.

One of the pathways we aimed to investigate pertains to autophagy within cortical neurons and cerebral organoids. In the previous study conducted in our laboratory, we uncovered the pivotal role of TBK1 in facilitating cytoprotective autophagy during the initial phases of HSV-1 infection (Ahmad et al., 2019). This discovery was made through the examination of $TBK1^{+/-}$ dermal fibroblasts harbouring the G159A substitution, a LoF variant associated with AD TBK1 deficiency in patients with HSE (Herman et al., 2012). The presence of this G159A TBK1 variant has been linked to uncontrolled HSV-1 infection propagation, impaired autophagy, and reduced HSV-1-induced IFN production (Ahmad et al., 2019). Notably, the findings revealed that HSV-1 triggers autophagy via a mechanism reliant on STING binding and TBK1 activity, independent of IFN signalling (Rasmussen et al., 2011; Liang et al., 2014; Ahmad et al., 2019; Liu et al., 2019; Yamashiro et al., 2020). However, the precise regulatory mechanisms governing these processes remain to be fully elucidated. Subsequently, an intriguing notion emerged, suggesting that the susceptibility of post-mitotic cells, particularly those within the CNS, to HSV1 infection might hinge more significantly on autophagy mechanisms rather than the conventional type 1 IFN responses offering a compelling direction for investigating the comparative roles of type 1 IFN and autophagy pathways across diverse cellular environments (Nikoletopoulou et al., 2015; Ahmad et al., 2019; Verzosa et al., 2021; Gomez-Virgilio et al., 2022). Consequently, it is natural for our subsequent investigations to delve into the autophagic response in this chapter following HSV-1 infection.

Autophagy, a highly regulated and evolutionarily conserved intracellular mechanism, oversees the degradation of cellular components, preserving functionality and eliminating protein aggregates and pathogens through a self-engulfing process involving autophagosomes that fuse with lysosomal vesicles (Klionsky & Ohsumi, 1999). The elevation in LC3BII levels serves as a reliable marker for autophagosome formation, while the autophagy receptor p62 interacts with the LC3B protein on the autophagosome (Kabeya et al., 2000; Stolz et al., 2014). In our cerebral organoid model, a notable increase in the expression of LC3 was observed, coupled with its colocalization with the HSV-1 viral protein, thereby corroborating our earlier findings that highlighted the upregulation of autophagy in cells subjected to HSV-1 infection (Ahmad et al., 2019). However, there is a need to capture the early autophagy timepoint for a more comprehensive understanding as it was seen in our previous observations that neighbouring cells surrounding the HSV-1 infected cells exhibit increased autophagy, indicating a cytoprotective effect in fibroblasts (Ahmad et al., 2019). Exploring whether such phenomena occur in cortical neurons and cerebral organoids adds an intriguing dimension to our ongoing investigation.

Clinicians exhibit reluctance to employ steroids in the treatment of HSE due to the inherent immunosuppressive effects of corticosteroids (Whitfield et al., 2021). Theoretically, this immunosuppression could create an environment conducive to heightened viral replication (Defres et al., 2017). As a result, the precise role of steroids in the management of HSE remains uncertain and is a matter of cautious consideration within the medical community (Portillo et al., 2016). Experiments conducted on animals have demonstrated an absence of correlation between steroid therapy and the dissemination or viral load of HSV-1 (Thompson et al., 2000). Moreover, even if there were an increase in viral load due to steroid therapy, other quantitative viral markers fail to exhibit a correlation with radiological changes (Meyding-Lamade et al., 1999) or clinical outcomes (Wildemann et al., 1997). The potential efficacy of corticosteroids in HSE is rooted in their ability to mitigate the activation of various inflammatory pathways (Sellner et al., 2005). In fact, adjunctive administration of corticosteroids has proven beneficial in addressing excessive inflammatory responses associated with other infectious diseases such as bacterial meningitis, tuberculous meningitis or herpetic keratitis (Wilhelmus et al., 1994; de Gans et al., 2002; Thwaites et al., 2004). In the context of HSE, both animal models and human

reports align in supporting the supplementary use of corticosteroids (Kamei et al., 2005). The application of steroids in HSE typically comes into consideration when there is evident disease progression despite ongoing aciclovir treatment, emphasizing their role as a supplementary therapeutic option in challenging cases (Kamei et al., 2005; Lizarraga et al., 2013; Ramos-Estebanez et al., 2014). Additionally, we are anticipating the outcomes of DexEnceph, an ongoing randomized controlled trial involving adults afflicted with HSV encephalitis (Whitfield et al., 2021). This trial involves the administration of dexamethasone in conjunction with the conventional antiviral therapy using aciclovir. The primary aim is to ascertain whether this combined treatment approach yields enhanced clinical outcomes when compared with individuals who solely undergo the standard treatment regimen. The findings from this trial hold profound implications for guiding future clinical practice in the management of adults suffering from this condition, potentially offering a significant stride forward in improving patient outcomes and quality of care. In our preliminary data of ESCs-derived cortical neurons, it was visually apparent that the combined administration of aciclovir and steroids yielded a more favourable outcome, although there was no significant difference in the viral load titres when compared to aciclovir alone. Despite these observations, the need for a comprehensive validation of the results persists, as there are additional outcome parameters that necessitate measurement to corroborate our findings. It is imperative to highlight that further repetitions of the experiments are essential to establish conclusive evidence regarding the efficacy and potential synergistic effects of the combined aciclovir and steroid treatment regimen.

Overall, while brain organoids present a markedly improved approach for *in vitro* brain modelling, they present certain limitations, most notably stemming from challenges related to the absence of vasculature, immunological components, and diverse non-neural cells within their structure, as compared to *in vivo* models. Additionally, these organoids have restricted nutrient and oxygen diffusion to the organoid core centers, imposing constraints on their size and rendering them susceptible to cellular demise at their core, a consequence likely attributed to the absence of a circulatory system (Lancaster et al., 2013). The generation of cerebral organoids often involves inhibiting the formation of mesoderm and endoderm to induce iPSCs into a neuroectoderm lineage, inadvertently leading to the absence of microglia, which is important for immune response studies as they originate from the mesoderm (Chambers et al., 2009). The exploration of neurotropic viral infections has posed significant challenges in both

in vitro and *in vivo* settings, primarily due to the limitations associated with the absence of multicellular compositions *in vitro* and disparities between human and murine brains *in vivo* (Hatzipetros et al., 2014). Moreover, while *in vivo* mouse models are frequently employed, they often fail to accurately replicate the intricacies of the human brain (Seok et al., 2013; Justice & Dhillon, 2016). Consequently, the continued potential of 3D cerebral brain organoids persists as a promising avenue for effectively modelling human neurotropic viral infections *in vitro*.

In summary, we have achieved a milestone by creating cortical neurons and cerebral organoid models derived from PSCs, providing us with valuable tools for studying HSV-1 infection. These models will be instrumental in our endeavours to explore the underlying genetic causes and functional immunology of severe or uncommon infectious diseases in children who were previously healthy and the absence of identifiable risk factors for infection. Our ultimate goal is to employ iPSCs obtained from such patients to explore deeper into the genetic etiologies and immune responses associated with these conditions.

Chapter 6

6. Discussion and future directions

6.1 General discussion

A prevalent characteristic observed in infectious diseases presented in this thesis is that the phenomenon that only a limited fraction of individuals who come into contact with the pathogen undergo the clinical progression of the disease. Furthermore, a considerable degree of variability is seen in the manifestations of the disease, giving rise to a range of phenotype outcomes. The diversity observed in the manifestation of the diseases highlights the complex nature of infectious diseases, wherein numerous factors contribute to give varied immune responses among individuals who have been exposed (Cooke & Hill, 2001). In recent times, advanced genetic methodologies, such as WES and gene enrichment studies, have been employed to identify classes of genes or proteins that exhibit over-representation within an extensive pool of genes (Subramanian et al., 2005). This pursuit involves analysing large cohorts of cases versus controls to unveil potential correlations with phenotypic class distinctions (Amos & Bryant, 2011; Amos et al., 2011). As a result of these advanced genetic approaches, there has been a notable breakthrough in the identification of monogenic IEI in the context of infectious diseases, with the identification of numerous novel gene defects bringing the total of IEI to 485 as of the year 2022 (Notarangelo et al., 2020; Bousfiha et al., 2022b; Tangye et al., 2022).

The infectious diseases within the scope of this thesis are characterised by substantial levels of both mortality and morbidity (Aurelius et al., 2002; Kennedy & Steiner, 2013; Zhang et al., 2023). In the case of HSE, over 70% of instances result in fatality when left untreated, with a mere approximately 11% of patients managing to recover normal function and leaving the majority with enduring neurological sequelae (Gkrania-Klotsas & Lever, 2008; Riancho et al., 2013; Wnek et al., 2016; Boucher et al., 2017; Mendez et al., 2018; Stahl & Mailles, 2019). Similarly, various studies indicate an increased risk of neurological sequalae morbidity following HSV-2 meningitis, as evidenced by a recent study revealing that individuals with

HSV-2 meningitis experienced a diminished quality of life compared to healthy controls during a one-year follow-up period (Aurelius et al., 2002; Schmidt et al., 2006; Omland et al., 2008; Miller et al., 2013; McGill et al., 2018). Moreover, HSV-2 meningitis emerges as a significant contributor to both morbidity and mortality among individuals with compromised immune systems (Mommeja-Marin et al., 2003; Noska et al., 2015). In a comprehensive analysis conducted in 2021 designed to calculate the pooled case fatality rate of COVID-19 from studies spanning various countries, using systematic review and meta-analysis techniques, the findings revealed an overall pooled case fatality rate of 10% (Alimohamadi et al., 2021). Upon further stratification, it was revealed that the pooled case fatality rate of COVID-19 within the general population stood at 1%, while among hospitalized patients, it surged to 13% (Alimohamadi et al., 2021).

It has been well documented that HSE can be attributed to IEI of TLR3-dependent IFNs immunity resulting from variants across genes under downstream of TLR3 pathway (Casrouge et al., 2006; Zhang et al., 2007; Perez de Diego et al., 2010; Audry et al., 2011; Guo et al., 2011; Sancho-Shimizu et al., 2011; Herman et al., 2012; Lim et al., 2014; Andersen et al., 2015). Additionally, there is evidence indicating that causative germline mutations in *TLR3*, *IRF7*, and *IRF9* genes are responsible for disrupting the TLR3-dependent induction of type I IFNs, as well as impeding the amplification pathway of type I interferons dependent on IRF7 and IRF9 and contributing to the development of life-threatening influenza pneumonia or ARDS (Ciancanelli et al., 2015; Hernandez et al., 2018; Lim et al., 2019). In this thesis, the focus was directed towards investigating various *TICAM1* variants with the aim of identifying novel genetic aetiologies responsible for HSE, recurrent HSV-2 meningitis or Mollaret's meningitis, and COVID-19. Moreover, beyond these investigations, the thesis also aimed to model the dynamics of HSV-1 infection within cerebral organoids, aiming to deepen our understanding of the mechanisms involved in neurotropic viral infections of the brain.

6.2 Main findings

The COVID Human Genetic Effort (COVIDHGE, https://www.covidhge.com) has proposed a hypothesis that IEI within pathways associated with viral influenza pneumonia might play a role in the development of COVID-19 pneumonia, exhibiting either complete or incomplete penetrance particularly in previously healthy and young individuals. Our study (Chapter 3) presents compelling evidence supporting the hypothesis where rare *TICAM1* variants identified in patients with COVID-19 pneumonia contribute to TICAM1 deficiencies within the TLR3-IFN signalling pathway. In our investigation, we identified three rare *TICAM1* variants (T4I, S60C, and Q392K) that exhibited loss of protein expression as evidenced by both immunoblotting and immunofluorescence analyses. Furthermore, these three distinct variants exhibited a significant reduction in the induction of both IFN-β and NF-κB promoter inductions, indicative of a loss of function (LoF) phenotype. Our research further indicates towards the notion that these three variants do not exert a dominant negative effect. The three patients harbouring these *TICAM1* variants did not carry candidate variants at other loci known to be involved in underlying inborn errors of immunity (Zhang et al., 2020). This evidence highlights the relationship between genetic variations and the compromised functionality of critical signalling pathways implicated in the immune response to COVID-19 infection.

An inherent challenge encountered in investigations involving TICAM1 overexpression is the phenomenon wherein the TICAM1 protein becomes constitutively active, thereby triggering cell apoptosis (Yamamoto et al., 2002; Han et al., 2004; Kaiser & Offermann, 2005; Sancho-Shimizu et al., 2011). This occurrence of cell apoptosis is generally not observed in cells that naturally that produce regulated and restricted quantities of endogenous TICAM1 (Funami et al., 2007; Funami et al., 2008). Consequently, the excessive amounts of TICAM1 protein produced in overexpression conditions in this study do not accurately reflect the physiologically relevant functions of TICAM1, as they result in constitutive activation and apoptosis. Nevertheless, despite this limitation, the transient transfection system has proven successful for numerous research groups in exploring the functional aspects of TICAM1 under overexpression system (Yamamoto et al., 2002; Oshiumi et al., 2003; Jiang et al., 2004; Kaiser & Offermann, 2005; Funami et al., 2008; Tatematsu et al., 2010; Sancho-Shimizu et al., 2011).

Our data suggests a critical role for type I IFN in the defence against life-threatening COVID-19 pneumonia, highlighting the significance of an intact TLR3-IFN signalling pathway (Zhang et al., 2020). Several significant risk factors have been linked to the onset of severe COVID-19, with being male, advanced age, obesity, and the presence of pre-existing comorbidities identified as primary contributors to heightened susceptibility (Grasselli et al., 2020; O'Driscoll et al., 2021; Lamers & Haagmans, 2022). Beyond these three *TICAM1* variants investigated in our laboratory, the collaborative efforts by diverse research groups within the COVIDHGE have also identified variants associated with deficiencies in TLR3, UNC93B1, TICAM1, TBK1, IRF3, IRF7, IFNAR1, and IFNAR2. These variants contribute to the impaired type I IFN immunity evidenced by a reduction or absence of type I IFNs, and their prevalence has been detected in at least 3.5% of individuals with life-threatening COVID-19 pneumonia (Zhang et al., 2020). In addition, an accompanying publication revealed that 10.2% of individuals suffering from life-threatening COVID-19 pneumonia harboured neutralising autoantibodies against type I IFNs at the onset of critical disease (Bastard et al., 2020). These autoantibodies effectively neutralised substantial concentrations of type I IFNs, compromising their effectiveness in inhibiting SARS-CoV-2 infection *in vitro*, thus demonstrating a B cell autoimmune phenocopy of inborn errors of type I IFN immunity could serve as a contributing factor to the development of life-threatening COVID-19 pneumonia (Bastard et al., 2020). Subsequently, in a follow up study, it was revealed that autoantibodies neutralising type I interferons were present in 20% of both critical COVID-19 cases among individuals over the age of 80 and in the overall population of fatal COVID-19 cases (Bastard et al., 2021). Taken together, this further emphasised the important significance of TLR3 and type-I immunity in mitigating and constraining the infection caused by SARS-CoV-2.

Mollaret's meningitis has recently been attributed to IEI involving autophagy, stemming from rare variants in *LC3B2* and *ATG4A* (Hait et al., 2020). This novel discovery marks the identification of a functionally significant antiviral role of autophagy in HSV-2 infections. These identified variants lead to compromised induction of autophagy upon HSV-2 infection, resulting in elevated viral loads and heightened cell death (Hait et al., 2020). In a separate investigation, Mollaret's meningitis has also been associated to IEI involving cGAS/STING pathway stemming from rare variant in *IKBKE*, which results in increased viral load, diminished phosphorylation of IRF3, and impaired production of type I IFNs following HSV-

2 infection (Reyahi et al., 2023). Introducing another dimension to these two IEIs, our research has unveiled the presence of pathogenic heterozygous variant (E429X) within the *TICAM1* gene in adult with Mollaret's meningitis with no prior history of hospitalization for viral illnesses, revealing additional insights into the complex genetic landscape influencing susceptibility to HSV-2 infection (Chapter 4). Our research provides evidence suggesting that the deficiency in *TICAM1* underlies cerebral infections caused by HSV-2 and also extends its impact to extra-cerebral manifestations.

This rare E429X *TICAM1* variant exhibited loss of protein expression, substantiated by both immunoblotting and immunofluorescence analyses. This variant also displayed an impaired ability in the activation of both IFN-β and NF-κB promoters, thus being categorised as LoF. Additionally, our investigations suggest that this variant does not exert a dominant negative effect. Instead, our immunoprecipitation of fibroblasts derived from patient exhibiting this E429X variant suggests TICAM1 haploinsufficiency as the underlying mechanism leading to the observed LoF phenotype. The LoE and LoF associated with the E429X allele result in the total elimination of TLR3-mediated signaling pathways, as well as the TICAM1-dependent TLR4 induction of IFNs and pro-inflammatory cytokines within fibroblast derived from the patient. Upon HSV-2 infection, the fibroblasts derived from the patient exhibited an inability to control the viral replication and impaired cytokines production including type I IFNs, resulting in an increased susceptibility. Our study highlights the important role of *TICAM1* in HSV-1 and HSV-2 infections, supporting the concept of TLR3 involved in detecting dsRNA intermediates originating derived from HSV-1 and HSV-2 infections. Our research is also consistent with the proposition that TLR3 coordinates the sustained production of IFN-β in fibroblasts and cortical neurons derived from iPSCs (Gao et al., 2021) where these collective findings reinforce the idea that TLR3-dependent IFN-β serves as a protective IFN, acting as an early defence mechanism against viral infections, highlighting the significance of maintaining constitutive interferon-β production in regulating the innate antiviral immunity.

The discovery of genetic variants in *TICAM1* and their correlation with severe manifestations of HSE, Mollaret's meningitis, and SARS-CoV-2 pneumonia suggests a wider significance of the TLR3-TICAM1-IFN pathway. This highlights susceptibility not only to HSV-1 and HSV-

2 but also highlights vulnerability to SARS-CoV-2, elucidating life-threatening consequences extending beyond the CNS. Remarkably, the evident incomplete penetrance observed within this particular family and similar families, introduces an intriguing proposition suggesting that the TLR3-TICAM1-IFN pathway could potentially be non-essential for host defence against HSV in specific individuals.

Over the past few years, cerebral brain organoids derived from human iPSCs have gained prominence as models that encapsulate diverse aspects of human brain development, tissue architecture, and physiology (Lancaster et al., 2013; Quadrato et al., 2017; Qian et al., 2018; D'Aiuto et al., 2019). Particularly, these cerebral brain organoids derived from human iPSCs are increasingly acknowledged as 3D models suitable for investigating viral infections (Salick et al., 2017; D'Aiuto et al., 2019; Krenn et al., 2021; Rybak-Wolf et al., 2023). Multiple transcriptomic studies demonstrate that the neuronal cell types generated within cerebral organoids closely resemble their counterparts present in the human embryonic brain (Camp et al., 2015; Qian et al., 2016; Quadrato et al., 2017). We have taken a significant stride forward in our research endeavours by successfully generating models of cortical neurons and cerebral organoids derived from PSCs (Chapter 5). These CNS models now serve as a tool for studying HSV-1 infection, offering a degree of relevance to the complex cellular environment of the human CNS. We also have shown that these models are susceptible to HSV-1 infection. Additionally, we successfully reprogrammed the PBMC from a patient with the assistance of Harry Leitch's lab, followed by the differentiation of these iPSCs into cortical neurons and cerebral organoids. This is particularly important given that 1024M possesses a *TLR3* variant (p.T650R) with an unknown significance and previous reports have indicated that deficiencies in TLR3 can result in heightened susceptibility to HSV-1 infection, potentially leading to development HSE. Thus, the utilisation of 1024M iPSCs which may potentially possess a defective TLR3-IFN pathway, provides a unique opportunity to investigate the intricacies of HSV-1 infection processes within iPSCs-derived CNS cells.

In our effort to evaluate pharmacological interventions, we are intrigued to test the potential effectiveness of various treatments for the management of HSV-1 infection. Clinicians hesitate to use steroids in treating HSE owing to the inherent immunosuppressive effects associated

with corticosteroids (Whitfield et al., 2021). The role of steroids in the treatment of HSE remains ambiguous and is a subject of careful deliberation among medical professionals (Portillo et al., 2016). Animal experiments have shown no correlation between the administration of steroid therapy and the spread or viral load of HSV-1 (Thompson et al., 2000). The potential effectiveness of corticosteroids in the management of HSE stems from their capacity to alleviate the activation of diverse inflammatory pathways (Sellner et al., 2005). The rationale that modulating inflammatory reactions through corticosteroid administration may contribute to alleviating the severity of HSE, presenting an avenue for further exploration and consideration within the medical community. In addition, the ongoing DexEnceph randomized controlled trial, investigating the efficacy of combining dexamethasone with standard antiviral therapy in adults with HSE, holds significant potential to advance clinical practice, potentially improving patient outcomes and care quality based on its anticipated outcomes (Whitfield et al., 2021). In our preliminary data from ESCs-derived cortical neurons, combined administration of aciclovir and steroids appeared to produce a more favourable outcome visually, despite no significant difference in viral load titres compared to aciclovir alone, necessitating further validation of additional outcome parameters to confirm findings and the essential repetition of experiments to establish conclusive evidence regarding the efficacy and potential synergistic effects of the combined treatment regimen (Chapter 5.5).

6.3 Future directions

In Chapters 3 and 4, we extensively evaluated various *TICAM1* variants across different domains to evaluate their functional characteristics and expressions. With this comprehensive collection of characterised *TICAM1* variants at our disposal, there is a compelling interest in augmenting this wealth of functional data by constructing a computational model of TICAM1's structure. This computational model is designed to identify specific residues associated with LoF and potentially predict additional sites that could contribute to diseases in the presence of a variant. The expectation is that this computational approach will serve as an educational or predictive tool to increase our understanding of the complexities surrounding *TICAM1* variants and their functional implications. Furthermore, exploring the impact of these *TICAM1* variants on TLR3 binding, particularly those situated within the TIR domain, as well as the LoF variants

identified in these chapters, presents an intriguing avenue for further investigation. Given our understanding that TLR3 interacts with TICAM1 through TIR-TIR domain interactions, a methodical approach to assess these bindings could involve immunoprecipitation (Fujita et al., 2003; Sasai et al., 2005; Funami et al., 2008; Han et al., 2010; Tatematsu et al., 2010). In this method, TLR3 antibodies would be attached to beads, serving as binding sites, while TICAM1-transfected protein lysates would adhere to these TLR3-coated beads. Subsequent steps would include running the bound material on an SDS gel, followed by probing with TICAM1 antibodies, thereby enabling the examination of binding interactions between TLR3 and TICAM1 at the molecular level.

In Chapter 4, a notable gap in our comprehensive dataset lies in the absence of viral titre data concerning the rescue of P1 fibroblast cells upon HSV-2 infection, which is crucial to substantiate the efficacy of the rescue process. Our efforts to perform a plaque assay were impeded by difficulties in quantifying the plaques, primarily due to the challenge of transfecting mammalian cells with bacterial, viral, or synthetic nucleic acids to induce type I IFN responses, thus complicating the assessment of HSV-2 replication (Huerfano et al., 2013). The next course of action for future investigations involves using CRISPR/Cas9 gene modification in P1 cells to introduce both the WT TICAM1 and its E429X variant. Subsequently, infecting these modified cells and evaluating outcomes, including IFN-β cytokine induction and viral titres, will provide a more comprehensive and robust assessment of the functional implications of the TICAM1 E429X variant in the context of HSV-2 infection. Additionally, this CRISPR/Cas9 gene modification approach can be extended to assess the wild-type rescue capability for the LoF variants identified in Chapter 3.

In Chapter 5, we have managed generating models of cortical neurons and cerebral organoids derived from PSCs. Our next phase involves the investigation of P1 cells, as discussed in Chapter 4, which harbour the E429X variant and have been reprogrammed from PBMC into iPSCs. Our plan includes the differentiation of these iPSCs into cortical neurons and cerebral organoids, followed by the testing of their susceptibility to HSV-2 infection. The particular significance of this investigation lies in the fact that P1 manifests Mollaret's meningitis, thereby offering a unique opportunity to shed light on the mechanisms underlying HSV-2 infection

within iPSCs-derived CNS cells with impaired TLR3-IFN signalling pathway. Furthermore, the natural progression of our study would involve an investigation of the *TICAM1* variants elucidated in Chapter 3 in the CNS cells. Our strategy involves introducing these *TICAM1* variants into PSCs using cutting-edge CRISPR-Cas9 technology, subsequently facilitating their differentiation into CNS cells. These PSCs-derived cells with *TICAM1* variants will then be subjected to viral infections which will contribute to the understanding of correlation between *TICAM1* variants and viral pathogenesis within the context of CNS cells.

While cerebral organoids represent an improved approach for *in vitro* modelling of the brain, it is essential to acknowledge they have limitations, as discussed in Chapter 5. However, recognising these limitations provides an opportunity for refinement and improvement of cerebral organoid models. For instance, the restricted diffusion of nutrients and oxygen within the central regions of cerebral organoids can be addressed by the implementation of vascularized organoids (Mansour et al., 2018; Pham et al., 2018; Sun et al., 2022). One approach involves embedding cerebral organoids with endothelial cells derived from the same iPSC line in the culture while another strategy involves the creation of assembloids by combining cerebral organoids with brain vascular organoids, effectively mirroring several characteristics of the blood-brain barrier (Pham et al., 2018; Sun et al., 2022). In murine studies, it has been documented that microglia play a pivotal role as the primary contributors to the expression of type I IFN in CNS cells following HSV-1 infection (Reinert et al., 2016). Additionally, the presence of microglia has been associated with a reduction in the lethality of HSV-1 in mice (Tsai et al., 2021). Given the significance of these findings, it highlights the importance of incorporating microglia into our cerebral organoid model to reflect the physiological environment and cellular interactions to understand HSV-1 infection within the CNS. A similar approach can be implemented involving the co-culture of cerebral organoids with microglia derived from the same iPSC line (Xu et al., 2021; Cakir et al., 2022).

An area of particular interest that we are keen to pursue revolves around autophagy within cortical neurons and cerebral organoids. In a prior research endeavour conducted within our laboratory, we observed the crucial involvement of TBK1 in promoting cytoprotective autophagy during the early stages of HSV-1 infection (Ahmad et al., 2019). A notion emerged

suggesting that HSV-1 infection of post-mitotic cells, particularly those within the CNS, may rely more significantly on autophagy mechanisms rather than type 1 IFN and this idea opens up a promising avenue for exploring the relative contributions of type 1 IFN versus autophagy pathways across various cellular contexts (Nikoletopoulou et al., 2015; Ahmad et al., 2019; Verzosa et al., 2021; Gomez-Virgilio et al., 2022). Utilising our PSCs-derived cortical neurons and cerebral organoids provides an excellent opportunity to explore these dynamics.

6.4 Concluding remarks

In summary, the comprehensive investigation conducted by the COVIDHGE sheds light on the intricate relationship between genetic variations and susceptibility to severe manifestations of COVID-19 pneumonia. The study, presented in Chapter 3, highlights the significant impact of rare *TICAM1* variants on the TLR3-IFN signalling pathway, emphasising their role in compromised immune responses, particularly in patients with life-threatening COVID-19 pneumonia. The findings extend beyond COVID-19 pneumonia, revealing a novel link between *TICAM1* variant and susceptibility to HSV-2 infections, as evidenced by the association with Mollaret's meningitis. This novel discovery expands our understanding of the genetic landscape influencing vulnerability to viral infections and highlights further the important role of TLR3 in antiviral immunity. Furthermore, this study introduces advanced research techniques, such as cerebral brain organoids derived from human PSCs, as valuable models for investigating viral infections, particularly HSV-1. Additionally, the exploration of potential pharmacological interventions, the combined administration of aciclovir and steroids, adds a practical dimension to the research. Overall, the research presented highlights the interplay between genetics and immune responses during viral infections, providing valuable insights that may inform future therapeutic approaches and enhance our ability to manage severe viral illnesses effectively.

References

Abe, Y., Fujii, K., Nagata, N., Takeuchi, O., Akira, S., Oshiumi, H., Matsumoto, M., Seya, T. & Koike, S. (2012) The toll-like receptor 3-mediated antiviral response is important for protection against poliovirus infection in poliovirus receptor transgenic mice. *J Virol.* 86 (1), 185-94.

Abel, L., Plancoulaine, S., Jouanguy, E., Zhang, S. Y., Mahfoufi, N., Nicolas, N., Sancho-Shimizu, V., Alcais, A., Guo, Y., Cardon, A., Boucherit, S., Obach, D., Clozel, T., Lorenzo, L., Amsallem, D., Berquin, P., Blanc, T., Bost-Bru, C., Chabrier, S., Chabrol, B., Cheuret, E., Dulac, O., Evrard, P., Heron, B., Lazaro, L., Mancini, J., Pedespan, J. M., Rivier, F., Vallee, L., Lebon, P., Rozenberg, F., Casanova, J. L. & Tardieu, M. (2010) Age-dependent Mendelian predisposition to herpes simplex virus type 1 encephalitis in childhood. *J Pediatr.* 157 (4), 623-9, 629 e1.

Aboul-Soud, M. A. M., Alzahrani, A. J. & Mahmoud, A. (2021) Induced Pluripotent Stem Cells (iPSCs)-Roles in Regenerative Therapies, Disease Modelling and Drug Screening. *Cells.* 10 (9).

Abu Khattab, M., Al Soub, H., Al Maslamani, M., Al Khuwaiter, J. & El Deeb, Y. (2009) Herpes simplex virus type 2 (Mollaret's) meningitis: a case report. *Int J Infect Dis.* 13 (6), e476-9.

Abu-Raddad, L. J., Magaret, A. S., Celum, C., Wald, A., Longini, I. M., Jr., Self, S. G. & Corey, L. (2008) Genital herpes has played a more important role than any other sexually transmitted infection in driving HIV prevalence in Africa. *PLoS One.* 3 (5), e2230.

Agirman, G., Broix, L. & Nguyen, L. (2017) Cerebral cortex development: an outside-in perspective. *FEBS Lett.* 591 (24), 3978-3992.

Ahmad, L., Mashbat, B., Leung, C., Brookes, C., Hamad, S., Krokowski, S., Shenoy, A. R., Lorenzo, L., Levin, M., O'Hare, P., Zhang, S. Y., Casanova, J. L., Mostowy, S. & Sancho-Shimizu, V. (2019) Human TANK-binding kinase 1 is required for early autophagy induction upon herpes simplex virus 1 infection. *J Allergy Clin Immunol.* 143 (2), 765-769 e7.

Ahmad, S. & Alsaeed, M. (2023) Recurrent Benign Lymphocytic Meningitis Due to HSV-2: A Case Report. *Dr. Sulaiman Al Habib Medical Journal.* 5 (4), 159-161.

Akira, S. & Takeda, K. (2004) Toll-like receptor signalling. *Nat Rev Immunol.* 4 (7), 499-511.

Akira, S., Takeda, K. & Kaisho, T. (2001) Toll-like receptors: critical proteins linking innate and acquired immunity. *Nat Immunol.* 2 (8), 675-80.

Akira, S., Uematsu, S. & Takeuchi, O. (2006) Pathogen recognition and innate immunity. *Cell.* 124 (4), 783-801.

Al-Khatib, K., Williams, B. R., Silverman, R. H., Halford, W. & Carr, D. J. (2004) Distinctive roles for 2',5'-oligoadenylate synthetases and double-stranded RNA-dependent protein kinase

R in the in vivo antiviral effect of an adenoviral vector expressing murine IFN-beta. *J Immunol.* 172 (9), 5638-47.

Al-Shekhlee, A., Kocharian, N. & Suarez, J. J. (2006) Re-evaluating the diagnostic methods in herpes simplex encephalitis. *Herpes.* 13 (1), 17-9.

Alexopoulou, L., Holt, A. C., Medzhitov, R. & Flavell, R. A. (2001) Recognition of double-stranded RNA and activation of NF-kappaB by Toll-like receptor 3. *Nature.* 413 (6857), 732-8.

Alimohamadi, Y., Tola, H. H., Abbasi-Ghahramanloo, A., Janani, M. & Sepandi, M. (2021) Case fatality rate of COVID-19: a systematic review and meta-analysis. *J Prev Med Hyg.* 62 (2), E311-E320.

Alipoor, B., Ghaedi, H., Omrani, M. D., Bastami, M., Meshkani, R. & Golmohammadi, T. (2016) A Bioinformatics Approach to Prioritize Single Nucleotide Polymorphisms in TLRs Signaling Pathway Genes. *Int J Mol Cell Med.* 5 (2), 65-79.

Allison, A. C. (1954) Protection afforded by sickle-cell trait against subtertian malareal infection. *Br Med J.* 1 (4857), 290-4.

Amos, W. & Bryant, C. (2011) Using human demographic history to infer natural selection reveals contrasting patterns on different families of immune genes. *Proc Biol Sci.* 278 (1711), 1587-94.

Amos, W., Driscoll, E. & Hoffman, J. I. (2011) Candidate genes versus genome-wide associations: which are better for detecting genetic susceptibility to infectious disease? *Proc Biol Sci.* 278 (1709), 1183-8.

Amoutzias, G. D., Nikolaidis, M., Tryfonopoulou, E., Chlichlia, K., Markoulatos, P. & Oliver, S. G. (2022) The Remarkable Evolutionary Plasticity of Coronaviruses by Mutation and Recombination: Insights for the COVID-19 Pandemic and the Future Evolutionary Paths of SARS-CoV-2. *Viruses.* 14 (1).

Andersen, L. L., Mork, N., Reinert, L. S., Kofod-Olsen, E., Narita, R., Jorgensen, S. E., Skipper, K. A., Honing, K., Gad, H. H., Ostergaard, L., Orntoft, T. F., Hornung, V., Paludan, S. R., Mikkelsen, J. G., Fujita, T., Christiansen, M., Hartmann, R. & Mogensen, T. H. (2015) Functional IRF3 deficiency in a patient with herpes simplex encephalitis. *J Exp Med.* 212 (9), 1371-9.

Antinone, S. E. & Smith, G. A. (2010) Retrograde axon transport of herpes simplex virus and pseudorabies virus: a live-cell comparative analysis. *J Virol.* 84 (3), 1504-12.

Arlotta, P., Molyneaux, B. J., Chen, J., Inoue, J., Kominami, R. & Macklis, J. D. (2005) Neuronal subtype-specific genes that control corticospinal motor neuron development in vivo. *Neuron.* 45 (2), 207-21.

Arlotta, P. & Pasca, S. P. (2019) Cell diversity in the human cerebral cortex: from the embryo to brain organoids. *Curr Opin Neurobiol.* 56, 194-198.

Arthur, J. L., Scarpini, C. G., Connor, V., Lachmann, R. H., Tolkovsky, A. M. & Efstathiou, S. (2001) Herpes simplex virus type 1 promoter activity during latency establishment, maintenance, and reactivation in primary dorsal root neurons in vitro. *J Virol.* 75 (8), 3885-95.

Asher, Y., Heller, M. & Becker, Y. (1969) Incorporation of lipids into herpes simplex virus particles. *J Gen Virol.* 4 (1), 65-76.

Ashkar, A. A., Yao, X. D., Gill, N., Sajic, D., Patrick, A. J. & Rosenthal, K. L. (2004) Toll-like receptor (TLR)-3, but not TLR4, agonist protects against genital herpes infection in the absence of inflammation seen with CpG DNA. *J Infect Dis.* 190 (10), 1841-9.

Astuti, I. & Ysrafil (2020) Severe Acute Respiratory Syndrome Coronavirus 2 (SARS-CoV-2): An overview of viral structure and host response. *Diabetes Metab Syndr.* 14 (4), 407-412.

Audry, M., Ciancanelli, M., Yang, K., Cobat, A., Chang, H. H., Sancho-Shimizu, V., Lorenzo, L., Niehues, T., Reichenbach, J., Li, X. X., Israel, A., Abel, L., Casanova, J. L., Zhang, S. Y., Jouanguy, E. & Puel, A. (2011) NEMO is a key component of NF-kappaB- and IRF-3-dependent TLR3-mediated immunity to herpes simplex virus. *J Allergy Clin Immunol.* 128 (3), 610-7 e1-4.

Aurelius, E., Forsgren, M., Gille, E. & Skoldenberg, B. (2002) Neurologic morbidity after herpes simplex virus type 2 meningitis: a retrospective study of 40 patients. *Scand J Infect Dis.* 34 (4), 278-83.

Babaei, A., Shatizadeh Malekshahi, S., Pirbonyeh, N. & Moattari, A. (2021) Prevalence and clinical manifestations of herpes simplex virus infection among suspected patients of herpes simplex encephalitis in Shiraz, Iran. *Virusdisease.* 32 (2), 266-271.

Balachandran, S., Roberts, P. C., Brown, L. E., Truong, H., Pattnaik, A. K., Archer, D. R. & Barber, G. N. (2000) Essential role for the dsRNA-dependent protein kinase PKR in innate immunity to viral infection. *Immunity.* 13 (1), 129-41.

Bansode, Y. D., Chattopadhyay, D. & Saha, B. (2019) Innate immune response in astrocytes infected with herpes simplex virus 1. *Arch Virol.* 164 (5), 1433-1439.

Baringer, J. R. & Swoveland, P. (1973) Recovery of herpes-simplex virus from human trigeminal ganglions. *N Engl J Med.* 288 (13), 648-50.

Barnard, D. L., Day, C. W., Bailey, K., Heiner, M., Montgomery, R., Lauridsen, L., Chan, P. K. & Sidwell, R. W. (2006) Evaluation of immunomodulators, interferons and known in vitro SARS-coV inhibitors for inhibition of SARS-coV replication in BALB/c mice. *Antivir Chem Chemother.* 17 (5), 275-84.

Barreras, P., Pamies, D., Monaco, M. C., Munoz, L. S., Zhong, X., Major, E. O., Hogberg, H. T., Hartung, T. & Pardo, C. A. (2022) A human-derived 3D brain organoid model to study JC virus infection. *J Neurovirol.* 28 (1), 17-26.

Bastard, P. & Gervais, A. & Le Voyer, T. & Rosain, J. & Philippot, Q. & Manry, J. & Michailidis, E. & Hoffmann, H. H. & Eto, S. & Garcia-Prat, M. & Bizien, L. & Parra-Martinez, A. & Yang, R. & Haljasmagi, L. & Migaud, M. & Sarekannu, K. & Maslovskaja, J. & de Prost,

N. & Tandjaoui-Lambiotte, Y. & Luyt, C. E. & Amador-Borrero, B. & Gaudet, A. & Poissy, J. & Morel, P. & Richard, P. & Cognasse, F. & Troya, J. & Trouillet-Assant, S. & Belot, A. & Saker, K. & Garcon, P. & Riviere, J. G. & Lagier, J. C. & Gentile, S. & Rosen, L. B. & Shaw, E. & Morio, T. & Tanaka, J. & Dalmau, D. & Tharaux, P. L. & Sene, D. & Stepanian, A. & Megarbane, B. & Triantafyllia, V. & Fekkar, A. & Heath, J. R. & Franco, J. L. & Anaya, J. M. & Sole-Violan, J. & Imberti, L. & Biondi, A. & Bonfanti, P. & Castagnoli, R. & Delmonte, O. M. & Zhang, Y. & Snow, A. L. & Holland, S. M. & Biggs, C. & Moncada-Velez, M. & Arias, A. A. & Lorenzo, L. & Boucherit, S. & Coulibaly, B. & Anglicheau, D. & Planas, A. M. & Haerynck, F. & Duvlis, S. & Nussbaum, R. L. & Ozcelik, T. & Keles, S. & Bousfiha, A. A. & El Bakkouri, J. & Ramirez-Santana, C. & Paul, S. & Pan-Hammarstrom, Q. & Hammarstrom, L. & Dupont, A. & Kurolap, A. & Metz, C. N. & Aiuti, A. & Casari, G. & Lampasona, V. & Ciceri, F. & Barreiros, L. A. & Dominguez-Garrido, E. & Vidigal, M. & Zatz, M. & van de Beek, D. & Sahanic, S. & Tancevski, I. & Stepanovskyy, Y. & Boyarchuk, O. & Nukui, Y. & Tsumura, M. & Vidaur, L. & Tangye, S. G. & Burrel, S. & Duffy, D. & Quintana-Murci, L. & Klocperk, A. & Kann, N. Y. & Shcherbina, A. & Lau, Y. L. & Leung, D. & Coulongeat, M. & Marlet, J. & Koning, R. & Reyes, L. F. & Chauvineau-Grenier, A. & Venet, F. & Monneret, G. & Nussenzweig, M. C. & Arrestier, R. & Boudhabhay, I. & Baris-Feldman, H. & Hagin, D. & Wauters, J. & Meyts, I. & Dyer, A. H. & Kennelly, S. P. & Bourke, N. M. & Halwani, R. & Sharif-Askari, N. S. & Dorgham, K. & Sallette, J. & Sedkaoui, S. M. & AlKhater, S. & Rigo-Bonnin, R. & Morandeira, F. & Roussel, L. & Vinh, D. C. & Ostrowski, S. R. & Condino-Neto, A. & Prando, C. & Bonradenko, A. & Spaan, A. N. & Gilardin, L. & Fellay, J. & Lyonnet, S. & Bilguvar, K. & Lifton, R. P. & Mane, S. & Lab, H. & Clinicians, C. & Clinicians, C.-S. & Group, N. I. R. t. C. & Group, N.-C. S. & Danish, C. & Danish Blood Donor, S. & St. James's, H. & group, S. C. I. & French, C. C. S. G. & Imagine, C.-G. & Milieu Interieur, C. & Co, V. C. C. & Amsterdam, U. M. C. C. & Biobank, I. & Effort, C. H. G. & cohort, C. & Study, C. D. & Cerba, H.-C. & Etablissement du Sang study, g. & Anderson, M. S. & Boisson, B. & Beziat, V. & Zhang, S. Y. & Vandreakos, E. & Hermine, O. & Pujol, A. & Peterson, P. & Mogensen, T. H. & Rowen, L. & Mond, J. & Debette, S. & de Lamballerie, X. & Duval, X. & Mentre, F. & Zins, M. & Soler-Palacin, P. & Colobran, R. & Gorochov, G. & Solanich, X. & Susen, S. & Martinez-Picado, J. & Raoult, D. & Vasse, M. & Gregersen, P. K. & Piemonti, L. & Rodriguez-Gallego, C. & Notarangelo, L. D. & Su, H. C. & Kisand, K. & Okada, S. & Puel, A. & Jouanguy, E. & Rice, C. M. & Tiberghien, P. & Zhang, Q. & Cobat, A. & Abel, L. & Casanova, J. L. (2021) Autoantibodies neutralizing type I IFNs are present in ~4% of uninfected individuals over 70 years old and account for ~20% of COVID-19 deaths. *Sci Immunol.* 6 (62).

Bastard, P. & Rosen, L. B. & Zhang, Q. & Michailidis, E. & Hoffmann, H. H. & Zhang, Y. & Dorgham, K. & Philippot, Q. & Rosain, J. & Beziat, V. & Manry, J. & Shaw, E. & Haljasmagi, L. & Peterson, P. & Lorenzo, L. & Bizien, L. & Trouillet-Assant, S. & Dobbs, K. & de Jesus, A. A. & Belot, A. & Kallaste, A. & Catherinot, E. & Tandjaoui-Lambiotte, Y. & Le Pen, J. & Kerner, G. & Bigio, B. & Seeleuthner, Y. & Yang, R. & Bolze, A. & Spaan, A. N. & Delmonte, O. M. & Abers, M. S. & Aiuti, A. & Casari, G. & Lampasona, V. & Piemonti, L. & Ciceri, F. & Bilguvar, K. & Lifton, R. P. & Vasse, M. & Smadja, D. M. & Migaud, M. & Hadjadj, J. & Terrier, B. & Duffy, D. & Quintana-Murci, L. & van de Beek, D. & Roussel, L. & Vinh, D. C. & Tangye, S. G. & Haerynck, F. & Dalmau, D. & Martinez-Picado, J. & Brodin, P. & Nussenzweig, M. C. & Boisson-Dupuis, S. & Rodriguez-Gallego, C. & Vogt, G. & Mogensen, T. H. & Oler, A. J. & Gu, J. & Burbelo, P. D. & Cohen, J. I. & Biondi, A. & Bettini, L. R. & D'Angio, M. & Bonfanti, P. & Rossignol, P. & Mayaux, J. & Rieux-Laucat, F. & Husebye, E. S. & Fusco, F. & Ursini, M. V. & Imberti, L. & Sottini, A. & Paghera, S. & Quiros-Roldan, E. & Rossi, C. & Castagnoli, R. & Montagna, D. & Licari, A. & Marseglia, G. L. & Duval, X. &

Ghosn, J. & Lab, H. & Group, N.-U. I. R. t. C. & Clinicians, C. & Clinicians, C.-S. & Imagine, C. G. & French, C. C. S. G. & Milieu Interieur, C. & Co, V. C. C. & Amsterdam, U. M. C. C.-B. & Effort, C. H. G. & Tsang, J. S. & Goldbach-Mansky, R. & Kisand, K. & Lionakis, M. S. & Puel, A. & Zhang, S. Y. & Holland, S. M. & Gorochov, G. & Jouanguy, E. & Rice, C. M. & Cobat, A. & Notarangelo, L. D. & Abel, L. & Su, H. C. & Casanova, J. L. (2020) Autoantibodies against type I IFNs in patients with life-threatening COVID-19. *Science.* 370 (6515).

Behzadi, P., Garcia-Perdomo, H. A. & Karpinski, T. M. (2021) Toll-Like Receptors: General Molecular and Structural Biology. *J Immunol Res.* 2021, 9914854.

Bellin, M., Marchetto, M. C., Gage, F. H. & Mummery, C. L. (2012) Induced pluripotent stem cells: the new patient? *Nat Rev Mol Cell Biol.* 13 (11), 713-26.

Belouzard, S., Chu, V. C. & Whittaker, G. R. (2009) Activation of the SARS coronavirus spike protein via sequential proteolytic cleavage at two distinct sites. *Proc Natl Acad Sci U S A.* 106 (14), 5871-6.

Bernard, J. J., Cowing-Zitron, C., Nakatsuji, T., Muehleisen, B., Muto, J., Borkowski, A. W., Martinez, L., Greidinger, E. L., Yu, B. D. & Gallo, R. L. (2012) Ultraviolet radiation damages self noncoding RNA and is detected by TLR3. *Nat Med.* 18 (8), 1286-90.

Bjorck, L. & Kronvall, G. (1984) Purification and some properties of streptococcal protein G, a novel IgG-binding reagent. *J Immunol.* 133 (2), 969-74.

Bodakuntla, S., Jijumon, A. S., Villablanca, C., Gonzalez-Billault, C. & Janke, C. (2019) Microtubule-Associated Proteins: Structuring the Cytoskeleton. *Trends Cell Biol.* 29 (10), 804-819.

Bodilsen, J., Tattevin, P., Tong, S. Y. C., Naucler, P. & Nielsen, H. (2022) Treatment of Herpes Simplex Virus Type 2 Meningitis: A Survey Among Infectious Diseases Specialists in France, Sweden, Australia, and Denmark. *Open Forum Infect Dis.* 9 (12), ofac644.

Booy, F. P., Trus, B. L., Davison, A. J. & Steven, A. C. (1996) The capsid architecture of channel catfish virus, an evolutionarily distant herpesvirus, is largely conserved in the absence of discernible sequence homology with herpes simplex virus. *Virology.* 215 (2), 134-41.

Borish, L., Ayars, A. G. & Kirkpatrick, C. H. (2011) Common variable immunodeficiency presenting as herpes simplex virus encephalitis. *J Allergy Clin Immunol.* 127 (2), 541-3.

Boucher, A., Herrmann, J. L., Morand, P., Buzele, R., Crabol, Y., Stahl, J. P. & Mailles, A. (2017) Epidemiology of infectious encephalitis causes in 2016. *Med Mal Infect.* 47 (3), 221-235.

Boulling, A., Le Marechal, C., Trouve, P., Raguenes, O., Chen, J. M. & Ferec, C. (2007) Functional analysis of pancreatitis-associated missense mutations in the pancreatic secretory trypsin inhibitor (SPINK1) gene. *Eur J Hum Genet.* 15 (9), 936-42.

Bousfiha, A., Moundir, A., Tangye, S. G., Picard, C., Jeddane, L., Al-Herz, W., Rundles, C. C., Franco, J. L., Holland, S. M., Klein, C., Morio, T., Oksenhendler, E., Puel, A., Puck, J.,

Seppanen, M. R. J., Somech, R., Su, H. C., Sullivan, K. E., Torgerson, T. R. & Meyts, I. (2022a) The 2022 Update of IUIS Phenotypical Classification for Human Inborn Errors of Immunity. *J Clin Immunol.* 42 (7), 1508-1520.

Bousfiha, A., Moundir, A., Tangye, S. G., Picard, C., Jeddane, L., Al-Herz, W., Rundles, C. C., Franco, J. L., Holland, S. M., Klein, C., Morio, T., Oksenhendler, E., Puel, A., Puck, J., Seppänen, M. R. J., Somech, R., Su, H. C., Sullivan, K. E., Torgerson, T. R. & Meyts, I. (2022b) The 2022 Update of IUIS Phenotypical Classification for Human Inborn Errors of Immunity. *J Clin Immunol.* 42 (7), 1508-1520.

Bradshaw, M. J. & Venkatesan, A. (2016) Herpes Simplex Virus-1 Encephalitis in Adults: Pathophysiology, Diagnosis, and Management. *Neurotherapeutics.* 13 (3), 493-508.

Bruyn, G. W., Straathof, L. J. & Raymakers, G. M. (1962) Mollaret's meningitis. Differential diagnosis and diagnostic pitfalls. *Neurology.* 12, 745-53.

Bsibsi, M., Ravid, R., Gveric, D. & van Noort, J. M. (2002) Broad expression of Toll-like receptors in the human central nervous system. *J Neuropathol Exp Neurol.* 61 (11), 1013-21.

Burdette, D. L., Monroe, K. M., Sotelo-Troha, K., Iwig, J. S., Eckert, B., Hyodo, M., Hayakawa, Y. & Vance, R. E. (2011) STING is a direct innate immune sensor of cyclic di-GMP. *Nature.* 478 (7370), 515-8.

Burgoyne, R. D., Cambray-Deakin, M. A., Lewis, S. A., Sarkar, S. & Cowan, N. J. (1988) Differential distribution of beta-tubulin isotypes in cerebellum. *EMBO J.* 7 (8), 2311-9.

Cai, X., Chiu, Y. H. & Chen, Z. J. (2014) The cGAS-cGAMP-STING pathway of cytosolic DNA sensing and signaling. *Mol Cell.* 54 (2), 289-96.

Cakir, B., Tanaka, Y., Kiral, F. R., Xiang, Y., Dagliyan, O., Wang, J., Lee, M., Greaney, A. M., Yang, W. S., duBoulay, C., Kural, M. H., Patterson, B., Zhong, M., Kim, J., Bai, Y., Min, W., Niklason, L. E., Patra, P. & Park, I. H. (2022) Expression of the transcription factor PU.1 induces the generation of microglia-like cells in human cortical organoids. *Nat Commun.* 13 (1), 430.

Camp, J. G., Badsha, F., Florio, M., Kanton, S., Gerber, T., Wilsch-Brauninger, M., Lewitus, E., Sykes, A., Hevers, W., Lancaster, M., Knoblich, J. A., Lachmann, R., Paabo, S., Huttner, W. B. & Treutlein, B. (2015) Human cerebral organoids recapitulate gene expression programs of fetal neocortex development. *Proc Natl Acad Sci U S A.* 112 (51), 15672-7.

Campadelli-Fiume, G., Amasio, M., Avitabile, E., Cerretani, A., Forghieri, C., Gianni, T. & Menotti, L. (2007) The multipartite system that mediates entry of herpes simplex virus into the cell. *Reviews in medical virology.* 17 (5), 313-326.

Carr, D. J., Tomanek, L., Silverman, R. H., Campbell, I. L. & Williams, B. R. (2005) RNA-dependent protein kinase is required for alpha-1 interferon transgene-induced resistance to genital herpes simplex virus type 2. *J Virol.* 79 (14), 9341-5.

Carsana, L., Sonzogni, A., Nasr, A., Rossi, R. S., Pellegrinelli, A., Zerbi, P., Rech, R., Colombo, R., Antinori, S., Corbellino, M., Galli, M., Catena, E., Tosoni, A., Gianatti, A. &

Nebuloni, M. (2020) Pulmonary post-mortem findings in a series of COVID-19 cases from northern Italy: a two-centre descriptive study. *Lancet Infect Dis.* 20 (10), 1135-1140.

Casanova, J. L. & Abel, L. (2021) Lethal Infectious Diseases as Inborn Errors of Immunity: Toward a Synthesis of the Germ and Genetic Theories. *Annu Rev Pathol.* 16, 23-50.

Casanova, J. L. & Anderson, M. S. (2023) Unlocking life-threatening COVID-19 through two types of inborn errors of type I IFNs. *J Clin Invest.* 133 (3).

Casanova, J. L., Conley, M. E., Seligman, S. J., Abel, L. & Notarangelo, L. D. (2014) Guidelines for genetic studies in single patients: lessons from primary immunodeficiencies. *J Exp Med.* 211 (11), 2137-49.

Casrouge, A., Zhang, S. Y., Eidenschenk, C., Jouanguy, E., Puel, A., Yang, K., Alcais, A., Picard, C., Mahfoufi, N., Nicolas, N., Lorenzo, L., Plancoulaine, S., Senechal, B., Geissmann, F., Tabeta, K., Hoebe, K., Du, X., Miller, R. L., Heron, B., Mignot, C., de Villemeur, T. B., Lebon, P., Dulac, O., Rozenberg, F., Beutler, B., Tardieu, M., Abel, L. & Casanova, J. L. (2006) Herpes simplex virus encephalitis in human UNC-93B deficiency. *Science.* 314 (5797), 308-12.

Cerveny, L., Straskova, A., Dankova, V., Hartlova, A., Ceckova, M., Staud, F. & Stulik, J. (2013) Tetratricopeptide repeat motifs in the world of bacterial pathogens: role in virulence mechanisms. *Infect Immun.* 81 (3), 629-35.

Chambers, S. M., Fasano, C. A., Papapetrou, E. P., Tomishima, M., Sadelain, M. & Studer, L. (2009) Highly efficient neural conversion of human ES and iPS cells by dual inhibition of SMAD signaling. *Nat Biotechnol.* 27 (3), 275-80.

Chan, J. K. (2014) The wonderful colors of the hematoxylin-eosin stain in diagnostic surgical pathology. *Int J Surg Pathol.* 22 (1), 12-32.

Chang, C. Y., Ting, H. C., Liu, C. A., Su, H. L., Chiou, T. W., Lin, S. Z., Harn, H. J. & Ho, T. J. (2020) Induced Pluripotent Stem Cell (iPSC)-Based Neurodegenerative Disease Models for Phenotype Recapitulation and Drug Screening. *Molecules.* 25 (8).

Chapgier, A., Wynn, R. F., Jouanguy, E., Filipe-Santos, O., Zhang, S., Feinberg, J., Hawkins, K., Casanova, J. L. & Arkwright, P. D. (2006) Human complete Stat-1 deficiency is associated with defective type I and II IFN responses in vitro but immunity to some low virulence viruses in vivo. *J Immunol.* 176 (8), 5078-83.

Chaplin, D. D. (2010) Overview of the immune response. *J Allergy Clin Immunol.* 125 (2 Suppl 2), S3-23.

Chentoufi, A. A. & Benmohamed, L. (2012) Mucosal herpes immunity and immunopathology to ocular and genital herpes simplex virus infections. *Clin Dev Immunol.* 2012, 149135.

Chiu, Y. H., Macmillan, J. B. & Chen, Z. J. (2009) RNA polymerase III detects cytosolic DNA and induces type I interferons through the RIG-I pathway. *Cell.* 138 (3), 576-91.

Choi, M. K., Wang, Z., Ban, T., Yanai, H., Lu, Y., Koshiba, R., Nakaima, Y., Hangai, S., Savitsky, D., Nakasato, M., Negishi, H., Takeuchi, O., Honda, K., Akira, S., Tamura, T. & Taniguchi, T. (2009) A selective contribution of the RIG-I-like receptor pathway to type I interferon responses activated by cytosolic DNA. *Proc Natl Acad Sci U S A.* 106 (42), 17870-5.

Choudhry, H., Bakhrebah, M. A., Abdulaal, W. H., Zamzami, M. A., Baothman, O. A., Hassan, M. A., Zeyadi, M., Helmi, N., Alzahrani, F., Ali, A., Zakaria, M. K., Kamal, M. A., Warsi, M. K., Ahmed, F., Rasool, M. & Jamal, M. S. (2019) Middle East respiratory syndrome: pathogenesis and therapeutic developments. *Future Virol.* 14 (4), 237-246.

Chun, Y. S., Byun, K. & Lee, B. (2011) Induced pluripotent stem cells and personalized medicine: current progress and future perspectives. *Anat Cell Biol.* 44 (4), 245-55.

Ciancanelli, M. J., Huang, S. X., Luthra, P., Garner, H., Itan, Y., Volpi, S., Lafaille, F. G., Trouillet, C., Schmolke, M., Albrecht, R. A., Israelsson, E., Lim, H. K., Casadio, M., Hermesh, T., Lorenzo, L., Leung, L. W., Pedergnana, V., Boisson, B., Okada, S., Picard, C., Ringuier, B., Troussier, F., Chaussabel, D., Abel, L., Pellier, I., Notarangelo, L. D., Garcia-Sastre, A., Basler, C. F., Geissmann, F., Zhang, S. Y., Snoeck, H. W. & Casanova, J. L. (2015) Infectious disease. Life-threatening influenza and impaired interferon amplification in human IRF7 deficiency. *Science.* 348 (6233), 448-53.

Cliffe, A. R., Garber, D. A. & Knipe, D. M. (2009) Transcription of the herpes simplex virus latency-associated transcript promotes the formation of facultative heterochromatin on lytic promoters. *J Virol.* 83 (16), 8182-90.

Cocchi, F., Fusco, D., Menotti, L., Gianni, T., Eisenberg, R. J., Cohen, G. H. & Campadelli-Fiume, G. (2004) The soluble ectodomain of herpes simplex virus gD contains a membrane-proximal pro-fusion domain and suffices to mediate virus entry. *Proc Natl Acad Sci U S A.* 101 (19), 7445-50.

Cohen, J. I. (2020) Herpesvirus latency. *J Clin Invest.* 130 (7), 3361-3369.

Compagnucci, C., Nizzardo, M., Corti, S., Zanni, G. & Bertini, E. (2014) In vitro neurogenesis: development and functional implications of iPSC technology. *Cell Mol Life Sci.* 71 (9), 1623-39.

Cooke, G. S. & Hill, A. V. (2001) Genetics of susceptibility to human infectious disease. *Nat Rev Genet.* 2 (12), 967-77.

Croen, K. D., Ostrove, J. M., Dragovic, L. & Straus, S. E. (1991) Characterization of herpes simplex virus type 2 latency-associated transcription in human sacral ganglia and in cell culture. *J Infect Dis.* 163 (1), 23-8.

Cui, J., Li, F. & Shi, Z. L. (2019) Origin and evolution of pathogenic coronaviruses. *Nat Rev Microbiol.* 17 (3), 181-192.

D'Aiuto, L., Bloom, D. C., Naciri, J. N., Smith, A., Edwards, T. G., McClain, L., Callio, J. A., Jessup, M., Wood, J., Chowdari, K., Demers, M., Abrahamson, E. E., Ikonomovic, M. D., Viggiano, L., De Zio, R., Watkins, S., Kinchington, P. R. & Nimgaonkar, V. L. (2019)

Modeling Herpes Simplex Virus 1 Infections in Human Central Nervous System Neuronal Cells Using Two- and Three-Dimensional Cultures Derived from Induced Pluripotent Stem Cells. *J Virol.* 93 (9).

D'Aiuto, L., Di Maio, R., Heath, B., Raimondi, G., Milosevic, J., Watson, A. M., Bamne, M., Parks, W. T., Yang, L., Lin, B., Miki, T., Mich-Basso, J. D., Arav-Boger, R., Sibille, E., Sabunciyan, S., Yolken, R. & Nimgaonkar, V. (2012) Human induced pluripotent stem cell-derived models to investigate human cytomegalovirus infection in neural cells. *PLoS One.* 7 (11), e49700.

Dahlstrand, J., Lardelli, M. & Lendahl, U. (1995) Nestin mRNA expression correlates with the central nervous system progenitor cell state in many, but not all, regions of developing central nervous system. *Brain Res Dev Brain Res.* 84 (1), 109-29.

Davies, N., Tang, J. & Ward, K. N. (2004) Herpes simplex virus type 2 and recurrent meningitis. *Lancet.* 364 (9433), 501-2.

Davis, L. E., Guerre, J. & Gerstein, W. H. (2010) Recurrent herpes simplex virus type 2 meningitis in elderly persons. *Arch Neurol.* 67 (6), 759-60.

Davison, A., Eberle, R. & Hayward, G. (2005) *Family herpesviridae.* Elsevier/Academic Press.

Davison, K. L., Crowcroft, N. S., Ramsay, M. E., Brown, D. W. & Andrews, N. J. (2003) Viral encephalitis in England, 1989-1998: what did we miss? *Emerg Infect Dis.* 9 (2), 234-40.

de Gans, J., van de Beek, D. & European Dexamethasone in Adulthood Bacterial Meningitis Study, I. (2002) Dexamethasone in adults with bacterial meningitis. *N Engl J Med.* 347 (20), 1549-56.

Defres, S., Keller, S. S., Das, K., Vidyasagar, R., Parkes, L. M., Burnside, G., Griffiths, M., Kopelman, M., Roberts, N., Solomon, T. & group, E. U. s. (2017) A Feasibility Study of Quantifying Longitudinal Brain Changes in Herpes Simplex Virus (HSV) Encephalitis Using Magnetic Resonance Imaging (MRI) and Stereology. *PLoS One.* 12 (1), e0170215.

Dendrou, C. A., Petersen, J., Rossjohn, J. & Fugger, L. (2018) HLA variation and disease. *Nat Rev Immunol.* 18 (5), 325-339.

Derk, J., Jones, H. E., Como, C., Pawlikowski, B. & Siegenthaler, J. A. (2021) Living on the Edge of the CNS: Meninges Cell Diversity in Health and Disease. *Front Cell Neurosci.* 15, 703944.

Desai, P. & Person, S. (1998) Incorporation of the green fluorescent protein into the herpes simplex virus type 1 capsid. *J Virol.* 72 (9), 7563-8.

Dinn, J. J. (1980) Transolfactory spread of virus in herpes simplex encephalitis. *Br Med J.* 281 (6252), 1392.

Dupuis, S., Jouanguy, E., Al-Hajjar, S., Fieschi, C., Al-Mohsen, I. Z., Al-Jumaah, S., Yang, K., Chapgier, A., Eidenschenk, C., Eid, P., Al Ghonaium, A., Tufenkeji, H., Frayha, H., Al-Gazlan, S., Al-Rayes, H., Schreiber, R. D., Gresser, I. & Casanova, J. L. (2003) Impaired

response to interferon-alpha/beta and lethal viral disease in human STAT1 deficiency. *Nat Genet.* 33 (3), 388-91.

Easter, S. S., Jr., Ross, L. S. & Frankfurter, A. (1993) Initial tract formation in the mouse brain. *J Neurosci.* 13 (1), 285-99.

Elkabetz, Y., Panagiotakos, G., Al Shamy, G., Socci, N. D., Tabar, V. & Studer, L. (2008) Human ES cell-derived neural rosettes reveal a functionally distinct early neural stem cell stage. *Genes Dev.* 22 (2), 152-65.

Ellermann-Eriksen, S., Justesen, J. & Mogensen, S. C. (1986a) Genetically determined difference in the antiviral action of alpha/beta interferon in cells from mice resistant or susceptible to herpes simplex virus type 2. *J Gen Virol.* 67 (Pt 9), 1859-66.

Ellermann-Eriksen, S., Liberto, M. C., Iannello, D. & Mogensen, S. C. (1986b) X-linkage of the early in vitro alpha/beta interferon response of mouse peritoneal macrophages to herpes simplex virus type 2. *J Gen Virol.* 67 (Pt 6), 1025-33.

Elsink, K., Huibers, M. M. H., Hollink, I., Simons, A., Zonneveld-Huijssoon, E., van der Veken, L. T., Leavis, H. L., Henriet, S. S. V., van Deuren, M., van de Veerdonk, F. L., Potjewijd, J., Berghuis, D., Dalm, V., Vermont, C. L., van de Ven, A., Lambeck, A. J. A., Abbott, K. M., van Hagen, P. M., de Bree, G. J., Kuijpers, T. W., Frederix, G. W. J., van Gijn, M. E., van Montfrans, J. M. & Genetics First for Primary Immunodeficiency Disorders, C. (2021) Implementation of Early Next-Generation Sequencing for Inborn Errors of Immunity: A Prospective Observational Cohort Study of Diagnostic Yield and Clinical Implications in Dutch Genome Diagnostic Centers. *Front Immunol.* 12, 780134.

Englund, C., Fink, A., Lau, C., Pham, D., Daza, R. A., Bulfone, A., Kowalczyk, T. & Hevner, R. F. (2005) Pax6, Tbr2, and Tbr1 are expressed sequentially by radial glia, intermediate progenitor cells, and postmitotic neurons in developing neocortex. *J Neurosci.* 25 (1), 247-51.

Enokizono, Y., Kumeta, H., Funami, K., Horiuchi, M., Sarmiento, J., Yamashita, K., Standley, D. M., Matsumoto, M., Seya, T. & Inagaki, F. (2013) Structures and interface mapping of the TIR domain-containing adaptor molecules involved in interferon signaling. *Proc Natl Acad Sci U S A.* 110 (49), 19908-13.

Falke, D., Siegert, R. & Vogell, W. (1959) [Electron microscopic findings on the problem of double membrane formation in herpes simplex virus]. *Arch Gesamte Virusforsch.* 9, 484-96.

Farazmand, P., Woolley, P. D. & Kinghorn, G. R. (2011) Mollaret's meningitis and herpes simplex virus type 2 infections. *Int J STD AIDS.* 22 (6), 306-7.

Ferreira, A. & Caceres, A. (1992) Expression of the class III beta-tubulin isotype in developing neurons in culture. *J Neurosci Res.* 32 (4), 516-29.

Finkel, Y., Mizrahi, O., Nachshon, A., Weingarten-Gabbay, S., Morgenstern, D., Yahalom-Ronen, Y., Tamir, H., Achdout, H., Stein, D., Israeli, O., Beth-Din, A., Melamed, S., Weiss, S., Israely, T., Paran, N., Schwartz, M. & Stern-Ginossar, N. (2021) The coding capacity of SARS-CoV-2. *Nature.* 589 (7840), 125-130.

Fitzgerald, K. A., McWhirter, S. M., Faia, K. L., Rowe, D. C., Latz, E., Golenbock, D. T., Coyle, A. J., Liao, S. M. & Maniatis, T. (2003a) IKKepsilon and TBK1 are essential components of the IRF3 signaling pathway. *Nat Immunol.* 4 (5), 491-6.

Fitzgerald, K. A., Rowe, D. C., Barnes, B. J., Caffrey, D. R., Visintin, A., Latz, E., Monks, B., Pitha, P. M. & Golenbock, D. T. (2003b) LPS-TLR4 signaling to IRF-3/7 and NF-kappaB involves the toll adapters TRAM and TRIF. *J Exp Med.* 198 (7), 1043-55.

Forni, D., Cagliani, R., Arrigoni, F., Benvenuti, M., Mozzi, A., Pozzoli, U., Clerici, M., De Gioia, L. & Sironi, M. (2021) Adaptation of the endemic coronaviruses HCoV-OC43 and HCoV-229E to the human host. *Virus Evol.* 7 (2), veab061.

Forrester, A., Farrell, H., Wilkinson, G., Kaye, J., Davis-Poynter, N. & Minson, T. (1992) Construction and properties of a mutant of herpes simplex virus type 1 with glycoprotein H coding sequences deleted. *J Virol.* 66 (1), 341-8.

Fujita, F., Taniguchi, Y., Kato, T., Narita, Y., Furuya, A., Ogawa, T., Sakurai, H., Joh, T., Itoh, M., Delhase, M., Karin, M. & Nakanishi, M. (2003) Identification of NAP1, a regulatory subunit of IkappaB kinase-related kinases that potentiates NF-kappaB signaling. *Mol Cell Biol.* 23 (21), 7780-93.

Funami, K., Sasai, M., Ohba, Y., Oshiumi, H., Seya, T. & Matsumoto, M. (2007) Spatiotemporal mobilization of Toll/IL-1 receptor domain-containing adaptor molecule-1 in response to dsRNA. *J Immunol.* 179 (10), 6867-72.

Funami, K., Sasai, M., Oshiumi, H., Seya, T. & Matsumoto, M. (2008) Homo-oligomerization is essential for Toll/interleukin-1 receptor domain-containing adaptor molecule-1-mediated NF-kappaB and interferon regulatory factor-3 activation. *J Biol Chem.* 283 (26), 18283-91.

Furlong, D., Swift, H. & Roizman, B. (1972) Arrangement of herpesvirus deoxyribonucleic acid in the core. *J Virol.* 10 (5), 1071-4.

Gabriel, E., Ramani, A., Karow, U., Gottardo, M., Natarajan, K., Gooi, L. M., Goranci-Buzhala, G., Krut, O., Peters, F., Nikolic, M., Kuivanen, S., Korhonen, E., Smura, T., Vapalahti, O., Papantonis, A., Schmidt-Chanasit, J., Riparbelli, M., Callaini, G., Kronke, M., Utermohlen, O. & Gopalakrishnan, J. (2017) Recent Zika Virus Isolates Induce Premature Differentiation of Neural Progenitors in Human Brain Organoids. *Cell Stem Cell.* 20 (3), 397-406 e5.

Gao, D., Ciancanelli, M. J., Zhang, P., Harschnitz, O., Bondet, V., Hasek, M., Chen, J., Mu, X., Itan, Y., Cobat, A., Sancho-Shimizu, V., Bigio, B., Lorenzo, L., Ciceri, G., McAlpine, J., Anguiano, E., Jouanguy, E., Chaussabel, D., Meyts, I., Diamond, M. S., Abel, L., Hur, S., Smith, G. A., Notarangelo, L., Duffy, D., Studer, L., Casanova, J. L. & Zhang, S. Y. (2021) TLR3 controls constitutive IFN-beta antiviral immunity in human fibroblasts and cortical neurons. *J Clin Invest.* 131 (1).

Gill, N., Deacon, P. M., Lichty, B., Mossman, K. L. & Ashkar, A. A. (2006) Induction of innate immunity against herpes simplex virus type 2 infection via local delivery of Toll-like receptor ligands correlates with beta interferon production. *J Virol.* 80 (20), 9943-50.

Giordani, N. V., Neumann, D. M., Kwiatkowski, D. L., Bhattacharjee, P. S., McAnany, P. K., Hill, J. M. & Bloom, D. C. (2008) During herpes simplex virus type 1 infection of rabbits, the ability to express the latency-associated transcript increases latent-phase transcription of lytic genes. *J Virol.* 82 (12), 6056-60.

Gitlin, L., Barchet, W., Gilfillan, S., Cella, M., Beutler, B., Flavell, R. A., Diamond, M. S. & Colonna, M. (2006) Essential role of mda-5 in type I IFN responses to polyriboinosinic:polyribocytidylic acid and encephalomyocarditis picornavirus. *Proc Natl Acad Sci U S A.* 103 (22), 8459-64.

Gkrania-Klotsas, E. & Lever, A. M. (2008) Herpes simplex I encephalitis presenting as a brain haemorrhage with normal cerebrospinal fluid analysis: a case report. *J Med Case Rep.* 2, 387.

Gnann, J. W., Jr., Barton, N. H. & Whitley, R. J. (1983) Acyclovir: mechanism of action, pharmacokinetics, safety and clinical applications. *Pharmacotherapy.* 3 (5), 275-83.

Gnann, J. W., Jr. & Whitley, R. J. (2017) Herpes Simplex Encephalitis: an Update. *Curr Infect Dis Rep.* 19 (3), 13.

Goldsmith, K., Chen, W., Johnson, D. C. & Hendricks, R. L. (1998) Infected cell protein (ICP)47 enhances herpes simplex virus neurovirulence by blocking the CD8+ T cell response. *J Exp Med.* 187 (3), 341-8.

Gomez-Virgilio, L., Silva-Lucero, M. D., Flores-Morelos, D. S., Gallardo-Nieto, J., Lopez-Toledo, G., Abarca-Fernandez, A. M., Zacapala-Gomez, A. E., Luna-Munoz, J., Montiel-Sosa, F., Soto-Rojas, L. O., Pacheco-Herrero, M. & Cardenas-Aguayo, M. D. (2022) Autophagy: A Key Regulator of Homeostasis and Disease: An Overview of Molecular Mechanisms and Modulators. *Cells.* 11 (15).

Gordon, C. J., Tchesnokov, E. P., Woolner, E., Perry, J. K., Feng, J. Y., Porter, D. P. & Gotte, M. (2020) Remdesivir is a direct-acting antiviral that inhibits RNA-dependent RNA polymerase from severe acute respiratory syndrome coronavirus 2 with high potency. *J Biol Chem.* 295 (20), 6785-6797.

Gore, A., Li, Z., Fung, H. L., Young, J. E., Agarwal, S., Antosiewicz-Bourget, J., Canto, I., Giorgetti, A., Israel, M. A., Kiskinis, E., Lee, J. H., Loh, Y. H., Manos, P. D., Montserrat, N., Panopoulos, A. D., Ruiz, S., Wilbert, M. L., Yu, J., Kirkness, E. F., Izpisua Belmonte, J. C., Rossi, D. J., Thomson, J. A., Eggan, K., Daley, G. Q., Goldstein, L. S. & Zhang, K. (2011) Somatic coding mutations in human induced pluripotent stem cells. *Nature.* 471 (7336), 63-7.

Goyal, T. & Ali, I. (2020) Recurrent Herpes Simplex Virus 2 Lymphocytic Meningitis in Patient with IgG Subclass 2 Deficiency. *Emerg Infect Dis.* 26 (4), 748-750.

Grasselli, G., Pesenti, A. & Cecconi, M. (2020) Critical Care Utilization for the COVID-19 Outbreak in Lombardy, Italy: Early Experience and Forecast During an Emergency Response. *JAMA.* 323 (16), 1545-1546.

Grinney, M. & Mohseni, M. M. (2022) Recurrent benign lymphocytic (Mollaret's) meningitis due to herpes simplex virus type 2. *Proc (Bayl Univ Med Cent).* 35 (6), 820-821.

Guan, H., Shen, A., Lv, X., Yang, X., Ren, H., Zhao, Y., Zhang, Y., Gong, Y., Ni, P., Wu, H., Zhu, Y. & Cui, L. (2016) Detection of virus in CSF from the cases with meningoencephalitis by next-generation sequencing. *J Neurovirol.* 22 (2), 240-5.

Guo, Y., Audry, M., Ciancanelli, M., Alsina, L., Azevedo, J., Herman, M., Anguiano, E., Sancho-Shimizu, V., Lorenzo, L., Pauwels, E., Philippe, P. B., Perez de Diego, R., Cardon, A., Vogt, G., Picard, C., Andrianirina, Z. Z., Rozenberg, F., Lebon, P., Plancoulaine, S., Tardieu, M., Valerie, D., Jouanguy, E., Chaussabel, D., Geissmann, F., Abel, L., Casanova, J. L. & Zhang, S. Y. (2011) Herpes simplex virus encephalitis in a patient with complete TLR3 deficiency: TLR3 is otherwise redundant in protective immunity. *J Exp Med.* 208 (10), 2083-98.

Habel, A. H. & Brown, J. K. (1972) Dexamethasone in herpes-simplex encephalitis. *Lancet.* 1 (7752), 695.

Hacker, H., Redecke, V., Blagoev, B., Kratchmarova, I., Hsu, L. C., Wang, G. G., Kamps, M. P., Raz, E., Wagner, H., Hacker, G., Mann, M. & Karin, M. (2006) Specificity in Toll-like receptor signalling through distinct effector functions of TRAF3 and TRAF6. *Nature.* 439 (7073), 204-7.

Hait, A. S., Olagnier, D., Sancho-Shimizu, V., Skipper, K. A., Helleberg, M., Larsen, S. M., Bodda, C., Moldovan, L. I., Ren, F., Brinck Andersen, N. S., Thomsen, M. M., Freytag, M. R., Darmalinggam, S., Parkes, I., Kadekar, D. D., Rahbek, S. H., van der Horst, D., Kristensen, L. S., Eriksson, K., Kjems, J., Mostowy, S., Christiansen, M., Mikkelsen, J. G., Brandt, C. T., Paludan, S. R. & Mogensen, T. H. (2020) Defects in LC3B2 and ATG4A underlie HSV2 meningitis and reveal a critical role for autophagy in antiviral defense in humans. *Sci Immunol.* 5 (54).

Han, K. J., Su, X., Xu, L. G., Bin, L. H., Zhang, J. & Shu, H. B. (2004) Mechanisms of the TRIF-induced interferon-stimulated response element and NF-kappaB activation and apoptosis pathways. *J Biol Chem.* 279 (15), 15652-61.

Han, K. J., Yang, Y., Xu, L. G. & Shu, H. B. (2010) Analysis of a TIR-less splice variant of TRIF reveals an unexpected mechanism of TLR3-mediated signaling. *J Biol Chem.* 285 (17), 12543-50.

Hao, M., Cao, Z., Wang, Z., Xin, J., Kong, B., Xu, J., Zhang, L. & Chen, P. (2022) Patient-Derived Organoid Model in the Prediction of Chemotherapeutic Drug Response in Colorectal Cancer. *ACS Biomater Sci Eng.* 8 (8), 3515-3525.

Hartenian, E., Nandakumar, D., Lari, A., Ly, M., Tucker, J. M. & Glaunsinger, B. A. (2020) The molecular virology of coronaviruses. *J Biol Chem.* 295 (37), 12910-12934.

Hatzipetros, T., Bogdanik, L. P., Tassinari, V. R., Kidd, J. D., Moreno, A. J., Davis, C., Osborne, M., Austin, A., Vieira, F. G., Lutz, C. & Perrin, S. (2014) C57BL/6J congenic Prp-TDP43A315T mice develop progressive neurodegeneration in the myenteric plexus of the colon without exhibiting key features of ALS. *Brain Res.* 1584, 59-72.

Herbst-Kralovetz, M. M. & Pyles, R. B. (2006) Quantification of poly(I:C)-mediated protection against genital herpes simplex virus type 2 infection. *J Virol.* 80 (20), 9988-97.

Herman, M., Ciancanelli, M., Ou, Y. H., Lorenzo, L., Klaudel-Dreszler, M., Pauwels, E., Sancho-Shimizu, V., Perez de Diego, R., Abhyankar, A., Israelsson, E., Guo, Y., Cardon, A., Rozenberg, F., Lebon, P., Tardieu, M., Heropolitanska-Pliszka, E., Chaussabel, D., White, M. A., Abel, L., Zhang, S. Y. & Casanova, J. L. (2012) Heterozygous TBK1 mutations impair TLR3 immunity and underlie herpes simplex encephalitis of childhood. *J Exp Med.* 209 (9), 1567-82.

Hernandez, N., Melki, I., Jing, H., Habib, T., Huang, S. S. Y., Danielson, J., Kula, T., Drutman, S., Belkaya, S., Rattina, V., Lorenzo-Diaz, L., Boulai, A., Rose, Y., Kitabayashi, N., Rodero, M. P., Dumaine, C., Blanche, S., Lebras, M. N., Leung, M. C., Mathew, L. S., Boisson, B., Zhang, S. Y., Boisson-Dupuis, S., Giliani, S., Chaussabel, D., Notarangelo, L. D., Elledge, S. J., Ciancanelli, M. J., Abel, L., Zhang, Q., Marr, N., Crow, Y. J., Su, H. C. & Casanova, J. L. (2018) Life-threatening influenza pneumonitis in a child with inherited IRF9 deficiency. *J Exp Med.* 215 (10), 2567-2585.

Herold, B. C., WuDunn, D., Soltys, N. & Spear, P. G. (1991) Glycoprotein C of herpes simplex virus type 1 plays a principal role in the adsorption of virus to cells and in infectivity. *J Virol.* 65 (3), 1090-8.

Hillen, H. S. (2021) Structure and function of SARS-CoV-2 polymerase. *Curr Opin Virol.* 48, 82-90.

Hocke, A. C., Becher, A., Knepper, J., Peter, A., Holland, G., Tonnies, M., Bauer, T. T., Schneider, P., Neudecker, J., Muth, D., Wendtner, C. M., Ruckert, J. C., Drosten, C., Gruber, A. D., Laue, M., Suttorp, N., Hippenstiel, S. & Wolff, T. (2013) Emerging human middle East respiratory syndrome coronavirus causes widespread infection and alveolar damage in human lungs. *Am J Respir Crit Care Med.* 188 (7), 882-6.

Hoebe, K., Du, X., Georgel, P., Janssen, E., Tabeta, K., Kim, S. O., Goode, J., Lin, P., Mann, N., Mudd, S., Crozat, K., Sovath, S., Han, J. & Beutler, B. (2003) Identification of Lps2 as a key transducer of MyD88-independent TIR signalling. *Nature.* 424 (6950), 743-8.

Hoefflin, S. & Carter, D. A. (2014) Neuronal expression of SOX2 is enriched in specific hypothalamic cell groups. *J Chem Neuroanat.* 61-62, 153-60.

Hoffmann, M., Kleine-Weber, H., Schroeder, S., Kruger, N., Herrler, T., Erichsen, S., Schiergens, T. S., Herrler, G., Wu, N. H., Nitsche, A., Muller, M. A., Drosten, C. & Pohlmann, S. (2020) SARS-CoV-2 Cell Entry Depends on ACE2 and TMPRSS2 and Is Blocked by a Clinically Proven Protease Inhibitor. *Cell.* 181 (2), 271-280 e8.

Horng, T., Barton, G. M. & Medzhitov, R. (2001) TIRAP: an adapter molecule in the Toll signaling pathway. *Nat Immunol.* 2 (9), 835-41.

Huerfano, S., Ryabchenko, B. & Forstova, J. (2013) Nucleofection of expression vectors induces a robust interferon response and inhibition of cell proliferation. *DNA Cell Biol.* 32 (8), 467-79.

Huff, V., Cai, W., Glorioso, J. C. & Levine, M. (1988) The carboxy-terminal 41 amino acids of herpes simplex virus type 1 glycoprotein B are not essential for production of infectious virus particles. *J Virol.* 62 (11), 4403-6.

IHME, I. o. H. M. a. E. (2019) *Global Burden of Disease (GBD).* https://www.healthdata.org/research-analysis/gbd.

Inomata, M., Niida, S., Shibata, K. & Into, T. (2012) Regulation of Toll-like receptor signaling by NDP52-mediated selective autophagy is normally inactivated by A20. *Cell Mol Life Sci.* 69 (6), 963-79.

Israel, L., Wang, Y., Bulek, K., Della Mina, E., Zhang, Z., Pedergnana, V., Chrabieh, M., Lemmens, N. A., Sancho-Shimizu, V., Descatoire, M., Lasseau, T., Israelsson, E., Lorenzo, L., Yun, L., Belkadi, A., Moran, A., Weisman, L. E., Vandenesch, F., Batteux, F., Weller, S., Levin, M., Herberg, J., Abhyankar, A., Prando, C., Itan, Y., van Wamel, W. J. B., Picard, C., Abel, L., Chaussabel, D., Li, X., Beutler, B., Arkwright, P. D., Casanova, J. L. & Puel, A. (2017) Human Adaptive Immunity Rescues an Inborn Error of Innate Immunity. *Cell.* 168 (5), 789-800 e10.

Iwasaki, A. (2010) Antiviral immune responses in the genital tract: clues for vaccines. *Nat Rev Immunol.* 10 (10), 699-711.

Jack, C. S., Arbour, N., Manusow, J., Montgrain, V., Blain, M., McCrea, E., Shapiro, A. & Antel, J. P. (2005) TLR signaling tailors innate immune responses in human microglia and astrocytes. *J Immunol.* 175 (7), 4320-30.

Jacobs, B. L. & Langland, J. O. (1996) When two strands are better than one: the mediators and modulators of the cellular responses to double-stranded RNA. *Virology.* 219 (2), 339-49.

Janeway, C. A., Jr. (1989) Approaching the asymptote? Evolution and revolution in immunology. *Cold Spring Harb Symp Quant Biol.* 54 Pt 1, 1-13.

Jennische, E., Eriksson, C. E., Lange, S., Trybala, E. & Bergstrom, T. (2015) The anterior commissure is a pathway for contralateral spread of herpes simplex virus type 1 after olfactory tract infection. *J Neurovirol.* 21 (2), 129-47.

Ji, J., Ng, S. H., Sharma, V., Neculai, D., Hussein, S., Sam, M., Trinh, Q., Church, G. M., McPherson, J. D., Nagy, A. & Batada, N. N. (2012) Elevated coding mutation rate during the reprogramming of human somatic cells into induced pluripotent stem cells. *Stem Cells.* 30 (3), 435-40.

Jiang, Z., Mak, T. W., Sen, G. & Li, X. (2004) Toll-like receptor 3-mediated activation of NF-kappaB and IRF3 diverges at Toll-IL-1 receptor domain-containing adapter inducing IFN-beta. *Proc Natl Acad Sci U S A.* 101 (10), 3533-8.

Jiang, Z., Zamanian-Daryoush, M., Nie, H., Silva, A. M., Williams, B. R. & Li, X. (2003) Poly(I-C)-induced Toll-like receptor 3 (TLR3)-mediated activation of NFkappa B and MAP kinase is through an interleukin-1 receptor-associated kinase (IRAK)-independent pathway employing the signaling components TLR3-TRAF6-TAK1-TAB2-PKR. *J Biol Chem.* 278 (19), 16713-9.

Johnsen, I. B., Nguyen, T. T., Ringdal, M., Tryggestad, A. M., Bakke, O., Lien, E., Espevik, T. & Anthonsen, M. W. (2006) Toll-like receptor 3 associates with c-Src tyrosine kinase on endosomes to initiate antiviral signaling. *EMBO J.* 25 (14), 3335-46.

Jones, C. A. (2009) Vertical transmission of genital herpes: prevention and treatment options. *Drugs.* 69 (4), 421-34.

Juillard, F., De Leon Vazquez, E., Tan, M., Li, S. & Kaye, K. M. (2019) Kaposi's Sarcoma-Associated Herpesvirus LANA-Adjacent Regions with Distinct Functions in Episome Segregation or Maintenance. *J Virol.* 93 (6).

Justice, M. J. & Dhillon, P. (2016) Using the mouse to model human disease: increasing validity and reproducibility. *Dis Model Mech.* 9 (2), 101-3.

Kabeya, Y., Mizushima, N., Ueno, T., Yamamoto, A., Kirisako, T., Noda, T., Kominami, E., Ohsumi, Y. & Yoshimori, T. (2000) LC3, a mammalian homologue of yeast Apg8p, is localized in autophagosome membranes after processing. *EMBO J.* 19 (21), 5720-8.

Kaiser, W. J. & Offermann, M. K. (2005) Apoptosis induced by the toll-like receptor adaptor TRIF is dependent on its receptor interacting protein homotypic interaction motif. *J Immunol.* 174 (8), 4942-52.

Kallio-Laine, K., Seppanen, M., Kautiainen, H., Lokki, M. L., Lappalainen, M., Valtonen, V., Farkkila, M. & Kalso, E. (2009) Recurrent lymphocytic meningitis positive for herpes simplex virus type 2. *Emerg Infect Dis.* 15 (7), 1119-22.

Kamei, S., Sekizawa, T., Shiota, H., Mizutani, T., Itoyama, Y., Takasu, T., Morishima, T. & Hirayanagi, K. (2005) Evaluation of combination therapy using aciclovir and corticosteroid in adult patients with herpes simplex virus encephalitis. *J Neurol Neurosurg Psychiatry.* 76 (11), 1544-9.

Kamei, S., Taira, N., Ishihara, M., Sekizawa, T., Morita, A., Miki, K., Shiota, H., Kanno, A., Suzuki, Y., Mizutani, T., Itoyama, Y., Morishima, T. & Hirayanagi, K. (2009) Prognostic value of cerebrospinal fluid cytokine changes in herpes simplex virus encephalitis. *Cytokine.* 46 (2), 187-93.

Kastrukoff, L. F., Lau, A. S. & Thomas, E. E. (2012) The effect of mouse strain on herpes simplex virus type 1 (HSV-1) infection of the central nervous system (CNS). *Herpesviridae.* 3, 4.

Kato, H., Takeuchi, O., Mikamo-Satoh, E., Hirai, R., Kawai, T., Matsushita, K., Hiiragi, A., Dermody, T. S., Fujita, T. & Akira, S. (2008) Length-dependent recognition of double-stranded ribonucleic acids by retinoic acid-inducible gene-I and melanoma differentiation-associated gene 5. *J Exp Med.* 205 (7), 1601-10.

Katsetos, C. D., Frankfurter, A., Christakos, S., Mancall, E. L., Vlachos, I. N. & Urich, H. (1993) Differential localization of class III, beta-tubulin isotype and calbindin-D28k defines distinct neuronal types in the developing human cerebellar cortex. *J Neuropathol Exp Neurol.* 52 (6), 655-66.

Katsetos, C. D., Herman, M. M. & Mork, S. J. (2003) Class III beta-tubulin in human development and cancer. *Cell Motil Cytoskeleton.* 55 (2), 77-96.

Kawai, T. & Akira, S. (2008) Toll-like receptor and RIG-I-like receptor signaling. *Ann N Y Acad Sci.* 1143, 1-20.

Kawai, T. & Akira, S. (2010) The role of pattern-recognition receptors in innate immunity: update on Toll-like receptors. *Nat Immunol.* 11 (5), 373-84.

Kawasaki, T. & Kawai, T. (2014) Toll-like receptor signaling pathways. *Front Immunol.* 5, 461.

Kenji Ohgane, H. Y. (2019) *Quantification of Gel Bands by an Image J Macro, Band/Peak Quantification Tool.* https://www.protocols.io/view/quantification-of-gel-bands-by-an-image-j-macro-ba-bp2l6n4bkgqe/v1.

Kennedy, P. G. & Steiner, I. (2013) Recent issues in herpes simplex encephalitis. *J Neurovirol.* 19 (4), 346-50.

Kesson, A. M. (2001) Management of neonatal herpes simplex virus infection. *Paediatr Drugs.* 3 (2), 81-90.

Key, F. M., Teixeira, J. C., de Filippo, C. & Andres, A. M. (2014) Advantageous diversity maintained by balancing selection in humans. *Curr Opin Genet Dev.* 29, 45-51.

Khandaker, G., Jung, J., Britton, P. N., King, C., Yin, J. K. & Jones, C. A. (2016) Long-term outcomes of infective encephalitis in children: a systematic review and meta-analysis. *Dev Med Child Neurol.* 58 (11), 1108-1115.

Kim, Y. M., Brinkmann, M. M., Paquet, M. E. & Ploegh, H. L. (2008) UNC93B1 delivers nucleotide-sensing toll-like receptors to endolysosomes. *Nature.* 452 (7184), 234-8.

King, W., Thomas-Powell, A. L., Raab-Traub, N., Hawke, M. & Kieff, E. (1980) Epstein-Barr virus RNA. V. Viral RNA in a restringently infected, growth-transformed cell line. *J Virol.* 36 (2), 506-18.

Kirkland, Z., Jeffery, R. E., Conte, J., George, J. & Mercado, R. (2020) Recurrent Aseptic Meningitis From Herpes Simplex Virus-2: Mollaret's Meningitis in a 30-Year-Old Female. *Cureus.* 12 (11), e11623.

Kleine-Weber, H., Elzayat, M. T., Hoffmann, M. & Pohlmann, S. (2018) Functional analysis of potential cleavage sites in the MERS-coronavirus spike protein. *Sci Rep.* 8 (1), 16597.

Klionsky, D. J. & Ohsumi, Y. (1999) Vacuolar import of proteins and organelles from the cytoplasm. *Annu Rev Cell Dev Biol.* 15, 1-32.

Knipe, D., Howley, P., Griffin, D., Lamb, R., Martin, M., Roizman, B. & Straus, S. (2013) *Fields Virology, Volumes 1 and 2.* Lippincott Williams & Wilkins: Philadelphia, PA, USA.

Knotts, F. B., Cook, M. L. & Stevens, J. G. (1973) Latent herpes simplex virus in the central nervous system of rabbits and mice. *J Exp Med.* 138 (3), 740-4.

Krenn, V., Bosone, C., Burkard, T. R., Spanier, J., Kalinke, U., Calistri, A., Salata, C., Rilo Christoff, R., Pestana Garcez, P., Mirazimi, A. & Knoblich, J. A. (2021) Organoid modeling of Zika and herpes simplex virus 1 infections reveals virus-specific responses leading to microcephaly. *Cell Stem Cell.* 28 (8), 1362-1379 e7.

Krug, A., Luker, G. D., Barchet, W., Leib, D. A., Akira, S. & Colonna, M. (2004) Herpes simplex virus type 1 activates murine natural interferon-producing cells through toll-like receptor 9. *Blood.* 103 (4), 1433-7.

Kumar, A., Haque, J., Lacoste, J., Hiscott, J. & Williams, B. R. (1994) Double-stranded RNA-dependent protein kinase activates transcription factor NF-kappa B by phosphorylating I kappa B. *Proc Natl Acad Sci U S A.* 91 (14), 6288-92.

Kumeta, H., Sakakibara, H., Enokizono, Y., Ogura, K., Horiuchi, M., Matsumoto, M., Seya, T. & Inagaki, F. (2014) The N-terminal domain of TIR domain-containing adaptor molecule-1, TICAM-1. *J Biomol NMR.* 58 (3), 227-30.

Kuo, C. Y., Ku, C. L., Lim, H. K., Hsia, S. H., Lin, J. J., Lo, C. C., Ding, J. Y., Kuo, R. L., Casanova, J. L., Zhang, S. Y., Chang, L. Y. & Lin, T. Y. (2022) Life-Threatening Enterovirus 71 Encephalitis in Unrelated Children with Autosomal Dominant TLR3 Deficiency. *J Clin Immunol.* 42 (3), 606-617.

Kurt-Jones, E. A., Orzalli, M. H. & Knipe, D. M. (2017) Innate immune mechanisms and herpes simplex virus infection and disease. *Cell Biology of Herpes Viruses.* 49-75.

Lafaille, F. G., Harschnitz, O., Lee, Y. S., Zhang, P., Hasek, M. L., Kerner, G., Itan, Y., Ewaleifoh, O., Rapaport, F., Carlile, T. M., Carter-Timofte, M. E., Paquet, D., Dobbs, K., Zimmer, B., Gao, D., Rojas-Duran, M. F., Kwart, D., Rattina, V., Ciancanelli, M. J., McAlpine, J. L., Lorenzo, L., Boucherit, S., Rozenberg, F., Halwani, R., Henry, B., Amenzoui, N., Alsum, Z., Marques, L., Church, J. A., Al-Muhsen, S., Tardieu, M., Bousfiha, A. A., Paludan, S. R., Mogensen, T. H., Quintana-Murci, L., Tessier-Lavigne, M., Smith, G. A., Notarangelo, L. D., Studer, L., Gilbert, W., Abel, L., Casanova, J. L. & Zhang, S. Y. (2019) Human SNORA31 variations impair cortical neuron-intrinsic immunity to HSV-1 and underlie herpes simplex encephalitis. *Nat Med.* 25 (12), 1873-1884.

Lafaille, F. G., Pessach, I. M., Zhang, S. Y., Ciancanelli, M. J., Herman, M., Abhyankar, A., Ying, S. W., Keros, S., Goldstein, P. A., Mostoslavsky, G., Ordovas-Montanes, J., Jouanguy, E., Plancoulaine, S., Tu, E., Elkabetz, Y., Al-Muhsen, S., Tardieu, M., Schlaeger, T. M., Daley, G. Q., Abel, L., Casanova, J. L., Studer, L. & Notarangelo, L. D. (2012) Impaired intrinsic immunity to HSV-1 in human iPSC-derived TLR3-deficient CNS cells. *Nature.* 491 (7426), 769-73.

Lafferty, W. E., Coombs, R. W., Benedetti, J., Critchlow, C. & Corey, L. (1987) Recurrences after oral and genital herpes simplex virus infection. Influence of site of infection and viral type. *N Engl J Med.* 316 (23), 1444-9.

Lamers, M. M. & Haagmans, B. L. (2022) SARS-CoV-2 pathogenesis. *Nat Rev Microbiol.* 20 (5), 270-284.

Lancaster, M. A., Corsini, N. S., Wolfinger, S., Gustafson, E. H., Phillips, A. W., Burkard, T. R., Otani, T., Livesey, F. J. & Knoblich, J. A. (2017) Guided self-organization and cortical plate formation in human brain organoids. *Nat Biotechnol.* 35 (7), 659-666.

Lancaster, M. A. & Knoblich, J. A. (2014) Generation of cerebral organoids from human pluripotent stem cells. *Nat Protoc.* 9 (10), 2329-40.

Lancaster, M. A., Renner, M., Martin, C. A., Wenzel, D., Bicknell, L. S., Hurles, M. E., Homfray, T., Penninger, J. M., Jackson, A. P. & Knoblich, J. A. (2013) Cerebral organoids model human brain development and microcephaly. *Nature.* 501 (7467), 373-9.

Lebre, M. C., van der Aar, A. M., van Baarsen, L., van Capel, T. M., Schuitemaker, J. H., Kapsenberg, M. L. & de Jong, E. C. (2007) Human keratinocytes express functional Toll-like receptor 3, 4, 5, and 9. *J Invest Dermatol.* 127 (2), 331-41.

Lederberg, J. (1999) J. B. S. Haldane (1949) on infectious disease and evolution. *Genetics.* 153 (1), 1-3.

Lee, M. K., Tuttle, J. B., Rebhun, L. I., Cleveland, D. W. & Frankfurter, A. (1990) The expression and posttranslational modification of a neuron-specific beta-tubulin isotype during chick embryogenesis. *Cell Motil Cytoskeleton.* 17 (2), 118-32.

Lei, C., Yang, J., Hu, J. & Sun, X. (2021) On the Calculation of TCID(50) for Quantitation of Virus Infectivity. *Virol Sin.* 36 (1), 141-144.

Lendahl, U., Zimmerman, L. B. & McKay, R. D. (1990) CNS stem cells express a new class of intermediate filament protein. *Cell.* 60 (4), 585-95.

Leoni, V., Gianni, T., Salvioli, S. & Campadelli-Fiume, G. (2012) Herpes simplex virus glycoproteins gH/gL and gB bind Toll-like receptor 2, and soluble gH/gL is sufficient to activate NF-kappaB. *J Virol.* 86 (12), 6555-62.

Li, T., Diner, B. A., Chen, J. & Cristea, I. M. (2012) Acetylation modulates cellular distribution and DNA sensing ability of interferon-inducible protein IFI16. *Proc Natl Acad Sci U S A.* 109 (26), 10558-63.

Liang, F., Glans, H., Enoksson, S. L., Kolios, A. G. A., Lore, K. & Nilsson, J. (2020) Recurrent Herpes Zoster Ophthalmicus in a Patient With a Novel Toll-Like Receptor 3 Variant Linked to Compromised Activation Capacity in Fibroblasts. *J Infect Dis.* 221 (8), 1295-1303.

Liang, Q., Seo, G. J., Choi, Y. J., Kwak, M. J., Ge, J., Rodgers, M. A., Shi, M., Leslie, B. J., Hopfner, K. P., Ha, T., Oh, B. H. & Jung, J. U. (2014) Crosstalk between the cGAS DNA sensor and Beclin-1 autophagy protein shapes innate antimicrobial immune responses. *Cell Host Microbe.* 15 (2), 228-38.

Ligas, M. W. & Johnson, D. C. (1988) A herpes simplex virus mutant in which glycoprotein D sequences are replaced by beta-galactosidase sequences binds to but is unable to penetrate into cells. *J Virol.* 62 (5), 1486-94.

Lim, H. K., Huang, S. X. L., Chen, J., Kerner, G., Gilliaux, O., Bastard, P., Dobbs, K., Hernandez, N., Goudin, N., Hasek, M. L., Garcia Reino, E. J., Lafaille, F. G., Lorenzo, L., Luthra, P., Kochetkov, T., Bigio, B., Boucherit, S., Rozenberg, F., Vedrinne, C., Keller, M. D., Itan, Y., Garcia-Sastre, A., Celard, M., Orange, J. S., Ciancanelli, M. J., Meyts, I., Zhang, Q., Abel, L., Notarangelo, L. D., Snoeck, H. W., Casanova, J. L. & Zhang, S. Y. (2019) Severe influenza pneumonitis in children with inherited TLR3 deficiency. *J Exp Med.* 216 (9), 2038-2056.

Lim, H. K., Seppanen, M., Hautala, T., Ciancanelli, M. J., Itan, Y., Lafaille, F. G., Dell, W., Lorenzo, L., Byun, M., Pauwels, E., Ronnelid, Y., Cai, X., Boucherit, S., Jouanguy, E., Paetau, A., Lebon, P., Rozenberg, F., Tardieu, M., Abel, L., Yildiran, A., Vergison, A., Roivainen, R., Etzioni, A., Tienari, P. J., Casanova, J. L. & Zhang, S. Y. (2014) TLR3 deficiency in herpes simplex encephalitis: high allelic heterogeneity and recurrence risk. *Neurology.* 83 (21), 1888-97.

Lin, S. C., Lo, Y. C. & Wu, H. (2010) Helical assembly in the MyD88-IRAK4-IRAK2 complex in TLR/IL-1R signalling. *Nature.* 465 (7300), 885-90.

Liu, D., Wu, H., Wang, C., Li, Y., Tian, H., Siraj, S., Sehgal, S. A., Wang, X., Wang, J., Shang, Y., Jiang, Z., Liu, L. & Chen, Q. (2019) STING directly activates autophagy to tune the innate immune response. *Cell Death Differ.* 26 (9), 1735-1749.

Liu, D. X., Liang, J. Q. & Fung, T. S. (2021) Human coronavirus-229E,-OC43,-NL63, and-HKU1 (Coronaviridae). *Encyclopedia of virology.* 428.

Liu, S., Cai, X., Wu, J., Cong, Q., Chen, X., Li, T., Du, F., Ren, J., Wu, Y. T., Grishin, N. V. & Chen, Z. J. (2015) Phosphorylation of innate immune adaptor proteins MAVS, STING, and TRIF induces IRF3 activation. *Science.* 347 (6227), aaa2630.

Liu, X., Taylor, A., Poo, Y. S., Ng, W. H., Herrero, L. J., Tang, P. C. H., Zaid, A. & Mahalingam, S. (2022) TIR-Domain-Containing Adapter-Inducing Interferon-beta (TRIF)-Dependent Antiviral Responses Protect Mice against Ross River Virus Disease. *mBio.* 13 (1), e0336321.

Lizarraga, K. J., Alexandre, L. C., Ramos-Estebanez, C. & Merenda, A. (2013) Are steroids a beneficial adjunctive therapy in the immunosuppressed patient with herpes simplex virus encephalitis? *Case Rep Neurol.* 5 (1), 52-5.

Looker, K. J., Elmes, J. A. R., Gottlieb, S. L., Schiffer, J. T., Vickerman, P., Turner, K. M. E. & Boily, M. C. (2017) Effect of HSV-2 infection on subsequent HIV acquisition: an updated systematic review and meta-analysis. *Lancet Infect Dis.* 17 (12), 1303-1316.

Loser, P., Schirm, J., Guhr, A., Wobus, A. M. & Kurtz, A. (2010) Human embryonic stem cell lines and their use in international research. *Stem Cells.* 28 (2), 240-6.

Lukassen, S., Chua, R. L., Trefzer, T., Kahn, N. C., Schneider, M. A., Muley, T., Winter, H., Meister, M., Veith, C., Boots, A. W., Hennig, B. P., Kreuter, M., Conrad, C. & Eils, R. (2020) SARS-CoV-2 receptor ACE2 and TMPRSS2 are primarily expressed in bronchial transient secretory cells. *EMBO J.* 39 (10), e105114.

Mansour, A. A., Goncalves, J. T., Bloyd, C. W., Li, H., Fernandes, S., Quang, D., Johnston, S., Parylak, S. L., Jin, X. & Gage, F. H. (2018) An in vivo model of functional and vascularized human brain organoids. *Nat Biotechnol.* 36 (5), 432-441.

Marcocci, M. E., Napoletani, G., Protto, V., Kolesova, O., Piacentini, R., Li Puma, D. D., Lomonte, P., Grassi, C., Palamara, A. T. & De Chiara, G. (2020) Herpes Simplex Virus-1 in the Brain: The Dark Side of a Sneaky Infection. *Trends Microbiol.* 28 (10), 808-820.

Marei, H. E., Althani, A., Lashen, S., Cenciarelli, C. & Hasan, A. (2017) Genetically unmatched human iPSC and ESC exhibit equivalent gene expression and neuronal differentiation potential. *Sci Rep.* 7 (1), 17504.

Martinez-Salas, E., Francisco-Velilla, R., Fernandez-Chamorro, J. & Embarek, A. M. (2017) Insights into Structural and Mechanistic Features of Viral IRES Elements. *Front Microbiol.* 8, 2629.

Matsumoto, M., Kikkawa, S., Kohase, M., Miyake, K. & Seya, T. (2002) Establishment of a monoclonal antibody against human Toll-like receptor 3 that blocks double-stranded RNA-mediated signaling. *Biochem Biophys Res Commun.* 293 (5), 1364-9.

McGill, F., Griffiths, M. J., Bonnett, L. J., Geretti, A. M., Michael, B. D., Beeching, N. J., McKee, D., Scarlett, P., Hart, I. J., Mutton, K. J., Jung, A., Adan, G., Gummery, A., Sulaiman, W. A. W., Ennis, K., Martin, A. P., Haycox, A., Miller, A., Solomon, T. & Investigators, U. K. M. S. (2018) Incidence, aetiology, and sequelae of viral meningitis in UK adults: a multicentre prospective observational cohort study. *Lancet Infect Dis.* 18 (9), 992-1003.

McGrath, N., Anderson, N. E., Croxson, M. C. & Powell, K. F. (1997) Herpes simplex encephalitis treated with acyclovir: diagnosis and long term outcome. *J Neurol Neurosurg Psychiatry.* 63 (3), 321-6.

Medzhitov, R. (2013) Pattern recognition theory and the launch of modern innate immunity. *J Immunol.* 191 (9), 4473-4.

Medzhitov, R. & Janeway, C. A., Jr. (1998) Innate immune recognition and control of adaptive immune responses. *Semin Immunol.* 10 (5), 351-3.

Melchjorsen, J., Rintahaka, J., Soby, S., Horan, K. A., Poltajainen, A., Ostergaard, L., Paludan, S. R. & Matikainen, S. (2010) Early innate recognition of herpes simplex virus in human primary macrophages is mediated via the MDA5/MAVS-dependent and MDA5/MAVS/RNA polymerase III-independent pathways. *J Virol.* 84 (21), 11350-8.

Menasria, R., Boivin, N., Lebel, M., Piret, J., Gosselin, J. & Boivin, G. (2013) Both TRIF and IPS-1 adaptor proteins contribute to the cerebral innate immune response against herpes simplex virus 1 infection. *J Virol.* 87 (13), 7301-8.

Mendez, A. A., Bosco, A., Abdel-Wahed, L., Palmer, K., Jones, K. A. & Killoran, A. (2018) A Fatal Case of Herpes Simplex Encephalitis with Two False-Negative Polymerase Chain Reactions. *Case Rep Neurol.* 10 (2), 217-222.

Mercurio, S., Serra, L., Motta, A., Gesuita, L., Sanchez-Arrones, L., Inverardi, F., Foglio, B., Barone, C., Kaimakis, P., Martynoga, B., Ottolenghi, S., Studer, M., Guillemot, F., Frassoni, C., Bovolenta, P. & Nicolis, S. K. (2019a) Sox2 Acts in Thalamic Neurons to Control the Development of Retina-Thalamus-Cortex Connectivity. *iScience.* 15, 257-273.

Mercurio, S., Serra, L. & Nicolis, S. K. (2019b) More than just Stem Cells: Functional Roles of the Transcription Factor Sox2 in Differentiated Glia and Neurons. *Int J Mol Sci.* 20 (18).

Meurs, E., Chong, K., Galabru, J., Thomas, N. S., Kerr, I. M., Williams, B. R. & Hovanessian, A. G. (1990) Molecular cloning and characterization of the human double-stranded RNA-activated protein kinase induced by interferon. *Cell.* 62 (2), 379-90.

Meyding-Lamade, U., Seyfer, S., Haas, J., Dvorak, F., Kehm, R., Lamade, W., Hacke, W. & Wildemann, B. (2002) Experimental herpes simplex virus encephalitis: inhibition of the expression of inducible nitric oxide synthase in mouse brain tissue. *Neurosci Lett.* 318 (1), 21-4.

Meyding-Lamade, U. K., Lamade, W. R., Wildemann, B. T., Sartor, K. & Hacke, W. (1999) Herpes simplex virus encephalitis: chronic progressive cerebral magnetic resonance imaging abnormalities in patients despite good clinical recovery. *Clin Infect Dis.* 28 (1), 148-9.

Meyding-Lamade, U. K., Oberlinner, C., Rau, P. R., Seyfer, S., Heiland, S., Sellner, J., Wildemann, B. T. & Lamade, W. R. (2003) Experimental herpes simplex virus encephalitis: a combination therapy of acyclovir and glucocorticoids reduces long-term magnetic resonance imaging abnormalities. *J Neurovirol.* 9 (1), 118-25.

Meylan, E., Burns, K., Hofmann, K., Blancheteau, V., Martinon, F., Kelliher, M. & Tschopp, J. (2004) RIP1 is an essential mediator of Toll-like receptor 3-induced NF-kappa B activation. *Nat Immunol.* 5 (5), 503-7.

Milek, J. & Blicharz-Domanska, K. (2018) Coronaviruses in Avian Species - Review with Focus on Epidemiology and Diagnosis in Wild Birds. *J Vet Res.* 62 (3), 249-255.

Miller, S., Mateen, F. J. & Aksamit, A. J., Jr. (2013) Herpes simplex virus 2 meningitis: a retrospective cohort study. *J Neurovirol.* 19 (2), 166-71.

Min, Z. & Baddley, J. W. (2014) Mollaret's meningitis. *Lancet Infect Dis.* 14 (10), 1022.

Miot, C., Imai, K., Imai, C., Mancini, A. J., Kucuk, Z. Y., Kawai, T., Nishikomori, R., Ito, E., Pellier, I., Dupuis Girod, S., Rosain, J., Sasaki, S., Chandrakasan, S., Pachlopnik Schmid, J., Okano, T., Colin, E., Olaya-Vargas, A., Yamazaki-Nakashimada, M., Qasim, W., Espinosa Padilla, S., Jones, A., Krol, A., Cole, N., Jolles, S., Bleesing, J., Vraetz, T., Gennery, A. R., Abinun, M., Gungor, T., Costa-Carvalho, B., Condino-Neto, A., Veys, P., Holland, S. M., Uzel, G., Moshous, D., Neven, B., Blanche, S., Ehl, S., Doffinger, R., Patel, S. Y., Puel, A., Bustamante, J., Gelfand, E. W., Casanova, J. L., Orange, J. S. & Picard, C. (2017) Hematopoietic stem cell transplantation in 29 patients hemizygous for hypomorphic IKBKG/NEMO mutations. *Blood.* 130 (12), 1456-1467.

Mirakhur, B. & McKenna, M. (2004) Recurrent herpes simplex type 2 virus (Mollaret) meningitis. *J Am Board Fam Pract.* 17 (4), 303-5.

Mollaret, P. (1945) Benign Recurrent Endo-thelio-Leucocytic Meningitis: a New Syndrome or Disease? *Ann. Inst. Pasteur.* 71 (1-2), 1-17.

Mommeja-Marin, H., Lafaurie, M., Scieux, C., Galicier, L., Oksenhendler, E. & Molina, J. M. (2003) Herpes simplex virus type 2 as a cause of severe meningitis in immunocompromised adults. *Clin Infect Dis.* 37 (11), 1527-33.

Moody, S. A., Quigg, M. S. & Frankfurter, A. (1989) Development of the peripheral trigeminal system in the chick revealed by an isotype-specific anti-beta-tubulin monoclonal antibody. *J Comp Neurol.* 279 (4), 567-80.

Morgan, C., Rose, H. M., Holden, M. & Jones, E. P. (1959) Electron microscopic observations on the development of herpes simplex virus. *J Exp Med.* 110 (4), 643-56.

Mork, N., Kofod-Olsen, E., Sorensen, K. B., Bach, E., Orntoft, T. F., Ostergaard, L., Paludan, S. R., Christiansen, M. & Mogensen, T. H. (2015) Mutations in the TLR3 signaling pathway and beyond in adult patients with herpes simplex encephalitis. *Genes Immun.* 16 (8), 552-66.

Morshead, C. M., Reynolds, B. A., Craig, C. G., McBurney, M. W., Staines, W. A., Morassutti, D., Weiss, S. & van der Kooy, D. (1994) Neural stem cells in the adult mammalian forebrain: a relatively quiescent subpopulation of subependymal cells. *Neuron.* 13 (5), 1071-82.

Murad, S. (2014) Toll-like receptor 4 in inflammation and angiogenesis: a double-edged sword. *Front Immunol.* 5, 313.

Murphy, P. M. (1993) Molecular mimicry and the generation of host defense protein diversity. *Cell.* 72 (6), 823-6.

Naqvi, A. A. T., Fatima, K., Mohammad, T., Fatima, U., Singh, I. K., Singh, A., Atif, S. M., Hariprasad, G., Hasan, G. M. & Hassan, M. I. (2020) Insights into SARS-CoV-2 genome, structure, evolution, pathogenesis and therapies: Structural genomics approach. *Biochim Biophys Acta Mol Basis Dis.* 1866 (10), 165878.

Negishi, H., Osawa, T., Ogami, K., Ouyang, X., Sakaguchi, S., Koshiba, R., Yanai, H., Seko, Y., Shitara, H., Bishop, K., Yonekawa, H., Tamura, T., Kaisho, T., Taya, C., Taniguchi, T. & Honda, K. (2008) A critical link between Toll-like receptor 3 and type II interferon signaling pathways in antiviral innate immunity. *Proc Natl Acad Sci U S A.* 105 (51), 20446-51.

Nicholson, M. W., Ting, C. Y., Chan, D. Z. H., Cheng, Y. C., Lee, Y. C., Hsu, C. C., Huang, C. Y. & Hsieh, P. C. H. (2022) Utility of iPSC-Derived Cells for Disease Modeling, Drug Development, and Cell Therapy. *Cells.* 11 (11).

Nicoll, M. P., Hann, W., Shivkumar, M., Harman, L. E., Connor, V., Coleman, H. M., Proenca, J. T. & Efstathiou, S. (2016) The HSV-1 Latency-Associated Transcript Functions to Repress Latent Phase Lytic Gene Expression and Suppress Virus Reactivation from Latently Infected Neurons. *PLoS Pathog.* 12 (4), e1005539.

Nie, L., Cai, S. Y., Shao, J. Z. & Chen, J. (2018) Toll-Like Receptors, Associated Biological Roles, and Signaling Networks in Non-Mammals. *Front Immunol.* 9, 1523.

Nikoletopoulou, V., Papandreou, M. E. & Tavernarakis, N. (2015) Autophagy in the physiology and pathology of the central nervous system. *Cell Death Differ.* 22 (3), 398-407.

Noska, A., Kyrillos, R., Hansen, G., Hirigoyen, D. & Williams, D. N. (2015) The role of antiviral therapy in immunocompromised patients with herpes simplex virus meningitis. *Clin Infect Dis.* 60 (2), 237-42.

Notarangelo, L. D., Bacchetta, R., Casanova, J. L. & Su, H. C. (2020) Human inborn errors of immunity: An expanding universe. *Sci Immunol.* 5 (49).

O'Driscoll, M., Ribeiro Dos Santos, G., Wang, L., Cummings, D. A. T., Azman, A. S., Paireau, J., Fontanet, A., Cauchemez, S. & Salje, H. (2021) Age-specific mortality and immunity patterns of SARS-CoV-2. *Nature.* 590 (7844), 140-145.

Omland, L. H., Vestergaard, B. F. & Wandall, J. H. (2008) Herpes simplex virus type 2 infections of the central nervous system: A retrospective study of 49 patients. *Scand J Infect Dis.* 40 (1), 59-62.

Orth, G. (2008) Host defenses against human papillomaviruses: lessons from epidermodysplasia verruciformis. *Curr Top Microbiol Immunol.* 321, 59-83.

Oshiumi, H., Matsumoto, M., Funami, K., Akazawa, T. & Seya, T. (2003) TICAM-1, an adaptor molecule that participates in Toll-like receptor 3-mediated interferon-beta induction. *Nat Immunol.* 4 (2), 161-7.

Oshiumi, H., Okamoto, M., Fujii, K., Kawanishi, T., Matsumoto, M., Koike, S. & Seya, T. (2011) The TLR3/TICAM-1 pathway is mandatory for innate immune responses to poliovirus infection. *J Immunol.* 187 (10), 5320-7.

Paik, D. T., Chandy, M. & Wu, J. C. (2020) Patient and Disease-Specific Induced Pluripotent Stem Cells for Discovery of Personalized Cardiovascular Drugs and Therapeutics. *Pharmacol Rev.* 72 (1), 320-342.

Pal, M., Berhanu, G., Desalegn, C. & Kandi, V. (2020) Severe Acute Respiratory Syndrome Coronavirus-2 (SARS-CoV-2): An Update. *Cureus.* 12 (3), e7423.

Pasca, A. M., Sloan, S. A., Clarke, L. E., Tian, Y., Makinson, C. D., Huber, N., Kim, C. H., Park, J. Y., O'Rourke, N. A., Nguyen, K. D., Smith, S. J., Huguenard, J. R., Geschwind, D. H., Barres, B. A. & Pasca, S. P. (2015) Functional cortical neurons and astrocytes from human pluripotent stem cells in 3D culture. *Nat Methods.* 12 (7), 671-8.

Pavoni, S., Jarray, R., Nassor, F., Guyot, A. C., Cottin, S., Rontard, J., Mikol, J., Mabondzo, A., Deslys, J. P. & Yates, F. (2018) Small-molecule induction of Abeta-42 peptide production in human cerebral organoids to model Alzheimer's disease associated phenotypes. *PLoS One.* 13 (12), e0209150.

Pedersen, E. B., Haahr, S. & Mogensen, S. C. (1983) X-linked resistance of mice to high doses of herpes simplex virus type 2 correlates with early interferon production. *Infect Immun.* 42 (2), 740-6.

Perez de Diego, R., Sancho-Shimizu, V., Lorenzo, L., Puel, A., Plancoulaine, S., Picard, C., Herman, M., Cardon, A., Durandy, A., Bustamante, J., Vallabhapurapu, S., Bravo, J., Warnatz, K., Chaix, Y., Cascarrigny, F., Lebon, P., Rozenberg, F., Karin, M., Tardieu, M., Al-Muhsen, S., Jouanguy, E., Zhang, S. Y., Abel, L. & Casanova, J. L. (2010) Human TRAF3 adaptor molecule deficiency leads to impaired Toll-like receptor 3 response and susceptibility to herpes simplex encephalitis. *Immunity.* 33 (3), 400-11.

Pham, A. M., Santa Maria, F. G., Lahiri, T., Friedman, E., Marie, I. J. & Levy, D. E. (2016) PKR Transduces MDA5-Dependent Signals for Type I IFN Induction. *PLoS Pathog.* 12 (3), e1005489.

Pham, M. T., Pollock, K. M., Rose, M. D., Cary, W. A., Stewart, H. R., Zhou, P., Nolta, J. A. & Waldau, B. (2018) Generation of human vascularized brain organoids. *Neuroreport.* 29 (7), 588-593.

Piret, J. & Boivin, G. (2020) Immunomodulatory Strategies in Herpes Simplex Virus Encephalitis. *Clin Microbiol Rev.* 33 (2).

Pizzato, M., Baraldi, C., Boscato Sopetto, G., Finozzi, D., Gentile, C., Gentile, M. D., Marconi, R., Paladino, D., Raoss, A. & Riedmiller, I. (2022) SARS-CoV-2 and the host cell: A tale of interactions. *Frontiers in Virology.* 1.

Portillo, J. B., Vilella, L. P., Tamayo, D. A. A., Ballesteros, L. V. & Garcia-Monco, J. C. (2016) Viral encephalitis in the adult: a review. *Medical Research Archives.* 4 (5).

Potapov, I., Kanneganti, T. D. & Del Sol, A. (2022) Fostering experimental and computational synergy to modulate hyperinflammation. *Trends Immunol.* 43 (1), 4-7.

Prabantu, V. M., Naveenkumar, N. & Srinivasan, N. (2020) Influence of Disease-Causing Mutations on Protein Structural Networks. *Front Mol Biosci.* 7, 620554.

Prehaud, C., Megret, F., Lafage, M. & Lafon, M. (2005) Virus infection switches TLR-3-positive human neurons to become strong producers of beta interferon. *J Virol.* 79 (20), 12893-904.

Qian, X., Jacob, F., Song, M. M., Nguyen, H. N., Song, H. & Ming, G. L. (2018) Generation of human brain region-specific organoids using a miniaturized spinning bioreactor. *Nat Protoc.* 13 (3), 565-580.

Qian, X., Nguyen, H. N., Song, M. M., Hadiono, C., Ogden, S. C., Hammack, C., Yao, B., Hamersky, G. R., Jacob, F., Zhong, C., Yoon, K. J., Jeang, W., Lin, L., Li, Y., Thakor, J., Berg, D. A., Zhang, C., Kang, E., Chickering, M., Nauen, D., Ho, C. Y., Wen, Z., Christian, K. M., Shi, P. Y., Maher, B. J., Wu, H., Jin, P., Tang, H., Song, H. & Ming, G. L. (2016) Brain-Region-Specific Organoids Using Mini-bioreactors for Modeling ZIKV Exposure. *Cell.* 165 (5), 1238-1254.

Qian, X., Song, H. & Ming, G. L. (2019) Brain organoids: advances, applications and challenges. *Development.* 146 (8).

Quadrato, G., Nguyen, T., Macosko, E. Z., Sherwood, J. L., Min Yang, S., Berger, D. R., Maria, N., Scholvin, J., Goldman, M., Kinney, J. P., Boyden, E. S., Lichtman, J. W., Williams, Z. M., McCarroll, S. A. & Arlotta, P. (2017) Cell diversity and network dynamics in photosensitive human brain organoids. *Nature.* 545 (7652), 48-53.

Rahman, M. S., Islam, M. R., Alam, A., Islam, I., Hoque, M. N., Akter, S., Rahaman, M. M., Sultana, M. & Hossain, M. A. (2021) Evolutionary dynamics of SARS-CoV-2 nucleocapsid protein and its consequences. *J Med Virol.* 93 (4), 2177-2195.

Ramani, A., Muller, L., Ostermann, P. N., Gabriel, E., Abida-Islam, P., Muller-Schiffmann, A., Mariappan, A., Goureau, O., Gruell, H., Walker, A., Andree, M., Hauka, S., Houwaart, T., Dilthey, A., Wohlgemuth, K., Omran, H., Klein, F., Wieczorek, D., Adams, O., Timm, J., Korth, C., Schaal, H. & Gopalakrishnan, J. (2020) SARS-CoV-2 targets neurons of 3D human brain organoids. *EMBO J.* 39 (20), e106230.

Ramos, P. S., Shedlock, A. M. & Langefeld, C. D. (2015) Genetics of autoimmune diseases: insights from population genetics. *J Hum Genet.* 60 (11), 657-64.

Ramos-Estebanez, C., Lizarraga, K. J. & Merenda, A. (2014) A systematic review on the role of adjunctive corticosteroids in herpes simplex virus encephalitis: is timing critical for safety and efficacy? *Antivir Ther.* 19 (2), 133-9.

Rasmussen, S. B., Horan, K. A., Holm, C. K., Stranks, A. J., Mettenleiter, T. C., Simon, A. K., Jensen, S. B., Rixon, F. J., He, B. & Paludan, S. R. (2011) Activation of autophagy by alpha-herpesviruses in myeloid cells is mediated by cytoplasmic viral DNA through a mechanism dependent on stimulator of IFN genes. *J Immunol.* 187 (10), 5268-76.

Rasmussen, S. B., Jensen, S. B., Nielsen, C., Quartin, E., Kato, H., Chen, Z. J., Silverman, R. H., Akira, S. & Paludan, S. R. (2009) Herpes simplex virus infection is sensed by both Toll-like receptors and retinoic acid-inducible gene- like receptors, which synergize to induce type I interferon production. *J Gen Virol.* 90 (Pt 1), 74-8.

Rebendenne, A., Valadao, A. L. C., Tauziet, M., Maarifi, G., Bonaventure, B., McKellar, J., Planes, R., Nisole, S., Arnaud-Arnould, M., Moncorge, O. & Goujon, C. (2021) SARS-CoV-2 triggers an MDA-5-dependent interferon response which is unable to control replication in lung epithelial cells. *J Virol.* 95 (8).

Rebsamen, M., Meylan, E., Curran, J. & Tschopp, J. (2008) The antiviral adaptor proteins Cardif and Trif are processed and inactivated by caspases. *Cell Death Differ.* 15 (11), 1804-11.

Reinert, L. S., Harder, L., Holm, C. K., Iversen, M. B., Horan, K. A., Dagnaes-Hansen, F., Ulhoi, B. P., Holm, T. H., Mogensen, T. H., Owens, T., Nyengaard, J. R., Thomsen, A. R. & Paludan, S. R. (2012) TLR3 deficiency renders astrocytes permissive to herpes simplex virus infection and facilitates establishment of CNS infection in mice. *J Clin Invest.* 122 (4), 1368-76.

Reinert, L. S., Lopusna, K., Winther, H., Sun, C., Thomsen, M. K., Nandakumar, R., Mogensen, T. H., Meyer, M., Vaegter, C., Nyengaard, J. R., Fitzgerald, K. A. & Paludan, S. R. (2016) Sensing of HSV-1 by the cGAS-STING pathway in microglia orchestrates antiviral defence in the CNS. *Nat Commun.* 7, 13348.

Reubinoff, B. E., Pera, M. F., Fong, C. Y., Trounson, A. & Bongso, A. (2000) Embryonic stem cell lines from human blastocysts: somatic differentiation in vitro. *Nat Biotechnol.* 18 (4), 399-404.

Reyahi, A., Studahl, M., Skouboe, M. K., Fruhwurth, S., Narita, R., Ren, F., Bjerhem Viklund, M., Iversen, M. B., Christiansen, M., Svensson, A., Mogensen, T. H., Eriksson, K. & Paludan, S. R. (2023) An IKBKE variant conferring functional cGAS/STING pathway deficiency and susceptibility to recurrent HSV-2 meningitis. *JCI Insight.* 8 (21).

Reynolds, B. A. & Weiss, S. (1992) Generation of neurons and astrocytes from isolated cells of the adult mammalian central nervous system. *Science.* 255 (5052), 1707-10.

Riancho, J., Delgado-Alvarado, M., Sedano, M. J., Polo, J. M. & Berciano, J. (2013) Herpes simplex encephalitis: clinical presentation, neurological sequelae and new prognostic factors. Ten years of experience. *Neurol Sci.* 34 (10), 1879-81.

Richards, A. L., Sollars, P. J., Pitts, J. D., Stults, A. M., Heldwein, E. E., Pickard, G. E. & Smith, G. A. (2017) The pUL37 tegument protein guides alpha-herpesvirus retrograde axonal transport to promote neuroinvasion. *PLoS Pathog.* 13 (12), e1006741.

Rocha, N. D., de Moura, S. K., da Silva, G. A. B., Mattiello, R. & Sato, D. K. (2023) Neurological sequelae after encephalitis associated with herpes simplex virus in children: systematic review and meta-analysis. *BMC Infect Dis.* 23 (1), 55.

Roizman, B. & Whitley, R. J. (2013) An inquiry into the molecular basis of HSV latency and reactivation. *Annu Rev Microbiol.* 67, 355-74.

Roop, C., Hutchinson, L. & Johnson, D. C. (1993) A mutant herpes simplex virus type 1 unable to express glycoprotein L cannot enter cells, and its particles lack glycoprotein H. *J Virol.* 67 (4), 2285-97.

Rosenberg, J. & Galen, B. T. (2017) Recurrent Meningitis. *Curr Pain Headache Rep.* 21 (7), 33.

Rubin, D., Chan-Tack, K., Farley, J. & Sherwat, A. (2020) FDA Approval of Remdesivir - A Step in the Right Direction. *N Engl J Med.* 383 (27), 2598-2600.

Ruckdeschel, K., Pfaffinger, G., Haase, R., Sing, A., Weighardt, H., Hacker, G., Holzmann, B. & Heesemann, J. (2004) Signaling of apoptosis through TLRs critically involves toll/IL-1 receptor domain-containing adapter inducing IFN-beta, but not MyD88, in bacteria-infected murine macrophages. *J Immunol.* 173 (5), 3320-8.

Rybak-Wolf, A., Wyler, E., Pentimalli, T. M., Legnini, I., Oliveras Martinez, A., Glazar, P., Loewa, A., Kim, S. J., Kaufer, B. B., Woehler, A., Landthaler, M. & Rajewsky, N. (2023) Modelling viral encephalitis caused by herpes simplex virus 1 infection in cerebral organoids. *Nat Microbiol.* 8 (7), 1252-1266.

Sabate-Soler, S., Kurniawan, H. & Schwamborn, J. C. (2024) Advanced brain organoids for neuroinflammation disease modeling. *Neural Regen Res.* 19 (1), 154-155.

Sajic, D., Ashkar, A. A., Patrick, A. J., McCluskie, M. J., Davis, H. L., Levine, K. L., Holl, R. & Rosenthal, K. L. (2003) Parameters of CpG oligodeoxynucleotide-induced protection against intravaginal HSV-2 challenge. *J Med Virol.* 71 (4), 561-8.

Salgado, B., Sastre, I., Bullido, M. J. & Aldudo, J. (2023) Herpes Simplex Virus Type 1 Induces AD-like Neurodegeneration Markers in Human Progenitor and Differentiated ReNcell VM Cells. *Microorganisms.* 11 (5).

Salick, M. R., Wells, M. F., Eggan, K. & Kaykas, A. (2017) Modelling Zika Virus Infection of the Developing Human Brain In Vitro Using Stem Cell Derived Cerebral Organoids. *J Vis Exp.* (127).

Sameer, A. S. & Nissar, S. (2021) Toll-Like Receptors (TLRs): Structure, Functions, Signaling, and Role of Their Polymorphisms in Colorectal Cancer Susceptibility. *Biomed Res Int.* 2021, 1157023.

Sancho-Shimizu, V., Perez de Diego, R., Lorenzo, L., Halwani, R., Alangari, A., Israelsson, E., Fabrega, S., Cardon, A., Maluenda, J., Tatematsu, M., Mahvelati, F., Herman, M., Ciancanelli, M., Guo, Y., AlSum, Z., Alkhamis, N., Al-Makadma, A. S., Ghadiri, A., Boucherit, S., Plancoulaine, S., Picard, C., Rozenberg, F., Tardieu, M., Lebon, P., Jouanguy, E., Rezaei, N., Seya, T., Matsumoto, M., Chaussabel, D., Puel, A., Zhang, S. Y., Abel, L., Al-Muhsen, S. & Casanova, J. L. (2011) Herpes simplex encephalitis in children with autosomal recessive and dominant TRIF deficiency. *J Clin Invest.* 121 (12), 4889-902.

Sasai, M., Oshiumi, H., Matsumoto, M., Inoue, N., Fujita, F., Nakanishi, M. & Seya, T. (2005) Cutting Edge: NF-kappaB-activating kinase-associated protein 1 participates in TLR3/Toll-IL-1 homology domain-containing adapter molecule-1-mediated IFN regulatory factor 3 activation. *J Immunol.* 174 (1), 27-30.

Sasai, M., Tatematsu, M., Oshiumi, H., Funami, K., Matsumoto, M., Hatakeyama, S. & Seya, T. (2010) Direct binding of TRAF2 and TRAF6 to TICAM-1/TRIF adaptor participates in activation of the Toll-like receptor 3/4 pathway. *Mol Immunol.* 47 (6), 1283-91.

Sato, S., Sugiyama, M., Yamamoto, M., Watanabe, Y., Kawai, T., Takeda, K. & Akira, S. (2003) Toll/IL-1 receptor domain-containing adaptor inducing IFN-beta (TRIF) associates with TNF receptor-associated factor 6 and TANK-binding kinase 1, and activates two distinct transcription factors, NF-kappa B and IFN-regulatory factor-3, in the Toll-like receptor signaling. *J Immunol.* 171 (8), 4304-10.

Sawyer, M. H. & Rotbart, H. A. (2004) Viral meningitis and aseptic meningitis syndrome. *Infections of the central nervous system. Philadelphia: Lippincott Williams & Wilkins.* 75-93.

Schenten, D. & Medzhitov, R. (2011) The control of adaptive immune responses by the innate immune system. *Adv Immunol.* 109, 87-124.

Schmidt, H., Heimann, B., Djukic, M., Mazurek, C., Fels, C., Wallesch, C. W. & Nau, R. (2006) Neuropsychological sequelae of bacterial and viral meningitis. *Brain.* 129 (Pt 2), 333-45.

Schneweis, K. E. (1962) [Serological relations of types 1 and 2 of Herpesvirus hominis to Herpesvirus simiae]. *Z Immun exp ther.* 124, 337-41.

Schulz, T. C., Noggle, S. A., Palmarini, G. M., Weiler, D. A., Lyons, I. G., Pensa, K. A., Meedeniya, A. C., Davidson, B. P., Lambert, N. A. & Condie, B. G. (2004) Differentiation of human embryonic stem cells to dopaminergic neurons in serum-free suspension culture. *Stem Cells.* 22 (7), 1218-38.

Schulz, T. C., Palmarini, G. M., Noggle, S. A., Weiler, D. A., Mitalipova, M. M. & Condie, B. G. (2003) Directed neuronal differentiation of human embryonic stem cells. *BMC Neurosci.* 4, 27.

Sehl, J., Holper, J. E., Klupp, B. G., Baumbach, C., Teifke, J. P. & Mettenleiter, T. C. (2020) An improved animal model for herpesvirus encephalitis in humans. *PLoS Pathog.* 16 (3), e1008445.

Sellner, J., Dvorak, F., Zhou, Y., Haas, J., Kehm, R., Wildemann, B. & Meyding-Lamade, U. (2005) Acute and long-term alteration of chemokine mRNA expression after anti-viral and anti-inflammatory treatment in herpes simplex virus encephalitis. *Neurosci Lett.* 374 (3), 197-202.

Seok, J., Warren, H. S., Cuenca, A. G., Mindrinos, M. N., Baker, H. V., Xu, W., Richards, D. R., McDonald-Smith, G. P., Gao, H., Hennessy, L., Finnerty, C. C., Lopez, C. M., Honari, S., Moore, E. E., Minei, J. P., Cuschieri, J., Bankey, P. E., Johnson, J. L., Sperry, J., Nathens, A. B., Billiar, T. R., West, M. A., Jeschke, M. G., Klein, M. B., Gamelli, R. L., Gibran, N. S., Brownstein, B. H., Miller-Graziano, C., Calvano, S. E., Mason, P. H., Cobb, J. P., Rahme, L. G., Lowry, S. F., Maier, R. V., Moldawer, L. L., Herndon, D. N., Davis, R. W., Xiao, W., Tompkins, R. G., Inflammation & Host Response to Injury, L. S. C. R. P. (2013) Genomic responses in mouse models poorly mimic human inflammatory diseases. *Proc Natl Acad Sci U S A.* 110 (9), 3507-12.

Shalabi, M. & Whitley, R. J. (2006) Recurrent benign lymphocytic meningitis. *Clin Infect Dis.* 43 (9), 1194-7.

Sharma, S., tenOever, B. R., Grandvaux, N., Zhou, G. P., Lin, R. & Hiscott, J. (2003) Triggering the interferon antiviral response through an IKK-related pathway. *Science.* 300 (5622), 1148-51.

Shen, Y., Li, N. L., Wang, J., Liu, B., Lester, S. & Li, K. (2012) TRIM56 is an essential component of the TLR3 antiviral signaling pathway. *J Biol Chem.* 287 (43), 36404-13.

Shi, Y., Kirwan, P. & Livesey, F. J. (2012) Directed differentiation of human pluripotent stem cells to cerebral cortex neurons and neural networks. *Nat Protoc.* 7 (10), 1836-46.

Sison, S. L., O'Brien, B. S., Johnson, A. J., Seminary, E. R., Terhune, S. S. & Ebert, A. D. (2019) Human Cytomegalovirus Disruption of Calcium Signaling in Neural Progenitor Cells and Organoids. *J Virol.* 93 (17).

Slee, E. A., Zhu, H., Chow, S. C., MacFarlane, M., Nicholson, D. W. & Cohen, G. M. (1996) Benzyloxycarbonyl-Val-Ala-Asp (OMe) fluoromethylketone (Z-VAD.FMK) inhibits apoptosis by blocking the processing of CPP32. *Biochem J.* 315 (Pt 1) (Pt 1), 21-4.

Smiley, J. R. (2004) Herpes simplex virus virion host shutoff protein: immune evasion mediated by a viral RNase? *J Virol.* 78 (3), 1063-8.

Snijder, E. J., Limpens, R., de Wilde, A. H., de Jong, A. W. M., Zevenhoven-Dobbe, J. C., Maier, H. J., Faas, F., Koster, A. J. & Barcena, M. (2020) A unifying structural and functional model of the coronavirus replication organelle: Tracking down RNA synthesis. *PLoS Biol.* 18 (6), e3000715.

Sola, I., Almazan, F., Zuniga, S. & Enjuanes, L. (2015) Continuous and Discontinuous RNA Synthesis in Coronaviruses. *Annu Rev Virol.* 2 (1), 265-88.

Soltani, M. H., Pichardo, R., Song, Z., Sangha, N., Camacho, F., Satyamoorthy, K., Sangueza, O. P. & Setaluri, V. (2005) Microtubule-associated protein 2, a marker of neuronal differentiation, induces mitotic defects, inhibits growth of melanoma cells, and predicts metastatic potential of cutaneous melanoma. *Am J Pathol.* 166 (6), 1841-50.

Spear, P. G., Eisenberg, R. J. & Cohen, G. H. (2000) Three classes of cell surface receptors for alphaherpesvirus entry. *Virology.* 275 (1), 1-8.

Stahl, J. P. & Mailles, A. (2019) Herpes simplex virus encephalitis update. *Curr Opin Infect Dis.* 32 (3), 239-243.

Stanifer, M. L., Pervolaraki, K. & Boulant, S. (2019) Differential Regulation of Type I and Type III Interferon Signaling. *Int J Mol Sci.* 20 (6).

Steiner, I. & Benninger, F. (2013) Update on herpes virus infections of the nervous system. *Curr Neurol Neurosci Rep.* 13 (12), 414.

Steiner, I., Spivack, J. G., Deshmane, S. L., Ace, C. I., Preston, C. M. & Fraser, N. W. (1990) A herpes simplex virus type 1 mutant containing a nontransinducing Vmw65 protein establishes latent infection in vivo in the absence of viral replication and reactivates efficiently from explanted trigeminal ganglia. *J Virol.* 64 (4), 1630-8.

Stoeger, T. & Adler, H. (2018) "Novel" Triggers of Herpesvirus Reactivation and Their Potential Health Relevance. *Front Microbiol.* 9, 3207.

Stolz, A., Ernst, A. & Dikic, I. (2014) Cargo recognition and trafficking in selective autophagy. *Nat Cell Biol.* 16 (6), 495-501.

Su, X., Yue, P., Kong, J., Xu, X., Zhang, Y., Cao, W., Fan, Y., Liu, M., Chen, J., Liu, A. & Bao, F. (2021) Human Brain Organoids as an In Vitro Model System of Viral Infectious Diseases. *Front Immunol.* 12, 792316.

Subramanian, A., Tamayo, P., Mootha, V. K., Mukherjee, S., Ebert, B. L., Gillette, M. A., Paulovich, A., Pomeroy, S. L., Golub, T. R., Lander, E. S. & Mesirov, J. P. (2005) Gene set

enrichment analysis: a knowledge-based approach for interpreting genome-wide expression profiles. *Proc Natl Acad Sci U S A.* 102 (43), 15545-50.

Sun, L., Wu, J., Du, F., Chen, X. & Chen, Z. J. (2013) Cyclic GMP-AMP synthase is a cytosolic DNA sensor that activates the type I interferon pathway. *Science.* 339 (6121), 786-91.

Sun, N., Meng, X., Liu, Y., Song, D., Jiang, C. & Cai, J. (2021) Applications of brain organoids in neurodevelopment and neurological diseases. *J Biomed Sci.* 28 (1), 30.

Sun, X. Y., Ju, X. C., Li, Y., Zeng, P. M., Wu, J., Zhou, Y. Y., Shen, L. B., Dong, J., Chen, Y. J. & Luo, Z. G. (2022) Generation of vascularized brain organoids to study neurovascular interactions. *Elife.* 11.

Sungnak, W., Huang, N., Becavin, C., Berg, M., Queen, R., Litvinukova, M., Talavera-Lopez, C., Maatz, H., Reichart, D., Sampaziotis, F., Worlock, K. B., Yoshida, M., Barnes, J. L. & Network, H. C. A. L. B. (2020) SARS-CoV-2 entry factors are highly expressed in nasal epithelial cells together with innate immune genes. *Nat Med.* 26 (5), 681-687.

Svensson, A., Bellner, L., Magnusson, M. & Eriksson, K. (2007) Role of IFN-alpha/beta signaling in the prevention of genital herpes virus type 2 infection. *J Reprod Immunol.* 74 (1-2), 114-23.

Takahashi, K., Tanabe, K., Ohnuki, M., Narita, M., Ichisaka, T., Tomoda, K. & Yamanaka, S. (2007) Induction of pluripotent stem cells from adult human fibroblasts by defined factors. *Cell.* 131 (5), 861-72.

Takaoka, A., Wang, Z., Choi, M. K., Yanai, H., Negishi, H., Ban, T., Lu, Y., Miyagishi, M., Kodama, T., Honda, K., Ohba, Y. & Taniguchi, T. (2007) DAI (DLM-1/ZBP1) is a cytosolic DNA sensor and an activator of innate immune response. *Nature.* 448 (7152), 501-5.

Takemura, N., Kawasaki, T., Kunisawa, J., Sato, S., Lamichhane, A., Kobiyama, K., Aoshi, T., Ito, J., Mizuguchi, K., Karuppuchamy, T., Matsunaga, K., Miyatake, S., Mori, N., Tsujimura, T., Satoh, T., Kumagai, Y., Kawai, T., Standley, D. M., Ishii, K. J., Kiyono, H., Akira, S. & Uematsu, S. (2014) Blockade of TLR3 protects mice from lethal radiation-induced gastrointestinal syndrome. *Nat Commun.* 5, 3492.

Tangye, S. G., Al-Herz, W., Bousfiha, A., Cunningham-Rundles, C., Franco, J. L., Holland, S. M., Klein, C., Morio, T., Oksenhendler, E., Picard, C., Puel, A., Puck, J., Seppanen, M. R. J., Somech, R., Su, H. C., Sullivan, K. E., Torgerson, T. R. & Meyts, I. (2022) Human Inborn Errors of Immunity: 2022 Update on the Classification from the International Union of Immunological Societies Expert Committee. *J Clin Immunol.* 42 (7), 1473-1507.

Tao, S., Zhu, L., Lee, P., Lee, W. M., Knox, K., Chen, J., Di, Y. P. & Chen, Y. (2012) Negative control of TLR3 signaling by TICAM1 down-regulation. *Am J Respir Cell Mol Biol.* 46 (5), 660-7.

Tatematsu, M., Ishii, A., Oshiumi, H., Horiuchi, M., Inagaki, F., Seya, T. & Matsumoto, M. (2010) A molecular mechanism for Toll-IL-1 receptor domain-containing adaptor molecule-1-mediated IRF-3 activation. *J Biol Chem.* 285 (26), 20128-36.

Taylor, T. J., Brockman, M. A., McNamee, E. E. & Knipe, D. M. (2002) Herpes simplex virus. *Front Biosci.* 7, d752-64.

Tedder, D. G., Ashley, R., Tyler, K. L. & Levin, M. J. (1994) Herpes simplex virus infection as a cause of benign recurrent lymphocytic meningitis. *Ann Intern Med.* 121 (5), 334-8.

Thompson, K. A., Blessing, W. W. & Wesselingh, S. L. (2000) Herpes simplex replication and dissemination is not increased by corticosteroid treatment in a rat model of focal Herpes encephalitis. *J Neurovirol.* 6 (1), 25-32.

Thwaites, G. E., Nguyen, D. B., Nguyen, H. D., Hoang, T. Q., Do, T. T., Nguyen, T. C., Nguyen, Q. H., Nguyen, T. T., Nguyen, N. H., Nguyen, T. N., Nguyen, N. L., Nguyen, H. D., Vu, N. T., Cao, H. H., Tran, T. H., Pham, P. M., Nguyen, T. D., Stepniewska, K., White, N. J., Tran, T. H. & Farrar, J. J. (2004) Dexamethasone for the treatment of tuberculous meningitis in adolescents and adults. *N Engl J Med.* 351 (17), 1741-51.

Torii, M., Hashimoto-Torii, K., Levitt, P. & Rakic, P. (2009) Integration of neuronal clones in the radial cortical columns by EphA and ephrin-A signalling. *Nature.* 461 (7263), 524-8.

Totura, A. L., Whitmore, A., Agnihothram, S., Schafer, A., Katze, M. G., Heise, M. T. & Baric, R. S. (2015) Toll-Like Receptor 3 Signaling via TRIF Contributes to a Protective Innate Immune Response to Severe Acute Respiratory Syndrome Coronavirus Infection. *mBio.* 6 (3), e00638-15.

Tsai, M. S., Wang, L. C., Tsai, H. Y., Lin, Y. J., Wu, H. L., Tzeng, S. F., Hsu, S. M. & Chen, S. H. (2021) Microglia Reduce Herpes Simplex Virus 1 Lethality of Mice with Decreased T Cell and Interferon Responses in Brains. *Int J Mol Sci.* 22 (22).

Tunkel, A. R., Glaser, C. A., Bloch, K. C., Sejvar, J. J., Marra, C. M., Roos, K. L., Hartman, B. J., Kaplan, S. L., Scheld, W. M., Whitley, R. J. & Infectious Diseases Society of, A. (2008) The management of encephalitis: clinical practice guidelines by the Infectious Diseases Society of America. *Clin Infect Dis.* 47 (3), 303-27.

Twomey, J. A., Barker, C. M., Robinson, G. & Howell, D. A. (1979) Olfactory mucosa in herpes simplex encephalitis. *J Neurol Neurosurg Psychiatry.* 42 (11), 983-7.

Tyler, K. L. (2004) Herpes simplex virus infections of the central nervous system: encephalitis and meningitis, including Mollaret's. *Herpes.* 11 Suppl 2, 57A-64A.

Upton, A. R., Barwick, D. D. & Foster, J. B. (1971) Dexamethasone treatment in herpes-simplex encephalitis. *Lancet.* 1 (7693), 290-1.

V'Kovski, P., Kratzel, A., Steiner, S., Stalder, H. & Thiel, V. (2021) Coronavirus biology and replication: implications for SARS-CoV-2. *Nat Rev Microbiol.* 19 (3), 155-170.

Verzosa, A. L., McGeever, L. A., Bhark, S. J., Delgado, T., Salazar, N. & Sanchez, E. L. (2021) Herpes Simplex Virus 1 Infection of Neuronal and Non-Neuronal Cells Elicits Specific Innate Immune Responses and Immune Evasion Mechanisms. *Front Immunol.* 12, 644664.

Vollstedt, S., Arnold, S., Schwerdel, C., Franchini, M., Alber, G., Di Santo, J. P., Ackermann, M. & Suter, M. (2004) Interplay between alpha/beta and gamma interferons with B, T, and natural killer cells in the defense against herpes simplex virus type 1. *J Virol.* 78 (8), 3846-50.

Wald, A., Koelle, D. M., Fife, K., Warren, T., Leclair, K., Chicz, R. M., Monks, S., Levey, D. L., Musselli, C. & Srivastava, P. K. (2011) Safety and immunogenicity of long HSV-2 peptides complexed with rhHsc70 in HSV-2 seropositive persons. *Vaccine.* 29 (47), 8520-9.

Wang, C., Deng, L., Hong, M., Akkaraju, G. R., Inoue, J. & Chen, Z. J. (2001) TAK1 is a ubiquitin-dependent kinase of MKK and IKK. *Nature.* 412 (6844), 346-51.

Wang, L. & Xiang, Y. (2020) Spike Glycoprotein-Mediated Entry of SARS Coronaviruses. *Viruses.* 12 (11).

Wang, Q. Y., Zhou, C., Johnson, K. E., Colgrove, R. C., Coen, D. M. & Knipe, D. M. (2005) Herpesviral latency-associated transcript gene promotes assembly of heterochromatin on viral lytic-gene promoters in latent infection. *Proc Natl Acad Sci U S A.* 102 (44), 16055-9.

Wang, T., Town, T., Alexopoulou, L., Anderson, J. F., Fikrig, E. & Flavell, R. A. (2004) Toll-like receptor 3 mediates West Nile virus entry into the brain causing lethal encephalitis. *Nat Med.* 10 (12), 1366-73.

Wang, Y., Liu, L., Davies, D. R. & Segal, D. M. (2010) Dimerization of Toll-like receptor 3 (TLR3) is required for ligand binding. *J Biol Chem.* 285 (47), 36836-41.

Wang, Z. & Moult, J. (2001) SNPs, protein structure, and disease. *Hum Mutat.* 17 (4), 263-70.

Whitfield, T., Fernandez, C., Davies, K., Defres, S., Griffiths, M., Hooper, C., Tangney, R., Burnside, G., Rosala-Hallas, A., Moore, P., Das, K., Zuckerman, M., Parkes, L., Keller, S., Roberts, N., Easton, A., Touati, S., Kneen, R., Stahl, J. P. & Solomon, T. (2021) Protocol for DexEnceph: a randomised controlled trial of dexamethasone therapy in adults with herpes simplex virus encephalitis. *BMJ Open.* 11 (7), e041808.

Whitley, R. J. (2006) Herpes simplex encephalitis: adolescents and adults. *Antiviral Res.* 71 (2-3), 141-8.

Whitley, R. J. & Gnann, J. W. (2002) Viral encephalitis: familiar infections and emerging pathogens. *Lancet.* 359 (9305), 507-13.

Whitley, R. J. & Kimberlin, D. W. (2005) Herpes simplex encephalitis: children and adolescents. *Semin Pediatr Infect Dis.* 16 (1), 17-23.

Whitley, R. J. & Roizman, B. (2001) Herpes simplex virus infections. *Lancet.* 357 (9267), 1513-8.

WHO, W. H. O. (2023) *Herpes simplex virus.* https://www.who.int/news-room/fact-sheets/detail/herpes-simplex-virus.

Widener, R. W. & Whitley, R. J. (2014) Herpes simplex virus. *Handbook of clinical neurology*, Elsevier, pp. 251-263.

Wikstrom, M., Sjobring, U., Drakenberg, T., Forsen, S. & Bjorck, L. (1995) Mapping of the immunoglobulin light chain-binding site of protein L. *J Mol Biol.* 250 (2), 128-33.

Wildemann, B., Ehrhart, K., Storch-Hagenlocher, B., Meyding-Lamade, U., Steinvorth, S., Hacke, W. & Haas, J. (1997) Quantitation of herpes simplex virus type 1 DNA in cells of cerebrospinal fluid of patients with herpes simplex virus encephalitis. *Neurology.* 48 (5), 1341-6.

Wildy, P. & Watson, D. H. (1962) Electron microscopic studies on the architecture of animal viruses. *Cold Spring Harb Symp Quant Biol.* 27, 25-47.

Wilhelmus, K. R., Gee, L., Hauck, W. W., Kurinij, N., Dawson, C. R., Jones, D. B., Barron, B. A., Kaufman, H. E., Sugar, J., Hyndiuk, R. A. & et al. (1994) Herpetic Eye Disease Study. A controlled trial of topical corticosteroids for herpes simplex stromal keratitis. *Ophthalmology.* 101 (12), 1883-95; discussion 1895-6.

Wille, M. & Holmes, E. C. (2020) Wild birds as reservoirs for diverse and abundant gamma- and deltacoronaviruses. *FEMS microbiology reviews.* 44 (5), 631-644.

Wnek, M., Ressel, L., Ricci, E., Rodriguez-Martinez, C., Guerrero, J. C., Ismail, Z., Smith, C., Kipar, A., Sodeik, B., Chinnery, P. F., Solomon, T. & Griffiths, M. J. (2016) Herpes simplex encephalitis is linked with selective mitochondrial damage; a post-mortem and in vitro study. *Acta Neuropathol.* 132 (3), 433-51.

Wong, J. P., Saravolac, E. G., Sabuda, D., Levy, H. B. & Kende, M. (1995) Prophylactic and therapeutic efficacies of poly(IC.LC) against respiratory influenza A virus infection in mice. *Antimicrob Agents Chemother.* 39 (11), 2574-6.

Wu, A., Peng, Y., Huang, B., Ding, X., Wang, X., Niu, P., Meng, J., Zhu, Z., Zhang, Z., Wang, J., Sheng, J., Quan, L., Xia, Z., Tan, W., Cheng, G. & Jiang, T. (2020) Genome Composition and Divergence of the Novel Coronavirus (2019-nCoV) Originating in China. *Cell Host Microbe.* 27 (3), 325-328.

Wu, J., Sun, L., Chen, X., Du, F., Shi, H., Chen, C. & Chen, Z. J. (2013) Cyclic GMP-AMP is an endogenous second messenger in innate immune signaling by cytosolic DNA. *Science.* 339 (6121), 826-30.

Xu, R., Boreland, A. J., Li, X., Erickson, C., Jin, M., Atkins, C., Pang, Z. P., Daniels, B. P. & Jiang, P. (2021) Developing human pluripotent stem cell-based cerebral organoids with a controllable microglia ratio for modeling brain development and pathology. *Stem Cell Reports.* 16 (8), 1923-1937.

Xue, Q., Zhou, Z., Lei, X., Liu, X., He, B., Wang, J. & Hung, T. (2012) TRIM38 negatively regulates TLR3-mediated IFN-beta signaling by targeting TRIF for degradation. *PLoS One.* 7 (10), e46825.

Yadav, R., Chaudhary, J. K., Jain, N., Chaudhary, P. K., Khanra, S., Dhamija, P., Sharma, A., Kumar, A. & Handu, S. (2021) Role of Structural and Non-Structural Proteins and Therapeutic Targets of SARS-CoV-2 for COVID-19. *Cells.* 10 (4).

Yamamoto, M., Sato, S., Hemmi, H., Hoshino, K., Kaisho, T., Sanjo, H., Takeuchi, O., Sugiyama, M., Okabe, M., Takeda, K. & Akira, S. (2003a) Role of adaptor TRIF in the MyD88-independent toll-like receptor signaling pathway. *Science.* 301 (5633), 640-3.

Yamamoto, M., Sato, S., Hemmi, H., Uematsu, S., Hoshino, K., Kaisho, T., Takeuchi, O., Takeda, K. & Akira, S. (2003b) TRAM is specifically involved in the Toll-like receptor 4-mediated MyD88-independent signaling pathway. *Nat Immunol.* 4 (11), 1144-50.

Yamamoto, M., Sato, S., Mori, K., Hoshino, K., Takeuchi, O., Takeda, K. & Akira, S. (2002) Cutting edge: a novel Toll/IL-1 receptor domain-containing adapter that preferentially activates the IFN-beta promoter in the Toll-like receptor signaling. *J Immunol.* 169 (12), 6668-72.

Yamashiro, L. H., Wilson, S. C., Morrison, H. M., Karalis, V., Chung, J. J., Chen, K. J., Bateup, H. S., Szpara, M. L., Lee, A. Y., Cox, J. S. & Vance, R. E. (2020) Interferon-independent STING signaling promotes resistance to HSV-1 in vivo. *Nat Commun.* 11 (1), 3382.

Yang, Q., Liu, T. T., Lin, H., Zhang, M., Wei, J., Luo, W. W., Hu, Y. H., Zhong, B., Hu, M. M. & Shu, H. B. (2017) TRIM32-TAX1BP1-dependent selective autophagic degradation of TRIF negatively regulates TLR3/4-mediated innate immune responses. *PLoS Pathog.* 13 (9), e1006600.

Yang, W., Gu, Z., Zhang, H. & Hu, H. (2020) To TRIM the Immunity: From Innate to Adaptive Immunity. *Front Immunol.* 11, 02157.

Ye, W., Hu, M. M., Lei, C. Q., Zhou, Q., Lin, H., Sun, M. S. & Shu, H. B. (2017) TRIM8 Negatively Regulates TLR3/4-Mediated Innate Immune Response by Blocking TRIF-TBK1 Interaction. *J Immunol.* 199 (5), 1856-1864.

Yi, S. A., Nam, K. H., Yun, J., Gim, D., Joe, D., Kim, Y. H., Kim, H. J., Han, J. W. & Lee, J. (2020) Infection of Brain Organoids and 2D Cortical Neurons with SARS-CoV-2 Pseudovirus. *Viruses.* 12 (9).

Yin, X., Riva, L., Pu, Y., Martin-Sancho, L., Kanamune, J., Yamamoto, Y., Sakai, K., Gotoh, S., Miorin, L., De Jesus, P. D., Yang, C. C., Herbert, K. M., Yoh, S., Hultquist, J. F., Garcia-Sastre, A. & Chanda, S. K. (2021) MDA5 Governs the Innate Immune Response to SARS-CoV-2 in Lung Epithelial Cells. *Cell Rep.* 34 (2), 108628.

Yoneyama, M., Kikuchi, M., Natsukawa, T., Shinobu, N., Imaizumi, T., Miyagishi, M., Taira, K., Akira, S. & Fujita, T. (2004) The RNA helicase RIG-I has an essential function in double-stranded RNA-induced innate antiviral responses. *Nat Immunol.* 5 (7), 730-7.

York, I. A., Roop, C., Andrews, D. W., Riddell, S. R., Graham, F. L. & Johnson, D. C. (1994) A cytosolic herpes simplex virus protein inhibits antigen presentation to CD8+ T lymphocytes. *Cell.* 77 (4), 525-35.

Yu, J., Vodyanik, M. A., Smuga-Otto, K., Antosiewicz-Bourget, J., Frane, J. L., Tian, S., Nie, J., Jonsdottir, G. A., Ruotti, V., Stewart, R., Slukvin, II & Thomson, J. A. (2007) Induced pluripotent stem cell lines derived from human somatic cells. *Science.* 318 (5858), 1917-20.

Zandi, M., Soltani, S. & Feyzi, K. (2021) SARS-CoV-2 as a betacoronavirus comprises five structural proteins? *Infect Genet Evol.* 94, 105011.

Zhang, J. J., Dong, X., Liu, G. H. & Gao, Y. D. (2023) Risk and Protective Factors for COVID-19 Morbidity, Severity, and Mortality. *Clin Rev Allergy Immunol.* 64 (1), 90-107.

Zhang, K., Wang, S., Gou, H., Zhang, J. & Li, C. (2021) Crosstalk Between Autophagy and the cGAS-STING Signaling Pathway in Type I Interferon Production. *Front Cell Dev Biol.* 9, 748485.

Zhang, Q. (2020) Human genetics of life-threatening influenza pneumonitis. *Hum Genet.* 139 (6-7), 941-948.

Zhang, Q. & Bastard, P. & Liu, Z. & Le Pen, J. & Moncada-Velez, M. & Chen, J. & Ogishi, M. & Sabli, I. K. D. & Hodeib, S. & Korol, C. & Rosain, J. & Bilguvar, K. & Ye, J. & Bolze, A. & Bigio, B. & Yang, R. & Arias, A. A. & Zhou, Q. & Zhang, Y. & Onodi, F. & Korniotis, S. & Karpf, L. & Philippot, Q. & Chbihi, M. & Bonnet-Madin, L. & Dorgham, K. & Smith, N. & Schneider, W. M. & Razooky, B. S. & Hoffmann, H. H. & Michailidis, E. & Moens, L. & Han, J. E. & Lorenzo, L. & Bizien, L. & Meade, P. & Neehus, A. L. & Ugurbil, A. C. & Corneau, A. & Kerner, G. & Zhang, P. & Rapaport, F. & Seeleuthner, Y. & Manry, J. & Masson, C. & Schmitt, Y. & Schluter, A. & Le Voyer, T. & Khan, T. & Li, J. & Fellay, J. & Roussel, L. & Shahrooei, M. & Alosaimi, M. F. & Mansouri, D. & Al-Saud, H. & Al-Mulla, F. & Almourfi, F. & Al-Muhsen, S. Z. & Alsohime, F. & Al Turki, S. & Hasanato, R. & van de Beek, D. & Biondi, A. & Bettini, L. R. & D'Angio, M. & Bonfanti, P. & Imberti, L. & Sottini, A. & Paghera, S. & Quiros-Roldan, E. & Rossi, C. & Oler, A. J. & Tompkins, M. F. & Alba, C. & Vandernoot, I. & Goffard, J. C. & Smits, G. & Migeotte, I. & Haerynck, F. & Soler-Palacin, P. & Martin-Nalda, A. & Colobran, R. & Morange, P. E. & Keles, S. & Colkesen, F. & Ozcelik, T. & Yasar, K. K. & Senoglu, S. & Karabela, S. N. & Rodriguez-Gallego, C. & Novelli, G. & Hraiech, S. & Tandjaoui-Lambiotte, Y. & Duval, X. & Laouenan, C. & Clinicians, C.-S. & Clinicians, C. & Imagine, C. G. & French, C. C. S. G. & Co, V. C. C. & Amsterdam, U. M. C. C.-B. & Effort, C. H. G. & Group, N.-U. T. C. I. & Snow, A. L. & Dalgard, C. L. & Milner, J. D. & Vinh, D. C. & Mogensen, T. H. & Marr, N. & Spaan, A. N. & Boisson, B. & Boisson-Dupuis, S. & Bustamante, J. & Puel, A. & Ciancanelli, M. J. & Meyts, I. & Maniatis, T. & Soumelis, V. & Amara, A. & Nussenzweig, M. & Garcia-Sastre, A. & Krammer, F. & Pujol, A. & Duffy, D. & Lifton, R. P. & Zhang, S. Y. & Gorochov, G. & Beziat, V. & Jouanguy, E. & Sancho-Shimizu, V. & Rice, C. M. & Abel, L. & Notarangelo, L. D. & Cobat, A. & Su, H. C. & Casanova, J. L. (2020) Inborn errors of type I IFN immunity in patients with life-threatening COVID-19. *Science.* 370 (6515).

Zhang, S. Y., Clark, N. E., Freije, C. A., Pauwels, E., Taggart, A. J., Okada, S., Mandel, H., Garcia, P., Ciancanelli, M. J., Biran, A., Lafaille, F. G., Tsumura, M., Cobat, A., Luo, J., Volpi, S., Zimmer, B., Sakata, S., Dinis, A., Ohara, O., Garcia Reino, E. J., Dobbs, K., Hasek, M., Holloway, S. P., McCammon, K., Hussong, S. A., DeRosa, N., Van Skike, C. E., Katolik, A., Lorenzo, L., Hyodo, M., Faria, E., Halwani, R., Fukuhara, R., Smith, G. A., Galvan, V., Damha, M. J., Al-Muhsen, S., Itan, Y., Boeke, J. D., Notarangelo, L. D., Studer, L., Kobayashi, M., Diogo, L., Fairbrother, W. G., Abel, L., Rosenberg, B. R., Hart, P. J., Etzioni, A. & Casanova, J. L. (2018) Inborn Errors of RNA Lariat Metabolism in Humans with Brainstem Viral Infection. *Cell.* 172 (5), 952-965 e18.

Zhang, S. Y., Jouanguy, E., Ugolini, S., Smahi, A., Elain, G., Romero, P., Segal, D., Sancho-Shimizu, V., Lorenzo, L., Puel, A., Picard, C., Chapgier, A., Plancoulaine, S., Titeux, M., Cognet, C., von Bernuth, H., Ku, C. L., Casrouge, A., Zhang, X. X., Barreiro, L., Leonard, J., Hamilton, C., Lebon, P., Heron, B., Vallee, L., Quintana-Murci, L., Hovnanian, A., Rozenberg, F., Vivier, E., Geissmann, F., Tardieu, M., Abel, L. & Casanova, J. L. (2007) TLR3 deficiency in patients with herpes simplex encephalitis. *Science.* 317 (5844), 1522-7.

Zhang, W., Ross, P. J., Ellis, J. & Salter, M. W. (2022) Targeting NMDA receptors in neuropsychiatric disorders by drug screening on human neurons derived from pluripotent stem cells. *Transl Psychiatry.* 12 (1), 243.

Zhang, X., Shi, H., Wu, J., Zhang, X., Sun, L., Chen, C. & Chen, Z. J. (2013) Cyclic GMP-AMP containing mixed phosphodiester linkages is an endogenous high-affinity ligand for STING. *Mol Cell.* 51 (2), 226-35.

Zhang, Z., Miteva, M. A., Wang, L. & Alexov, E. (2012) Analyzing effects of naturally occurring missense mutations. *Comput Math Methods Med.* 2012, 805827.

Zhao, J., Wohlford-Lenane, C., Zhao, J., Fleming, E., Lane, T. E., McCray, P. B., Jr. & Perlman, S. (2012) Intranasal treatment with poly(I*C) protects aged mice from lethal respiratory virus infections. *J Virol.* 86 (21), 11416-24.

Zheng, M., Karki, R., Williams, E. P., Yang, D., Fitzpatrick, E., Vogel, P., Jonsson, C. B. & Kanneganti, T. D. (2021) TLR2 senses the SARS-CoV-2 envelope protein to produce inflammatory cytokines. *Nat Immunol.* 22 (7), 829-838.

Zhou, P., Yang, X. L., Wang, X. G., Hu, B., Zhang, L., Zhang, W., Si, H. R., Zhu, Y., Li, B., Huang, C. L., Chen, H. D., Chen, J., Luo, Y., Guo, H., Jiang, R. D., Liu, M. Q., Chen, Y., Shen, X. R., Wang, X., Zheng, X. S., Zhao, K., Chen, Q. J., Deng, F., Liu, L. L., Yan, B., Zhan, F. X., Wang, Y. Y., Xiao, G. F. & Shi, Z. L. (2020) A pneumonia outbreak associated with a new coronavirus of probable bat origin. *Nature.* 579 (7798), 270-273.

Zhu, N., Zhang, D., Wang, W., Li, X., Yang, B., Song, J., Zhao, X., Huang, B., Shi, W., Lu, R., Niu, P., Zhan, F., Ma, X., Wang, D., Xu, W., Wu, G., Gao, G. F., Tan, W., China Novel Coronavirus, I. & Research, T. (2020) A Novel Coronavirus from Patients with Pneumonia in China, 2019. *N Engl J Med.* 382 (8), 727-733.

Zimmer, B., Ewaleifoh, O., Harschnitz, O., Lee, Y. S., Peneau, C., McAlpine, J. L., Liu, B., Tchieu, J., Steinbeck, J. A., Lafaille, F., Volpi, S., Notarangelo, L. D., Casanova, J. L., Zhang, S. Y., Smith, G. A. & Studer, L. (2018) Human iPSC-derived trigeminal neurons lack constitutive TLR3-dependent immunity that protects cortical neurons from HSV-1 infection. *Proc Natl Acad Sci U S A.* 115 (37), E8775-E8782.

Appendix

7. Appendix

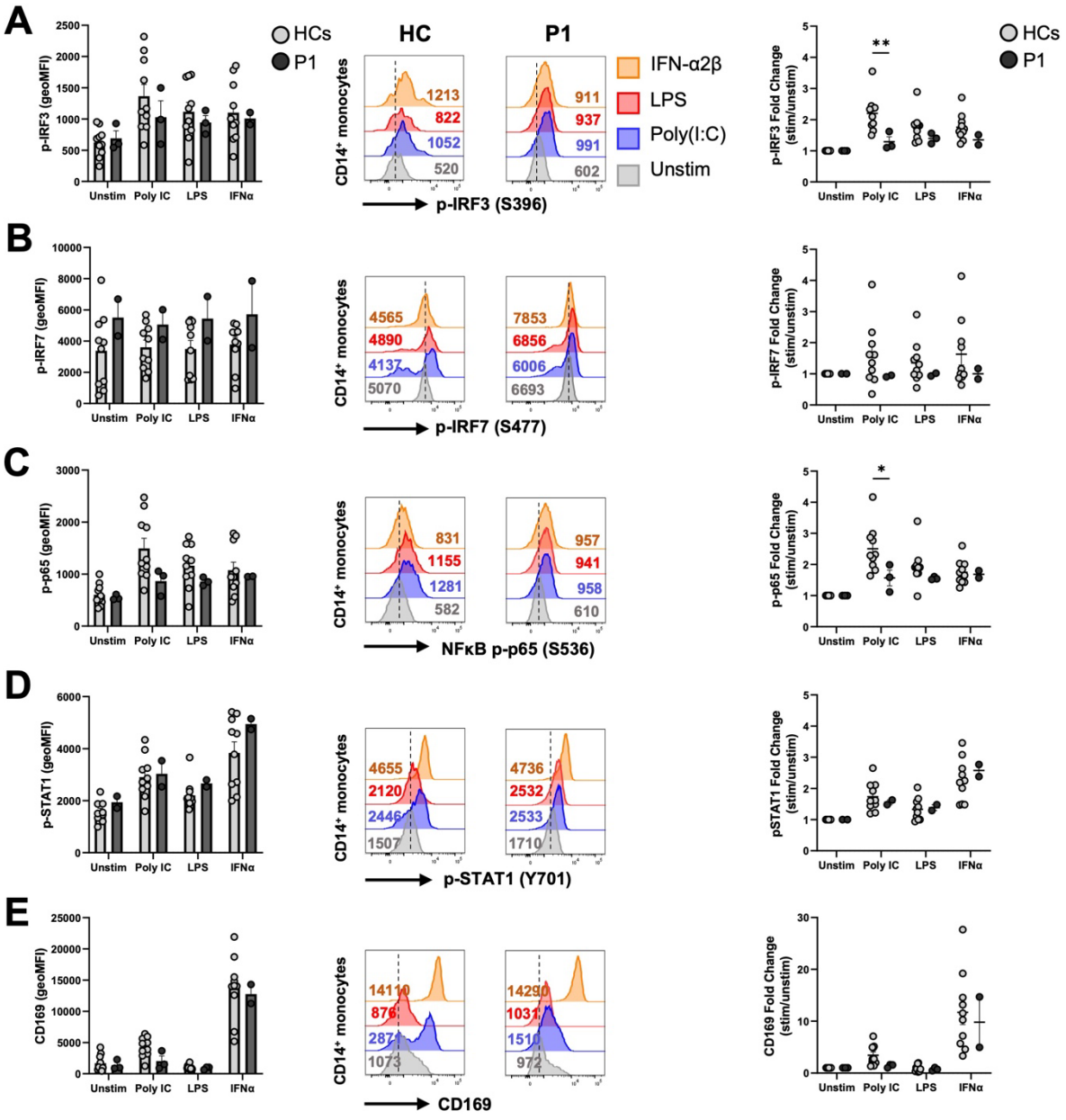


Figure 7.1 P1 PBMCs responses to poly(I:C), LPS and IFN-α.

Phosphoflow analysis was conducted on stimulated peripheral blood mononuclear cells (PBMCs) from both healthy controls (HCs) (N=10) and individual P1. The cells were treated with poly(I:C), LPS, and IFN-α2β for 24 hours to assess the phosphorylation status of A) pIRF3 (S396), B) pIRF7(S477), C) NF-κB pp65 (S536), D) pSTAT1, and E) CD169. Left panels show the quantification of the geometric within the CD14 positive monocyte population. Middle panels show representative histogram overlays of CD14 positive monocytes of a healthy control (HC) and P1. Values depicted next to histograms represent the

corresponding geometric. Right panels show fold change in geometric. Fold change was calculated normalising to the expression in unstimulated CD14+ cells. Data are represented in bar graphs or dot plots with mean ± SEM. The results shown are of 3 independent experiments; HC (N=10) and P1 (N=2-3; 3 different blood withdrawals). p-values were calculated using a Two-Way ANOVA test with Sidak's multiple-comparison test; * $p<0.05$ and ** $p<0.01$. This was performed by Dr Dorit Verhoeven and she generated all the data and legend. Dr. Dorit Verhoeven conducted this, producing both the data and the accompanying legend.

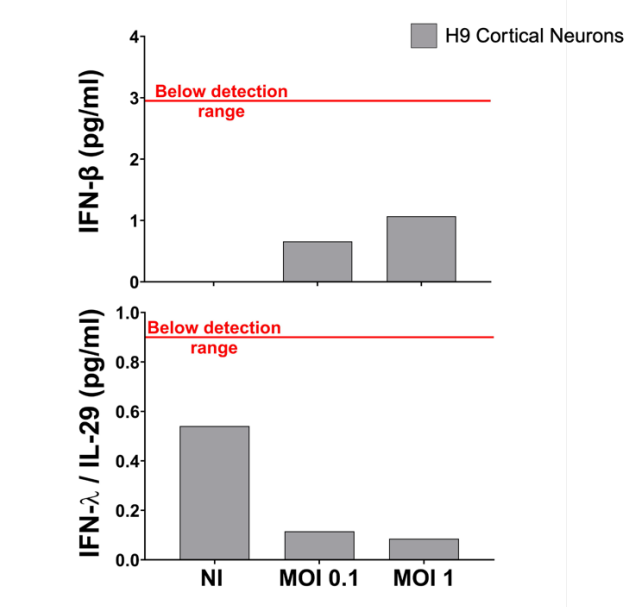


Figure 7.2 Production of cytokines by H9 ESCs-derived cortical neurons.

H9 ESCs-derived cortical neurons left uninfected (NI) or infected with HSV-1 at different MOIs for 24 hours. Supernatants collected from the infected cells were assayed for production of cytokines IFN-β, and IFN-λ/IL-29 by Meso Scale Discovery immunoassays. This experiment has only been performed once.

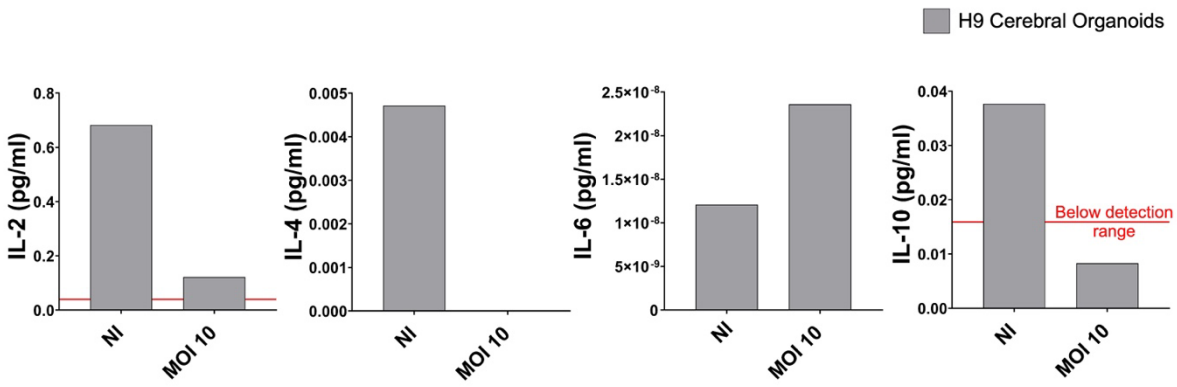


Figure 7.3 Production of cytokines by H9 ESCs-derived cerebral organoids.

H9 ESCs-derived cerebral organoids left uninfected (NI) or infected with HSV-1 at MOI 10 for 24 hours. Supernatants collected from the infected cells were assayed for production of cytokines IL-2, IL-4, IL-6 and IL-10 by Meso Scale Discovery immunoassays. This experiment has only been performed once.

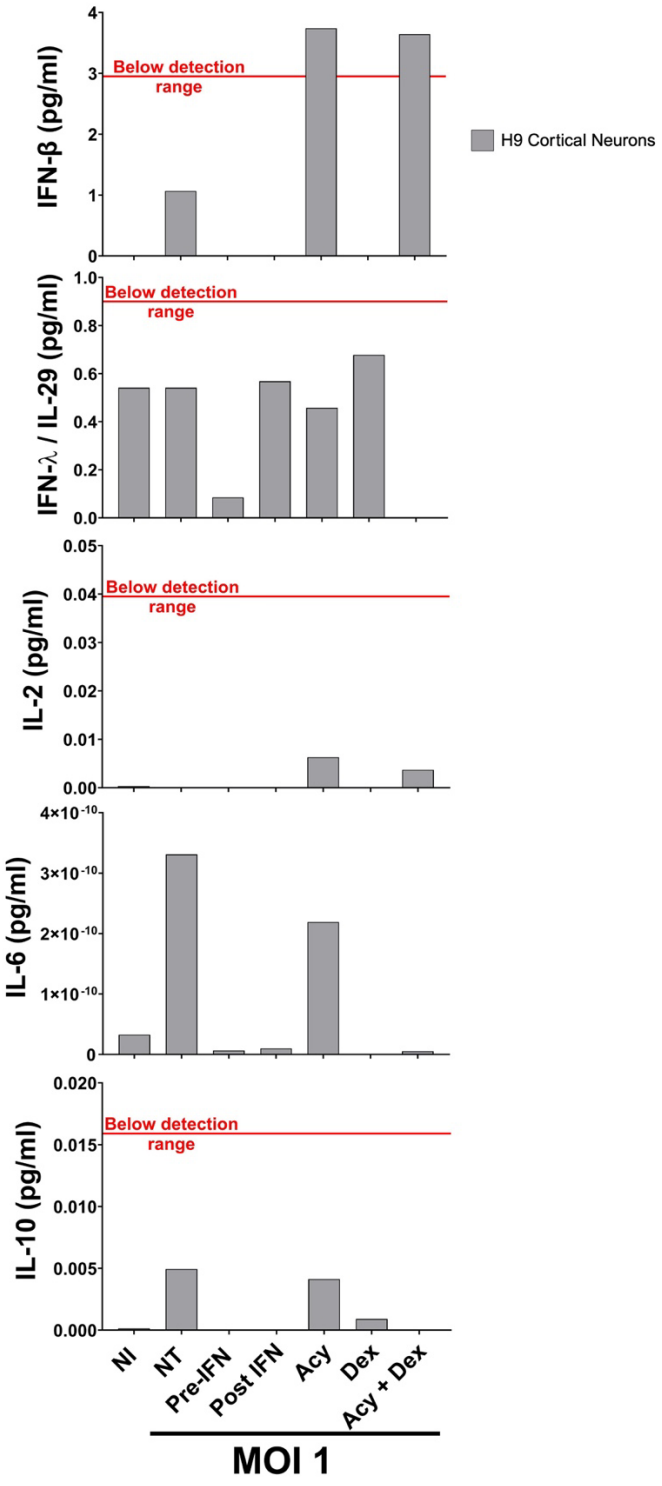


Figure 7.4 Production of cytokines by H9 ESCs-derived cortical neurons with treatments.

H9 ESCs-derived cortical neurons left uninfected (NI) or infected with HSV-1 at MOI I. Various treatments were added and allowed to proceed for 24 hours post-infection. Supernatants collected from the infected cells were assayed for production of cytokines IFN-β, and IFN-λ/IL-29 by Meso Scale Discovery immunoassays. This experiment has only been performed once.